Consiglio Nazionale delle Ricerche

Study Commission for the Drafting and Analysis of Technical Standards for Constructions

CNR-DT 200/2025

Guidelines for the Design, Execution, and Inspection of Structural Strengthening Interventions Using Fiber-Reinforced Composites

Materials, Reinforced and Prestressed Concrete Structures, Masonry Structures

CNR-DT 200 R2/2025

TABLE OF CONTENTS

1 PREAMBLE

1.1 PREAMBLE TO THIS REVISION (DT 200 R2) OF THE CNR-DT 200/2004 INSTRUCTIONS

Approximately ten years after the publication of the R1 revision of DT 200, the CNR Study Commission for the preparation and analysis of technical standards related to construction has undertaken a second revision of the Instructions. The purpose is to align the document with the latest international and national regulations and to integrate innovative topics and applications recently covered in scientific and technical literature.

The original Study Group, with some modifications and additions, was tasked with this revision. The final composition of the group is included at the end of the document.

The original intent of both being informative and explanatory has been preserved, aiming to disseminate essential mechanical and technological knowledge regarding the use of polymer matrix composite materials in the professional sector. This approach differs from that of a design guideline, which typically focuses exclusively on providing practical application rules for using fiber-reinforced composites in structural strengthening of existing buildings.

The revision addresses various topics and is supported by scientific studies endorsed by the scientific and technical communities and published in leading international journals. Each topic includes a concise bibliography for readers interested in further exploration.

A comprehensive update was carried out in **Chapter 2**, dedicated to **Materials**, to reflect the significant technological advancements of the last decade. This includes the introduction of new types of fibers and resins on the market, some of which, while not directly within the scope of these Instructions (limited to aramid, carbon, and glass fibers, steel wires or strands, and thermosetting resins), are discussed to inform the reader.

Specifically, an updated overview of material qualification is provided, incorporating the requirements of current Italian regulations and detailing the procedure for obtaining CE marking [1]. **Appendices A and B**, primarily didactic/informative, were revised accordingly, incorporating content from Professor Roberto Frassine's recent book [2], with his kind permission. **Appendix C**, with a similar purpose and scope, remains unchanged from previous editions.

Chapter 3, focusing on **Basic Reinforcement Design Concepts and Special Issues**, underwent revisions concerning partial factors for FRP materials and conversion factors. These revisions consider results from extensive experimental campaigns assessing uncertainties related to the variability of FRP material properties [3, 4] and approaches proposed in European standards [5–7] for accounting for all material-related uncertainties affecting design resistance using a single partial factor.

Chapter 4, addressing the **Strengthening of RC and PC Structures**, also underwent significant revisions. Notably, it now includes reinforcement systems embedded in substrate grooves (**NSM systems**, Near Surface Mounted) alongside externally bonded reinforcement systems (**EBR systems**), which were the sole focus of previous versions of the Instructions. Similar updates were made to the section on masonry structures in **Chapter 5**, with an essential bibliography provided [8–19].

For EBR systems, the calibration of the coefficient k_G was updated using results from composite-to-concrete adhesion tests conducted as part of the WP1 activities—**Polymer Matrix Composites** of the ReLUIS-DPC 2019-2021 Project. Similar updates were made to the k_G coefficient for EBR systems applied to masonry structures, covered in **Chapter 5**.

Additionally, the R2 revision introduces specifications for using anchoring devices with composite frayed anchors [20–31] and mechanical connectors [32–34], absent in previous versions. Details of the mechanical formulations underlying predictive formulas for debonding failure, applicable to both EBR and NSM systems, are included in the revised **Appendix D**.

Further updates in **Chapter 4** include additional guidelines for predicting crack widths in Serviceability Limit States [5, 7, 35–36] and evaluating diagonal tensile capacity of panel joints in beam-column connections, particularly for seismic applications [37–39].

Finally, **Chapter 6**, on **Monitoring and Control of the Intervention**, was updated to reflect regulatory advancements and practical experiences gained in the last decade.

This technical document was prepared by a study group composed of:

AIELLO Prof. Maria Antonietta	- University of Salento
ASCIONE Prof. Luigi	- University of Salerno
BALSAMO Prof. Alberto	- University "Federico II" - Naples
BARATTA Prof. Alessandro	- University "Federico II" - Naples
BATTISTA Dr. Umberto	- SACEN S.r.l. Restorations - Naples
BELLIAZZI Eng. Stefano	- University "Pegaso" - Naples
BENEDETTI Prof. Andrea	- University of Bologna
BERARDI Prof. Valentino Paolo	- University of Salerno
BILOTTA Prof. Antonio	- University "Federico II" - Naples
BONATI Eng. Antonio	- National Research Council, ITC
CAMATA Prof. Guido	- University "G. d'Annunzio" - Chieti-Pescara
CAMPANINI Eng. Davide	- Kerakoll S.p.a. - Sassuolo (MO)
CANESTRI Prof. Matteo	- University "G. d'Annunzio" - Chieti-Pescara
CERONI Prof. Francesca	- University "Parthenope" - Naples
CERSOSIMO Eng. Giuseppe	- Interbau S.r.l. - Milan
CORBI Geol. Ileana	- University "Federico II" - Naples
CORBI Prof. Ottavia	- University "Federico II" - Naples
COSENZA Prof. Edoardo	- University "Federico II" - Naples
D'ANTINO Prof. Tommaso	- Polytechnic University of Milan
DE FELICE Prof. Gianmarco	- Roma Tre University - Rome
DE SANTIS Prof. Stefano	- Roma Tre University - Rome
DEL ZOPPO Eng. Marta	- University "Federico II" - Naples
DEL VECCHIO Prof. Ciro	- University of Sannio - Benevento
DI LUDOVICO Prof. Marco	- University "Federico II" - Naples
FEO Prof. Luciano	- University of Salerno
FERRACUTI Prof. Barbara	- "Cusano" University - Rome
FERRETTI Eng. Francesca	- University of Bologna
FOCACCI Prof. Francesco	- eCampus University
FRANCO Eng. Annalisa	- National Research Council, ITC
FRASSINE Prof. Roberto	- Polytechnic University of Milan
GALATI Eng. Nessa	- Structural Technologies – Columbia, Maryland (USA)
GIACOMIN Eng. Giorgio	- G&P Intech S.r.l. - Altavilla Vicentina (VI)

LA MENDOLA Prof. Lidia	- University of Palermo
LA TEGOLA Prof. Antonio	- University of Salento
LIGNOLA Prof. Gian Piero	- University "Federico II" - Naples
LUCIANO Prof. Raimondo	- University "Parthenope" - Naples
MANFREDI Prof. Gaetano	- University "Federico II" - Naples
MARTINELLI Prof. Enzo	- University of Salerno
MAZZOTI Prof. Claudio	- University of Bologna
MONTI Prof. Giorgio	- "La Sapienza" University - Rome
MORANDINI Eng. Giulio	- Mapei S.p.a. - Milan
MORONI Eng. Federico	- Sika Italia S.p.a. - Milan
NANNI Prof. Antonio	- University of Miami - USA
NAPOLI Eng. Annalisa	- University of Salerno
NIGRO Prof. Emidio	- University "Federico II" - Naples
OCCHIUZZI Prof. Antonio	- University "Parthenope" - Naples & CNR-ITC
OLIVITO Prof. Renato Sante	- University of Calabria - Cosenza
PECCE Prof. Maria Rosaria	- University "Federico II" - Naples
PISANI Prof. Marco Andrea	- Polytechnic University of Milan
POGGI Prof. Carlo	- Polytechnic University of Milan
PROTA Prof. Andrea	- University "Federico II" - Naples
REALFONZO Prof. Roberto	- University of Salerno
ROSATI Prof. Luciano	- University "Federico II" - Naples
SAVOIA Prof. Marco	- University of Bologna
ZAMPA Eng. Andrea	- Fibre Net S.r.l. - Udine

Coordinators:

- For the chapter on "Materials":

FRASSINE Prof. Roberto, POGGI Prof. Carlo, PROTA Prof. Andrea

- For the chapter on "Basic Concepts of Strengthening Design and Special Issues":

MONTI Prof. Giorgio, NANNI Prof. Antonio, SAVOIA Prof. Marco

- For the chapter on "Reinforced and Prestressed Concrete Structures":

ASCIONE Prof. Luigi, BENEDETTI Prof. Andrea, MANFREDI Prof. Gaetano, MONTI Prof. Giorgio, PROTA Prof. Andrea

- For the chapter on "Masonry Structures":

BENEDETTI Prof. Andrea, AIELLO Prof. Maria Antonietta, CERONI Prof. Francesca

- For the chapter on "Control and Monitoring of the Intervention":

OLIVITO Prof. Renato Sante, FEO Prof. Luciano, PECCE Prof. Maria Rosaria

General Coordinator:
ASCIONE Prof. Luigi

Technical Secretariat:
LIGNOLA Prof. Gian Piero

This Technical Document was approved in its preliminary version on November 20, 2024, and submitted for public inquiry by the "Study Commission for the Preparation and Analysis of Technical Standards for Construction," composed as follows:

ANGOTTI Prof. Franco	-	University of Florence
ASCIONE Prof. Luigi	-	University of Salerno
AURICCHIO Prof. Ferdinando	-	University of Pavia
AVERSA Prof. Stefano	-	"Parthenope" University – Naples
BARATTA Prof. Alessandro	-	"Federico II" University – Naples
BONATI Eng. Antonio	-	National Research Council CNR-ITC
COSENZA Prof. Edoardo	-	"Federico II" University – Naples
DA PORTO Prof. Francesca	-	University of Padua
DI PRISCO Prof. Marco	-	Polytechnic University of Milan
IERVOLINO Prof. Iunio	-	"Federico II" University – Naples
LAGOMARSINO Prof. Sergio	-	University of Genoa
MANCINI Prof. Giuseppe	-	Polytechnic University of Turin
MAZZOLANI Prof. Federico Massimo	-	"Federico II" University – Naples
OCCHIUZZI Prof. Antonio, President	-	"Parthenope" University – Naples and CNR-ITC
PECCE Prof. Maria Rosaria	-	"Federico II" University – Naples
PINTO Prof. Paolo Emilio	-	"La Sapienza" University – Rome
POGGI Prof. Carlo	-	Polytechnic University of Milan
PROTA Prof. Andrea	-	Federico II" University – Naples
RENZI Eng. Emanuale	-	Ansfisa
ROYER CARFAGNI Prof. Gianni	-	University of Parma
SAETTA Prof. Anna	-	University of Venice
SAVOIA Prof. Marco	-	University of Bologna
URBANO Prof. Carlo	-	Polytechnic University of Milan
ZANON Prof. Paolo	-	University of Trento

The document was approved in its final version on March 10, 2025, at the conclusion of the public inquiry, incorporating the resulting changes, by the "Study Commission for the Preparation and Analysis of Technical Standards for Construction," composed as follows:

ANGOTTI Prof. Franco	-	University of Florence
ASCIONE Prof. Luigi	-	University of Salerno
AURICCHIO Prof. Ferdinando	-	University of Pavia
AVERSA Prof. Stefano	-	"Parthenope" University – Naples
BARATTA Prof. Alessandro	-	"Federico II" University – Naples
BONATI Eng. Antonio	-	National Research Council CNR-ITC
COSENZA Prof. Edoardo	-	"Federico II" University – Naples
DA PORTO Prof. Francesca	-	University of Padua
DI PRISCO Prof. Marco	-	Polytechnic University of Milan
IERVOLINO Prof. Iunio	-	"Federico II" University – Naples
LAGOMARSINO Prof. Sergio	-	University of Genoa
MANCINI Prof. Giuseppe	-	Polytechnic University of Turin
MAZZOLANI Prof. Federico Massimo	-	"Federico II" University – Naples
OCCHIUZZI Prof. Antonio, President	-	"Parthenope" University – Naples and CNR-ITC
PECCE Prof. Maria Rosaria	-	"Federico II" University – Naples
PINTO Prof. Paolo Emilio	-	"La Sapienza" University – Rome
POGGI Prof. Carlo	-	Polytechnic University of Milan
PROTA Prof. Andrea	-	Federico II" University – Naples
RENZI Eng. Emanuale	-	Ansfisa
ROYER CARFAGNI Prof. Gianni	-	University of Parma
SAETTA Prof. Anna	-	University of Venice
SAVOIA Prof. Marco	-	University of Bologna
URBANO Prof. Carlo	-	Polytechnic University of Milan
ZANON Prof. Paolo	-	University of Trento

ESSENTIAL BIBLIOGRAPHY SUPPORTING THE REVISION

[1] Bonati, A., Franco, A., De Luca, G., Coppola, O., Mirto, C., Occhiuzzi, A., L'attuazione del D.Lgs. 106/2017, in La marcatura CE dei Prodotti da Costruzione – ed. A. Rissotto, S. Fusco, Hoepli, 2020.

[2] Frassine, R., Tecnologie e proprietà dei materiali compositi: appunti del corso, Amazon Publ., ISBN-13 979-8712973958, (2021).

[3] Salzano, P., Bonati, A., Ceroni, F., Crisci, G., Franco, A., Occhiuzzi, A., Statistical analysis on mechanical properties of frp materials for structural strengthening, COMPDYN 2019, 7th ECCOMAS, (2019).

[4] Occhiuzzi, A., Ceroni, F., Franco, A., Salzano, P., Bonati, A., Experimental results of a national technical assessment procedure on commercial FRP for structural strenghening: wet-lay-up systems, Materials and Structures, 53:9, (2020).

[5] CEN-TC 250-SC 2_N2087, Background to EN 1992-1-1:2023 Eurocode 2 - Design of concrete structures - Part 1-1: General rules and rules for buildings, bridges and civil engineering structures, (2022).

[6] Eurocode 2 - Design of concrete structures - Part 1-1: General rules and rules for buildings, bridges and civil engineering structures, EN 1992-1-1, 2023, EUROPEAN COMMITTEE FOR STANDARDIZATION.

[7] *fib* Model Code for Concrete Structures 2020 (MC2020), (2020).

[8] Al-Zu'bi, M., Fan, M., Bertolesi, E., Anguilano, L., A review on retrofitting concrete members with near-surface mounted-fiber reinforced polymer composites. Structural Concrete 25(3): 2242–2268. https://doi.org/10.1002/suco.202300382, (2024).
[9] Bilotta, A., Ceroni, F., Barros, J., Costa, I., Palmieri, A., Szabo, Z., Nigro, E., Matthys, S., Balazs, G., Pecce, M., Bond of NSM FRP strengthened concrete: Round Robin Test initiative, ASCE Journal of Composites for Construction, 20 (1), (2016). https://doi.org/10.1061/(ASCE)CC.1943-5614.0000579.
[10] Novidis, D.G., Pantazopoulou S.J., Bond Tests of Short NSM-FRP and Steel Bar Anchorages Journal of Composites for Construction, 2008, Vol. 12(3), https://doi.org/10.1061/(ASCE)1090-0268(2008)12:3(323).
[11] Lee, D., Cheng, L., Hui J.Y., Bond Characteristics of Various NSM FRP Reinforcements in Concrete, Journal of Composites for Construction, Vol. 17(1), 2013, https://doi.org/10.1061/(ASCE)CC.1943-5614.0000318
[12] Sharaky, I.A., Torres, L., Baena, M., Miàs, C., An experimental study of different factors affecting the bond of NSM FRP bars in concrete, Composite Structures, 2013, https://doi.org/10.1016/j.compstruct.2012.12.014.
[13] Barris C., Baena M., Jahani Y., Codina A., Torres L. Experimental Study on Flexural Cracking and Deformation of Reinforced-Concrete Beams Strengthened with NSM FRP Reinforcement, Journal of Composites for Construction, 27(2), (2023). https://doi.org/10.1061/JCCOF2.CCENG-3907.
[14] Zhang, Y., Elsayed, M., Zhang, L. V., Nehdi, M. L., Flexural behavior of reinforced concrete T-section beams strengthened by NSM FRP bars, Engineering Structures, 233:111922, (2021).
[15] Kashyap, J., Willis, C.R., Griffith, M.C., Ingham, J.M., Masia, M.J., Debonding resistance of FRP-to-clay brick masonry joints, Engineering Structures 41 (2012) 186–198. http://dx.doi.org/10.1016/j.engstruct.2012.03.032.
[16] Maljaee, H., Ghiassi, B., Lourenço, P.B., Bond behavior in NSM-strengthened masonry, Engineering Structures 166: 302-313, https://doi.org/10.1016/j.engstruct.2018.03.091, (2018).
[17] Ceroni, F., Barros, J.A.O., Pecce, M., Ianniciello, M., Assessment of non linear bond laws for Near Surface Mounted systems in concrete elements, Composites Part B: Engineering, 45: 666–681, (2013).
[18] D'Antino, T., Pisani, M.A., General Analytical Model for the Bond Capacity of NSM FRP-Concrete Joints, Journal of Composites for Construction ASCE, 24(6). https://doi.org/10.1061/(ASCE)CC.1943-5614.0001076, (2020).
[19] Wang, X., Cheng L., Bond characteristics and modeling of near-surface mounted CFRP in concrete, Composite Structures 255 (2021), https://doi.org/10.1016/j.compstruct.2020.113011.
[20] Muciaccia, G., Khorasani, M., Mostofinejad, D., Effect of different parameters on the performance of FRP anchors in combination with EBR-FRP strengthening systems: A review. Construction and Building Materials, 354. https://doi.org/10.1016/j.conbuildmat.2022.129181, (2022).
[21] Alotaibi, N. K., Evaluating the impact of different anchor configurations and patch arrangements on the performance of fiber-reinforced polymer (FRP) anchors. Construction and Building Materials, 415. https://doi.org/10.1016/j.conbuildmat.2024.135110, (2024).
[22] Smith, S.T., Zhang, H., Wang, Z., Influence of FRP anchors on the strength and ductility of FRP-strengthened RC slabs, Construction and Building Materials, 2013, https://doi.org/10.1016/j.conbuildmat.2013.02.006.
[23] Jacobs, R.R., Williams, C.S., Evaluation of flexural strengthening methods for beams with simulated deterioration using spike-anchored FRP externally bonded sheets and near-surface-mounted strips, Composite Structures, Vol. 305, 2023, https://doi.org/10.1016/j.compstruct.2022.116463.
[24] del Rey Castillo, E., Dizhur, D., Griffith, M., Ingham, J., Strengthening RC structures using FRP spike anchors in combination with EBR systems, Composite Structures, 2019, https://doi.org/10.1016/j.compstruct.2018.10.093.

[25] del Rey Castillo, E., Griffith, M., Ingham, J., Seismic behavior of RC columns flexurally strengthened with FRP sheets and FRP anchors, Compos Struct, vol. 203, pp. 382–395, 2018, doi: 10.1016/j.compstruct.2018.07.029.
[26] Villanueva Llauradó. P., Ibell, T., Fernández Gómez, J., González Ramos, F.J., Pull-out and shear-strength models for FRP spike anchors, Compos B Eng, vol. 116, pp. 239–252, 2017, 10.1016/j.compositesb.2017.02.029.
[27] Cortez Flore, I.A., Gómez, J.F., Villanueva Llauradó, P., Influence of multiple anchor arrangement in the behaviour of FRP-to-concrete anchored joints, Composite Structures 230, 2019, https://doi.org/10.1016/j.compstruct.2019.111528.
[28] Alshami G. S., Hawileh R. A., Tatar J., Abdalla, J.A., Influence of CFRP Spike Anchors on the Performance of Flexural CFRP Sheets Externally Bonded to Concrete, J. of Composites for Construction, vol. 27, no. 5, 2023, doi: 10.1061/jccof2.cceng-4182.
[29] Ceroni F., Bond tests to evaluate the effectiveness of anchoring devices for CFRP sheets epoxy bonded over masonry elements, Compos B Eng, vol. 113, pp. 317–330, 2017, doi: 10.1016/j.compositesb.2017.01.042.
[30] Fagone, M., Ranocchiai, G., Caggegi, C., Briccoli Bati, S., Cuomo, M., The efficiency of mechanical anchors in CFRP strengthening of masonry: An experimental analysis, Compos B Eng, vol. 64, pp. 1–15, 2014, doi: 10.1016/j.compositesb.2014.03.018.
[31] Ozbakkaloglu T., Fang C., Gholampour A., Influence of FRP anchor configuration on the behavior of FRP plates externally bonded on concrete members, Eng Struct, vol. 133, pp. 133–150, Feb. 2017, doi: 10.1016/j.engstruct.2016.12.005.
[32] Barris, C., Correia, L., Sena-Cruz, J., Experimental study on the bond behaviour of a transversely compressed mechanical anchorage system for externally bonded reinforcement, Composite Structures 200: 217-228. https://doi.org/10.1016/j.compstruct.2018.05.084, (2018).
[33] Zhou, Y., Wang, X., Sui, L., Xing, F., Huang, Z., Chen, C., Li, P., Mei. L., Effect of mechanical fastening pressure on the bond behaviors of hybrid bonded FRP to concrete interface. Composite Structures 204:731-744. https://doi.org/10.1016/j.compstruct.2018.08.008, (2018).
[34] Gao, L., Zhang, F., Liu, J., Lu, X., Gao, H., Experimental and numerical study on the interfacial bonding characteristics of FRP-to-concrete joints with mechanical fastening, Construction and Building Materials 199: 456–470. https://doi.org/10.1016/j.conbuildmat.2018.12.033, (2019).
[35] Barris, C., Ceroni, F., Perez Caldentey, A., Assessment of Crack Spacing and Crack Width formulations in RC Elements Externally Strengthened with FRP Materials, ACI SP-360: Proceedings of the 16th International Symposium on Fiber-Reinforced Polymer (FRP) Reinforcement for Concrete Structures (FRPRCS-16), 23-24 March 2024, New Orleans, USA, ISBN: 9781641952439, (2024).
[36] *fib* bulletin 114, Serviceability Limit States of Concrete Structures: Background document of fib MC2020, (2025).
[37] Del Vecchio, C., Di Ludovico, M., Balsamo, A., Prota, A., Manfredi G., Dolce, M., Experimental investigation on exterior RC beam-column joints retrofitted with FRP systems, ASCE Journal of Composites for Construction, 18 (4), 1-13, (2014).
[38] Del Vecchio, C., Di Ludovico, M., Prota, A., Manfredi, G., Analytical model and design approach for FRP strengthening of non-conforming RC corner beam–column joints, Engineering Structures, 87, 8-20, (2015).
[39] Del Vecchio, C., Di Ludovico, M., Balsamo, A., Prota, A., Minimally Invasive FRP Strengthening of External Beam–Column Joints, ASCE Journal of Composites for Construction, Vol. 28, Issue 4, (2024) https://doi.org/10.1061/JCCOF2.CCENG-4525.

1.2 PREAMBLE TO THE R1 REVISION OF THE CNR-DT 200/2004 INSTRUCTIONS

More than five years after the approval of the first version of the CNR-DT 200/2004 Instructions, the CNR Study Commission for the preparation and analysis of technical standards related to construction initiated a revision of the document. The original Study Group was entrusted with updating the document to reflect the results of the most recent theoretical and experimental research conducted internationally over the five years before 2013, particularly research developed in Italy as part of the ReLUIS project (2005–2008) funded by the Department of Civil Protection. One section of this project was specifically dedicated to the topic of "Innovative Materials for Reducing Vulnerability in Existing Structures."

During the revision process, the Study Group also referred to the latest versions of the following international guidelines:

- **440.2R-08**: *Guide for the Design and Construction of Externally Bonded FRP Systems for Strengthening Concrete Structures*, American Concrete Institute (ACI), Committee 440, 2008.
- **ISIS Design Manual No. 4**: *FRP Rehabilitation of Reinforced Concrete Structures*, ISIS Canada Corporation, 2008.

The document underwent public inquiry from April to June 2013. Following this, modifications and/or additions were introduced to the text.

The updated document was discussed and approved by the "Commission for the preparation and analysis of technical standards related to construction" on October 10, 2013, at the CNR headquarters in Rome.

Gratitude is extended to the professionals, institutions, industries, and universities who actively participated in this process, which rightly involves the entire technical and scientific community of a modern and advanced nation.

1.3 PREAMBLE TO THE CNR-DT 200/2004 DOCUMENT

Among researchers and designers working in the field of strengthening with fiber-reinforced composite materials, there is a common perception that Italy is assuming a distinctive position internationally. This is due both to the value of its contributions to knowledge and to the presence of a particularly diverse and important architectural heritage. This heritage includes structures of significant historical and architectural value, as well as more recent masonry, reinforced concrete (RC), prestressed concrete (PC), and steel constructions. Many of these structures are over thirty years old and thus require varying degrees of urgent structural rehabilitation.

International initiatives to establish guidelines addressing these needs are well known, such as the Japanese standards (JSCE - 1997), American guidelines (ACI 440 - 2000), and European recommendations (FIP-CEB - 2001). Additionally, the CNR approved a study document in January 1999 titled *Use of Non-Metallic Reinforcements in RC Structures.* All these documents focus on structural systems with reinforced concrete frameworks.

The scientific interest in innovative FRP applications for structural rehabilitation and the unique characteristics of Italy's architectural heritage has, in recent years, attracted the attention of numerous researchers in the fields of Structural Mechanics, Construction, Structural Rehabilitation, and Seismic

Engineering. These efforts have resulted in a series of scientific programs funded by major Italian research entities, particularly MIUR and CNR.

A list of significant research projects on composite materials funded in the five years preceding the drafting of the 2004 document. Many of the authors of this document participated in these projects as national or local coordinators.

The drafting of an Italian Instruction document for the design, execution, and monitoring of static strengthening interventions using fiber-reinforced composites (FRPs) became essential. This need was particularly urgent for a document with broad applicability to the diverse structural types found in Italy's architectural heritage, including RC and PC structures, masonry constructions, timber structures, and metal structures.

The CNR, through its Commission tasked with providing opinions on technical construction standards, recognized this need and acted promptly to address it. To this end, it promoted a specific initiative within academic and industrial sectors, catalyzed by a group of faculty members specializing in Construction Science and Techniques. Some of the members of the Commission have been conducting FRP research for many years.

Nearly all Italian faculty members joined the initiative and researchers involved in this promising and emerging field of construction, as well as technical managers from major producers and installers of composite reinforcements, and representatives from organizations and companies using fiber-reinforced materials for the strengthening of structures and works of art.

Their names and affiliations are listed at the end of the 2004 edition of the text. Starting January 15, 2004, these professionals were engaged in drafting a document organized into the following sections:

- Materials
- Basic Concepts of FRP Strengthening and Special Issues
- Strengthening of RC and PC Structures
- Strengthening of Masonry Structures
- Strengthening of Metal Structures
- Strengthening of Timber Structures
- New Construction Using FRPs

The document was also conceived with an informative and explanatory purpose, essential for disseminating, within the professional field, the basic mechanical and technological knowledge necessary for the use of new materials.

After six months of intense and passionate work, the first four parts are ready for publication. The publication of the remaining sections is expected by the end of 2005.

Below is a list of significant research projects on composite materials, funded by the MIUR (Ministry of Education, University, and Research) and the CNR (National Research Council) over the five years preceding 2004, which contributed to creating the conditions for drafting this document.

- **1998–2000:** PRIN research project titled *"Composite Materials in Civil Construction,"* National Coordinator: Prof. Luigi Ascione;
- **2000–2002:** PRIN research project titled *"Structural Strengthening of Existing Structures with Composite Materials: Development of Design Guidelines for Reliability and Durability,"* National Coordinator: Prof. Luigi Ascione;

- **2002–2004:** PRIN research project titled *"Active and Passive Strengthening Using Composite Materials in Existing Structures and for Technological Innovation in Civil Construction,"* National Coordinator: Prof. Luigi Ascione;
- **2002–2003:** PRIN research project titled *"The Use of Composites for Seismic Strengthening of Reinforced Concrete Structures,"* National Coordinator: Prof. G. Manfredi;
- **2003–2005:** PRIN research project titled *"The Use of Microstructured Materials for the Technological Innovation of Civil Structures,"* National Coordinator: Prof. Franco Maceri;
- **2003–2005:** PRIN research project titled *"Behavior and Design Criteria for the Strengthening of Reinforced Concrete Structures with Composites,"* National Coordinator: Prof. Antonio Nanni;
- **2003–2005:** Research project titled *"Modeling of Innovative Materials for Structural Preservation,"* (Coordinator: Prof. Luigi Ascione), part of the MIUR Strategic Project (Law 449/97) titled *"Diagnosis and Preservation of Architectural Structures with Particular Attention to the Effects of Seismic Events and Other Natural Disasters,"* National Coordinator: Prof. Franco Maceri;
- **2003–2005:** Research project titled *"Effects of the Rheological Properties of Composite Materials in Structural Interventions for Civil Engineering,"* (Coordinator: Prof. Marco Savoia), part of the MIUR Strategic Project (Law 449/97) titled *"Composite Materials for Structural Applications of Significant Industrial Interest,"* National Coordinator: Prof. Sesto Viticoli;
- **2003–2005:** Research project titled *"Structures Made of Composite Material,"* (Coordinator: Prof. Franco Maceri), part of the MIUR Strategic Project (Law 449/97) titled *"Composite Materials for Structural Applications of Significant Industrial Interest,"* National Coordinator: Prof. Sesto Viticoli;
- **2003:** Center of Excellence on *"Structural Composites for Innovative Applications in Civil Engineering,"* based at the University of Naples, Director: Prof. Edoardo Cosenza.

1.4 CONTENT AND PURPOSE OF THE INSTRUCTIONS

The purpose of these Instructions is to provide, within the framework of the current regulations, a guideline for the design, execution, and monitoring of structural strengthening interventions using fiber-reinforced composite materials (FRPs). These materials consist of thermosetting polymer matrices and continuous long fibers of carbon, glass, aramid, or steel micro-strands. Commonly referred to as FRPs (or FRP systems), they are also more specifically categorized as CFRP (carbon fibers), GFRP (glass fibers), AFRP (aramid fibers), and SFRP (steel micro-strands).

The Guidelines, by their origin and nature, are not binding standards but are instead intended to assist professionals in navigating the extensive national and international literature available in this field. They provide a structured reference while leaving the final responsibility for decisions with the professionals themselves.

The document addresses the following topics:

- Materials
- Basic Concepts of FRP Strengthening and Special Issues
- Strengthening of RC and PC Structures
- Strengthening of Masonry Structures
- Examples of FRP System Design

Within the sections on strengthening RC, PC, and masonry structures, specific guidelines are also provided for seismic zones, aligning with the latest orientations adopted in both national and international standards.

The first topic includes detailed information in three dedicated appendices (Appendices A, B, and C) on the phases of FRPs, their physical-mechanical characteristics, production techniques, and constitutive behavior. These appendices are intentionally didactic in nature, aiming to provide less-experienced readers with basic technological and mechanical knowledge essential for the conscious use of composite materials in structural applications. Particular emphasis is placed on the unique characteristics of these materials compared to isotropic materials commonly used in construction, with a focus on constitutive relationships and resistance checks.

The remaining topics are structured in the typical style of technical documents published by the CNR, providing instructions in the structural field. The approach follows the widely accepted Eurocode methodology, where numbered clauses distinguish different provisions.

The document includes the following Appendices:

- **Appendix A**: Constituent phases of FRPs and their physical-mechanical characteristics
- **Appendix B**: Production techniques
- **Appendix C**: Constitutive relationship of FRPs and failure criteria
- **Appendix D**: Debonding of EBR and NSM reinforcements from the substrate
- **Appendix E**: Strengthening of RC elements under flexural compression
- **Appendix F**: Constitutive relationship of confined concrete
- **Appendix G**: Derivation of the crack width formula for RC elements strengthened with FRP materials
- **Appendix H**: Examples of FRP strengthening design for RC structures
- **Appendix I**: Examples of FRP strengthening design for masonry structures

1.5 NOMENCLATURE

Below is a list of the primary symbols used in the document and their meanings:

General Notations

$(.)_c$ Value of the quantity (.) referring to concrete.
$(.)_{cc}$ Value of the quantity (.) referring to confined concrete.
$(.)_d$ Design (or calculated) value of the quantity (.).
$(.)_f$ Value of the quantity (.) referring to fiber-reinforced composite (FRP).
$(.)_{fib}$ Value of the quantity (.) referring to fibers.
$(.)_k$ Characteristic value of the quantity (.).
$(.)_m$ Value of the quantity (.) referring to masonry.
$(.)_{mat}$ Value of the quantity (.) referring to the matrix.
$(.)_{mc}$ Value of the quantity (.) referring to confined masonry.
$(.)_R$ Value of the quantity (.) viewed as resistance.
$(.)_s$ Value of the quantity (.) referring to steel.
$(.)_S$ Value of the quantity (.) viewed as stress.

Uppercase Roman Letters

A_c Area of the concrete section, excluding metallic reinforcements.
$A_{c,ef}$ Effective tensile area of the concrete section.

A_f Area of FRP reinforcement.
$A_{f,i}$ Area of inclined FRP reinforcement.
A_{fib} Area of fibers.
A_F Fiber area in NSM systems.
A_{fv} Area of shear-resistant fiber stirrup.
A_R Resin area in NSM systems.
A_s Area of internal steel reinforcement.
A_{s1} Area of tensile steel reinforcement.
A_{s2} Area of compressive steel reinforcement.
A_t Effective cross-sectional area of a single strand.
B_f Width of anchored reinforcement.
B_p Width of the anchoring plate.
D Diameter of the circular concrete section.
E_c Elastic modulus of concrete.
$E_{c,eff}$ Effective elastic modulus of concrete.
E_d Design value of a general demand.
E_{ds} Reduced modulus of longitudinal steel reinforcement bars.
E_f Normal elastic modulus of FRP reinforcement.
E_F Normal elastic modulus of fiber-reinforced composite.
E_{fib} Normal elastic modulus of fibers.
E_h Elastic modulus of the homogenized system of reinforcement and leveling layer.
E_H Homogenized elastic modulus of the NSM system.
E_i Tangential modulus of steel reinforcements.
E_{mat} Normal elastic modulus of the matrix.
E_R Normal elastic modulus of the resin in NSM systems.
E_r Normal elastic modulus of the leveling layer.
E_s Normal elastic modulus of steel reinforcements.
FC Confidence factor.
$F_{A,1}$ Maximum force transmissible by an anchored FRP strip.
$F_{anc,d}$ Maximum tensile stress in an FRP strip anchored with frayed anchors
$F_{max,m}$ Mean value of the maximum tensile force transmissible by FRP reinforcement to the substrate.
$F_{max,d}$ Design value of the maximum tensile force transmissible by FRP reinforcement to the substrate.
F_{pd} Design value of the maximum anchoring force transmissible by FRP reinforcement bonded to masonry under normal action to the adhesion plane.
F_{fu} Ultimate force of FRP reinforcement.
G_a Tangential elastic modulus of the adhesive.
G_c Tangential elastic modulus of concrete.
I_o Moment of inertia of the uncracked and unreinforced RC section.
I_1 Moment of inertia of the cracked RC section reinforced with FRP.
I_2 Moment of inertia of the cracked RC section without external FRP reinforcement and with homogenized steel reinforcements.
I_{2r} Moment of inertia of the homogenized section considering both internal steel reinforcements and external FRP reinforcements, assumed partialized.
I_c Moment of inertia of the homogenized section.
I_f Moment of inertia of FRP reinforcement relative to its centroidal axis, parallel to the neutral axis of the beam.
L Width of the masonry panel.
L_s Length of the anchoring fiber.
M_{cr} Moment that induces cracking in the section.

M_{Rd} Design resistance moment of the section strengthened with FRP.
M_{Sd} Design bending moment acting on the section.
M_0 Bending moment acting on the RC section at the time of FRP reinforcement application.
M_1 Bending moment acting on the RC section strengthened with FRP due to loads applied after the intervention.
M_{max} Moment acting on the most stressed section of the element, evaluated for the characteristic load combination.
N_f Number of yarns per unit width.
N_M Total compressive force resulting from bolt tightening.
N_t Number of strands.
$N_{DB,k}$ Characteristic value of the maximum force causing debonding failure of the anchoring bundle from the FRP reinforcement.
$N_{FR,k}$ Characteristic value of the maximum force causing tensile failure of the fibers in the anchoring bundle.
$N_{S,m}$ Characteristic value of the maximum force causing shear failure.
$N_{PO,m}$ Characteristic value of the maximum force causing pull-out failure of the anchoring bundle from the substrate.
$N_{Rcc,d}$ Design resistance to axial compression of an RC element confined with FRP.
$N_{Rmc,d}$ Design resistance to axial compression of masonry confined with FRP.
N_{Sd} Design axial force acting on the section.
N_1 Compressive force resulting from the tightening of a single bolt.
P_{fib} Weight fraction of fibers.
P_{mat} Weight fraction of the matrix.
R_b Radius of curvature of the bend in anchoring fibers.
R_d Design value of a general resistance.
T_g Glass transition temperature of the resin.
T_{mat} Melting temperature of the matrix.
T_{Rd} Design torsional resistance of the RC element strengthened with FRP.
$T_{Rd,f}$ Resistance of the FRP reinforcement to torsion.
$T_{Rd,c}$ Resistance of the compressed concrete strut to torsion.
$T_{Rd,l}$ Resistance of the longitudinal steel reinforcement to torsion.
$T_{Rd,s}$ Resistance of the transverse steel reinforcement to torsion.
T_{Sd} Design torsional moment acting on the section.
T_x Yarn count in the x-direction.
V_{fib} Volume fraction of fibers.
V_{Rd} Design shear resistance of the element strengthened with FRP.
$V_{Rd,c}$ Contribution of the compressed concrete strut to design shear resistance.
$V_{Rd,s}$ Contribution of the transverse steel reinforcement to design shear resistance.
$V_{Rd,f}$ Contribution of the FRP reinforcement to design shear resistance.
V_{Sd} Design shear force acting on the section.
$V_{Rd,m}$ Contribution of masonry to design shear resistance of masonry strengthened with FRP.
X_k Characteristic value of a general resistance or deformation property of an FRP reinforcement.
X_d Design value of a general resistance or deformation property of an FRP reinforcement.

Lower Roman Letters

b Base of the section.
b_f Width of the FRP reinforcement.
b_G Distance of the NSM bar from the edge of the concrete beam.
b_h Width of the homogenized system.

c Maximum value between the vertical and horizontal concrete cover of the internal steel reinforcement.
d Effective depth of the section.
d_a Nominal diameter of the anchoring fibers.
d_g Depth of the groove in NSM systems.
d_{min} Minimum cross-sectional dimension of the element.
f_{bm} Mean compressive strength of the masonry blocks.
f_{btm} Mean tensile strength of the masonry blocks.
f_{bRm} Mean residual tangential stress in NSM systems.
f_{bd} Design bond strength between FRP reinforcement and concrete (or masonry).
f_c (Cylindrical) compressive strength of concrete.
f_{ccd} Design strength of confined concrete.
f_{cd} Design compressive strength of concrete.
f_{cm} Mean compressive strength of concrete.
f_{ctm} Mean tensile strength of concrete.
f_f Strength of FRP reinforcement.
f_{fd} Design strength of FRP reinforcement.
f_{fdm} Mean debonding strength of FRP reinforcement (Mode 1).
f_{fdd} Mean debonding strength of FRP reinforcement (Mode 1).
$f_{fdd,2}$ Design debonding strength of FRP reinforcement (Mode 2).
$f_{fdd,anc}$ Design debonding strength of FRP reinforcement in the presence of anchors.
$f_{fdd,rid}$ Reduced design debonding strength of FRP reinforcement.
f_{fed} Effective design shear strength of FRP reinforcement.
f_{fib} Strength of the fibers.
f_{fk} Characteristic strength of FRP reinforcement.
f_{fak} Characteristic tensile strength of the anchoring fibers.
f_{fpd} Design debonding strength of FRP reinforcement in a tangential direction.
f_l Confinement pressure.
$f_{l,eff}$ Effective confinement pressure.
f_{mat} Strength of the matrix.
f_{mm} Mean compressive strength of masonry.
f^h_{mm} Mean compressive strength of masonry in the horizontal direction.
f_{mcd} Design compressive strength of masonry confined with FRP.
f_{md} Design compressive strength of masonry.
f^h_{md} Design compressive strength of masonry in the horizontal direction.
f_{mtm} Mean tensile strength of masonry.
f_{vk} Characteristic shear strength of masonry.
f_{v0m} Mean shear strength in the absence of compressive stress in the concrete below the anchoring plate.
f_{vm} Mean shear strength of masonry.
f_y Design yield strength of longitudinal steel reinforcement.
f_{yd} Design yield strength of longitudinal steel reinforcement.
f_{Rck} Characteristic compressive strength of the resin used for anchoring fibers.
f_{Rm} Mean compressive strength of the resin in NSM systems.
f_{Rtk} Characteristic tensile strength of the resin used for anchoring fibers.
f_1 Deflection value calculated for an uncracked section.
f_2 Deflection value calculated for a cracked section.
h Height of the section.
$h_{c,ef}$ Effective height of the effective tensile area of the concrete section.
h_e Minimum anchorage depth of the anchoring fiber stem.
h_w Height of the beam web.

k_b Geometric correction coefficient.
k_c Experimentally calibrated coefficient equal to 2.0.
k_{eff} Efficiency coefficient of the confinement action.
k_{FAN} Correction coefficient equal to 0.5.
k_{FR} Correction coefficient of the residual tangential stress.
k_{SL} Correction coefficient for the maximum displacement of the bond.
k_k Experimentally calibrated coefficient for the characteristic maximum normal stress in the presence of frayed connectors.
k_{id} Coefficient accounting for the concentration of tangential and normal stresses.
k_q Correction coefficient based on the loading condition.
k_{Gk} Characteristic value (5% fractile) of the calibrated dimensionless coefficient.
$k_{Gm,2}$ Mean value of the calibrated correction coefficient.
k_H Horizontal efficiency coefficient.
k_I Force intensification coefficient for debonding.
k_V Vertical efficiency coefficient.
k_α Efficiency coefficient related to the inclination (α) of the fibers relative to the longitudinal axis of the confined element.
$k_{\phi/\rho}$ Coefficient dependent on the distribution of tangential stresses.
k_{fl} Factor accounting for stress distribution prior to cracking.
l Length of the beam.
l_E Transfer length (distance between the cracked section and the section without slip).
ℓ_b Bonded length of the reinforcement.
ℓ_{ed} Optimal design anchorage length.
$\ell_{ed,min}$ Minimum optimal anchorage length.
ℓ_{em} Mean optimal anchorage length.
ℓ_{e1}, ℓ_{e2} Limiting bond lengths in NSM systems.
n Number of layers of bars composing the internal reinforcement in the tension zone.
n_A Number of FRP anchors in half of the beam.
$n_{A,eff}$ Number of effective FRP anchors in half of the beam.
n_b Number of bolts securing the anchoring plate to the substrate.
n_s Number of faces of the joint panel reinforced.
n_{str} Number of strips applied to the joint panel.
n_z Number of FRP anchors on the FRP strip up to the z-coordinate.
p_b Distance between layers of bars in the confinement of masonry columns.
p_F Perimeter of the NSM reinforcement.
p_f Spacing of FRP strips or wraps.
p_G Perimeter of the groove wetted by the resin in NSM systems.
p_t Mass of fabric per unit area.
r_c Radius of curvature at the corner of the reinforced section.
s Interface slip.
s_G Distance between two consecutive NSM bars.
$s_{r,max}$ Maximum distance between cracks.
s_{max} Maximum slip
s_y Vertical distance between layers of bars composing the internal reinforcement in the tension zone.
s_u Interface slip corresponding to complete debonding from the substrate.
t_a Nominal thickness of the adhesive.
t_c Thickness of the concrete layer contributing to the deformability of the interface.
t_f Thickness of the FRP reinforcement.
t_r Mean thickness of the leveling layer.
t_h Thickness of the homogenized system composed of the reinforcement and the leveling layer.

u_s Perimeter of internal steel reinforcements in contact with concrete.
u_f Perimeter of the external FRP reinforcement in contact with concrete.
w_g Width of the groove in NSM systems.
w_f Width of a single strip in the FRP reinforcement system.
x Distance from the neutral axis to the extreme compressed fiber of the cross-section.
z Distances related to the positioning of the anchoring fibers.

Greek Letters (Uppercase)

Γ_{Fk} Characteristic value of specific fracture energy
Γ_{Fd} Design value of specific fracture energy.
Γ_{Fm} Mean value of specific fracture energy.
Γ_{F1m} Mean value of the specific fracture energy for the rigid-softening branch of the NSM bond model.
Δ Distance.

Greek Letters (Lowercase)

α_s Homogenization coefficient for steel reinforcement.
α_f Homogenization coefficient for FRP reinforcement.
α_{fl} Angle of inclination of fibers.
β Angle of inclination of fibers relative to the longitudinal axis of the element.
β_i Angle of inclination of fibers used to reinforce RC joints.
β_1 Coefficient accounting for the duration of load application.
γ Tension-stiffening coefficient.
γ_m Partial factor for materials or products.
γ_{Rd} Partial factor for resistance models.
δ Deformations.
ε_o Strain in concrete at the tension edge before applying reinforcement.
ε_c Strain in concrete at the compression edge.
ε_{cm} Mean strain in the concrete between two consecutive cracks.
ε_{ccu} Ultimate design strain of confined concrete.
ε_{co} Strain in concrete at the compressed edge before reinforcement application.
ε_f Strain in FRP reinforcement.
ε_{fd} Maximum design strain in FRP reinforcement.
ε_{fdd} Maximum design strain in FRP due to end debonding (Mode 1).
$\varepsilon_{fdd,anc}$ Maximum design strain in FRP due to debonding in the presence of anchors.
$\varepsilon_{fd,rid}$ Reduced maximum design strain of FRP reinforcement in confined RC or masonry elements.
ε_{fmax} Limiting strain in FRP reinforcement.
ε_{fk} Characteristic strain at tensile failure of FRP reinforcement.
ε_{fu} Ultimate strain in FRP reinforcement.
$\varepsilon_{fdd,2}$ Maximum design strain in FRP due to intermediate debonding (Mode 2).
ε_{mcu} Ultimate compressive strain of confined masonry.
ε_{mu} Ultimate compressive strain of confined masonry.
ε_{s1} Strain in tensile steel reinforcement.
ε_{s2} Strain in compressive steel reinforcement.
ε_{sm} Mean strain in internal steel reinforcement between two consecutive cracks.
ε_{sy} Calculated strain in preexisting reinforcement at yielding.
ε_{yd} Design value of the yield strain in steel reinforcement.
φ Viscosity coefficient of concrete.
ϕ_s Diameter of internal steel reinforcement bars.
λ Half-opening angle of the fibers in anchoring bundles.

μ_R Friction coefficient.
ϑ Crack inclination angle.
η Conversion factor.
η_a Environmental conversion factor.
ν_{fib} Poisson's ratio of the fibers.
ν_{mat} Poisson's ratio of the matrix.
ψ Resultant of compressive stresses in concrete.
ψ_a Bending angle of the embedded portion of anchoring fibers.
ρ_{fib} Density of the fibers.
ρ_{mat} Density of the matrix.
$\rho_{s+FRP,ef}$ Effective reinforcement ratio.
σ_c Tensile stress in concrete.
σ_f Tensile stress in FRP reinforcement.
σ_N Normal stress produced by bolt tightening.
$\sigma_{nt,Rd}$ Design diagonal tensile strength of the reinforced node.
$\sigma_{nt,Rd,c}$ Diagonal tensile capacity of concrete.
$\sigma_{nt,Rd,f}$ Diagonal tensile capacity of the FRP reinforcement system.
σ_s Stress in steel reinforcement under tension.
σ_{Sd} Normal stress acting on masonry at the adhesive surface between FRP and masonry.
σ_{sw} Tensile stress in stirrups.
$\tau_{b,e}$ Equivalent tangential stress at the adhesive-concrete interface.
τ_{bms} Average bond stress at the interface between internal steel reinforcement and concrete.
$\tau_{Rb,k}$ Characteristic tangential debonding stress of resin.
ξ^2_1 Dimensionless coefficient.

2 MATERIALS

2.1 INTRODUCTION

As previously mentioned, this document addresses some specific structural applications of composite materials made from thermoset polymer matrices and continuous fibers of carbon, glass, aramid, or steel microfibers, commonly referred to as FRP, an acronym for Fiber Reinforced Polymers (more specifically CFRP in the case of carbon fibers, GFRP for glass fibers, AFRP for aramid fibers, and SFRP for steel wire or microfibers). In the following, the term 'fibers' is also used to refer to the microfibers of SFRP (Steel Fiber Reinforced Polymers). From a structural standpoint, FRP materials are heterogeneous and anisotropic, exhibiting a predominantly linear elastic behavior up to failure. In addition to their varied and well-established applications in the fields of aerospace, naval, and mechanical engineering, they are widely used in the rehabilitation and strengthening of civil structures, to which these guidelines are specifically dedicated. The advantages of FRPs are numerous: they are lightweight, have high mechanical properties, and have anti-corrosive characteristics.

Composites for structural reinforcement are available in various geometries, ranging from pultruded laminates, characterized by a unidirectional fiber arrangement and typically used for cladding regular surfaces, to bidirectional fabrics, which are easily adaptable to the shape of the reinforced structural element. FRPs are competitive in cases where it is necessary to limit the aesthetic impact on the original structure or ensure adequate reversibility of the intervention (such as buildings of historical or artistic interest) or when limited space availability would make traditional techniques challenging to apply.

Other types of composite materials are also on the market, differing in the nature of the matrix (inorganic matrix) or the fibers (discontinuous or continuous fibers made from different materials, such as basalt). These composites have proven to be particularly promising for specific applications. Some of them are addressed in other or future technical documents published by the CNR.

Chapter 2 is dedicated to the classification of reinforcement systems made with FRP, their qualification, certification, and acceptance on-site, and the operators' tasks and responsibilities.

The reader who wishes to deepen their knowledge of the technologies for producing fiber-reinforced composite materials, their mechanical properties, and the relevant strength criteria can refer, in addition to the numerous texts available in the literature, to Appendices A, B, and C of these guidelines.

2.2 CLASSIFICATION OF REINFORCEMENT SYSTEMS

(1) From a morphological point of view, reinforcement systems made with FRP materials are classified into:

- Preformed systems (precured systems) (§ 2.2.2), consisting of components of various shapes (laminates, strips, bars, or others) prepared in the factory by pultrusion or other production processes of proven technological validity and bonded to the structural element to be reinforced.
- In-situ impregnated systems (e.g., wet lay-up systems) (§ 2.2.3), consisting of sheets, fabrics, or fiber strands (uni- or multi-directional) impregnated with a resin that can also serve as an adhesive to the substrate (e.g., concrete, masonry);
- Prepreg systems (§ 2.2.4), consisting of sheets or fabrics of uni- or multi-directional fibers pre-impregnated with partially polymerized resin and bonded to the substrate to be reinforced with (or without) the use of additional resins.

Reinforcement systems made with SFRP materials fall into the category of in-situ impregnated systems. For SFRP systems, the microfibers must be produced in accordance with the UNI EN ISO

16120 Parts 1-4 standard and, concerning the mechanical and geometric properties, including the torsion angle of the steel wires, in accordance with the ISO 17832 standard. As corrosion protection, the microfibers must have a galvanized coating made according to the UNI EN 10244-2 or ASTM A475 standard with a minimum mass of 22g/kg (0.35 oz./lb.).

(2) From a mechanical point of view, within the scope of these guidelines, the systems mentioned above are classified based on the values of the elastic modulus and the tensile strength. These quantities, evaluated under uniaxial tension in the direction of the fibers, should be referred, in the case of preformed reinforcement systems, to the total surface unit of the FRP composite (fibers and matrix); in the case of in-situ systems, to the area of only the dry fibers or the microfibers of the composite. The values of the elastic modulus and tensile strength must be suitably stable in relation to degradation induced on the composite by environmental actions.

The classification above is consistent with that adopted in Italy in the "Guidelines for the identification, qualification, and acceptance control of polymer matrix fiber-reinforced composites (FRP) to be used for the structural strengthening of existing buildings," as referenced in section 2.3.

2.2.1 Mechanical Properties of Reinforcement Systems

(1) In fiber-reinforced composites, the fibers serve as load-bearing elements in terms of both strength and stiffness. The matrix protects the fibers and serves as a medium for transferring stresses between the fibers and the structural element being reinforced. In most cases, the composites consist of fibers characterized by high strength and stiffness, while the ultimate strain is lower than that of the matrix. Figure 2-1 qualitatively illustrates the constitutive bonds of a unidirectional fiber-reinforced material, including its constituent phases: the matrix and fibers. The composite has lower stiffness than the fibers and the same ultimate strain, $\varepsilon_{\text{fib,max}}$. Once the ultimate strain of the fibers is reached, no stress transfer between the matrix and the fibers is possible.

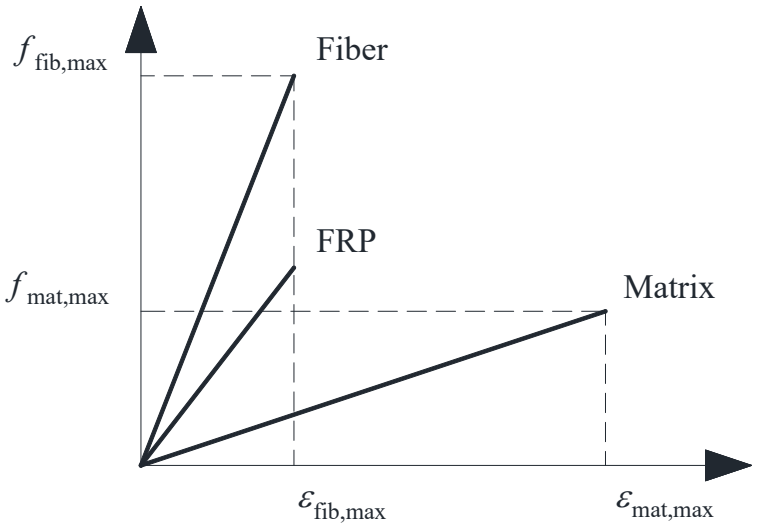

Figure 2-1 – Comparison of mechanical properties of a preformed system with those of the corresponding fibers.

For illustrative purposes, Table 2-1 compares the average values of some mechanical properties of a unidirectional preformed system with those of the corresponding fibers. The values of the axial elastic modulus and tensile strength of the composite in the direction of the fibers are lower than those of the fibers. In contrast, the values of the ultimate tensile strains for both fibers and composite are comparable.

Table 2-1 – Comparison of mechanical properties of a preformed system with those of the corresponding fibers.

Preformed Systems	**Normal Elastic Modulus [GPa]**		**Tensile Strength [MPa]**		**Ultimate Strain [%]**	
	FRP E_f	Fibre E_{fib}	FRP f_f	Fibre f_{fib}	FRP ε_{fu}	Fibre $\varepsilon_{fib,u}$
CFRP (high strength)	160	210-230	2800	3500-4800	1.6	1.4-2.0
CFRP (high modulus)	300	350-500	1500	2500-3100	0.5	0.4-0.9

(2) In the case of unidirectional composites, it is possible, with reasonable approximation, to estimate their mechanical behavior using micromechanical models; for example, by applying the rule of mixtures (eq. (9.5) in Appendix C):

$$E_f = V_{fib} \cdot E_{fib} + (1 - V_{fib}) \cdot E_{mat} \tag{2.1}$$

$$f_f \cong V_{fib} \cdot E_{fib} + (1 - V_{fib}) \cdot f_{mat} \tag{2.2}$$

where, in addition to the quantities already introduced in Table 2-1, V_{fib} is the volume fraction of the fibers (the ratio between the volume of the fibers and the total volume of the composite), E_{mat} and f_{mat} are the longitudinal elastic modulus and tensile strength of the matrix, respectively..
It is worth noting that the rule of mixtures, based on the assumption of perfect bonding between fibers and matrix, provides a reasonably accurate estimate of the longitudinal elastic modulus but is less reliable for strength.
The possible high values of the ratio between the reinforcement volume and the resin volume that may occur for SFRP materials suggest caution when using the rule of mixtures for these materials.

(3) For the evaluation of the elastic modulus and strength in a specific direction of an in-situ impregnated composite, it is customary to refer to the area of the cross-section of the dry fabric arranged in the given direction.
Referring to the net area of the fibers is justified by the difficulty in quantifying the volume fractions of the phases due to uncertainty about the actual amount of resin applied manually.
For example, consider a unidirectional fabric strip of 100 mm width (fiber area: A_{fib} = 70 mm^2), saturated with different amounts of resin The properties of the individual components are listed in Table 2-2. The influence of the resin content on the mechanical properties in the fiber direction is estimated using eqs. (2.1) and (2.2), is shown in Table 2-3 and Figure 2-2.

Table 2-2 – Properties of the components.

Fibers	Matrix
E_{fib} = 220 GPa	E_{mat} = 3 GPa
f_{fib} = 4000 MPa	f_{mat} = 80 N MPa

Table 2-3 – Influence of the volume fraction V_{fib} on the mechanical properties of a composite.

A_{fib} [mm^2]	A_{mat} [mm^2]	A_f [mm^2]	V_{fib} [%]	E_f [GPa]	f_f [MPa]	ε_{fu} [%]	F_{fu} [kN]	$E_f \cdot A_f$ [kN]
70	0	70	100	220.0	4000	1.81	280.0	15400
70	30	100	70	154.9	2824	1.82	282.4	15490
70	70	140	50	111.5	2040	1.83	285.6	15610

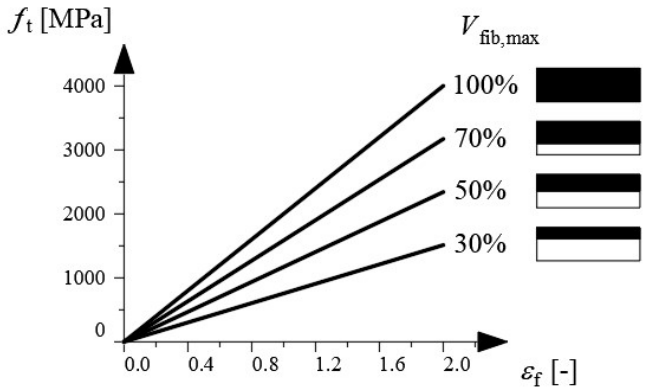

Figure 2-2 – Dependence of the constitutive bond of the composite on the volume fraction.

In Table 2-3 and Figure 2-2 considers values of V_{fib} between 30% and 70%. As a limiting case, the value of 100% for the fiber volume fraction is also considered.
Table 2-3 shows that the volume fraction V_{fib} significantly influences the mechanical properties of the composite (E_f and f_f).
This does not happen for the values of the ultimate axial force, $F_{fu} = f_f \cdot A_f$, and the axial stiffness, $E_f \cdot A_f$, of the composite strip, to which it is, therefore, preferable to refer.
Indeed, these quantities exhibit negligible variations (3-4%), as any reductions in the values of the factors Ef and ff are compensated by the increase in the other factor, namely, the total cross-sectional area of the saturated fabric, A_f.

2.2.2 Preformed Systems

(1) The mechanical properties of preformed composites, f_f and E_f, are evaluated through the following relations:

$$f_f = \frac{F_{fu}}{A_f} \tag{2.3}$$

$$E_f = \frac{F_{fu}}{A_f \cdot \varepsilon_{fu}} \tag{2.4}$$

where F_{fu} and ε_{fu}, respectively, represent the force and the ultimate deformation, determined experimentally, and A_f is the area of the cross-section of the preformed composite.

(2) Preformed composites are generally characterized by a unidirectional fiber arrangement, which allows, as a first approximation, the use of the rule of mixtures to determine the mechanical characteristics of stiffness and strength of the composite.

The approximation essentially arises from the fact that these values do not account for the influence of other parameters, such as the adhesion between fibers and matrix, production defects, the presence of voids, and/or imperfections in the distribution or alignment of the fibers. A more realistic assessment requires conducting a sufficient number of experimental tests to provide statistically significant results, taking into account the quality level of the manufacturing technique used.

(3) The volume fractions of the fibers typically range from 50% to 70%.

(4) Preformed systems, such as FRP bars or laminates, can be used as external reinforcement by applying them directly to the surface or in grooves on the surface of the elements to be reinforced, utilizing the NSM (Near Surface Mounted) reinforcement technique.

2.2.3 In-Situ Impregnated Systems

(1) In the case of manual impregnation, it is recommended to limit the amount of fabric present in the individual reinforcement layer so that the grammage does not exceed the value of 600 g/m². For higher grammages, it is advisable to check the completeness of the impregnation. In these cases, the use of mechanical application systems is recommended.

(2) The use of more than 5 fabric layers is discouraged.

2.2.3.1 Determination of A_{fib}

(1) The technical data sheet of the fabric used must be consulted to determine the resistant area, A_{fib}.
It must be referenced to each of its main directions and is generally expressed in mm² using the following relation:

$$A_{fib} = \frac{T_x \cdot N_f}{10^4 \cdot \rho_{fib}} \cdot b_f \tag{2.5}$$

were T_x is the yarn title, expressed in [g/km], N_f is the number of filaments per unit width [n°/cm], ρ_{fib} is the density of the fibers [g/cm^3], and b_f is the width of the fabric strip [mm].

Alternatively, in the case of fabrics (balanced grammage fabrics) that have the same number of fibers in the warp (longitudinal direction) and weft (horizontal direction), with p_t being the mass of the fabric per unit area (grammage), expressed in g/m², the resistant area – in each of the two directions – can be obtained using the relation:

$$A_{fib} = \frac{p_t}{2 \cdot \rho_{fib}} \cdot \frac{b_f}{10^3} \tag{2.6}$$

For a unidirectional fabric, the relation (2.6) simplifies to:

$$A_{\text{fib}} = \frac{p_{\text{t}}}{\rho_{\text{fib}}} \cdot \frac{b_{\text{f}}}{10^3} \tag{2.7}$$

Sometimes, for practical purposes and limited to unidirectional or balanced fabrics, the resistant area of the fabric is referred to as the thickness of an equivalent sheet made of only fiber material. The thickness of this sheet is assumed to be:

$$t_{\text{f}} = \frac{A_{\text{fib}}}{b_{\text{f}}} \tag{2.8}$$

As an example, the calculation of the resistant area of three carbon fiber-based fabric strips, all with a width of 10 cm, is shown: a plain weave unbalanced fabric (Fabric A); a plain weave but balanced fabric (Fabric B); and finally, a unidirectional fabric (Fabric C). The characteristics of these fabrics are summarized in Table 2-4.

Table 2-4 – Comparison between resistant areas of three carbon fiber-based strips.

Property		**Unit**	**Fabric A**	**Fabric B**	**Fabric C**
Grammage		g/m^2	187	240	304
Fiber Density		g/cm^3	1.76	1.76	1.8
N° di wires/cm	weft	n°/cm	4	6	--
	warp	n°/cm	8	6	3.8
Title	weft	tex	67	200	--
	warp	tex	200	200	800

In the case of the unbalanced fabric (Fabric A), applying relation (2.5), we get:

$A_{fib}^{welf} = \frac{67[tex]\cdot 4\left[\frac{wires}{cm}\right]}{10^4 \cdot 1.76\left[\frac{g}{cm^3}\right]} \cdot 100[mm] = 1.52mm^2$ (resistant area in the weft direction)

$A_{fib}^{warp} = \frac{200[tex]\cdot 8\left[\frac{wires}{cm}\right]}{10^4 \cdot 1.76\left[\frac{g}{cm^3}\right]} \cdot 100[mm] = 9.09mm^2$ (resistant area in the warp direction)

In the case of Fabric B, for both directions, we obtain:

$$A_{\text{fib}} = \frac{200\ [\text{Tex}]\cdot 6\ [\text{wires/cm}]}{10^4 \cdot 1.76\ [\text{g/cm}^3]} \cdot 100\ [\text{mm}] = 6.82\ \text{mm}^2$$

$$t_{\text{f}} = \frac{6.82[\text{mm}^2]}{100[\text{mm}]} = 0.068\ \text{mm}\ .$$

Using relation (2.6), for Fabric B, it can be verified that the same result is achieved.:

$$A_{\text{fib}} = \frac{240[\text{g/m}^2]}{2\cdot 10^3 \cdot 1.76\ [\text{g/cm}^3]}\ \cdot 100\ [\text{mm}] = 6.82\ \text{mm}^2\ .$$

Finally, for the unidirectional fabric (Fabric C), applying equations (2.7) and (2.8), we get:

$$A_{\text{fib}} = \frac{304[\text{g/m}^2]}{10^3 \cdot 1.80[\text{g/cm}^3]} \cdot 100\ [\text{mm}] = 16.89\ \text{mm}^2$$

$$t_{\text{f}} = \frac{16.89[\text{mm}^2]}{100[\text{mm}]} = 0.17\ \text{mm}\ .$$

(2) In the case of SFRP systems, the resistant area of the steel fibers, A_{fib}, expressed in mm², is equal to the product of the resistant area of the individual strand, A_{t}, and the number of strands N_{t} present in the width b_f of the steel fabric:

$$A_{fib} = N_t \cdot A_t \tag{2.9}$$

Equation (2.8) can still be applied to evaluate the thickness of the equivalent sheet.

2.2.3.2 Mechanical Properties of In-Situ Impregnated Systems

(1) Within the scope of these guidelines, it is agreed to treat the in-situ impregnated system as an equivalent composite made only of dry fabric ($A_f = A_{fib}$).
The mechanical properties of the impregnated composite, f_{f} and E_{f}, must be evaluated through the following relations:

$$f_{\text{f}} = F_{\text{fu}}/A_{\text{fib}} \tag{2.10}$$

$$E_{\text{f}} = F_{\text{fu}}/(A_{\text{fib}} \cdot \varepsilon_{\text{fu}}) \tag{2.11}$$

For practical applications, when required later, the thickness of the in-situ impregnated composite, t_f, must be evaluated according to Equation (2.8).

2.2.3.3 Comparison Between the Characteristics of a Preformed Laminate and an In-Situ Impregnated Fabric

The following illustrative considerations may be helpful for design purposes when comparing the mechanical properties of preformed composites with those of in-situ impregnated systems. Consider two types of reinforcement: System 1, which consists of a unidirectional carbon fiber fabric impregnated in situ; and System 2, which consists of a pultruded preformed composite. Assume that both reinforcement systems are applied using an epoxy adhesive.
Table 2-5 shows the mechanical properties of the materials taken from their respective technical data sheets.

Table 2-5 – Material properties of two CFRP systems.

System 1	System 2
Type: Unidirectional CFRP fabric and epoxy resin Installation: Wet lay-up technique	Type: Pultruded laminate CFRP and epoxy resin Installation: Bonding method
Mechanical Properties * $t_f = 0.45\ mm$	Mechanical Properties ** $t_f = 1.2\ mm$

f_f = 4200 MPa	f_f = 2800 MPa
ε_f = 1.8%	ε_f = 1.7%
E_f = 235000 MPa	E_f = 165000 MPa

* Properties of the composite refer to the area of dry fibers (or fibers) (eq. (2.9) and (2.10))

** Properties of the composite referred to the total area of the pultruded laminate (eq. (2.3) and (2.4)).

The procedure summarized in **Table 2-6** is recommended for performing the comparison.

Table 2-6 – Comparison between the two FRP systems in Table 2-5.

System 1	**System 2**
Type: Unidirectional CFRP fabric and epoxy resin Installation: Wet lay-up technique	Type: Pultruded laminate CFRP and epoxy resin Installation: Bonding method
1) Calculation of tensile strength per unit width $f_t \cdot t_f = 1890\,{}^{N}/_{mm}$	1) Calculation of tensile strength per unit width $f_t \cdot t_f = 3360\,{}^{N}/_{mm}$
2) Calculation of elastic modulus per unit width $E_f \cdot t_f = 105{,}750\,{}^{N}/_{mm}$	2) Calculation of elastic modulus per unit width $E_f \cdot t_f = 198{,}000\,{}^{N}/_{mm}$

3a) Comparison between the two systems for tensile strength

$$\frac{f_f^{(2)} \cdot t_f^{(2)}}{f_f^{(1)} \cdot t_f^{(1)}} = 1.77$$

3b) Comparison between the two systems for elastic modulus

$$\frac{E_f^{(2)} \cdot t_f^{(2)}}{E_f^{(1)} \cdot t_f^{(1)}} = 1.87$$

Therefore, two layers of unidirectional fabric (System 1) are necessary to achieve tensile strength and stiffness equivalent to those of the pultruded laminate (System 2).

2.2.4 Prepreg Systems

(1) Prepreg composites are impregnated directly in manufacturing facilities, and after possible pre-polymerization of the resin, they are wound into rolls. The prepreg is a thin sheet, typically about 0.15 mm thick, flexible, and moderately sticky, wrapped between two release films (such as silicone paper). The prepreg must be stored under controlled humidity and temperature conditions, and its curing must occur at the time of application using an appropriate thermal treatment.

2.3 MATERIAL CONTROL

2.3.1 Material Qualification

Current Italian regulations require the qualification of materials and construction products for structural use, specifying three cases:

A) Products falling within the scope of a harmonized standard (hEN): In this case, the CE marking of the product is mandatory, as required by EU Regulation 2024/3110, which came into force on January 7, 2025, and will soon replace EU Regulation 305/2011. CE marking represents the only acceptable method of qualification.
B) Products that do not fall under the scope of a hEN but whose qualification is explicitly regulated in technical standards.
C) Products that fall under neither Case A nor Case B. For these products, qualification is alternatively achieved through:

- CE marking based on a specific European Technical Assessment (ETA), which is prepared in accordance with a specific European Assessment Document (EAD);
- A Technical Evaluation Certificate (CVT) issued by the President of the Higher Council of Public Works, following review by the Central Technical Service, based on specific qualification guidelines established by the Higher Council of Public Works.

As mentioned in point A, CE marking for construction products is regulated by EU Regulation 305/2011 / 2024/3110 (CPR, Construction Products Regulation), which establishes harmonized procedures for placing construction products on the market within the European Union (EU).

These harmonized conditions are expressed through what are known as harmonized technical specifications (hTS). The basis for CE marking of construction products consists of:

1. Harmonized Standards (hEN): These are European standards developed by an organization accredited by the EU for standardization, such as the European Committee for Standardization (CEN), the European Committee for Electrotechnical Standardization (CENELEC), or the European Telecommunications Standards Institute (ETSI), with the contribution of all national standardization bodies (for Italy, this is UNI – Ente Italiano di Normazione). A harmonized standard is created in response to a mandate from the European Commission, issued to one of these organizations, chosen based on the product type.
   → CE marking based on harmonized standards constitutes "mandatory certification."
2. European Assessment Documents (EADs): These are harmonized technical specifications developed for construction products not yet covered by a harmonized standard, as per CPR, Articles 19 and 31. They are prepared by Technical Assessment Bodies (TABs) and adopted by the European Organization for Technical Assessment (EOTA).
   → EADs serve as the basis for issuing a European Technical Assessment (ETA).
   → CE marking based on an ETA is voluntary.

Before a construction product can receive CE marking, it must be characterized through experimental, analytical, and/or numerical methods. Once characterized, the ongoing production process must allow for the control, assessment, and verification of the product’s performance consistency.

Only after this process can the manufacturer issue the Declaration of Performance and Conformity (DoPC), which will soon replace the current Declaration of Performance (DoP), and affix the CE marking to the product.

The methods used for product characterization are always specified within the harmonized technical specifications (either harmonized standards or EADs), along with the criteria for performance assessment and verification (PAV), or, soon, the Assessment and Verification System (AVS), which will replace the PAV.

It is important to note that CE marking for construction products does not provide information on the product's safety, is not a quality mark, and does not imply suitability for use. Each Member State of the EU regulates the latter through national standards that define the conditions of use of the product in works.

Ultimately, CE marking for a construction product confirms that the accompanying information—summarized in the Declaration of Performance and Conformity (DoPC)—has been established in accordance with EU Regulation 305/2011 / 2024/3110 and must therefore be considered accurate and reliable. The manufacturer issues the Declaration of Performance (DoP) when placing the product on the market, assuming full responsibility for the product's compliance with the declared characteristics.

However, it is worth noting that although CE marking is generally not mandatory for materials and products not covered by harmonized standards, the situation changes when it comes to construction safety at the national level. As stated at the beginning of the section, Italian law requires that, for the qualification of construction products for structural use, the manufacturer must comply by marking the product with the CE mark based on a relevant European Technical Assessment (ETA). In Italy, voluntary certification thus becomes mandatory for structural materials and products (as stated in point C). Alternatively, if not CE marked, the structural material/product " must obtain a 'Technical Evaluation Certificate' issued by the President of the Higher Council of Public Works, after review by the Central Technical Service, also based on Guidelines for Qualification issued by the Higher Council of Public Works, where available."

The Technical Evaluation Certificate (TEC) can be defined as a national version of the ETA. It does not represent suitability for use and, to align with European rules that replaced European Technical Approvals (ETAs) with European Technical Assessments, it replaces what was previously known as the Technical Suitability Certificate (TSC).

It should be noted that some currently valid Guidelines for issuing TECs may still include, in addition to the methods for evaluation/qualification of the product, the minimum requirements ("thresholds") necessary for the product's use (authorization for use), as well as procedures for acceptance on-site. In the specific case of composite materials for structural reinforcement, the current "Guideline for the identification, qualification, and acceptance control of fiber-reinforced polymer composites (FRP) to be used for the structural strengthening of existing buildings," issued by the Higher Council of Public Works in May 2019, defines, for example, criteria for durability, based on thresholds of percentage reduction in tensile strength and elastic modulus measured after environmental conditioning compared to unconditioned samples. However, this aspect has been superseded by the "Guideline for the identification, qualification, and acceptance of FRP bars and stirrups for structural use," issued by the Higher Council of Public Works in December 2021. In this guideline, the percentage reduction in tensile strength and modulus values of samples subjected to cycles must still be reported in the laboratory test report. Still, they no longer need to meet specific acceptance criteria.

Currently, there are no harmonized standards (hEN) for composite materials used for structural reinforcement. However, various European Assessment Documents (EADs) are available for the qualification of these products, based on which CE marking can be obtained by preparing relevant European Technical Assessments (ETAs). EADs are available at the EOTA website, eota.eu/eads, and those related to the technical documents issued by the CNR can be found on the CNR website at https://www.cnr.it/it/norme-tecniche-costruzioni.

Additionally, the "Guideline for the Identification, Qualification, and Acceptance Control of Fiber-Reinforced Polymer Composites (FRP) to be Used for Structural Strengthening of Existing Buildings," issued by the Higher Council of Public Works in May 2019, is also helpful in preparing Technical Evaluation Certificates.

This guideline is also used to classify reinforcement systems.

For FRP bars used as NSM reinforcement systems or as confinement systems for reinforced concrete or masonry elements, applications for which this document provides design indications, a helpful reference may be the "Guideline for the identification, qualification, and acceptance of FRP bars and stirrups for structural use," issued by the Higher Council of Public Works in December 2021.

2.3.2 Responsibilities of Operators

This section outlines the duties and responsibilities of the professionals involved in the design, installation, and inspection of structural strengthening interventions. As further specified in the Guidelines issued by the Consiglio Superiore dei Lavori Pubblici (Higher Council of Public Works), the term Manufacturer is understood - pursuant to EU Regulation No. 305/2011 / 2024/3110 (Art. 2, point 193, letter 10) - to mean: “Any natural or legal person who manufactures a construction product or has such a product designed or manufactured and markets it under their name or trademark.”

Designer:

- In the design, the required mechanical properties for the reinforcement system must be clearly specified, and the classification outlined in Section 2.3.1 of the Guideline must be referenced.
- Depending on the importance and extent of the application, the project manager may suggest quality tests of the installation, specifically those related to detachment from the substrate, as outlined in Chapter 6.

Contracting Companies and Applicators:

- Must have specific and proven skills in the application of composite materials/systems on concrete and masonry structures, documented through prior experience. In particular, personnel assigned to installation must have specific and proven skills in applying FRP reinforcement systems for structural purposes.
- Must ensure that the products/systems conform to the specifications indicated by the Designer.

Project Manager:

- Plays a decisive role in accepting products.
- Must verify, at the time of delivery, the conformity of the supplied material with the Designer’s specifications.
- Must verify the origin of the supplied material.
- Must verify the mechanical and physical characteristics of the products by reviewing the Declaration of Performance and Conformity (DoPC), as defined by Regulation (EU) 2024/3110 (which will soon replace the DoP required by Regulation (EU) 305/2011), in the case of CE-marked products, or by referring to equivalent certifications in other cases.
- Depending on the importance and extent of the application, particularly in the case of products without CE marking, experimental tests may be requested to assess the material quality and verify

that the results correspond to the values provided by the Manufacturer. These tests must be conducted in laboratories with proven experience in the mechanical characterization of FRPs and equipped with suitable equipment for this purpose.
- Again, depending on the importance and extent of the application, specific tests may be requested to verify resistance to detachment from the substrate in comparison to the design forecasts.

Third-Party Inspector:

In the case where testing is required, the Third-Party Inspector must:

- verify the quality of the materials used by reviewing the Declaration of Performance and Conformity in accordance with Regulation (EU) 2024/3110 (DoPC, which will soon replace the DoP required by Regulation (EU) 305/2011) in the case of CE-marked products, or by relying on the accompanying supply certificates.
- Verify the project manager's acceptance of the materials.
- Verify the results of any experimental acceptance tests requested by the Project Manager and, if necessary, perform additional tests.

2.4 TRANSPORT, STORAGE, CONSERVATION, HANDLING, AND USE

The methods of transport, storage, conservation, handling, and use of materials that constitute reinforcement systems are essential for ensuring the preservation of both their physical and chemical properties and compliance with safety standards.

- **Transport:** The components of the reinforcement system must be adequately packaged and transported in compliance with any relevant regulations in force.
- **Storage:** Composite materials must be stored in accordance with the Manufacturer's recommendations to preserve the properties of the materials constituting the reinforcement system and ensure compliance with safety standards. In particular, to preserve the properties of fibers and resins, they should be stored under appropriate temperature conditions (recommended range: 10°-24°C) and in a sufficiently dry environment (humidity below 20%), unless otherwise specified by the Manufacturer. Laminates and other preformed elements can be damaged due to bending or improper stacking. Storage of specific components, such as reactive curing agents, initiators, catalysts, and solvents for cleaning surfaces, requires special precautions that must comply with the Manufacturer's instructions and any relevant regulations in force. Specifically, catalysts and initiators (usually peroxides) must be stored separately from other reagents to prevent accidental contact and the subsequent initiation of the curing reaction.
- **Conservation:** The properties of uncured resins may change over time, particularly when exposed to varying humidity and temperature conditions. These can also influence the reactivity of the mixture and the properties of the cured resin. The Manufacturer must specify the storage time (pot life) during which the properties of thermoset resin-based materials remain unchanged. Conservation, for a period not exceeding the pot life (usually between 1 and 2 years), can be carried out in cool, dry places in the original sealed packaging. The Manufacturer's instructions should always be followed. Once the package is opened, products must be used as soon as possible and always kept in the original, well-sealed container. After the original package is opened, it is crucial to avoid contamination by moisture, which can significantly compromise the product's reactivity. Additionally, it is essential to keep the product out of direct sunlight to prevent overheating. Any component that has exceeded its pot life or has been degraded or contaminated must not be used. All components deemed unusable must

be discarded in accordance with the manufacturer's instructions and in compliance with environmental protection regulations.

- **Handling:** The Manufacturer must provide the relevant technical data sheets for products placed on the market, including safety information (MSDS – Materials Safety Data Sheet).
- **Use:** It is noted that substances used in combination with thermosetting resins are typically curing agents, crosslinkers, initiators (peroxides), isocyanates, and fillers. Potential hazards associated with their use include:
    - Skin irritation and sensitization;
    - Inhalation of solvent vapors, thinners, and monomers;
    - Fire or explosion risks due to high concentrations of flammable substances in the air or contact with flames or sparks (including cigarettes);
    - Exothermic reactions between reagents, which can cause fires or accidents to people;
    - Presence of dust resulting from the handling or processing of fiber-reinforced composites.

Appropriate precautions should be taken when working with these products. The potential risks associated with their use require all operators to read labels and MSDSs carefully to avoid unpleasant accidents.
It is recommended to use disposable gloves, work clothing, or overalls to handle fibers and resins. Gloves made of rubber or plastic should be solvent-resistant. Additionally, when working with solvents or resin components, it is essential to wear protective goggles. Finally, as required by the manufacturers, respiratory protection should be used when handling fiber fragments, dust, or solvent vapors or while mixing and spreading resins. The work area must always be adequately ventilated.

3 FUNDAMENTAL CONCEPTS OF THE REINFORCEMENT DESIGN AND SPECIAL ISSUES

This Chapter addresses the fundamental concepts of the reinforcement design with FRP for existing structures, both concrete and masonry, when the requirements and safety checks prescribed by the current regulations are not met.
The same concepts apply to existing metal and wooden structures, which are not included in this document.

(1) It is assumed that:

- Qualified and experienced technicians carry out the selection and design of the reinforcement system;
- Workers carry out the subsequent execution of the intervention with an adequate level of capability and experience;
- Adequate supervision and quality control are ensured during the execution of the intervention;
- The construction materials and products used are identifiable, qualified, controlled, and accepted on-site.

(2) The design of the reinforcement system must meet the requirements for performance, durability, and resistance to collapse. In the event of a fire, the reinforcement's resistance must be adequate for the intended exposure time.

(3) The reinforcement system must be placed in areas where resistance to tensile stresses is required. The composite material should not be subjected to compressive stresses unless it involves well-confined elements (embedded in the reinforced components) or a pultruded composite that has adequate axial and flexural stiffness.

3.1 FUNDAMENTAL REQUIREMENTS

(1) The fundamental requirements for the reinforcement system design are:

- Identification, elimination, or reduction of risks to which the structure could be subjected;
- Selection of a reinforcement system configuration that is less sensitive to these risks and capable of withstanding localized damage if necessary;
- Elimination or postponement of existing brittle collapse phenomena before the reinforcement.

(2) The fundamental requirements outlined above can be considered satisfied if the following conditions are met:

- The selection of materials is in accordance with the guidelines provided in Chapter 2;
- The design, execution, and control of the intervention are in accordance with the instructions outlined in this Chapter and subsequent chapters.

(3) When the structural reinforcement concerns buildings of historical and monumental interest, a critical evaluation of the intervention is required with respect to the principles of conservation and restoration, in accordance with the Directive of the President of the Council of Ministers of 12/10/2007 (Official Gazette no. 24 of 29/01/2008 - Ordinary Supplement no. 24).

In particular, the actual effectiveness of the intervention must be demonstrated, along with its durability and reversibility, as well as the compatibility (physical-chemical and mechanical) of the reinforcement materials with those of the reinforced structures.

3.2 DURABILITY REQUIREMENTS

(1) The design of the reinforcement system must ensure the durability of the proposed intervention throughout the service life of the reinforced structure, even in relation to the expected degradation.

(2) To ensure the durability of the reinforcement intervention, the following factors must be duly considered:

- The intended use of the reinforced structure;
- The expected environmental conditions and load application methods;
- The composition, properties, and performance of the existing materials and FRPs, as well as the products used for the installation of the latter;
- The choice of reinforcement configuration, application methods, and construction details;
- The quality of the workers and the level of control;
- The adoption of specific protective measures, for example, against high temperatures and humidity;
- The expected maintenance during the service life.

(3) Special project issues (such as environmental actions and the applied loads) must be identified in the design phase so that their importance concerning the durability of the reinforcement can be assessed. Appropriate values for the conversion factors (§ 3.5) must be adopted, and suitable precautions for protecting the materials used must be planned.

(4) When reliable values for the conversion factors are not available for the specific issue under examination, the level of any degradation affecting the reinforcement must be accurately estimated. The estimation can be carried out based on theoretical models, experimental investigations, or experiences gained from previous interventions.

3.3 GENERAL PRINCIPLES OF REINFORCEMENT DESIGN

3.3.1 General Information

(1) The checks for the reinforced elements must be carried out in relation to the Ultimate Limit States (ULS) and, where required, the Serviceability Limit States (SLS). The limit states are defined in the current regulations.

(2) For each limit state, the following must be true:

$$E_d \leq R_d \tag{3.1}$$

where E_d and R_d represent, respectively, the design (or calculated) values of the general demand (design force, stress, or deformation) being considered and the corresponding capacity (in terms of strength or deformation).

(3) The calculation values are derived from the characteristic values using appropriate partial factors, whose values for the various limit states are codified in the current regulations. In the absence of specific regulatory indications for this particular field, these instructions suggest possible values for the partial factors.

3.3.2 Service Life and Calculation of Actions

(1) It is assumed that the service life of a reinforced structure is the same as that of a newly constructed one. Consequently, the partial factors to be used for the calculation of actions are the same as those prescribed by the current regulations for new constructions.

3.3.3 Material Properties and Corresponding Calculation Values

(1) The values of the material properties or products used to create the reinforcement system must be determined in accordance with the guidelines provided in Chapter 2.

(2) The values of the properties of the existing materials in the structure to be reinforced must be derived from the results of standardized tests conducted either in situ or in the laboratory, and, if available, from the original project documents or subsequent acquired documentation. These values should be considered as average values.

(3) The values to be used to quantify the strength and ultimate deformation of the FRP materials are the characteristic values (5% fractile). In accordance with the current regulations, the values to be used to quantify similar properties for the existing materials are the average values.

(4) The values assigned to the elastic moduli of the FRP materials and the existing materials are the average values.

(5) The design value, X_d, of a general strength or deformation property of an FRP material is expressed through a relation of the form:

$$X_{\mathrm{d}} = \eta \cdot \frac{X_{\mathrm{k}}}{\gamma_{\mathrm{f}}} \tag{3.2}$$

Where η, the conversion factor, accounts for special design issues (§ 3.5), X_k is the characteristic value of the property in question (§ 3.4) that accounts for all uncertainties related to the material.
In cases where both environmental factors and long-term load effects (Serviceability Limit States) need to be considered, the conversion factor η is obtained as the product of the environmental conversion factor (§ 3.5.1), η_a, and the long-term load effect conversion factor (§3.5.2), η_l.
In cases where only environmental factors need to be considered (Ultimate Limit States), the conversion factor η coincides with the environmental factor η_l (§ 3.5.1).

(6) The design value, X_d, of a general property of an existing material is obtained from the ratio between the average value, X_m, of that property (obtained based on what is stated in point 2) and an appropriate reduction factor corresponding to the level of knowledge required for the element being reinforced, which in Italian regulations is denoted by the symbol FC. This ratio may be further divided by the material partial factor where prescribed by the current regulations.

3.3.4 Design Capacity

(1) The general design capacity, R_d, can be expressed through a relation of the form:

$$R_{\mathrm{d}} = \frac{1}{\gamma_{\mathrm{Rd}}} \cdot R\left\{X_{\mathrm{d,i}}; a_{\mathrm{d,i}}\right\} \tag{3.3}$$

In equation (3.3), the symbol $R\{\cdot\}$ represents an appropriate function related to the specific mechanical model considered (for example, bending, shear, anchorage), and γ_{Rd} is a partial factor that accounts for the uncertainties inherent in the mentioned model. The terms of the function $R\{\cdot\}$ are the design values, $X_{d,i}$, of the FRP materials and existing materials, as well as the nominal values, $\alpha_{d,i}$, of the geometric parameters involved in the model.

(2) As a rule, the increase in the calculation capacity of the FRP-reinforced element cannot exceed 60% of that of the non-reinforced element. This limitation does not apply to exceptional and seismic actions.

3.4 PARTIAL FACTORS

3.4.1 Partial Factors γ_f for FRP Materials

(1) For the various limit states, the partial factor γ_f d for FRP materials can be assigned the reference values shown in Table 3-1. These values are applicable to preformed laminates and in-situ impregnated fabrics externally applied using resin (EBR technique), as well as to preformed laminates applied in resin-filled grooves as external reinforcement (NSM technique), depending on the ultimate limit state (ULS) being checked. For FRP bars applied in resin-filled grooves as external reinforcement (NSM technique) or used for confining masonry columns, the partial factor γ_f for the ULS of tensile failure must be evaluated based on what is indicated in CNR DT 203 guidelines and subsequent modifications.

Table 3-1 – Partial factors γ_f.

Limit State		
SLE	γ_{f0}	1.00
SLU: Tensile failure of FRP laminates	γ_{f1}	1.25
SLU: Tensile failure of in-situ impregnated fabrics	γ_{f1}	1.30
SLU: Detachment from the substrate for EBR systems	γ_{f2}	1.30
SLU: Detachment from the substrate for EBR systems with cord anchors	γ_{f2}	1.30
SLU: Detachment from the substrate for NSM systems:	γ_{f3}	
NSM with rough, deformed, or spirally wrapped surfaces		1.30
NSM with smooth laminates and bars or with resin-sand finished surfaces		1.70

3.4.2 Partial Factors γ_{Rd} for Resistance Models

(1) The recommended values for the partial factors, γ_{Rd}, for the different resistance models with respect to the Ultimate Limit States are shown in Table 3-2.

Table 3-2 – Partial factors γ_{Rd}.

Resistance Model	γ_{Rd}
Flexure/Combined Axial and Flexure	1.00
Shear/torsion	1.20
Confinement	1.10

3.5 SPECIAL DESIGN ISSUES AND CORRESPONDING CONVERSION FACTORS

Below are some reference values to be assigned to the conversion factors η (§ 3.3.3(5)) in relation to aspects that can influence the durability and behavior of FRPs in specific conditions.

3.5.1 Environmental Actions and Environmental Conversion Factor

(1) The mechanical properties (e.g., tensile strength, ultimate deformation, and longitudinal elastic modulus) of some FRP materials may degrade in certain conditions such as alkaline environments, high humidity (water and saline solutions), extreme temperatures, thermal cycles, freeze-thaw cycles, and ultraviolet (UV) radiation.

(2) Effects of the alkaline environment: The alkaline aqueous solution in the pores of concrete may, in some cases, cause degradation of the resin and/or the interface zones. Epoxy resins generally exhibit excellent resistance to alkaline environments, unlike polyester resins, which are sometimes used for reinforcing bars. Compared to these, more resistant resins, such as vinyl ester, should be preferred. Resin and fiber damage due to alkali attack can sometimes be more severe than the effect of moisture alone and must always be taken into consideration. It is, however, advisable to cure the resin before exposure to alkaline environments.

(3) Effects of moisture (water and saline solutions): The primary effects of moisture absorption on the resin are a reduction in glass transition temperature, strength, and stiffness. Moisture absorption depends on the type of resin, the composition and quality of the reinforcement system, thickness, curing conditions, and working conditions. Additionally, moisture can weaken the fiber-resin interface, particularly in the case of glass fibers, leading to a reduction in the mechanical properties of the composite material, especially its strength. This effect can be aggravated in the presence of saline solutions.

(4) Effects of extreme temperatures and thermal cycles: The primary effects of temperature concern the mechanical response of the resin, and therefore, the composite. As temperature increases, the typical elastic modulus of the resin decreases. If the temperature exceeds the glass transition temperature, the composite's performance level significantly decreases. Thermal cycles generally do not have deleterious effects, although they may promote the formation of microcracks in systems that use high-modulus resins. For temperature ranges typical of civil infrastructure, undesirable performance degradation can be avoided by selecting a reinforcement system that ensures the glass transition temperature is always higher than the maximum operating temperature. FRP materials should not be used in environments where the operating temperature exceeds the reduced glass transition temperature by 15°C. If necessary, thermal insulation protection should be provided.

(5) Freeze-thaw cycles: Exposure to freeze-thaw cycles generally does not affect the performance of fibers but reduces that of the resin and the fiber-resin interface due to detachment. For temperatures below 0°C, polymer-based systems can improve their performance by developing higher resistance and stiffness values. The effects of thermal degradation can be amplified in the presence of moisture. Cyclicity promotes the growth and propagation of microcracks caused by saline solutions in humid environments at the fiber-resin interface, an effect that saline solutions may exacerbate.

(6) Effects of ultraviolet (UV) radiation: UV radiation rarely degrades the mechanical properties of FRP reinforcement systems; however, some resins may experience surface embrittlement and erosion due to the radiation. In general, the most harmful effect related to UV exposure is the penetration of moisture and other aggressive agents through the damaged surface. UV radiation protection can be achieved by incorporating suitable additives into the resin and/or applying suitable coatings.

(7) Table 3-3 recommends reference values to assign to the environmental conversion factor η_a for various materials (preformed FRP systems, prepregs, and in-situ impregnated materials used for the EBR technique). These values are based on specific experimental studies conducted on the material used and under expected environmental conditions, using artificial aging tests of 1,000 hours for external exposure and 3,000 hours for exposure to aggressive environments. These values are, therefore, sufficiently conservative estimates that the Designer can refer to when more precise evaluations are not available.
The values in the table can be increased by 10% (but in any case, $\eta_a \leq 1$) if protective coatings are used, whose properties for mitigating the effects of environmental exposure have been experimentally proven, and provided maintenance is provided so that these coatings protect the FRP reinforcement for the entire service life.
In the case of FRP bars applied in resin-filled grooves as external reinforcement (NSM technique) or used for the confinement of reinforced concrete or masonry elements, the environmental conversion factor η_a must be evaluated based on the guidelines in CNR DT 203 and subsequent modifications. Alternatively, conservative values, as shown in Table 3-3, can be used.

Table 3-3 – Environmental conversion factor ηa for various exposure conditions and FRP systems with an epoxy resin matrix.

Exposure Condition	Type of Fiber	η_a
Indoor	Glass	0.75
	Aramid	0.85
	Carbon – Preformed	0.95
	Carbon – Prepreg and in-situ impregnated	0.95
	Steel	0.95
Outdoor	Glass	0.65
	Aramid	0.75
	Carbon – Preformed	0.95
	Carbon – Prepreg and in-situ impregnated	0.80
	Steel	0.80
Aggressive Environment	Glass	0.50
	Aramid	0.70
	Carbon – Preformed	0.90
	Carbon – Prepreg and in-situ impregnated	0.75
	Steel	0.75

(8) For applications on reinforced concrete, the exposure condition can be determined using the exposure classes specified by the UNI EN 206:2021 standard, as shown in Table 3-4. For masonry applications, the same approach can be used by analogy.

Table 3-4 – Exposure conditions for applications on reinforced concrete.

Exposure Condition	**Exposure Class**
Indoor	X0, XC1, XC2, XC3, XF1
Outdoor	XC4, XD1, XS1, XA1, XA2, XF2, XF3
Aggressive Environment	XD2, XD3, XS2, XS3, XA3, XF4

3.5.2 Loading Modes and Conversion Factor for Long-term Effects

(1) The mechanical properties (such as tensile strength, ultimate deformation, and longitudinal elastic modulus) of some FRP materials degrade due to creep and fatigue phenomena.

(2) Effects of long-term loads and deformations (viscosity and relaxation): The long-term strength and deformation of FRP materials depend on the properties of the resins and reinforcing fibers. Generally, thermosetting resins (e.g., unsaturated polyesters, vinyl esters, epoxy resins, and phenolic resins) are less viscous than thermoplastic resins (polypropylenes, nylons, polycarbonates). Since the presence of fibers counteracts the viscosity of the resins, these phenomena are more pronounced when loads are applied transversely to the fibers or in composites with a low volume percentage of fibers. The extent of delayed deformations due to long-term loads can be reduced by appropriately limiting the operational stresses in the composite. CFRP materials are less susceptible to failures from long-term loads; AFRP materials are moderately susceptible; GFRP materials are the most susceptible to this type of failure.

(3) Fatigue Effects: The performance of FRP materials under fatigue conditions is generally satisfactory. It depends on the matrix composition and, to a lesser extent, the type of fibers. The fibers effectively counteract crack formation and hinder crack propagation.

(4) To prevent the failure of FRP materials (preformed FRP systems, prepregs, and in-situ impregnated systems used for the EBR technique) under long-term or cyclic loads, the stress state in operating conditions can be appropriately controlled by reducing the design value using a conversion factor η_l, with suggested values shown in Table 3-5.
For FRP bars applied in resin-filled grooves as external reinforcement (NSM technique) or for the confinement of reinforced concrete or masonry elements, the conversion factor η_l should be evaluated based on what is indicated in the CNR DT 203 guidelines and subsequent modifications.

Table 3-5 - Conversion factor for long-term effects η_l for various FRP materials (service loads).

Loading Mode	**Fiber/Resin Type**	**Conversion Factor, η_l**
Long-term Load	Glass/Epoxy	0.30
	Aramid/Epoxy	0.50
	Carbon/Epoxy	0.80
Cyclic	All	0.50

3.5.3 Resistance to Impact and Explosion Actions

(1) Experimental tests conducted both in the laboratory and on portions of in-situ structures subjected to explosion actions have shown the greater effectiveness of AFRP composites compared to CFRP and GFRP. Full-scale tests on buildings have also shown that alternating layers of AFRP with

different elastic moduli, impregnated with epoxy matrices, along with layers of elastomeric resins (polyurethane) with very high deformation and toughness, allow the dissipation of energy from an impact or explosion, containing the devastating effects of deflagration and preventing debris from penetrating the structure.

3.5.4 Resistance to Actions Caused by Vandalism

(1) FRP materials are susceptible to engraving and tearing caused by cutting tools.

(2) In the case of FRP material applications on structural elements located in public areas, appropriate protective measures against vandalism should be taken. However, the safety of the structural elements in the situation following a vandalism event, without reinforcement, must be verified. The verification should be performed for the Ultimate Limit State (ULS) by adopting the combination of quasi-permanent actions with partial material factors for exceptional actions.

3.6 STRENGTHENING LIMITATIONS UNDER FIRE EXPOSURE

(1) FRP materials made with polymeric matrices are susceptible to exposure to high temperatures, such as those that may occur during a fire. When the operating temperature exceeds the glass transition temperature of the resin (or the melting temperature in the case of semi-crystalline materials), the strength and stiffness of FRP materials decrease drastically. Additionally, if FRP materials are applied externally to the reinforced elements, exposure to high temperatures leads to rapid deterioration of the FRP/support adhesion, resulting in detachment of the composite from the substrate and loss of the reinforcement intervention's effectiveness.

(2) Under fire conditions, the mechanical properties of externally applied FRP materials can be significantly improved by using appropriate protective coating thicknesses. Coatings should be appropriately certified according to the current regulations. Further specifications on the application of protective systems are provided in §§ 4.9.2.3 and 5.9.2.3**Errore. L'origine riferimento non è stata trovata.**.

(3) For constructions where fire risk must be limited for the safety of individuals, the public, neighboring properties, and assets directly exposed to fire, specific checks on the level of fire-resistance performance must be carried out.
In cases where fire-resistance safety checks are required, the reinforced structure must be verified in the following situations, where the symbol $E_{fi,d,t}$ represents the calculated value of the stresses for the combination of load in fire conditions, as defined by the current Technical Standards for Constructions or Building Code. The capacities of the elements $R_{fi,d,t}$, appropriately reduced to account for the exposure time to fire, must be calculated using unitary values of the material partial factors.

The following conditions may apply:

- **Verification with reinforcement:** This is considered when the reinforcement is to be considered effective in fire conditions and must, therefore, be designed for a specified exposure time to fire. If necessary to satisfy the verification, a suitable fire protection system for the reinforcement should be designed, taking into account the guidelines in §§ 4.9.2.3 and 5.9.2.3.
- **Verification without reinforcement:** In this case, the reinforcement is not considered effective in fire conditions, and therefore, the fire safety check must be conducted on the existing structure, disregarding the reinforcement.

4 REINFORCEMENT OF CONCRETE AND PRESTRESSED CONCRETE STRUCTURES

4.1 EVALUATION OF RESISTANCE AGAINST DETACHMENT FROM THE SUPPORT

This chapter provides predictive formulas for detachment from the support of reinforcement systems applied to the surface of the reinforced element (EBR systems, Externally Bonded Reinforcement, §4.1), as well as systems applied in grooves cut on the surface of the elements (NSM systems, Near Surface Mounted, §4.2).
Also provided are predictive formulas for flexural reinforcement (§4.3), shear reinforcement (§4.4), torsional reinforcement (§4.5) of concrete elements, and for the confinement of concrete columns (§4.6).

4.1.1 Failure Mechanisms for Detachment from the Support of EBR Systems

(1) In concrete reinforcement interventions using EBR systems, the role of the bond between concrete and the composite is crucial, as the detachment failure mechanism is brittle. According to the hierarchy of resistance criterion, this failure mechanism should not precede the collapse due to bending or shear of the reinforced element.

(2) Loss of bond between the composite and the concrete can occur either in the reinforcement system applied in the longitudinal direction to the underside of concrete beams (in the case of flexural reinforcement) or in systems applied in the transverse direction to the lateral faces (usually fabrics) in the case of shear reinforcement. In principle (Figure 4-1)), detachment of the composite from the support can occur within the adhesive, between the concrete and the adhesive, in the concrete itself, or within the reinforcement (for example, between overlapping layers of composite). In the case of correctly applied reinforcements, since the shear strength of the adhesive is generally much higher than that of the concrete, the failure occurs within the concrete, removing a layer of material ranging from a few millimeters thick to potentially affecting the entire cover.

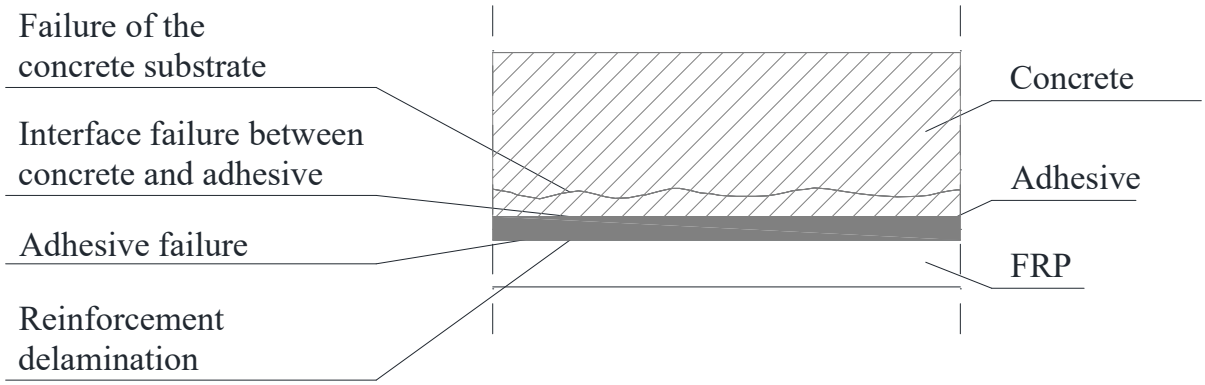

Figure 4-1 – Loss of bond between reinforcement and concrete.

(3) Detachment failure of flexural reinforcement applied to the underside of a beam can occur in one of the following four ways, schematically represented in Figure 4-2.

- Mode 1 (End detachment);
- Mode 2 (Intermediate detachment, caused by bending cracks in the beam);
- Mode 3 (Detachment caused by diagonal shear cracks in the beam);

- Mode 4 (Detachment caused by irregularities and roughness of the concrete surface).

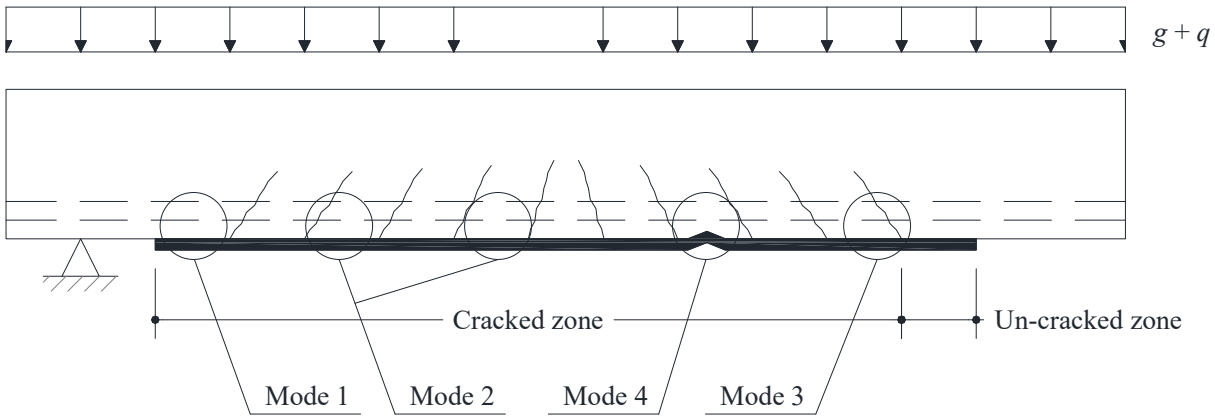

Figure 4-2 – Beam reinforced in flexure with FRP laminates: Failure modes are due to detachment from the support.

(4) Since modes 1 and 2 are more frequent, the following discussion refers exclusively to these two failure modes.
To mitigate the risk of the other two failure modes, the recommendations provided in § 4.9 of these guidelines can be followed, which concern the preliminary assessment of the support conditions as well as the preparation of the substrate.

(5) For further details on modes 1 and 2 of detachment failure and their verification criteria, please refer to Appendix D.

4.1.2 Safety Checks Against Detachment from the Support of EBR Systems

(1) The safety check for detachment failure from the support requires the evaluation of the maximum force that can be transmitted from the concrete element to the reinforcement, as well as the estimation of the stresses, both tangential and normal, mobilized at the concrete-FRP interface. The first requirement is necessary for the ULS (Ultimate Limit State) check, and the second for the SLS (Serviceability Limit State) check. The rules outlined in this document are based on the assumption of an interface law, or bond, of a cohesive type, which correlates the tangential stress mobilized at the interface between the support and reinforcement with the corresponding relative slip, which is bilinear. The graph of this relationship includes an initial elastic-linear branch followed by a softening branch. For ULS checks, it is acceptable to limit the analysis to the second branch (for more details and clarifications on the derivation of the formulas, please refer to Appendix D).

(2) Referring to a typical bond test, such as the one schematically represented in Figure 4-3, the ultimate value of the force that the FRP reinforcement can withstand before detachment from the support (end detachment) depends, under the same conditions, on the length, ℓ_b, until it reaches a maximum corresponding to a well-defined length, ℓ_e: further elongation of the bonding area does not result in any increase in the transmitted force.
The length ℓ_e is defined as the "optimal anchorage length". It corresponds to the minimum anchorage length that ensures the transmission of the maximum bond force (it corresponds to the full development of the bond).

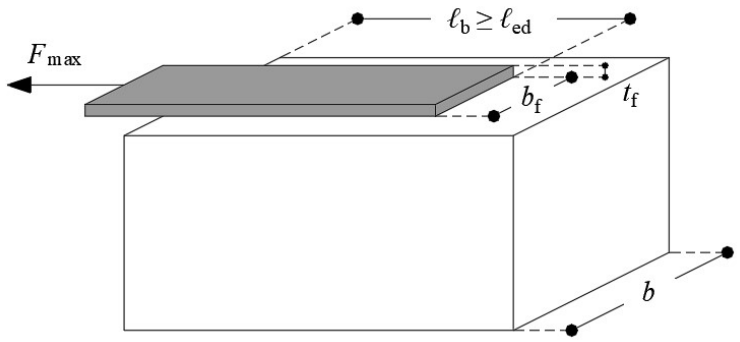

Figure 4-3 – Maximum force transferable by an FRP reinforcement.

(3) The optimal design anchorage length, ℓ_{ed}, can be estimated using the following formula:

$$\ell_{ed} = \max\left\{\ell_{ed,min};\ \gamma_{Rd}\frac{1}{f_{bm}}\sqrt{\frac{\pi^2 E_f t_f \Gamma_{Fm}}{2}}\right\} = \max\left\{\ell_{ed,min};\ \gamma_{Rd}\frac{\pi}{2}\sqrt{\frac{E_f t_f \cdot s_u}{f_{bm}}}\right\} \tag{4.1}$$

Where:

- E_f and t_f are, respectively, the elastic modulus of the FRP reinforcement in the direction of the force and its thickness, assumed to be constant along the reinforcement;
- f_{bm} is the average value of the maximum bond stress at the FRP-substrate interface;
- Γ_{Fm} is the average value of the specific fracture energy (energy strain release rate), i.e., the energy required to separate two adjacent unit surfaces (coincident with the area under the bond);
- $\gamma_{Rd} = 1.20$ is a partial factor for the model;
- $l_{ed,min}$ is the minimum value for the optimal anchorage length, which is 100 mm for in-situ impregnated composites and 250 mm for preformed composites.

The average value of the maximum tangential bond stress is assumed to be:

$$f_{bm} = k_{Gm} \cdot \frac{\sqrt{f_{cm} \cdot f_{ctm}}}{2 \cdot FC} \tag{4.2}$$

Where:

- f_{cm} and f_{ctm} are, respectively, the average values of the compressive and tensile strengths of the concrete, assessed in situ; the average tensile strength of the concrete is the minimum value between the experimentally assessed strength (if available) and the value derived from f_{cm} in accordance with the current regulations;
- k_{Gm} is the average value of a dimensionless coefficient calibrated experimentally, equal to 0.80 for preformed composites and 1.25 for in-situ impregnated FRP systems (see Appendix D);
- FC is the confidence factor that accounts for the level of knowledge of the substrate, evaluated with reference to valid regulatory standards.

The average value of the specific fracture energy, assuming a bilinear bond, can be assumed to be:

$$\Gamma_{\mathrm{Fm}} = \frac{1}{2} f_{\mathrm{bm}} s_{\mathrm{u}} = \frac{k_{\mathrm{Gm}}}{4} \frac{\sqrt{f_{\mathrm{cm}} f_{\mathrm{ctm}}}}{FC} s_{\mathrm{u}} \tag{4.3}$$

where s_{u} is the average value of the ultimate slip of the bond, which is assumed to be 0.25 mm.

4.1.3 Resistance to Ultimate Limit State for End Detachment (Mode 1) of EBR Systems

(1) In the assumption that the detachment involves the first layers of concrete and that the anchorage lengths are greater than or equal to the optimal length, the average and design values of the maximum tensile force, $F_{max,m}$ and $F_{max,d}$, and thus the maximum stress, f_{fdm} and f_{fdd}, to which the composite can be subjected without end detachment (Figure 4-3), are provided by the following relations:

$$F_{\mathrm{max},m} = k_{\mathrm{b}} b_{\mathrm{f}} \cdot \sqrt{2 E_{\mathrm{f}} t_{\mathrm{f}} \Gamma_{\mathrm{Fm}}} \tag{4.4}$$

$$F_{\mathrm{max,d}} = \frac{k_{\mathrm{b}} b_{\mathrm{f}}}{\gamma_{\mathrm{f2}}} \cdot \sqrt{2 E_{\mathrm{f}} t_{\mathrm{f}} \Gamma_{\mathrm{Fk}}} \tag{4.5}$$

$$f_{\mathrm{fdm}} = k_{\mathrm{b}} \cdot \sqrt{\frac{2 E_{\mathrm{f}} \Gamma_{\mathrm{Fm}}}{t_{\mathrm{f}}}} \tag{4.6}$$

$$f_{\mathrm{fdd}} = \frac{k_{\mathrm{b}}}{\gamma_{\mathrm{f2}}} \cdot \sqrt{\frac{2 E_{\mathrm{f}} \Gamma_{\mathrm{Fk}}}{t_{\mathrm{f}}}} \tag{4.7}$$

In these formulas and the ones that follow, the symbols used have the following meaning (Figure 4-3):

- b_f and l_b are, respectively, the width of the FRP reinforcement and the length of the bonded area responsible for anchorage, both assumed to be constant;
- γ_{f2} is the partial factor equal to 1.3 for ULS of detachment from the support, as indicated in § 3.4.1;
- k_b is a geometric correction coefficient, for which the following expression is admitted based on the ratio b_f/b between the width of the reinforcement and that of the reinforced element:

$$k_{\mathrm{b}} = \sqrt{\frac{2 - b_{\mathrm{f}} / b}{1 + b_{\mathrm{f}} / b}} \geq 1 \tag{4.8}$$

provided that $b_f/b \geq 0.25$ (for $b_f/b < 0.25$ the coefficient k_b is assigned the value 1.18, corresponding to $b_f/b = 0.25$). In the case of flexural reinforcement of a slab made with multiple adjacent FRP strips, each with a width b_f, the shape factor k_b can be calculated using equation (4.8), considering the distance between two adjacent reinforcement strips as the width b;

- Γ_{Fk} is the characteristic value of the maximum bond stress at the substrate-FRP interface, calculated as follows, in accordance with (4.9) and (4.10):

$$\Gamma_{Fk} = \frac{1}{2} f_{bk} s_u = \frac{k_{Gk}}{4} \frac{\sqrt{f_{cm} f_{ctm}}}{FC} \cdot s_u \tag{4.9}$$

$$f_{bk} = k_{Gk} \cdot \frac{\sqrt{f_{cm} \cdot f_{ctm}}}{2 \cdot FC} \tag{4.10}$$

where k_{Gk} is the characteristic (5% fractile) value of the dimensionless correction coefficient (see Appendix D), experimentally calibrated and equal to 0.35 for preformed composites and 0.60 for in-situ impregnated FRP systems. At the same time, the other symbols have meanings that were introduced earlier.

(2) In the case where the anchorage length, l_b, is smaller than the optimal length, l_{ed}, the design stress for end detachment must be appropriately reduced according to the following relation:

$$f_{fdd,rid} = f_{fdd} \cdot \frac{\ell_b}{\ell_{ed}} \cdot \left(2 - \frac{\ell_b}{\ell_{ed}} \right) \tag{4.11}$$

Where f_{fdd} is given by eq. (4.7).

(3) In the case of using fan-shaped flared connectors as anchorage devices, the guidelines provided in §4.1.5 apply.

(4) In the case of using mechanical connectors as anchorage devices, the guidelines provided in §4.1.6 apply.

(5) If particular anchorage devices (e.g., transverse composite bars, end wrapping with fabrics) are to be used to avoid end detachment or to achieve higher values of f_{fdd}, certification of the materials used (adhesives and reinforcements) and the specific systems used to improve anchorage is required, along with indications of the surface preparation steps, execution times, and environmental conditions for application. Specifically, the evaluation of the increase in f_{fdd} relative to the value given by (4.7) must be conducted through specific experimental investigations, following the approach suggested in EN1990 – Annex D (Design assisted by testing). For anchorage systems represented by flared anchors and post-installed mechanical connectors, the design formulations provided in 4.1.5 and 4.1.6 can be used, respectively.

4.1.4 Resistance to Ultimate Limit State for Intermediate Detachment (Mode 2) of EBR Systems

(1) To prevent the detachment failure according to Mode 2, it is necessary to verify that the change in stress, $\Delta\sigma_f$ in the FRP reinforcement between two consecutive cracks does not exceed an appropriate limiting value, $\Delta\sigma_r$. This limit generally depends on the characteristics of the bond (as defined in Appendix D), the distance between cracks, and the level of stress σ_f in the reinforcement and can be evaluated in accordance with proven regulatory standards and/or guidelines.

(2) Alternatively, a simplified procedure can be used, which involves verifying that, at the ULS, the maximum stress in the fiber-reinforced composite does not exceed the design value, $f_{\text{fdd,2}}$, provided by the following relation:

$$f_{\text{fdd,2}} = \frac{k_{\text{q}} k_{\text{b}}}{\gamma_{\text{f2}}} \sqrt{\frac{2E_{\text{f}} \frac{k_{\text{Gk,2}}}{4FC} \sqrt{f_{\text{cm}} f_{\text{ctm}}} \cdot s_{\text{u}}}{t_{\text{f}}}} \tag{4.12}$$

where the previously introduced symbols have the same meaning as specified above, and additionally:

- $k_{Gk,2}$ is the characteristic (5% fractile) value of a correction coefficient calibrated (see Appendix D) based on experimental results, assumed to be $k_{Gk,2} = 1.6$ regardless of the type of reinforcement;
- k_{q} is a coefficient that accounts for the loading condition, assumed to be 1.25 for predominantly distributed loads and 1.00 for all other cases;
- γ_{f2} is the partial factor equal to 1.3 for ULS of detachment from the support, as indicated in § 3.4.1.

Consequently, the maximum value that can be attributed to the deformation of the composite in the design stage to avoid intermediate detachment is:

$$\varepsilon_{\text{fdd,2}} = \frac{f_{\text{fdd,2}}}{E_{\text{f}}} \geq \varepsilon_{\text{sy}} - \varepsilon_0 \tag{4.13}$$

where ε_{fy} is the strain in the steel reinforcement at yielding and ε_0 is the pre-existing deformation at the application of the reinforcement at the extreme tensioned edge, calculated in accordance with the instructions in § 4.3.2.2.

The average value of the maximum stress in the fiber-reinforced composite, $f_{\text{fdm,2}}$, is given by the following relation:

$$f_{\text{fdm,2}} = k_{\text{q}} k_{\text{b}} \sqrt{\frac{2E_{\text{f}} \frac{k_{\text{Gm,2}}}{4FC} \sqrt{f_{\text{cm}} f_{\text{ctm}}} \cdot s_{\text{u}}}{t_{\text{f}}}} \tag{4.14}$$

Where $k_{Gm,2}$ is the average value of the calibrated correction coefficient (see Appendix D) based on experimental results, assumed to be $k_{Gm,2} = 5.1$, regardless of the type of reinforcement.

4.1.5 Anchorage Devices Using Flared Connectors for EBR Systems

(1) The end zones of FRP reinforcement strips can be reinforced with fan-shaped flared connectors (SOFS or Splays Of Fiber Spikes), hereafter referred to as 'spikes,' consisting of a part (stem) anchored inside holes made in the substrate of the element to be reinforced, and generally made from resin-impregnated fibers. The fibers are not impregnated and are flared and glued on top of the FRP strip (Figure 4-4c). The anchorage of the spikes in the substrate is achieved by making holes at an angle ψ_a relative to the plane of the reinforcement. "Inline spikes" can be made when, in some applications, the spike is anchored in a concrete element orthogonal to the one where the reinforcement is applied (Figure 4-4 a, '*straight anchor'*), in which case $\psi_a = 180°$. "Inclined spikes" are used when the spike is anchored in the same concrete element where the reinforcement is applied; in this case ψ_a can be different than 180°, and it is recommended to be between 90° and 135° (Figure 4-4 a-b, '*bent anchor*').

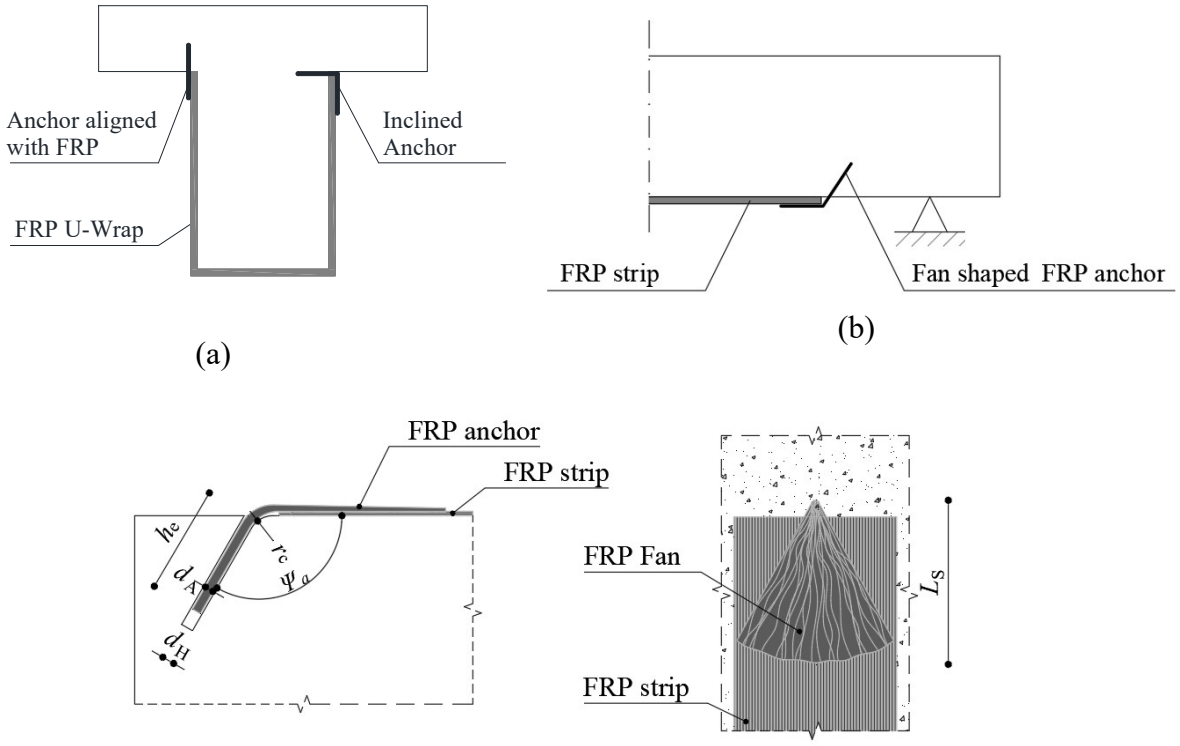

Figure 4-4 – a) Possible placements of the spike in case of end anchorage of shear reinforcement; b) Possible placement of the spike in case of flexural reinforcement anchorage; c) Parameters defining the geometry of fan-shaped anchors.

(2) In the absence of direct experimental data demonstrating the effectiveness of the adopted solution, the geometric parameters of the fan-shaped anchors (Figure 4-4 c) must comply with the following limits:

- The nominal diameter of the spike must be between 6 mm and 16 mm, and this is used to calculate the nominal area A_{fc} of the spike;
- In the case of inclined spikes ('bent anchor'), i.e., when the spike is anchored in the same element where the reinforcement is applied:
  - The bending angle ψ_a of the fixed part of the connector must be between 90° and 135°;
  - The radius of curvature r_c at the corner must be greater than 10 mm;
- The minimum anchorage depth h_e of the spike's stem must be at least:

  - For inclined spikes *('bent anchor')*: $\frac{2\psi_a}{180°}$ max(80mm,8d_a),
  - For inline spikes *('straight anchor')*: max(120mm,12d_a);
- The diameter of the hole d_h must be at least 1.20 d_a, with a lower limit of d_a + 2.0 mm
- The total length of the hole in which the spike is inserted must be equal to h_e+10 mm to allow complete resin penetration inside the hole;
- The semi-opening angle λ of the fibers must not exceed 30°;
- The width of the fan opening must cover at least 80% of the width of the FRP strip that is anchored if it is made from unidirectional fabric, while for quad-axial fabric, the coverage percentage can be reduced to 50% of the width of the strip; these requirements also apply to cases where multiple spikes are applied to a single strip, with the additional requirement that the distance between the inserted parts of the spikes is between 1.5h_e and 2h_e. For the same total resistant area of spikes, it is recommended to use a greater number of small-diameter spikes rather than fewer larger-diameter spikes.

The validity of the formulas provided below is limited to spikes that meet the above requirements. If spikes with different geometric characteristics are to be used, their effectiveness must be demonstrated through specific experimental tests. Specifically, alternative resistance values to those calculated with the formulas provided below may be used, provided they are evaluated following the approach suggested in EN1990 – Annex D (Design assisted by testing).

(3) The failure of the fan-shaped anchors can occur in different modes, each characterized by its limit resistance value (Figure 4-5). In particular, the following modes are distinguished:

a) Detachment of the spike from the substrate with the removal of a concrete wedge, which can affect the entire anchorage depth of the spike's stem or part of it (pull-out failure, PO, Figure 4-5a and Figure 4-5e), possibly accompanied by partial sliding of the spike's stem along the hole walls at the terminal end of the anchorage length (mixed failure);
b) Sliding of the spike's stem due to cohesive failure in the resin or in the concrete around the hole (sliding failure, S, (Figure 4-5b and Figure 4-5f);
c) Detachment of the flared part at the interface with the reinforcement fabric (debonding, DB, (Figure 4-5c and Figure 4-5g);
d) Rupture of the spike due to shear and/or tensile-flexural failure of the fibers in the cord (fiber failure, FR, (Figure 4-5d and Figure 4-5h).

Due to the anisotropic behavior of the fibers in the spike, fiber failure (FR) occurs for resistance values that depend on the inclination of the stem, with lower values for smaller angles ψ_a, due to the predominance of shear rather than tensile-flexural stresses in the fibers at the section of maximum curvature.
Pull-out (PO) and sliding (S) failures generally occur in inline spikes and are less common in inclined ones with angles between $90° < \psi_a \leq 135°$.
For inline spikes ($\psi_a = 180°$) and for inclined spikes with angles between $90° < \psi_a \leq 135$ the likelihood of pull-out (PO), sliding (S), or a mixed failure that includes both modes occurring before fiber failure depends on the insertion length, concrete strength, spike diameter, spike tensile strength, and resin strength. In particular, sliding failure due to cohesive failure in the resin occurs when very low-strength resins are used. To avoid such failure, the compressive strength, f_{Rcm}, and tensile strength, f_{Rtm}, of the resin used to bond the spikes must be at least 20% higher than the corresponding concrete strengths. Sliding failure with cohesive failure in the concrete may be limiting in the verification, especially for low-strength concrete or short anchorage lengths.
Therefore, for inline spikes ($\psi_a = 180°$) and for inclined spikes with angles between $90° < \psi_a \leq 135°$, all failure modes shown in Figure 4-5 must be considered, according to Eq. (4.15) and the formulations described below.

In the case of inclined spikes with ψ_a= 90°, since the force acting on the tensile reinforcement is predominantly shear in the spike's stem, pull-out (PO) and sliding (S) failures do not occur unless localized rupture happens in the concrete around the stem, as shown in Figure 4-5e. This eventuality can generally be avoided by adopting the minimum anchorage depth suggested earlier. Therefore, for inclined spikes with ψ_a = 90°, Eq. (4.15), should consider the minimum value between the resistance associated with the debonding (DB) and fiber shear failure (FR) mechanisms, according to the formulations provided below.

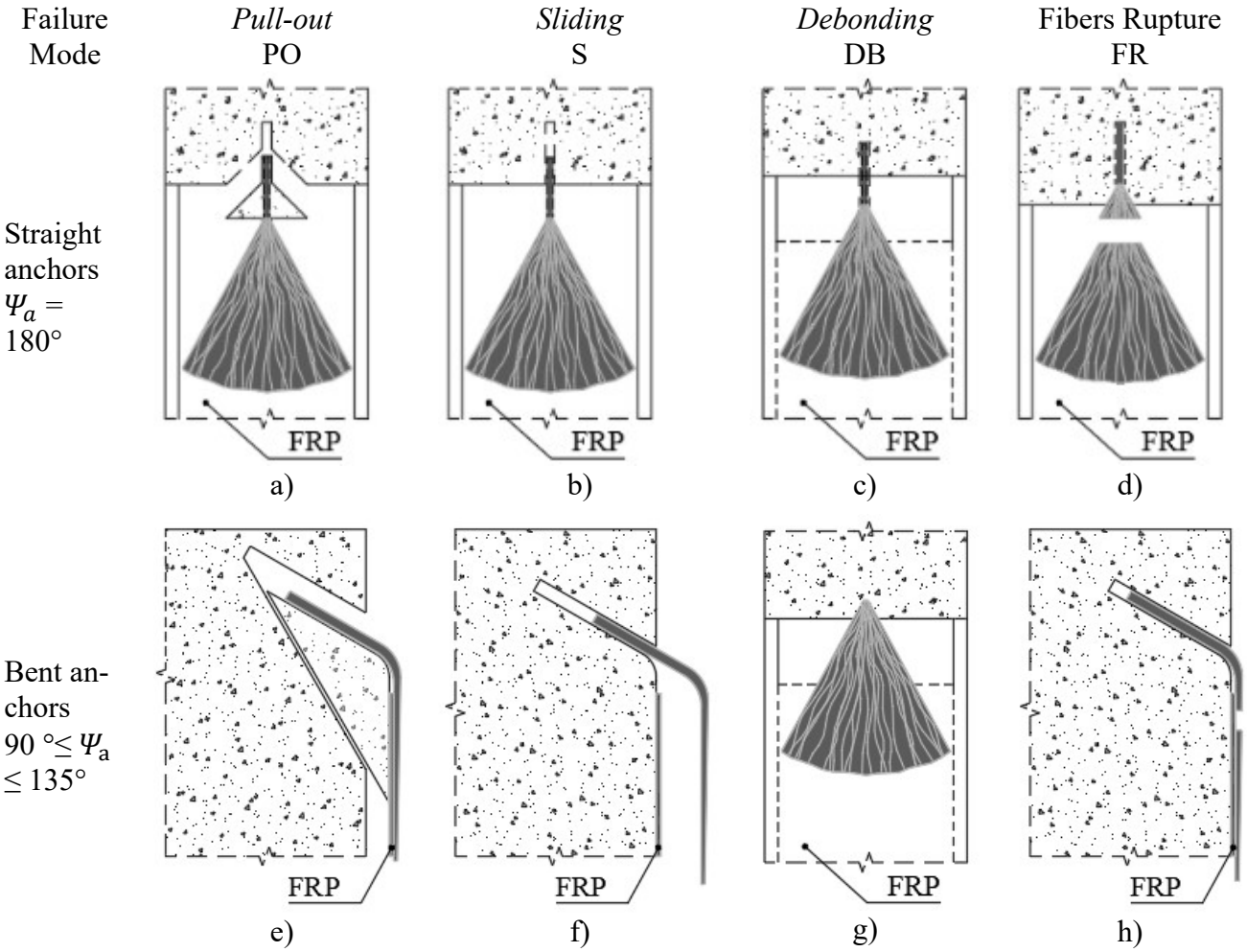

Figure 4-5 – Failure Modes of Fiber Spike Connectors.

(4) The maximum tensile force in a properly anchored FRP strip with spikes can be calculated in any section at a distance z from the end of the reinforcement by summing the force of end detachment of the reinforcement strip with the anchoring force provided by the connectors in the section between the end section of the reinforcement and the considered section, as follows:

$$F_{\mathrm{anc,d}}(\mathrm{z}) = \min\left(k_{\mathrm{k}} \cdot \frac{f_{\mathrm{f\,dm}} \cdot b_{\mathrm{f}} \cdot t_{\mathrm{f}} + \left[n_{\mathrm{z}} \cdot \min\{N_{\mathrm{PO,m}}, N_{\mathrm{S,m}}, N_{\mathrm{DB,k}}, N_{\mathrm{FR,k}}\} \right]}{\gamma_{\mathrm{f2}}} ; \frac{\eta_{\mathrm{a}} \cdot f_{\mathrm{fk}}}{\gamma_{\mathrm{f1}}} b_{\mathrm{f}} \cdot t_{\mathrm{f}} \right) \quad (4.15)$$

where:

- k_k is a coefficient, experimentally calibrated (Appendix D), equal to 0.7, which gives the characteristic value of the maximum axial stress in the presence of fiber spike connectors. If specific experimental tests are available for certain anchoring systems or systems characterized by different geometric parameters than those previously mentioned, and these tests show a resistance different from the one predicted by Equation (4.15), it is possible to adopt a different value for the k_k coefficient by calibrating it using the approach suggested in EN1990 – Annex D (Design assisted by testing);
- f_{fdm} is the average value of the end detachment resistance of the FRP strip, given by Equation (4.6) in the case of flexural reinforcement and by Equation (4.83) in the case of shear reinforcement, where f_{fdm} replaces f_{fdd};
- n_z is the number of connectors applied to the FRP strip up to the abscissa z, evaluated starting from the end of the reinforcement, including any side-by-side connectors;
- γ_{f2} is the partial factor to be assumed as 1.30 for the Ultimate Limit State (ULS) of end detachment in the presence of anchoring, as indicated in Section § 3.4.13.4.1;
- b_f and t_f are the width and thickness of the reinforcement in the case of flexural and shear reinforcement;
- f_{fk} is the characteristic tensile strength of the reinforcement fibers;
- η_a is the environmental conversion factor of the FRP reinforcement and γ_{f1} is the partial factor for ULS tensile rupture of the reinforcement fibers, as indicated in Section § 3.4.1.

The terms $N_{PO,m}$, $N_{S,m}$, $N_{DB,k}$, and $N_{FR,k}$ and others are described below and refer to failure modes such as pull-out of the spike from the substrate (PO), sliding (S), debonding of the spike from the FRP reinforcement (DB), and tensile rupture of the fibers of the spike (FR), as shown in Figure 4-5.

Based on (4.15), the corresponding design values for tensile stress and strain in the reinforcement strip are:

$$f_{\mathrm{fdd},anc}(z) = \frac{F_{\mathrm{anc,d}}(z)}{b_{\mathrm{f}} \cdot t_{\mathrm{f}}} \tag{4.16}$$

$$\varepsilon_{\mathrm{fdd,anc}}(z) = \frac{F_{\mathrm{anc,d}}(z)}{E_{\mathrm{f}} \cdot b_{\mathrm{f}} \cdot t_{\mathrm{f}}} \geq \varepsilon_{\mathrm{sy}} - \varepsilon_0 \tag{4.17}$$

(5) For straight spikes ($\psi_a = 180°$) and inclined spikes with angles $90° < \psi_a \leq 135°$, it is necessary to consider pull-out failure and calculate the corresponding force, $N_{PO,m}$, to be used in Equation (4.15), which depends on the anchoring depth and the strength of the concrete in which the spike is anchored, as follows:

$$N_{\mathrm{PO,m}} = k_{\mathrm{eff}} \sqrt{\frac{f_{\mathrm{cm}}}{FC}} \cdot \min(120\mathrm{mm}, h_{\mathrm{e}})^{1.5} \frac{1}{\cos(180 - \psi_{\mathrm{a}})} \tag{4.18}$$

Where:

- f_{cm} is the average compressive strength of the concrete in which the spike is inserted;
- FC is the confidence factor that takes into account the level of knowledge of the substrate and is evaluated according to widely recognized standards;

- k_{eff} is a coefficient experimentally calibrated for straight spikes, to be assumed as 8.5. Suppose specific experimental tests are available for certain anchoring systems or systems with different geometric parameters, and these tests show a different average resistance than predicted by Equation (4.10). In that case, it is possible to adopt a different value for the k_{eff} coefficient by calibrating it with the approach suggested in EN1990 – Annex D (Design assisted by testing).

Let c be the minimum distance between the anchor stem and the edge of the concrete element. If $c < 0.7 \cdot h_e$, the force $N_{PO,m}$ given by equation (4.18) must be reduced by the coefficient $\psi_c = \frac{c}{0.7h_e} \leq 1$. This ensures that the concrete cone is fully developed.

For inclined spike anchors with $\psi_a = 90°$, °, the force corresponding to pull-out failure does not need to be calculated.

(6) For straight spikes ($\psi_a = 180°$) and inclined spikes with angles $90° < \psi_a \leq 135°$, °, it is necessary to consider sliding (S) failure, assuming the failure to be cohesive in the concrete, and calculate the corresponding force $N_{S,m}$, to be used in Equation (4.15), which is proportional to the surface area of the hole wetted by resin $\pi \cdot d_h \cdot h_e$ and the cohesion of the concrete $\frac{\sqrt{f_{cm} \cdot f_{ctm}}}{2}$, as follows:

$$N_{S,m} = \pi \, d_h \, h_e \cdot k_c \cdot \frac{\sqrt{f_{cm} \cdot f_{ctm}}}{2FC} \frac{1}{\cos(180 - \psi_a)} \tag{4.19}$$

Where k_c is a coefficient experimentally calibrated, to be assumed as 2.0. Suppose specific experimental tests are available for certain anchoring systems or systems with different geometric parameters, and the tests show a significantly different average resistance than predicted by Equation (4.19). In that case, it is possible to adopt a different value for the k_c coefficient, or for the product $k_c \frac{\sqrt{f_{cm} f_{ctm}}}{2FC}$, by calibrating it with the approach suggested in EN1990 – Annex D (Design assisted by testing).

For inclined spike anchors with $\psi_a = 90°$, °, the force corresponding to sliding failure does not need to be calculated.

(7) For all types of fiber spike connectors, both straight and inclined, with reference to the debonding failure of the fan of fibers from the reinforcement, the force N_{DB}, to be used in Equation (4.15), depending on the shear strength of the resin used to apply the spikes to the FRP strip. The fan of fiber spikes creates balance in the longitudinal direction of the FRP strip, but also introduces parasitic tensile forces orthogonal to the strip's axis. The longitudinal and transverse components of the fiber adhesion force of the fan depend on the opening 2λ of the fan itself, and the characteristic values of the two components can be calculated as:

$$N_{DB,k} = F_{DB,k} \cdot \left(\frac{\sin \lambda}{\lambda} \right) \;,\; H_{DB,k} = F_{DB,k} \cdot \left(\frac{1 - \cos \lambda}{2\lambda} \right) \tag{4.20}$$

The total force that activates the debonding failure can be calculated based on the surface area of the fan connection and the shear strength of the resin:

$$F_{\mathrm{DB,k}} = \lambda L_{\mathrm{s}}^2 \cdot \tau_{\mathrm{Rb,k}} \tag{4.21}$$

where the resin's detachment strength can be assumed to be the cohesion of the resin:

$$\tau_{\mathrm{Rbk}} = \frac{1}{2}\sqrt{f_{\mathrm{Rck}} f_{\mathrm{Rtk}}} \tag{4.22}$$

where $f_{R,ck}$ and $f_{R,fk}$ are the characteristic values of the compressive and tensile strengths of the resin used for bonding.
The transverse component H_{FD} is distributed across the FRP strip orthogonally to the fiber axis. Assuming a linearly increasing distribution from the apex of the fiber spike to its tip, the tensile strength of the resin must be greater than the maximum tension due to $H_{\mathrm{FD,k}}$:

$$\frac{2H_{\mathrm{DB,k}}}{L_{\mathrm{S}} \cdot t_{\mathrm{f}}} \leq \frac{f_{\mathrm{Rtk}}}{\gamma_{\mathrm{Rd}}} \tag{4.23}$$

where t_f is the thickness of the anchored reinforcement strip and γ_{Rd} is a model coefficient for tensile rupture of the resin, assumed to be 1.30.

(8) For all types of fiber spike connectors, whether straight or inclined, with reference to the tensile rupture of the fiber spike fibers (FR), where A_{fc} is the nominal cross-sectional area of the spike, the characteristic value of the maximum force N_{FR}, to be used in Equation (4.15), that causes the rupture of the fibers is:

$$N_{\mathrm{FR,k}} = k_{\mathrm{FAN}} \cdot \frac{\psi_{\mathrm{a}}}{180°} A_{\mathrm{fc}} \cdot \eta_{\mathrm{a}} \cdot f_{\mathrm{fak}} \tag{4.24}$$

where:

- η_{a} is the environmental conversion factor of the FRP material, as indicated in Section § 3.4.1;
- f_{fak} is the characteristic tensile strength of the fiber spike anchor;
- k_{FAN} is a correction factor equal to 0.5 to account for a reduction in efficiency in the fibers due to the spiking, with the maximum opening of $\lambda = 30°$. Suppose specific experimental tests are available for certain anchoring systems or systems with different geometric parameters, and the tests show a characteristic resistance different from the one predicted by Equation (4.24). In that case, it is possible to adopt a different value for the k_{FAN} coefficient by calibrating it with the approach suggested in EN1990 – Annex D (Design assisted by testing).

(9) In the case of applying spikes to fabrics used for shear-tension reinforcement of beam-column joints, the product $b_{\mathrm{f}} \cdot t_{\mathrm{f}}$, in Equation (4.15) must be replaced by the area A_{f} given by Equations (4.108), (4.109), (4.110), and (4.111), which, for bidirectional or Quadri-axial fabrics, can be reduced by the contribution of the fibers arranged along the column axis, as given by Equation (4.109) for θ =90°.

Additionally, in the case of shear-tension reinforcement of beam-column joints, the number of anchors required to achieve the design strain can be determined by verifying the following relationship:

$$F_{\text{anc,d}}(z) \geq \varepsilon_{\text{fd}} \cdot A_{\text{f}} \cdot E_{\text{f}}$$

where $F_{\text{anc,d}}(z)$ is the strength of the bonded FRP fabric given by Equation (4.15), E_{f} is the elastic modulus of the FRP reinforcement applied at the joint, ε_{fd} is calculated using Equation (4.114), and the area A_{f} is given by Equations (4.108), (4.109), (4.110), (4.111).

4.1.6 Post-Installed Mechanical Anchor Devices for EBR Systems

(1) FRP strengthening elements can be anchored discontinuously using metal plates bonded with resin over the FRP reinforcement and fixed to the concrete with post-installed mechanical anchors. This creates a hybrid strengthening system, which functions through friction in the space between the metal plate and the FRP reinforcement, through simple adhesion between the anchors and the substrate, and through friction between the substrate and the FRP reinforcement in areas not equipped with anchorage devices.

(2) The anchors may be either mechanical (expansion type) or chemical. The plates may be made of steel or aluminum. The tightening of the screws for post-installed mechanical anchors must only be performed once the resin used to bond the FRP reinforcement to the substrate and to the metal plate has fully cured and hardened.

(3) For the qualification of the anchorage device, the requirements set by the applicable standards or by other recognized, validated guidelines for structural anchors must be followed.

(4) Anchorage devices must be designed to ensure that their strength is sufficient to reach the tensile failure of the FRP reinforcement being anchored. All components of the anchorage system (plates, anchors) must be designed and verified in accordance with the relevant codes or other recognized, validated guidelines for structural anchors.

(5) For construction details regarding the placement of post-installed mechanical anchors, the guidance provided in the applicable codes or other validated references for structural anchors must be followed.

(6) The application of anchorage devices using post-installed mechanical anchors requires an evaluation of the substrate's integrity, as described in section 4.9.

(7) Structural analysis of elements with mechanically anchored FRP reinforcements can be performed using standard models based on beam theory (planarity of the deformation diagram of each section) only up to the intermediate delamination tension of the FRP reinforcement. Beyond this state, the structural analysis must be developed considering the reinforcement disconnected from the structural element, and its deformation is constant in segments between each pair of mechanical anchors.

(8) Mechanical anchors can fail in three different modes: sliding between the reinforcement and the anchor (FS, "Fiber Slip"), failure of the interface with the structural element (ID, "Interface Debonding"), and plasticization of the anchor's metallic elements (DF, "Device Failure").

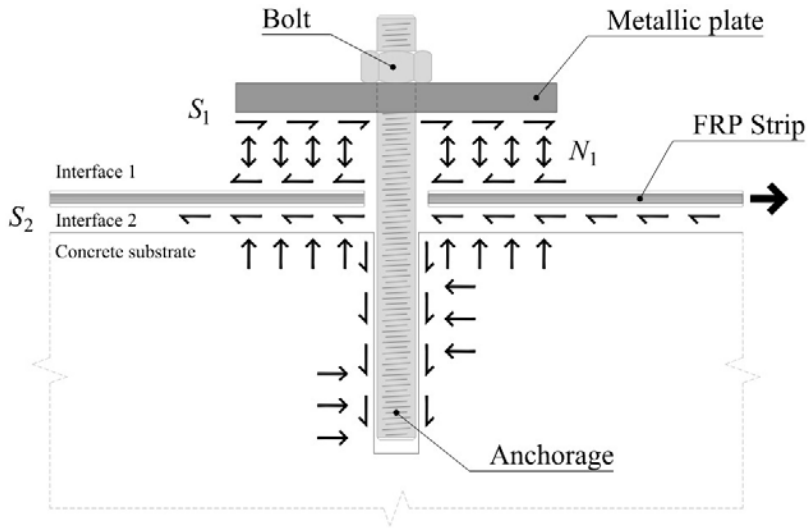

Figure 4-6 – Model of local stress development in mechanical anchors within the anchoring device, which consists of a plate and post-installed mechanical anchors.

(9) The operating pressure of the anchor, which is achieved by tightening the metallic plate, must be designed to prevent failure by sliding the reinforcement (FS). The adhesion surface of the reinforcement to the anchor is given by $B_f B_p$, where B_f is the width of the anchored reinforcement, and B_p is the width of the anchor plate (Figure 4-7). A compressive force $N_m = n_b N_1$ is applied to this surface, where N_1 is the load from tightening the individual bolt and n_b is the number of bolts fixing the anchor plate to the substrate.

The force N_1 can be calculated as $N_1 = \frac{T_s}{0.15d}$, where T_s is the tightening torque and d is the nominal diameter of the anchor. It must be verified that N_1 is less than the design resistance of the anchor, as evaluated in accordance with the provisions of the applicable standards or other recognized, valid guidelines.

The surface of the tightening nut must be lubricated with an anti-friction compound.

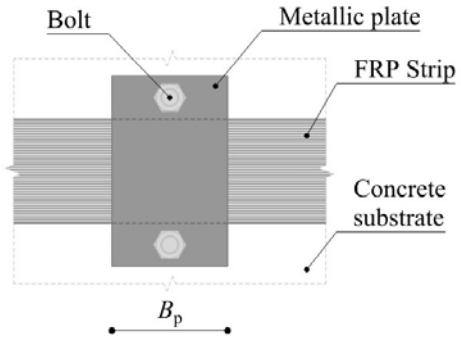

Figure 4-7 – Plan view of the localized mechanical connection of the anchorage device consisting of the metal plate and the post-installed mechanical anchors.

The friction force produced between the resin and the FRP reinforcement because of the compression N_M must be greater than the fracture strength of the FRP reinforcement fibers:

$$\mu_R N_M \geq B_f t_f \cdot \eta_a \cdot f_{fk} \tag{4.25}$$

where f_{fk} is the characteristic tensile strength of the FRP material, and η_a is the environmental conversion factor for the FRP reinforcement.
The friction coefficient μ_R can be determined based on the mechanical properties of the resin. In the absence of more precise determinations, it can be calculated as follows:

$$\phi_R = \arcsin\frac{f_{Rck} - f_{Rtk}}{f_{Rck} + f_{Rtk}} \ , \ \mu_R = \min\left\{\tan\phi_R; 0.5\right\} \tag{4.26}$$

(10) Regarding sliding failure at the interface with the structural element (ID), the shear-sliding resistance of the area $B_f B_p$ of the resin-concrete interface beneath the anchor plate must be at least half of the fracture strength of the FRP composite, leading to the following inequality:

$$(f_{v0m} + 0.4\sigma_N) B_f B_p \geq \frac{1}{2} B_f t_f \eta_a \cdot f_{fk} \tag{4.27}$$

where:

- $\sigma_N = \dfrac{N_M}{B_f B_p}$ is the normal stress acting on the area $B_f B_p$ produced by tightening the bolts;
- f_{v0m} is the average shear strength of the concrete below the anchor plate without compression, calculated as:

$$f_{v0m} = \frac{f_{cm} f_{ctm}}{\left(f_{cm} + f_{ctm}\right) FC} \tag{4.28}$$

where f_{cm} and f_{ctm} are the average compressive and tensile strengths of the concrete evaluated in situ; the average tensile strength of the concrete is given by the minimum of the experimentally determined strength (if available) and the value derived from f_{cm} in accordance with current regulations.

(11) Suppose the above conditions are met, particularly if the inequalities expressed in equations (4.27) and (4.28) are satisfied. In that case, the design tensile strength of the reinforcement can be assumed to be equal to the tensile strength of the FRP composite, calculated as:

$$f_{fd} = \eta_a \frac{f_{fk}}{\gamma_{f1}} \tag{4.29}$$

where:

- f_{fk} is the characteristic tensile strength of the reinforcement fibers;
- η_a is the environmental conversion factor for the FRP reinforcement;

- γ_{f1} is the partial factor for the ultimate limit state for the tensile failure of the reinforcement fibers, as indicated in § 3.4.1.

(12) The load-extension diagram for FRP reinforcement with discontinuous mechanical anchors presents a strain-hardening behavior with reduced stiffness after the intermediate delamination strength of the composite is reached (Figure 4-8).

In the calculation of flexural elements with externally anchored FRP reinforcement via discontinuous mechanical anchoring, the loss of linearity in the deformation diagram between successive anchor pairs must be considered, caused by the deformation difference between the structural element's interface and the reinforcement.
More precisely, when the separation force $P_1 = A_f f_{fdd}$ (Point A) occurs in the section, the assumption of plane section conservation is no longer valid. The reinforcement strip begins to elongate like a tendon with constant deformation between each successive pair of anchoring devices in a manner that is no longer consistent with the bending deformation of the concrete section. This elongation continues until the reinforcement fails (point C), when the tension of the fibers reaches the tensile failure f_{fd}, as given by Equation (4.29).

The elongations δ_0 and δ_u can be calculated as $\varepsilon_{fdd} \cdot \Delta_A$ and $\varepsilon_{fd} \cdot \Delta_A$, respectively, where Δ_A is the distance between two successive anchors and $\varepsilon_{fd} = f_{fd}/E_f$.

Suppose the distance Δ_A is greater than the optimal anchoring length ℓ_{ed}; a section of zero stiffness (section A-B) may occur, where delamination progresses at a constant tension while the concrete element increases its curvature.

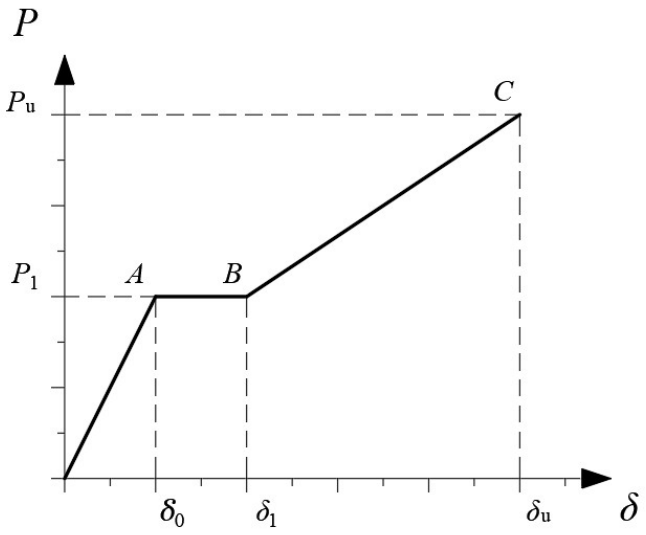

Figure 4-8 – Load-extension diagram for FRP reinforcement with discontinuous mechanical devices.

4.1.7 Interface Stress Check at the Serviceability Limit State for EBR Systems

(1) In a beam reinforced with FRP, shear and normal stress concentrations occur at the interface between concrete and reinforcement, particularly near the ends of the reinforcement, where transverse cracks in the concrete are most likely to develop. These stress concentrations can cause cracking at the interface, potentially leading to separation between the two materials.

(2) It is essential that, under service conditions, for non-seismic load combinations, the opening of these cracks does not occur, especially during load cycles and freeze/thaw cycles. The relevant check can be carried out by calculating the interface stresses using linear elastic models.

(3) It must be verified that at the adhesive-concrete interface, for the characteristic (or rare) load combination, the "equivalent" shear stress, denoted as $\tau_{b,e}$, defined below, is lower than the bond strength between the reinforcement and the concrete substrate, denoted as f_{bd}:

$$\tau_{b,e} \leq f_{bd} \tag{4.30}$$

(4) The design value of the bond strength between reinforcement and concrete, f_{bd}, is given by:

$$f_{bd} = \frac{f_{bk}}{\gamma_{fo}} \tag{4.31}$$

where f_{bk} is calculated from Equation (4.10), and γ_{fo} is the safety factor for serviceability checks, assumed to be 1.0 as specified in § 3.4.1.

(5) The "equivalent" shear stress, $\tau_{b,e,}$ is defined from the average shear stress, τ_m, measured at the adhesive-concrete interface along the bond line:

$$\tau_{b,e} = k_{id} \cdot \tau_m \tag{4.32}$$

The coefficient k_{id} (≥ 1), which accounts for the stress concentrations at the terminal zones (Appendix D), is given by the following relation:

$$k_{id} = \left(k_\sigma^{1.5} + 1.15 \cdot k_\tau^{1.5}\right)^{2/3} \tag{4.33}$$

where:

- $k_\sigma = k_\tau \cdot \beta_l \cdot t_f$,
- $k_\tau = 1 + \alpha \cdot a \cdot \dfrac{M_{(z=a)}}{V_{(z=a)} \cdot a}$,
- $M_{(z=a)}$ is the bending moment at the reinforcement termination section (Figure 4-9),
- $V_{(z=a)}$ is the shear at the reinforcement termination section, located at a distance z = a from the beam's end,
- $\alpha = \sqrt{\dfrac{K_l}{E_f \cdot t_f}}$,
- $\beta_l = \left(\dfrac{b_f \cdot 2.30 \cdot K_l}{4 \cdot E_f \cdot I_f}\right)^{1/4}$,

- $K_1 = \dfrac{1}{t_a/G_a + t_c/G_c}$,
- G_a and G_c are the shear moduli of the adhesive and concrete, respectively,
- t_a is the nominal thickness of the adhesive,
- t_c is the thickness of the concrete layer involved in the deformability of the interface (typically assumed to be between 20 and 30 mm).

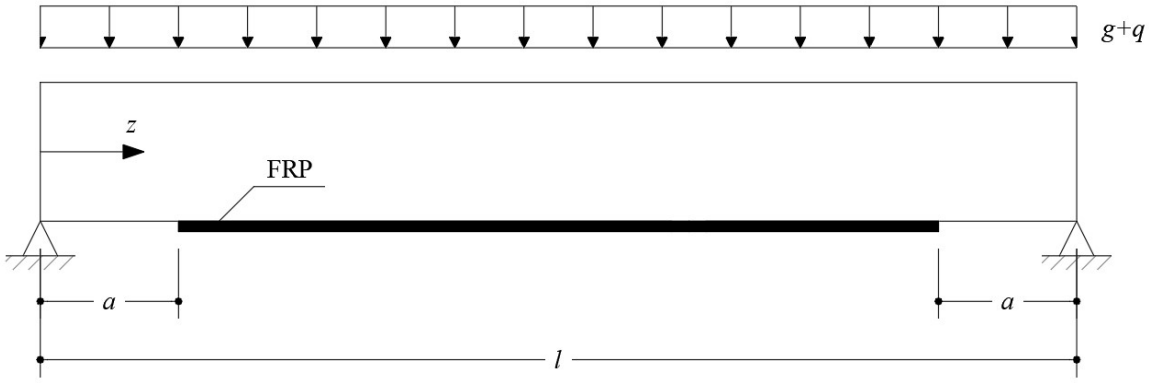

Figure 4-9 – Definition of the geometric parameters.

The average shear stress, τ_m, is calculated using Jourawski's approximation as follows:

$$\tau_m = \frac{V_{(z=a)} \cdot t_f \cdot (h - x)}{I_{2r}/\alpha_f} \tag{4.34}$$

where:

- h is the height of the section,
- I_{2r} is the moment of inertia, and x_{2r} is the corresponding distance from the neutral axis to the edge of the section at maximum compression, considering both the steel reinforcement and the external FRP reinforcement. If the section is uncracked, the moment of inertia in Equation (4.34) is the one corresponding to the homogenized uncracked section, I_{1r}, and the corresponding neutral axis distance, x_{1r};
- E_c is the compressive modulus of elasticity of the concrete.;
- $\alpha_f = E_f/E_c$ is the homogenization coefficient.

(5) If anchorages are provided at the strip ends, such as a U-wrap or fiber spike connectors, the effect of normal stresses for the interface check can be neglected. Thus, the coefficient If anchorages are provided at the strip ends, such as a U-wrap or fiber spike connectors, the effect of normal stresses for the interface check can be neglected. Thus, the coefficient k_σ can be assumed to be zero.

(6) For calculating anchorage stresses at the serviceability limit state, only the increases in the load characteristics resulting from loads applied after the reinforcement intervention should be taken into account.

4.2 ASSESSMENT OF THE RESISTANCE AGAINST DETACHMENT FROM THE SUBSTRATE OF REINFORCEMENTS INSERTED IN GROOVES (NSM)

4.2.1 General Concepts

(1) Reinforcement of concrete structures can be achieved by creating longitudinal or transverse grooves of appropriate length on the surface of the elements to be reinforced and gluing FRP plates or bars with circular or prismatic cross-sections into the grooves. The reinforcements are referred to by the acronym NSM (Near Surface Mounted).

(2) NSM reinforcements must be installed in grooves that have been roughened through surface scarification to dimensions appropriate for the reinforcement being placed inside. Installation can only be done using resin with mechanical properties superior to those of the concrete in which the reinforcement is applied.

(3) The minimum dimensions of the grooves depend on the dimensions of the reinforcement being installed, and in any case, they must be at least 2.0 mm greater than the reinforcement on each side. Figure 4-10 provides some indications of the dimensions of the grooves, d_G, and w_G, in which to insert the reinforcements, with d_F representing the diameter of the circular bar or the side of the square bar and t_F and b_F representing the thickness and height of the rectangular plate.

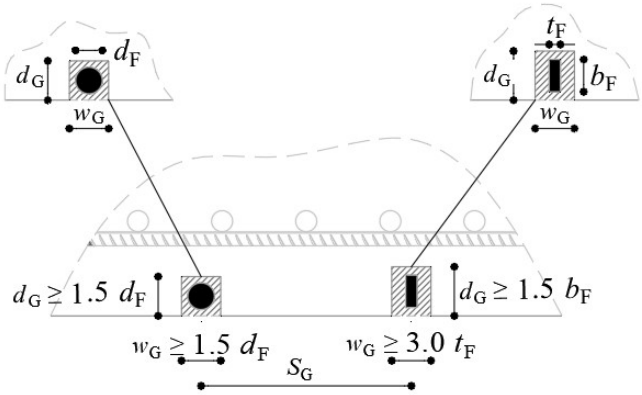

Figure 4-10 – Definition of geometric parameters in NSM reinforcements.

(4) The failure of the element reinforced with NSM systems can occur due to the detachment of the reinforcement from the substrate, which typically produces a fracture at the interface of the groove, with part of the concrete adhering to the resin used for the filling. The calculation of the detachment force can be carried out by assuming a fracture model based on a τ-s adhesion law that is trilinear (Figure 4-11). This model is characterized by two linear sections (an ascending section up to the peak shear stress and a softening section after the peak, in analogy with what is assumed for FRP-EBR systems) and by a constant section defined by a residual shear strength due to friction at the interface between the fracture surface and the intact concrete. This law closely approximates experimentally obtained adhesion laws. For technical purposes, it can be approximated with a rigid-softening law, neglecting the ascending branch and following the descending branch with a constant one, representing a residual shear strength (for details, see Appendix D).

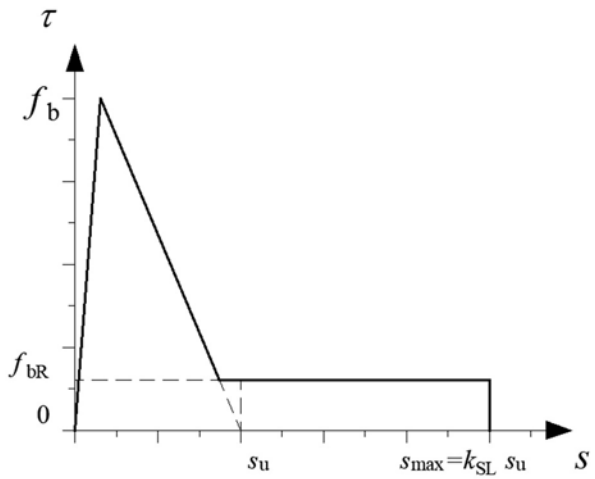

Figure 4-11 – Definition of the shear stress-slip diagram.

The average peak shear stress, f_{bm}, can be assumed to be equal to the cohesion of the concrete substrate:

$$f_{bm} = \frac{\sqrt{f_{cm} f_{ctm}}}{2 \cdot FC} \tag{4.35}$$

where f_{cm} and f_{ctm} are, respectively, the average values of the compression and tension resistances of the concrete measured in situ; the average tensile strength of the concrete is given by the minimum value between the experimentally evaluated strength (if available) and the value of f_{cm} calculated in accordance with the current standards.

The area under the rigid-softening branch of the adhesion law (variable s ranging from 0 and s_u) corresponds to a portion of the fracture energy associated with detachment from the concrete. The average value of this energy can be expressed as:

$$\Gamma_{F1m} = \frac{1}{2} \cdot s_u f_{bm} \tag{4.36}$$

In the absence of specific experimental data for a given NSM reinforcement system, s_u can be assumed to be 1.20 mm.
Similarly, in the absence of specific experimental data for a given NSM reinforcement system, the average residual shear stress, f_{bRm}, can be assumed to be equal to $f_{bRm} = k_{FR} f_{bm}$, in which $k_{FR} = 0.05$, and the maximum displacement of the adhesion law $s_{max} = k_{SL} \cdot s_u$, where $k_{SL} = 4.0$.

4.2.2 Calculation of the End Detachment Limit Force

(1) The following homogenized elastic modulus of the NSM system, composed of resin and the FRP reinforcement inserted into the groove, is introduced:

$$E_H = \frac{E_F A_F + E_R A_R}{w_G d_G} \quad , \; A_H = w_G d_G \quad , \; A_R = w_G d_G - A_F \quad , \; p_G = w_G + 2 d_G \tag{4.37}$$

Where E_R and A_R are the modulus of elasticity and area of the resin, E_F and A_F are the modulus of elasticity and area of the NSM reinforcement, w_G and d_G are the width and depth of the groove as defined earlier, and p_G is the perimeter of the groove wetted by the resin (Figure 4-10).
For the resin modulus of elasticity, E_R can be assumed $E_R = 50 f_{Rm}$, where f_{Rm} is the average compressive strength of the resin.

(2) The average and design values of the following two adhesion limit lengths, l_{e1} and l_{e2}, corresponding to the attainment of the previously defined slip values s_u and s_{max} in the adhesion law of the NSM reinforcements, are defined as follows:

$$\ell_{e1m} = \frac{\pi}{2}\sqrt{\frac{E_H A_H s_u}{p_G f_{bm}}} \quad , \quad \ell_{eld} = \gamma_{Rd} \cdot \ell_{elm} \tag{4.38}$$

$$\ell_{e2,d} = \gamma_{Rd} \cdot \ell_{e2,m} = \gamma_{Rd} \cdot \left(\ell_{e1,m} + \frac{F_{l,max,m}}{f_{bm} \cdot p_G \cdot k_{FR}} \left[\sqrt{1 + 2k_{FR}(k_{SL} - 1)} - 1 \right] \right) \tag{4.39}$$

Where $\gamma_{Rd} = 1.2$ is the model partial factor, and the other symbols are as defined earlier.

The average values of the maximum tensile forces that can be applied to each NSM reinforcement for the adhesive lengths $\ell_b = \ell_{e1m}$ is as follows:

$$F_{lm} = k_1 \sqrt{2E_H \cdot A_H \cdot p_G \cdot \Gamma_{Flm}} \tag{4.40}$$

where:

- Γ_{F1m} is the fracture energy under the rigid-softening branch of the adhesion law of the NSM reinforcement, as previously defined and given by equation (4.36);
- k_1 is an intensification coefficient for the detachment force, which, in the absence of more precise data, can be assumed to be:

$$k_1 = 0.95 \cdot \left(\frac{p_F}{p_G} \right)^{0.25} \left(\frac{f_{Rm}}{f_{cm}} \right)^{0.5} \tag{4.41}$$

in cui p_F and p_G are the perimeter of the NSM reinforcement and the perimeter of the groove wetted by the resin, respectively, and, f_{Rm} and f_{cm} are the average compressive strengths of the resin and concrete, respectively.

The average values of the maximum tensile forces that can be applied to each NSM reinforcement for the adhesive lengths $\ell_b \geq \ell_{e2,m}$ is as follows:

$$F_{2,\max,m} = F_{1,\max,m} \cdot \sqrt{1 + 2\,k_{FR}\,(k_{SL} - 1)} \tag{4.42}$$

(3) Depending on the value of the bonded length ℓ_b of the NSM FRP reinforcement, the design values of the maximum tensile forces applicable to the reinforcement are calculated as follows:

$$\text{for } \ell_b < \ell_{e1,d}: \; F_{1,d}(\ell_b) = \frac{k_{\ell_b} \cdot k_I \cdot k_{k,NSM}}{\gamma_f} \sqrt{E_H A_H \cdot p_G \cdot f_{bm} \cdot s_u} \qquad k_{\ell_b} = \frac{2\ell_b}{\ell_b + \ell_{e1d}} \tag{4.43}$$

$$\text{for } \ell_b = \ell_{e1,d}: \; F_{1,\max,d} = \frac{k_I \cdot k_{k,NSM}}{\gamma_f} \sqrt{E_H A_H \cdot p_G \cdot f_{bm} \cdot s_u} \tag{4.44}$$

$$\text{for } \ell_{e1,d} < \ell_b < \ell_{e2,d}: \; F_{2,d}(\ell_b) = F_{1,\max,d} + \left(\ell_b - \ell_{e1,d}\right) \cdot \left(\frac{F_{2,\max,d} - F_{1,\max,d}}{\ell_{e2,d} - \ell_{e1,d}} \right) \tag{4.45}$$

$$\text{for } \ell_b \geq \ell_{e2,d}: \; F_{2,\max,d} = F_{1,\max,d} \cdot \sqrt{1 + 2k_{FR} \cdot (k_{SL} - 1)} \tag{4.46}$$

where:

- $k_{k,NSM} = 0.7$ is a coefficient that provides the characteristic value (fractile 5%) of the maximum force from the average prediction given by the equation (4.40), based on the guidelines in EN1990 – Annex D - Design assisted by testing (see Appendix D);
- γ_{f3} is the partial safety factor for NSM FRP reinforcement at the Ultimate Limit State for debonding from the substrate. It should be taken as 1.30 for NSM systems consisting of ribbed, indented, or helically wrapped FRP bars (possibly sand-coated), and as 1.70 for FRP strips or bars with a smooth or sand-coated surface.

(4) The maximum stress in the reinforcement due to debonding from the substrate must be lower than the design tensile strength of the FRP element inserted into the groove. By calculating the maximum value of the force $F_{i,d}\left(\ell_b\right)$ using equation (4.43) or (4.45), depending on the bonded length ℓb, it is given by:

$$f_{\max,d}(\ell_b) = \frac{F_{\max,d}(\ell_b)}{A_F} \leq \eta_a \frac{f_{ftk}}{\gamma_{f1}} \tag{4.47}$$

Where η_a and γ_{fl} are defined in § 3.4.1.

The corresponding maximum strain in the NSM reinforcement is:

$$\varepsilon_{fdd}(\ell_b) = \frac{F_{\max,d}(\ell_b)}{E_F A_F} \geq \varepsilon_{sy} - \varepsilon_0 \tag{4.48}$$

For $\ell_b = \ell_{e1,d}$ or $\ell_b \geq \ell_{e2,d}$ the force $F_{i,d}\left(\ell_b\right)$ is determined as $F_{1,\max,d}$ or $F_{2,\max,d}$, respectively.

(5) The mean values of the maximum force in the NSM FRP reinforcement for bonded lengths $\ell_b < \ell_{e1m}$ or $\ell_{e1,m} < \ell_b < \ell_{e2,m}$, can be calculated using relations analogous to equations (4.43) and

(4.45) respectively, by using the mean values $F_{1,max,m}$ and $F_{2,max,m}$ instead of $F_{1,max,d}$ and $F_{2,max,d}$, and lengths $\ell_{e1,m}, \ell_{e2,m}$ in place of $\ell_{e1,d}, \ell_{e2,d}$.

(6) To ensure that the detachment resistance of the NSM reinforcement from the substrate is higher than the detachment resistance of the groove interface, the following inequality must hold:

$$\sqrt{\frac{f_{Rck} f_{Rtk}}{f_{cm} f_{ctm}}} \geq \frac{E_H A_H p_G}{E_F A_F p_F} \tag{4.49}$$

where f_{Rck} and f_{Rtk} are the characteristic values for compression and tensile strengths of the resin.

4.3 FLEXURAL STRENGTHENING

4.3.1 General Concepts

(1) Flexural strengthening is necessary for structural elements subjected to a design bending moment greater than the corresponding resistance. For illustrative purposes, the case of pure bending is discussed below, which occurs when the axis of loading coincides with an axis of symmetry of the cross-section of the reinforced element.

(2) Flexural reinforcement with composite materials can be realized by applying one or more preformed composite laminates to the tension side of the element to be reinforced or one or more layers of FRP or SFRP fabrics impregnated in situ. The FRP and SFRP fabrics impregnated in situ can also be anchored with one or more rows of fiber spike connectors placed symmetrically (Figure 4-12) relative to the section of maximum moment.

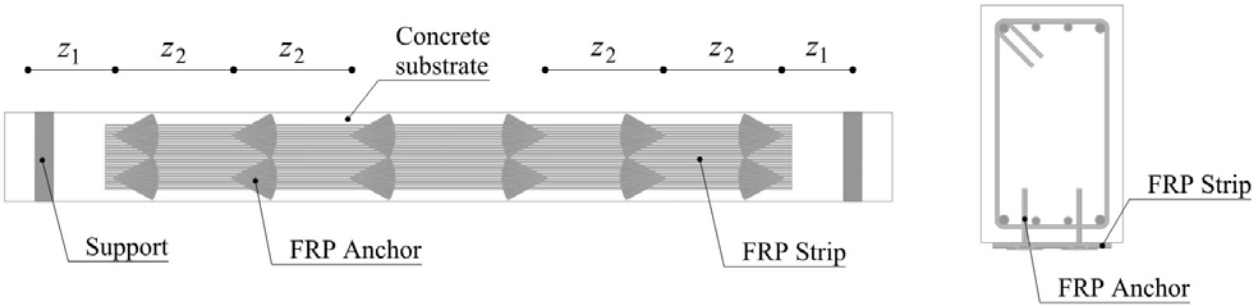

Figure 4-12 – View of the underside of the beam with EBR strips anchored with spike anchors.

(3) Both preformed FRP composites and in-situ impregnated FRP composites can be anchored by attaching metal plates to the substrate using metal post-installed anchoring devices. In this case, the anchors must be placed at a specified distance and symmetrically relative to the point of maximum bending moment.

(4) Flexural strengthening can also be achieved using the NSM technique, which involves creating one or more grooves on the tension face of the beams and inserting round or prismatic FRP elements within them. The spacing of the reinforcements must respect the limits $s_G \geq 3\ w_G$. The distance of the outermost groove from the edge must respect the limit $b_G \geq 3\ w_G$ (see Figure 4-13 for geometric characteristics).

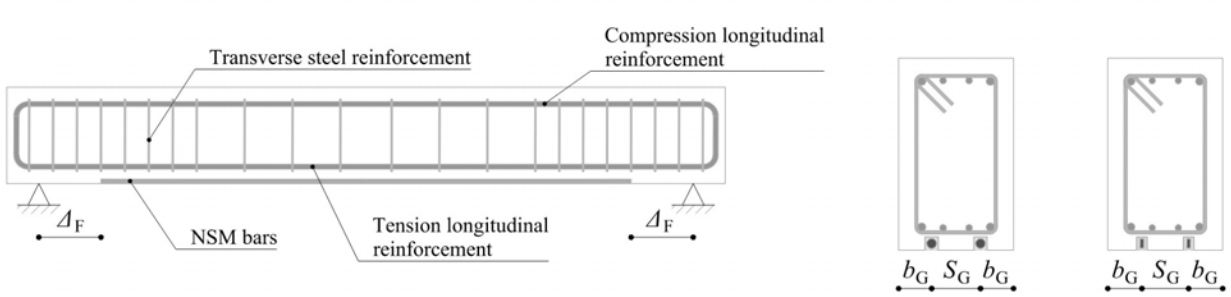

Figure 4-13 – View of the cross-section of a beam reinforced with NSM systems.

4.3.2 Analysis of the Ultimate Limit State

4.3.2.1 General Concepts

(1) The ultimate limit state design requires the determination of the amount of FRP reinforcement so that the resisting moment of the reinforced section, M_{Rd}, exceeds the design moment, M_{Sd}:

$$M_{\mathrm{Sd}} \leq M_{\mathrm{Rd}} \tag{4.50}$$

(2) The fundamental assumptions for the ultimate limit state analysis of concrete sections reinforced with FRP are as follows:

- Negligible tensile strength of concrete;
- Conservation of the flatness of the section until failure so that the diagram of normal deformations in the compressed concrete, the internal steel reinforcement, and the external FRP reinforcement remains linear;
- Perfect adhesion between concrete and internal steel reinforcement in the compressed zone;
- Constitutive laws for concrete and steel in accordance with current regulations;
- Linear elastic constitutive law for the FRP composite until failure.

(3) Reinforcement is recommended for sections with weak internal steel reinforcement (tension-controlled failure). The following rules apply to this situation or when the internal steel reinforcement reaches its yield point.

(4) It is assumed that bending failure occurs when one of the following conditions is met:

- The maximum plastic deformation in the concrete in compression, ε_{cu}, is reached, as defined by the current regulations;
- The maximum deformation in the FRP reinforcement, ε_{fd}, is reached, calculated as:

$$\varepsilon_{\mathrm{fd}} = \min\left\{\eta_{\mathrm{a}} \cdot \frac{\varepsilon_{\mathrm{fk}}}{\gamma_{\mathrm{f1}}}, \varepsilon_{\mathrm{fdd}}\right\} \tag{4.51}$$

Where $\varepsilon_{\mathrm{fk}}$ is the tensile strength of the reinforcement and γ_{f1} and η_{a} are the factors defined in Table 3-2 and Table 3-3, and $\varepsilon_{\mathrm{fdd}}$ is the maximum strain of the FRP, defined as follows:

- EBR Reinforcements**:** For the verification of sections subjected to intermediate delamination, it is assumed that $\varepsilon_{\mathrm{fdd}} = \varepsilon_{\mathrm{fdd2}}$ where $\varepsilon_{\mathrm{fdd2}}$ is given by Equation (4.13) (detachment from the

support in mode 2). For the verification of sections subjected to end delamination, it is assumed that $\varepsilon_{\mathrm{fdd}} = \frac{f_{\mathrm{fdd}}}{E_{\mathrm{f}}}$, where f_{fdd} is given by Equation (4.7) (detachment from the support in mode 1);

- NSM Reinforcements**:** The deformation $\varepsilon_{\mathrm{fdd}}$ is given by equation (4.48) as a function of the distance of the section from the end of the reinforcement.

In all cases, the maximum stress in the FRP reinforcement is equal to $f_{\mathrm{fd}} = E_{\mathrm{f}}\varepsilon_{\mathrm{fd}}$.

(7) For external FRP reinforcements with n_{z} spike anchors at the ends, the maximum stress in the reinforcement of the section at coordinate z where the flexural check is performed, with reference to the verification for detachment from the support at the ends, is defined by equation (4.15), which can be used instead of Equation (4.13) to determine the strain $\varepsilon_{\mathrm{fdd}}$ to be used in Equation (4.51). For the verification of the detachment from the support due to intermediate delamination (mode 2), the maximum strain in the FRP reinforcement is given by $\varepsilon_{\mathrm{fdd}}$ calculated according to the Equation (4.13), as this mode of failure is not affected by the presence of spike anchors at the ends.

(8) In the case of external FRP reinforcements with 2 n_{A} "bent" spike anchors positioned along the entire FRP strip at a constant pitch $\Delta z = L / (2\, n_{\mathrm{A}} - 1)$), symmetrically with respect to the section of maximum stress (generally the midspan), the detachment force increases from the end to the section at coordinate z as a function of the number of connectors n_z present in that portion of the beam. Because of equilibrium, the force at the coordinate z, cannot exceed the force calculated for the portion of the beam between the section at maximum stress with n_{A} connectors and the section at coordinate z (the portion of the beam with $n_{\mathrm{A}} - n_{\mathrm{z}}$ connectors). Therefore, if the maximum force is reached at the midspan, the maximum force that the FRP reinforcement can withstand due to the distribution of n_{A} connectors between the end and the midspan is reached at the section $z_{crit} = \left(n_{\mathrm{A,eff}} - 1\right) \cdot \Delta z$, where the end detachment force, calculated taking into account the tension f_{fdm} given by equation (4.6) and the additional contribution of the n_{z} connectors, according to equation (4.15), is equal to the intermediate detachment force, calculated at the midspan considering the contribution of the remaining $n_{\mathrm{A}} - n_{\mathrm{z}}$ connectors according to equation (4.15), where the tension f_{fdm} is replaced by $f_{\mathrm{fdm,2}}$ given by equation (4.14). Finding the section z_{crit} is equivalent to determining the number of effective connectors starting from the section of the end (the number of effective connectors, $n_{\mathrm{A,eff}} < n_{\mathrm{A}}$) that causes the equality between the two forces, where $z_{\mathrm{crit}} = \left(n_{\mathrm{A,eff}} - 1\right) \cdot \Delta z$.

Therefore, the maximum force that an FRP strip anchored with n_{A} spike bent anchors can transmit between the mid-span (or the point of maximum moment) and the end of the strip can be evaluated by determining the number of effective connectors $n_{\mathrm{A,eff}}$ as follows:

$$n_{\mathrm{A,eff}} = \frac{1}{2}\left[n_A + \frac{A_{\mathrm{f}} \cdot \left(f_{\mathrm{fdm,2}} - f_{\mathrm{fdm}} \right)}{F_{\mathrm{A,l}}} \right] \tag{4.52}$$

$$F_{\mathrm{A,l}} = \min\{N_{\mathrm{PO,m}}, N_{\mathrm{S,m}}, N_{\mathrm{FD,k}}, N_{\mathrm{FR,k}}\} \tag{4.53}$$

Where the terms $N_{\mathrm{PO,m}}$, $N_{\mathrm{S,m}}$, $N_{\mathrm{FD,k}}$, and $N_{\mathrm{FR,k}}$ are defined in Section 4.1.5 by Equations (4.18), (4.19), (4.20) e (4.24), respectively.

Given the number of effective anchors $n_{\mathrm{A,eff}}$, the maximum force in the section located at a distance z_{crit} from the end of the FRP strip can be obtained by substituting $n_{\mathrm{A,eff}}$ in place of n_z in Equation

(4.15). In this equation, the contribution of the $n_{\mathrm{A,eff}}$ anchors is added to the end debonding stress f_{fdm}, given by Equation (4.6), as follows:

$$F_{anc,\mathrm{d}} = k_{\mathrm{k}} \cdot \frac{f_{\mathrm{fd\,m}} \cdot b_{\mathrm{f}} \cdot t_{\mathrm{f}} + \left[n_{\mathrm{A,eff}} \cdot \min\{N_{\mathrm{PO,m}}, N_{\mathrm{S,m}}, N_{\mathrm{FD,k}}, N_{\mathrm{FR,k}}\} \right]}{\gamma_{\mathrm{f2}}} \leq \frac{\eta_{\mathrm{a}} \cdot f_{\mathrm{fk}}}{\gamma_{\mathrm{f1}}} b_{\mathrm{f}} \cdot t_{\mathrm{f}} \qquad (4.54)$$

The maximum resisting force given by Equation (4.54) can be considered to act throughout the portion of the beam between z_{crit} and $L/2$ (or the section of the maximum moment) since the force in the FRP strip at the section at maximum stress can only increase until debonding occurs at the critical section.

The design strain to be used in Equation (4.51) is obtained by substituting $\varepsilon_{\mathrm{fdd}}$ with the strain at the section at z_{crit}, as follows:

$$\varepsilon_{\mathrm{fdd},anc} = \frac{F_{\mathrm{anc,d}}}{E_{\mathrm{f}} \cdot b_{\mathrm{f}} \cdot t_{\mathrm{f}}} \qquad (4.55)$$

(9) In the case of externally bonded FRP strips with mechanical anchors only at the ends, referring to the verification for end support debonding (Mode 1 failure), the design stress of the reinforcement at the end is equal to the tensile rupture strength of the FRP composite based on Equation (4.29). For verification against intermediate delamination (Mode 2 failure), the maximum strain in the FRP reinforcement remains limited to the value related to debonding from the support, as given by Equation (4.13).

(10) In the case of externally bonded FRP reinforcements with mechanical anchors distributed along the entire FRP strip length, the stress in the composite can be considered constant in sections between consecutive pairs of anchors. Local equilibrium and compatibility conditions define this stress, and it can reach, at most, the tensile rupture strength of the FRP reinforcement, as given by Equation (4.29), as specified in item (8) of Section 4.1.6.

(11) It is essential to verify that the shear strength of the reinforced element is greater than that associated with the bending moment diagram of the design for which the flexural reinforcement was deemed necessary. Any required increase in shear strength must be achieved in accordance with the provisions given in Section 4.4.

4.3.2.2 Condition of the Structure at the Time of Strengthening

(1) Since FRP reinforcement is usually applied to a structure that is already subjected to loads, the deformation state of the structure at the time of strengthening must be taken into account..

(2) If the pre-existing bending moment at the time of reinforcement application, M_0, is lower than the cracking moment, the initial deformation state can be neglected.

(3) The deformation state of the structure at the time of reinforcement can be evaluated by assuming a linear elastic behavior of the two materials constituting the beam (concrete and steel), assuming the concrete in tension is ineffective.

4.3.2.3 Design Flexural Strength of an FRP-Reinforced Element

(1) The flexural strength of the reinforced section is evaluated in accordance with the assumptions specified in § **Errore. L'origine riferimento non è stata trovata.**. This is done by using the equilibrium equation for translation along the beam's axis and the equilibrium equation for rotation about the centroid of the tensile reinforcement parallel to the neutral axis.

(2) Referring to the illustrative case shown in Figure 4-14, two failure modes can be distinguished, depending on whether the maximum tensile strain in the FRP reinforcement (Zone 1) or the maximum compressive strain in the concrete (Zone 2) is reached.

(3) Zone 1 Failure – FRP Rupture: In Zone 1, failure occurs when the FRP reaches its design tensile strain limit. Any strain distribution diagram corresponding to this failure mode has the fixed reference point of the ultimate FRP strain ε_{fd}, as defined in Equation (4.51).
The strains corresponding to different fibers in the cross-section parallel to the neutral axis can be determined using the assumption of linear strain distribution through the following relationships:

- (FRP) $\varepsilon_f = \varepsilon_{fd}$,
- (concrete at the compressed edge) $\varepsilon_c = (\varepsilon_{fd} + \varepsilon_0) \cdot \frac{x}{(h-x)} \leq \varepsilon_{cu}$,
- (steel in compression) $\varepsilon_{s2} = (\varepsilon_{fd} + \varepsilon_0) \cdot \frac{x - d_2}{(h-x)}$,
- (steel in tension) $\varepsilon_{s1} = (\varepsilon_{fd} + \varepsilon_0) \cdot \frac{d - x}{(h-x)}$,

where the notation follows Figure 4-14. In particular:

- x is the distance from the neutral axis to the extreme compressed fiber of the section;
- ε_{fd} is given by Equation (4.51);
- ε_{cu} is the ultimate design strain of the concrete in compression.
- ε_0 is the pre-existing strain at the extreme tensile fiber at the time of reinforcement application, calculated as per§ 4.3.2.2.

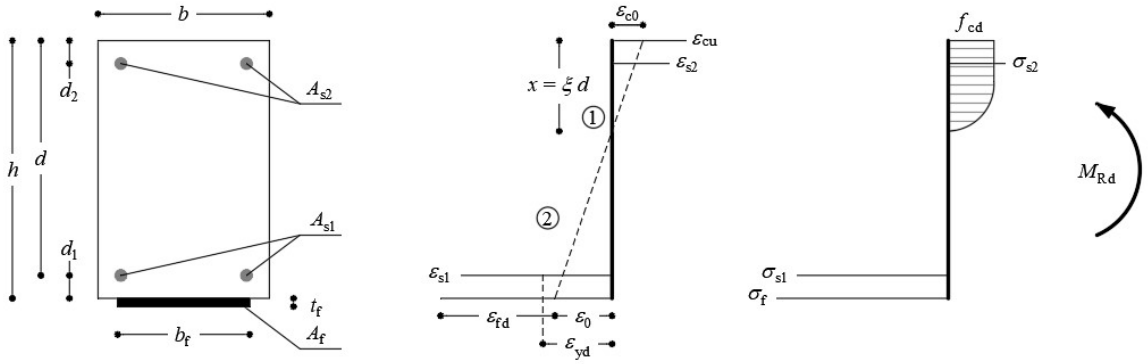

Figure 4-14 – Failure Modes of an RC Section with Externally Bonded FRP Reinforcement.

If the assumed constitutive model for steel reinforcement is bilinear with strain hardening, it is generally unnecessary to check the strain in the tensile steel at the Ultimate Limit State (ULS). This is because, for typical values of ultimate strain in FRP, ε_{fd}, and concrete, ε_{cu}, the steel strain at failure does not exceed its design limit. However, suppose the ultimate strain of the steel prescribed by current standards is exceeded. In that case, this must be accounted for in the calculation of the neutral axis position and, consequently, in determining the resisting moment.

(4) Zone 2 Failure – Concrete Crushing: In Zone 2, failure occurs due to concrete crushing while the tensile steel reinforcement has yielded, and the FRP strain does not exceed its ultimate limit. In this case, the maximum design strain in the compressed concrete, ε_{cu}, is set as a fixed value. Based on this assumption, the strains in the other materials can be determined using the principle of linear strain distribution:

- (FRP) $\varepsilon_f = \frac{\varepsilon_{cu}}{x} \cdot (h - x) - \varepsilon_0 \le \varepsilon_{fd}$,
- (Concrete at the compressed edge) $\varepsilon_c = \varepsilon_{cu}$,
- (Steel in compression) $\varepsilon_{s2} = \varepsilon_{cu} \cdot \frac{x - d_2}{x}$,
- (Steel in tension) $\varepsilon_{s1} = \varepsilon_{cu} \cdot \frac{d - x}{x}$.

(5) Neutral Axis Position and Resisting Moment Calculation: For both failure modes (neutral axis in Zone 1 or Zone 2), the neutral axis depth, *x*, is determined using the equilibrium equation for translation along the beam's axis:

$$0 = \psi \cdot b \cdot x \cdot f_{cd} + A_{s2} \cdot \sigma_{s2} - A_{s1} \cdot \sigma_{s1} - A_f \cdot \sigma_f \tag{4.56}$$

where:
f_{cd} is the design compressive strength of the existing concrete, calculated according to§ 3.3.3(6).
σ_f, σ_{s1} and σ_{s2} are the normal stresses in the FRP reinforcement, tensile steel, and compressive steel, respectively, evaluated based on the strain values determined in (3) or (4).

A reduction factor may be necessary to account for long-term strength effects in interventions on young concrete.

The design resisting moment, M_{Rd}, is determined using the equilibrium equation for rotation about the centroid of the tensile reinforcement parallel to the neutral axis:

$$M_{Rd} = \frac{1}{\gamma_{Rd}} \cdot \left[\psi \cdot b \cdot x \cdot f_{cd} \cdot (d - \lambda \cdot x) + A_{s2} \cdot \sigma_{s2} \cdot (d - d_2) + A_f \cdot \sigma_f \cdot d_1 \right] \tag{4.57}$$

where the model partial factor γ_{Rd} is taken as 1.00 (Table 3-2, § 3.4.2).

In Equations (4.56) and (4.57), the dimensionless coefficients ψ and λ represent:

- ψ, the intensity of the resultant compressive force, expressed as a fraction of f_{cd}.
- λ, the normalized distance of the resultant of the compressive force from the most compressed fiber, expressed as a fraction of *x*.

For Zone 2 failure, these coefficients take fixed values:

- $\psi = 0.8095$
- $\lambda = 0.4160$,

These values correspond to a fully developed compressive stress-strain relationship in the concrete,

where $\varepsilon_c = \varepsilon_{cu}$.

4.3.2.4 Design Flexural Strength of an FRP-Reinforced Element Under Axial Force (Combined Axial and Bending Forces)

(1) The principles and application rules introduced in § 4.3.2.1**Errore. L'origine riferimento non è stata trovata.**, from point (1) to point (5), remain valid. Additionally, the design value of the resisting moment of the reinforced section, M_{rd}, must be considered in relation to the applied axial force, N_{Sd}.

(2) The effectiveness of the reinforcement in the nodal regions must be ensured by adopting appropriate construction solutions that provide both adequate anchorage of the composite and the proper transfer of tensile forces from the reinforcement to the node. Furthermore, the flexural-compression strengthening system must be designed to ensure that failure occurs due to FRP rupture rather than premature debonding from the substrate. This condition can be achieved, for example, through transverse confinement. Consequently, the ultimate strain $\varepsilon_{\mathrm{fd}}$ can be taken as the first term in parentheses in Equation (4.51).

The achievement of these structural objectives must be validated through appropriate experimental investigations.

(3) The application rules introduced in § 4.3.2.3, from point (2) to point (6), remain valid, with the only modification being that the applied axial force, N_{Sd}, must be included in the left-hand side of the Equation (4.56).

(4) As an alternative to the approach outlined in point (5) of § 4.3.2.3. The simplified method described in Appendix E can be used to determine the design flexural strength of an FRP-strengthened element under axial force.

4.3.2.5 Identification of the FRP Anchorage Section

(1) End debonding depends on various factors, including the location of crack formation, the type of cracks (shear and/or flexural cracks), irregularities on the substrate surface, and stress concentrations in the anchorage zones.

(2) For reinforced concrete flexural elements strengthened with externally bonded reinforcement (EBR) systems, once the section requiring FRP reinforcement to increase flexural strength is identified (defined as the anchorage section), it must be verified that the tensile stress in the reinforcement, due to the applied moment under the Ultimate Limit State (ULS) load combination, does not exceed the maximum allowable end debonding stress (Mode 1), f_{fdd}, given by Equation (4.5). Alternatively, it must be verified that the applied moment in this section under the ULS load combination, M_{sd}, is less than the resisting moment, M_{rd}, of the strengthened section, where the FRP strain in Equation (4.51) corresponds to the end debonding strain, $\varepsilon_{\mathrm{fdd}} = \frac{f_{\mathrm{fdd}}}{E_{\mathrm{f}}}$.
If the verification at the identified anchorage section is not satisfied, it must be shifted to a location with a lower applied moment. Alternatively, end anchorage systems may be implemented to increase the maximum allowable tensile stress in the reinforcement for end debonding, according to Equation (4.16**)** for splayed connectors or Equation (4.29) for mechanical connectors.

(3) For EBR systems, in addition to the anchorage section identified in point (2), an additional bonded length of reinforcement must be provided, at least equal to the optimal anchorage length, ℓ_{ed}, defined

in Equation (4.1); this ensures that the verifications at the anchorage section (located at least ℓ_{ed} from the reinforcement end) can be performed using the end debonding stress, f_{fdd}, given by Equation (4.5) (or Equation (4.16) for splayed connectors, or Equation (4.29) for mechanical connectors).
If a bonded length is smaller than ℓ_{ed}, the verification of the anchorage section must be conducted by replacing f_{fdd} with $f_{fdd,Rid}$ given in Equation (4.11).

(4) For EBR systems, if verification at the anchorage section is not performed as described in point (2), then:

- For continuous beams, the anchorage section must coincide with the point of zero moment.
- For simply supported beams, the anchorage section must coincide with the section where the applied moment under the ULS load combination reaches the cracking moment of the section.

In both cases, beyond these sections, an additional bonded length of reinforcement must be provided, at least equal to the optimal anchorage length, ℓ_{ed}, as defined in Equation (4.1).

(5) For Near-Surface Mounted (NSM) FRP reinforcement, the maximum stress values in the reinforcement leading to debonding failure are given by Equation (4.48), which provides the stress values as a function of any distance from the reinforcement end. Therefore, at any section along the beam, the resisting moment of the NSM-strengthened section can be determined using the reinforcement stress from Equation (4.47), and it must be verified that this moment is greater than the applied moment at the same section.

(6) If the reinforcement end is located in a region primarily subjected to shear forces, which may induce inclined cracks, the applied moment at the anchorage section must be determined by considering an appropriate shift of the bending moment diagram by a distance a_1. This shift must be applied in the direction that increases the absolute value of the bending moment (Figure 4-15).

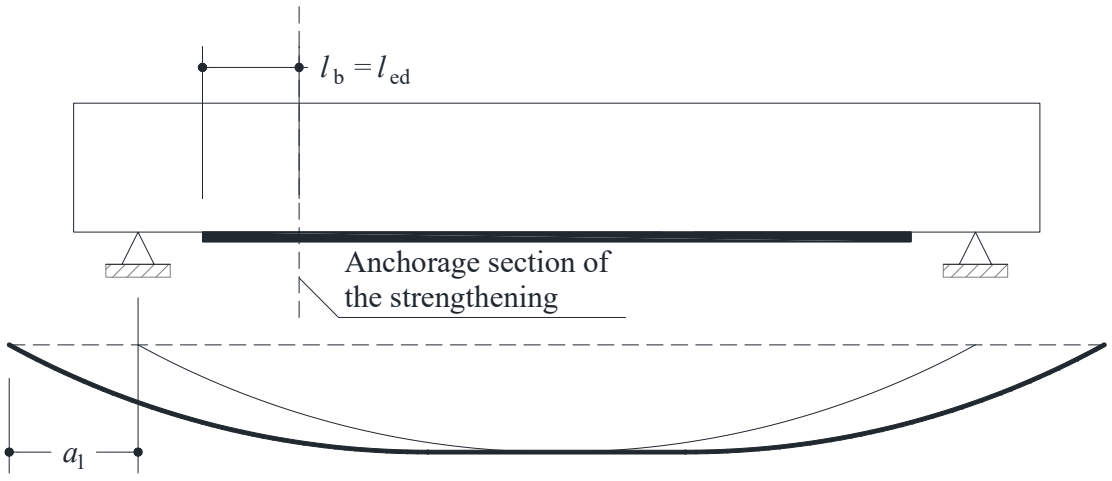

Figure 4-15 – Shift of the Bending Moment Diagram.

From a practical standpoint, the design applied moment must generally be increased by the following amount:

$$M = V_{Sd} \cdot a_1 \tag{4.58}$$

where:

- V_{Sd} is the design shear force,
- $\alpha_1 = 0.9d \cot \alpha$,
- α is the inclination of the shear reinforcement,
- d is the effective depth of the section.

4.3.3 Serviceability Limit State

4.3.3.1 Basis of Calculation

This section considers the following Serviceability Limit States (SLS):

- Stress limitation (§4.3.3.2);
- Deflection control (§4.3.3.3);
- Crack control (§4.3.3.4).

Other serviceability limit states not explicitly listed in these guidelines may also be relevant in specific situations.

(1) Under service loads, the following verifications must be performed:

- Stress levels in the materials must be appropriately limited to prevent steel yielding and mitigate the effects of creep in both the concrete and the external reinforcement.
- Deformations and deflections must remain within acceptable limits to ensure proper structural functionality, prevent damage to non-structural elements, and avoid psychological discomfort for users.
- Cracking must be controlled appropriately since excessive or widely spaced cracks could significantly reduce the structure's durability and functionality, compromise its appearance, and weaken the bond at the FRP-concrete interface.

(2) Serviceability verifications must account for any pre-existing deformations at the time of reinforcement application. The assumptions underlying the calculations include:

- Preservation of plane sections: cross-sections remain plane during deformation.
- Linear elastic behavior of both the steel reinforcement and the FRP reinforcement.
- Linear elastic behavior in compression for concrete, with limited capacity to resist tensile stresses, potentially considering the effects of tension stiffening.
- Equal strain compatibility among concrete fibers, steel reinforcement, and FRP reinforcement at the same depth.

(3) These assumptions establish proportional relationships between stresses in different materials:

- In the compressed zone, the stress in the steel reinforcement and the stress in the adjacent compressed concrete fibers follow the relation:

$$\frac{\sigma_{\mathrm{s}}}{\sigma_{\mathrm{c}}} = \frac{E_{\mathrm{s}}}{E_{\mathrm{c}}} = \alpha_{\mathrm{s}}$$

- In the tensile zone, the stresses in the steel reinforcement, FRP reinforcement, and adjacent tensile concrete fibers follow:

$$\frac{\sigma_s}{\sigma_c} = \frac{E_s}{E_c} = \alpha_s,\ \frac{\sigma_f}{\sigma_c} = \frac{E_f}{E_c} = \alpha_f$$

These ratios are known as homogenization coefficients.

The values of the homogenization coefficients must be determined while considering the long-term evolution of concrete deformations. This requires distinguishing between short-term and long-term verifications based on the assumed service load combination (e.g., rare or quasi-permanent load combinations).

In the calculation of stresses and deflections, it may also be necessary to account for additional effects, including:

- Thermal variations
- Creep effects
- Shrinkage
- Other potential distortions.

4.3.3.2 Stress Verification

(1) For the characteristic (or rare) load combination**,** the stresses in the materials must satisfy the following limitations:

$$\begin{aligned} \sigma_c &\le 0.60 f_{ck} \\ \sigma_s &\le 0.80 f_{yk} \\ \sigma_f &\le 0.80 f_{yk} \cdot \frac{E_f}{E_s} \end{aligned} \tag{4.59}$$

(2) For the quasi-permanent load combination, the stresses in the fiber-reinforced composite must meet the following limitations:

$$\sigma_f \le \eta \cdot f_{fk} \tag{4.60a}$$

where:

- f_{fk} is the characteristic tensile strength of the reinforcement,
- η is the conversion factor, with values suggested in §3.5.

Under this load combination, it must also be verified that the maximum compressive stress in the concrete does not exceed the following:

$$\sigma_c \le 0.45 f_{ck} \tag{4.61b}$$

(3) Effect of Pre-Existing and Additional Moments

If a moment M_0 is acting on the section at the time of reinforcement application—where M_0 has

already caused cracking in the section—and an additional moment ΔM results from loads applied after reinforcement, the total moment $M=M_0+\Delta M$ can be used to determine stresses additively as follows:

- Compressive stress in concrete:

$$\sigma_c = \sigma_{c0} + \Delta\sigma_c, \qquad \sigma_{c0} = \frac{M_0}{I_2} x_2, \qquad \Delta\sigma_c = \frac{\Delta M}{I_{2r}} x_{2r}; \tag{4.62}$$

- Tensile stress in steel reinforcement:

$$\sigma_s = \sigma_{s0} + \Delta\sigma_s, \qquad \sigma_{s0} = \frac{\alpha_s \cdot M_0}{I_2} \left(d - x_2\right), \qquad \Delta\sigma_s = \frac{\alpha_s \cdot \Delta M}{I_{2r}} \left(d - x_{2r}\right); \tag{4.63}$$

- Tensile stress in the FRP reinforcement:

$$\sigma_f = \frac{\alpha_f \cdot \Delta M}{I_{2r}} \left(h - x_{2r}\right) \cdot \tag{4.64}$$

With reference to Figure 4-14, the variables in the above equations are defined as follows:

- I_2 is the moment of inertia of the cracked RC section without external FRP reinforcement, with steel reinforcement homogenized using α_s.
- x_2 is the corresponding distance from the neutral axis to the extreme compressed fiber.
- I_{2r} è is the moment of inertia of the cracked RC section with both steel and external FRP reinforcement, homogenized using α_s and α_f, respectively.
- x_{2r} is the corresponding distance from the neutral axis to the extreme compressed fiber.
- h is the overall height of the section, and d is its effective depth.
- α_s and α_f are the homogenization coefficients, defined as:

$$\alpha_s = \frac{E_s}{E_c}, \ \alpha_f = \frac{E_f}{E_c}$$

where

- E_c is the elastic modulus of concrete, which may be taken as an effective modulus to account for time-dependent deformations using the relation:

$$E_{c,eff} = \frac{E_c}{1+\varphi(t,t_0)},$$

where $\varphi(t,t_0)$ s the creep coefficient of concrete, to be determined based on the applicable standards or other validated recommendations.

For a simplified approach, when calculating stresses, the creep coefficient can be assumed as $\varphi(t,t_0) = 1$ to compute the values of α_s and α_f used in the moment of inertia calculations and Equations (4.63) and (4.64).

If the bending moment M_0 is lower than the cracking moment M_{cr} of the section, the initial stresses σ_{c0} and σ_{s0} must be calculated using:

- The moment of inertia I_1 of the uncracked RC section without FRP reinforcement and
- The corresponding neutral axis depth is x_1.

4.3.3.3 Deflection Verification

(1) Structures strengthened with FRP must comply with the deflection limitations imposed by current regulations.

(2) The adopted mechanical model must accurately simulate the structure's actual behavior, ensuring a level of precision appropriate for the design objectives**.** In particular, the model must account for the possible presence of cracking and its effects on the deformation of both the tensile and compressed regions of the section.

(3) Where appropriate, the mechanical model should consider the following factors:

- Effects of creep and shrinkage;
- Stiffening effect of the tensioned concrete between cracks;
- Pre-existing cracks caused by loads applied before reinforcement installation;
- Influence of other potential distortions, such as those due to thermal effects;
- Loading conditions, whether static or dynamic;
- Appropriate modulus of elasticity for concrete, considering its curing stage at the time of loading.

(4) Integrating the curvature diagram can perform a Deflection calculation for reinforced concrete beams strengthened with FRP. Curvatures can be determined through a nonlinear analysis that accounts for cracking and the stiffening effect of the tensioned concrete. In nonlinear deflection calculations, the principle of superposition does not apply.

(5) Alternatively, simplified analysis methods can be used, similar to those applied to conventional reinforced concrete sections, including the following equation:

$$f = f_1 \cdot (1-\gamma) + f_2 \cdot \gamma$$
$$\gamma = 1 - \beta \left(\frac{M_{cr}}{M_{max}} \right)^2 \tag{4.65}$$

where:

- f_1 and f_2 are the deflections calculated assuming an uncracked and a cracked section, respectively, based on the chosen service load combination;
- γ is the tension-stiffening coefficient, where:
- β accounts for the type of load and is taken as 1.0 for short-term loads and 0.5 for long-term or repeated cyclic loads;
- M_{cr} is the cracking moment of the RC section;
- M_{max} is the maximum applied moment in the most stressed section, evaluated based on the characteristic load combination (since this represents the highest moment experienced during the structure's service life).

Effect of Pre-Existing and Additional Moments

If a moment M_0 is acting on the section at the time of reinforcement application and an additional moment ΔM results from loads applied after reinforcement, the total moment $M = M_0 + \Delta M$, can be used to determine deflections f_1 and f_2 at the most stressed section under the service load combination.

Deflections can be evaluated using an elastic analysis of the section, considering:

- For f_1,
  - The loads corresponding to M_0 applied to the uncracked section without external FRP reinforcement (moment of inertia I_1)
  - The loads corresponding to ΔM applied to the uncracked section with external FRP reinforcement (moment of inertia I_{1r}).
  - It is noted that for calculating I_1 and $I_{1r,}$ the contribution of both internal steel reinforcement and external FRP may be neglected.
- For f_2,
  - The loads corresponding to M_0 applied to the cracked section without external FRP reinforcement (moment of inertia I_2)
  - he loads corresponding to ΔM applied to the cracked section with external FRP reinforcement (moment of inertia I_{2r}).

Example: Simply Supported Beam with a Central Point Load or Uniform Load

For a simply supported beam subjected to either a central point load or a uniformly distributed load, the deflections f_1 and f_2, induced by the total moment $M = M_0 + \Delta M$, can be expressed as:

$$f_1 = k \cdot l^2 \left(\frac{M_0}{E_c I_1} + \frac{\Delta M}{E_c I_{1r}} \right)$$
$$f_2 = k \cdot l^2 \left(\frac{M_0}{E_c I_2} + \frac{\Delta M}{E_c I_{2r}} \right) \quad (4.66)$$

in cui:

- $k = 1/$ for a central point load, and $k = 40/384$ for a uniformly distributed load;
- E_c is the elastic modulus of concrete, which may be adjusted as:

  $$E_{c,eff} = \frac{E_c}{1 + \varphi(t, t_0)}$$

  to account for creep effects based on the selected service load combination. The creep coefficient $\varphi(t, t_0)$ must be determined in accordance with current standards or other validated recommendations.
- l is the span length of the beam.

4.3.3.4 Crack Width Verification

(1) To protect the internal steel reinforcement and ensure the serviceability of structural elements, appropriate limits on crack widths must be established under service conditions.

The load combinations used for crack width calculations and the corresponding allowable limits may be taken from current standards or other validated guidelines for reinforced concrete structures.

(2) The literature has developed several empirical formulations to modify existing equations for conventional reinforced concrete sections, incorporating the effects of external reinforcement.

In particular, similar to the formulations for reinforced concrete elements, and removing the assumption of equal strain between concrete, steel reinforcement, and FRP in the tensile zone, the design crack width for an externally FRP-strengthened reinforced concrete element can be calculated as:

$$w_k = k_{1/r} \cdot s_{r,max} \cdot \left(\varepsilon_{sm} - \varepsilon_{cm}\right) \tag{4.67}$$

Where:

- $k_{1/r} = \dfrac{h - x_{2r}}{d - x_{2r}}$ is a factor accounting for beam curvature effects on crack width, with
  - h = total section height,
  - d = effective depth,
  - x_{2r} = depth of the neutral axis from the compressed edge in the cracked section, considering both internal steel reinforcement and external FRP reinforcement, as previously defined.

The maximum crack spacing, $\boldsymbol{s_{r,max}}$, in the presence of external FRP reinforcement can be estimated as:

$$s_{r,max} = \beta_w \cdot \left(k_c c + k_{\phi/\rho} \cdot k_{fl} \cdot k_b \frac{f_{ctm} \cdot \phi_s}{\tau_{bms} \cdot \rho_{s+FRP,ef}} \right) \tag{4.68}$$

where:

- β_w =1.7 (for stabilized cracking conditions) converts average crack spacing to maximum crack spacing.
- k_c =1.5 is an empirical coefficient.
- c is the maximum concrete cover (excluding bar diameters) in either the vertical or horizontal direction.
- $k_{\phi/\rho}$ =0.25, a coefficient related to shear stress distribution (assuming uniform stress).
- k_{fl} accounts for stress distribution before cracking, defined as::

  $$k_{fl} = \frac{h - h_{c,ef}}{h},$$

  where $h_{c,ef}$ is the effective tensile concrete height, defined later.
  - For pure flexure, k_{fl} is calculated using the equation above.
  - For pure tension, k_{fl} = 1.0;
- k_b accounts for the bond quality of internal steel reinforcement, with:
  - k_b = 0.9 for bottom reinforcement (poor bond conditions),

- k_b = 1.2 for poor bond conditions (e.g., top bars, smooth bars).

- f_{ctm} is the mean tensile strength of concrete.
- ϕ_s is the diameter of internal steel reinforcement bars**.**
- For mixed bar sizes (n_1 bars of diameter and ϕ_1 e bars of diameter ϕ_2), an equivalent diameter is used:

$$\phi_{eq} = \frac{n_1\phi_1^2 + n_2\phi_2^2}{n_1\phi_1 + n_2\phi_2} \tag{4.69}$$

- τ_{bms} is the mean bond stress at the steel-concrete interface, calculated as:

$$\tau_{bms} = 1.8 \cdot f_{ctm};$$

- $\rho_{s+FRP,ef}$ is the effective reinforcement ratio, given by:

$$\rho_{s+FRP,ef} = \frac{A_s + \xi_1^2 \cdot A_f}{A_{c,ef}} \tag{4.70}$$

where:

- A_s = area of internal steel reinforcement.
- A_f = area of external FRP reinforcement.
- ξ_1^2 is a dimensionless coefficient defined as:

$$\xi_1^2 = \frac{\tau_{bmf}}{\tau_{bms}} \cdot \frac{A_s}{u_s} \cdot \frac{u_f}{A_f} \tag{4.71}$$

where

- u_s and u_f are the perimeters in contact with concrete for steel reinforcement and FRP reinforcement, respectively.

Crack Width Considerations for Different FRP Strengthening Systems

- For Externally Bonded Reinforcement (EBR) systems**:**
  since $\mathbf{A_f = b_f t_f}$, and $\boldsymbol{u_f = b_f}$, the effective reinforcement ratio simplifies to:

$$\xi_1^2 = \frac{\tau_{bmf}}{\tau_{bms}} \cdot \frac{\phi_s}{4t_f} \tag{4.72}$$

where t_f is the total thickness of the FRP reinforcement system, and τ_{bmf} is the mean bond stress at the FRP-concrete interface.

- For Near-Surface Mounted (NSM) strip systems**:**

Given $\boldsymbol{A_f = n_f b_f t_f}$, and $\boldsymbol{u_f = n_f 2 b_f}$, with b_f, t_f e n_f as the width, thickness, and number of NSM strips**,** respectively, the reinforcement ratio is:

$$\xi_1^2 = \frac{\tau_{bmf}}{\tau_{bms}} \cdot \frac{\phi_s}{2t_f} \tag{4.73}$$

- For Near-Surface Mounted (NSM) bar systems**:**

  Given $\boldsymbol{A_f = n_f \frac{\pi \phi_f^2}{4}}$, and $\boldsymbol{u_f = n_f \pi \phi_f}$, with $\boldsymbol{\phi_f}$ and $\boldsymbol{n_f}$ as the diameter and number of NSM FRP bars**,** respectively, the reinforcement ratio is:

$$\xi_1^2 = \frac{\tau_{bmf}}{\tau_{bms}} \cdot \frac{\phi_s}{\phi_f} \tag{4.74}$$

Finally, τ_{bmf} is the mean bond stress at the FRP-concrete interface, given as::

$$\tau_{bmf} = 1.8 f_{ctm} \qquad \textit{(}\text{for NSM systems}\textit{)} \tag{4.75}$$

$$\tau_{bmf} = 1.0 f_{ctm} \qquad \textit{(}\text{for EBR systems}\textit{)} \tag{4.76}$$

In Equation (4.70), The effective tensile concrete area (see Figure 4-16) is given by:

$$A_{c,ef} = b \cdot h_{c,ef} \tag{4.77}$$

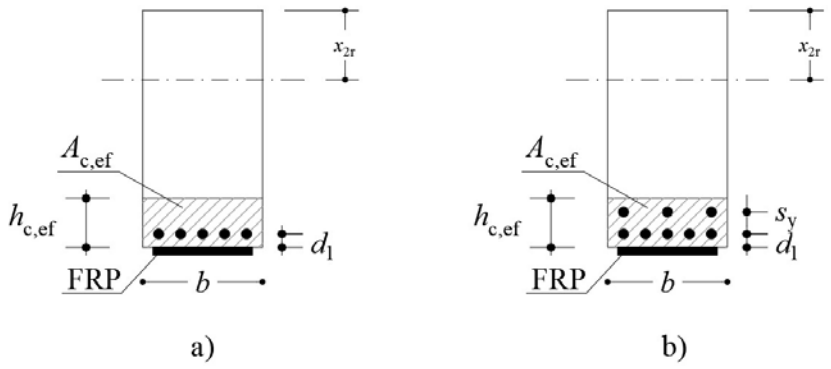

Figure 4-16 – Definition of the Effective Tensile Concrete Area:
(a) Single reinforcement layer; (b) Multiple reinforcement layers.

The effective height of this area, $h_{c,ef}$, is calculated as:

- For a single layer of bars (Figure 4-16.a):

$$h_{c,ef} = \min\left\{a_y + 5\phi_s; 10\phi_s; 3.5a_y; h - x_{2r}; h/2\right\} \tag{4.78}$$

- For multiple (*n)* reinforcement layers spaced s_y apart in the vertical direction (Figure 4-16.b):

$$h_{c,ef} = \min\left\{\min(a_y + 5\phi_s; 10\phi_s; 3.5a_y) + (n-1)s_y; h - x_{2r}; h/2\right\} \tag{4.79}$$

where

- a_y is the mechanical cover (measured from the center of the internal steel bars to the section's lower edge).

In Equation (4.67), the difference in average strain between the internal steel reinforcement and the tensioned concrete in the region between two consecutive cracks can be calculated as:

$$\varepsilon_{sm} - \varepsilon_{cm} = \left(\frac{\sigma_s}{E_s} - k_t \frac{f_{ctm}}{E_s \cdot \rho_{s+FRP,ef}} + k_t \frac{f_{ctm}}{E_c} \right) \geq \frac{\sigma_s}{E_s}(1 - k_t) \tag{4.80}$$

where:

- σ_s = stress in the internal steel reinforcement under the selected service load combination**.**
  - To be computed for a cracked section as per 4.2.1;
  - The stress σ_s, moment of inertia I_{2r}, and neutral axis depth x_{2r} may be adjusted for concrete creep effects using:

$$\boldsymbol{E_{c,eff} = \frac{E_c}{1 + \varphi(t, t_0)}}$$

- E_s = elastic modulus of internal steel reinforcement.
- E_c = elastic modulus of concrete (without creep effects)
- k_t is a coefficient that depends on load duration and nature
  k_t = 0.6 for short-term or instantaneous loads
  k_t = 0.4 for long-term or repeated cyclic loads

(3) More advanced models may be adopted, provided they are validated by experimental research.

4.3.4 Ductility

(1) The ductility of flexural elements, defined as their ability to undergo plastic deformation, depends on both the behavior of the section and the actual failure mode of the structural element as a whole.

A more ductile response is achieved when the tensile steel reinforcement yields and the curvature of the strengthened element at incipient failure is high.

If FRP debonding occurs before the yielding of the tensile steel reinforcement, ductility is effectively absent.

4.4 SHEAR STRENGTHENING

4.4.1 General Considerations

(1) Shear strengthening is required for structural elements where the design shear force—potentially evaluated using capacity design principles—exceeds the corresponding design shear resistance. The latter must be determined by considering both the contribution of concrete and any existing transverse steel reinforcement.

(2) Shear strengthening is verified only for the Ultimate Limit States (ULS).

(3) Different shear-strengthening configurations can be used, but the same type of reinforcement must be applied consistently within each structural element. Available options include:

- Laminates,
- Wet-layup fabric systems,
- FRP elements are inserted into grooves symmetrically and applied to the external surfaces of the structural element.

Alternatively, individual reinforcement elements—such as bars, laminates, or splayed fiber ropes—can be inserted into pre-drilled holes of specified geometry, filled with resin, within the structural core.

Note:
To date, shear strengthening of reinforced concrete (RC) and prestressed concrete (PC) elements using FRP systems remains uncommon. The scientific and technical literature on this subject is still limited.

4.4.2 Shear Strengthening Configurations

(1) Externally Bonded Reinforcement (EBR) for shear strengthening is applied by bonding one- or two-dimensional composite elements (typically fabrics) onto the external surface of the structural member (Figure 4-17). These elements consist of one or more layers of FRP material.

For one-dimensional reinforcement, composite strips can be placed:

- Adjacent to each other (continuous layout) or
- Discontinuously (spaced apart).

A similar configuration can be adopted for Near-Surface Mounted (NSM) reinforcement (Figure 4-18) where FRP strips are:

- Inserted into grooves cut into the external surface of the structural element or
- Embedded in holes drilled through the structural core.

.

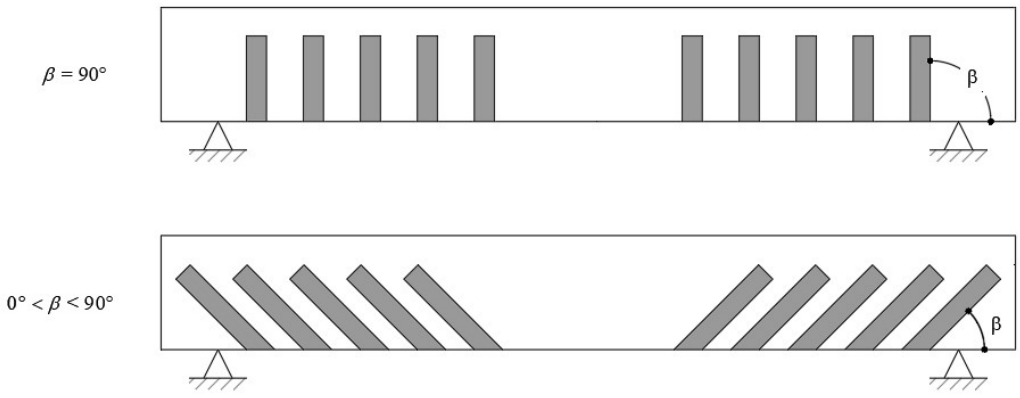

Figure 4-17 – Shear strengthening orientations using composite strips.

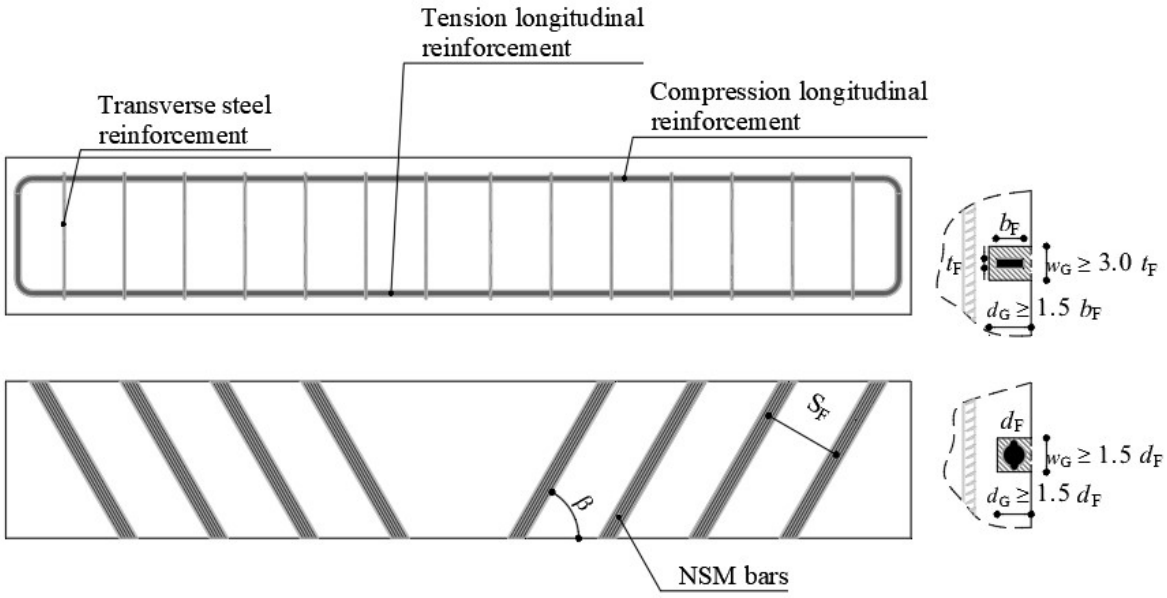

Figure 4-18 – Shear strengthening using NSM elements applied to vertical faces.

(2) Key design parameters for shear strengthening systems include:

- Geometry (thickness, width, and spacing of the composite strips adhered to the strengthened member), and
- Fiber orientation angle relative to the longitudinal axis of the element.

(3) Shear reinforcement can be arranged around the section in the following ways (Figure 4-19):

- U-jacketing, or
- Complete wrapping.

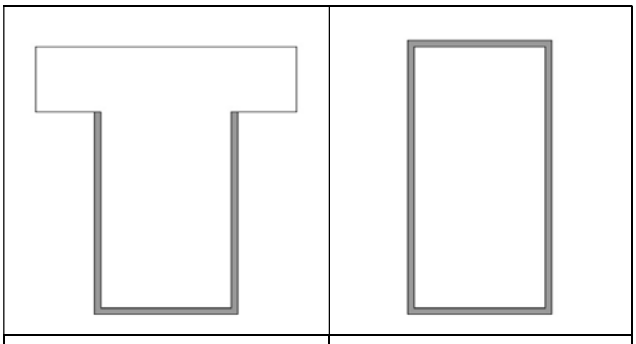

Figure 4-19 – Shear strengthening layouts around the section.

(4) For U-jacketing configurations applied to rectangular or T-sections, the effectiveness of the anchorage at the free ends of the FRP reinforcement - which is not fully wrapped around the section - can be improved using:

- Splayed fiber connectors or
- Mechanical end anchors for external stirrups.

If the effectiveness of these anchorage solutions is experimentally demonstrated, the behavior of a U-jacketed system can be considered equivalent to a fully wrapped system.

(5) For bars or splayed fiber cord anchors inserted into pre-drilled holes within the structural core, the efficacy of the strengthening system can be enhanced by:

- Flaring the fibers at the ends (fan-shaped anchorage) or
- An enlarged resin sleeve at both reinforcement ends is created to improve anchorage capacity.

4.4.3 Design Shear Strength of an FRP-Strengthened Element

4.4.3.1 Design Strength

(1) The design shear strength of the FRP-strengthened element can be calculated by adding the contribution of the FRP shear reinforcement, as calculated in points (2) and (4), to the shear capacity of the unstrengthened element, evaluated in accordance with the applicable standards.

Taking into proper account the ductility of the materials, the shear-tension contribution of the FRP reinforcement, expressed by equation (4.81) or (4.82), must be added to the shear-tension contribution of the existing transverse steel reinforcement. In any case, it must be ensured that the sum of the contributions of the two reinforcements does not exceed the shear-compression capacity of the concrete web, which is to be evaluated in accordance with the applicable standards.

.(2) For U-wrapped or fully wrapped FRP reinforcement on a rectangular section, the shear contribution of the FRP system, $V_{\mathrm{Rd,f}}$, can be evaluated using Mörsch's truss analogy, with the following equation:

$$V_{\mathrm{Rd,f}} = \frac{1}{\gamma_{\mathrm{Rd}}} f_{\mathrm{fed}} A_{\mathrm{fv}} \frac{0.9d}{\overline{p}_{\mathrm{f}}} (\cot\theta + \cot\beta)\sin\beta = \\ = \frac{1}{\gamma_{\mathrm{Rd}}} f_{\mathrm{fed}} A_{\mathrm{fv}} \frac{0.9d}{p_{\mathrm{f}}} (\cot\theta + \cot\beta)\sin^2\beta \tag{4.81}$$

where (Figure 4-20):

- d = effective depth of the section,
- f_{fed} = effective design strength of the FRP system, evaluated according to § 4.4.3.2,
- A_{fv} = shear-resisting area of the FRP stirrups, calculated as:
  - $A_{\mathrm{fv}} = 2b_{\mathrm{f}}t_{\mathrm{f}}$ for externally bonded strips,
  - $A_{\mathrm{fv}} = 2A_{\mathrm{f}}$ for NSM bars embedded in external grooves,
- p_{f} = spacing of strips or bars, measured perpendicular to the fiber direction.
  - If the FRP strips are continuous or in a 2D reinforcement system, assume $\frac{b_{\mathrm{f}}}{p_{\mathrm{f}}} = 1.0$

- γ_{Rd} = partial factor, provided in Table 3-2, § 3.4.2,

- β = angle of fiber orientation relative to the beam's longitudinal axis.
- θ is the inclination of the concrete struts with respect to the element's axis.

Based on the reference to the ductility of the materials, the angle θ can be conservatively assumed to be equal to 45° for the calculation of the shear–tension capacity of both the existing steel transverse reinforcement and the FRP shear strengthening system. Where applicable, the contribution of the concrete's resistant mechanisms can also be considered, following validated references.
Even in the presence of a compressive force, as in the case of columns, the angle θ can still be conservatively assumed to be equal to 45°, and the contribution of the axial compressive force can be considered, in accordance with validated methodologies.

Alternatively, the angle θ may be evaluated by considering the axial force acting on the element and may therefore be lower than 45°.

In equation (4.81), the spacing p_f can be measured perpendicular to the fiber direction instead of along the beam axis $\overline{p_f}$ (Figure 4-20), , using the equation $\overline{p}_f = p_f / \sin\beta$.

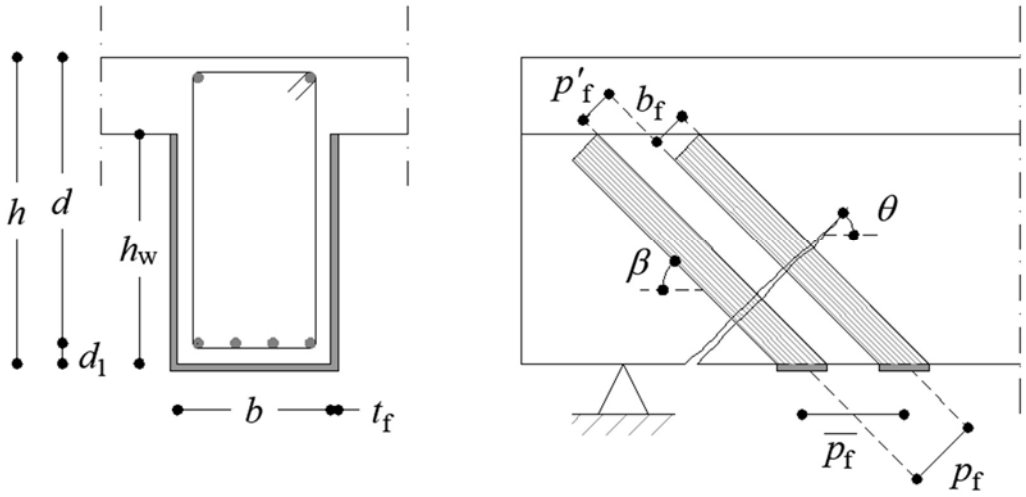

Figure 4-20 – Key Parameters for Shear Strengthening with FRP Strips.

(3) For discontinuous FRP strip reinforcement, the strip width b_f and spacing p_f (both in mm, measured perpendicular to the fibers) must meet the following limits:

$$50mm \leq b_f \leq 250mm \text{ and } p_f \leq min(0.5d, 3b_f, b_f + 200mm)$$

If the spacing exceeds the limit:

$$p_f > min(0.5d, 3b_f, b_f + 200mm)$$

a different reinforcement system must be used, either by modifying the geometry or mechanical properties.

(4) For continuous wrapping around circular sections (diameter D), where fibers are oriented orthogonally to the beam axis (β = 90°), the shear contribution of the FRP system, $V_{Rd,f}$, is given by:

$$V_{\mathrm{Rd,f}} = \frac{1}{\gamma_{\mathrm{Rd}}} \cdot D \cdot f_{\mathrm{fed}} \cdot \frac{\pi}{2} \cdot t_{\mathrm{f}} \cdot \cot\theta \tag{4.82}$$

4.4.3.2 Effective Strength

(1) Shear cracks induce stress concentrations at the concrete-FRP interface**,** which may lead to debonding failure (Mode 1 failure, § 4.1.3).
In the absence of a more detailed stress analysis, a simplified approach can be used. This method introduces an "effective tensile strength" for the FRP system, representing the expected tensile stress at incipient debonding**.**

(2) For U-jacketing reinforcement in rectangular sections, the effective design tensile strength of the FRP system, f_{fed}, is given by:

$$f_{\mathrm{fed}} = f_{\mathrm{fdd}} \cdot \left[1 - \frac{1}{3} \cdot \frac{\ell_{\mathrm{ed}} \cdot \sin\beta}{\min\{0.9 \cdot d, h_{\mathrm{w}}\}} \right] \tag{4.83}$$

where:

- f_{fdd} = design tensile stress for end debonding, calculated using Equation(4.7) and considering point (4) below,
- l_{ed} = Effective anchorage length, given by Equation (4.1),
- β = Fiber inclination angle relative to the beam's longitudinal axis,
- d = effective depth of the section,
- h_{w} = height of the web, which the U-wrap reinforcement must fully cover.

Special Considerations for Beams with Compressed Zones at the Bottom:

- In cases where the compression zone is located at the bottom of the beam (e.g., cantilever beams), shear cracks propagate upward (Figure 4-21).
- In such situations, proper anchorage of U-wrap FRP reinforcement is critical and may require:
  - Mechanical anchors, or
  - Additional anchorage measures.
- Equation (4.83) must always be used in such cases without applying Equation (4.84) (point three below).

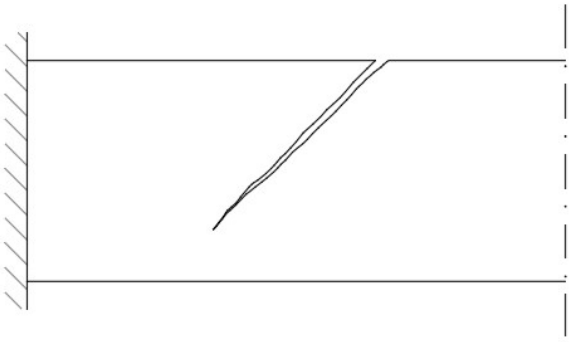

Figure 4-21 – Shear Crack Development in Beams with Bottom Compression Zones.

(3) For fully wrapped reinforcement in rectangular sections, the effective design tensile strength of the FRP system is given by:

$$f_{\text{fed}} = f_{\text{fdd}} \cdot \left[1 - \frac{1}{6} \cdot \frac{\ell_{\text{ed}} \cdot \sin\beta}{\min\{0.9 \cdot d, h_{\text{w}}\}}\right] + \frac{1}{2}(\phi_{\text{R}} \cdot f_{\text{fd}} - f_{\text{fdd}}) \cdot \left[1 - \frac{\ell_{\text{ed}} \cdot \sin\beta}{\min\{0.9 \cdot d, h_{\text{w}}\}}\right] \tag{4.84}$$

Where:

- f_{fdd} = design tensile stress for end debonding, from Equation(4.5),
- f_{fd} = design tensile stress in the FRP reinforcement, calculated as $f_{\text{fd}} = E_{\text{f}}\varepsilon_{\text{fd}}$, where ε_{fd} is calculated as $\varepsilon_{\text{fd}} = \eta_{\text{a}} \cdot \frac{\varepsilon_{\text{fk}}}{\gamma_{\text{fl}}}$,
- ϕ_{R} = coefficient accounting of radius at the section corner and the width of the section, and it is calculated as follows:

$$\phi_{\text{R}} = 0.2 + 1.6 \cdot \frac{r_{\text{c}}}{b}, \qquad 0 \le \frac{r_{\text{c}}}{b} \le 0.5 \tag{4.85}$$

where:

- r_{c} = radius of curvature at the section corners,
- b = width of the web.

- The second term in Equation (4.84) is included only if positive.

(4) For calculating the geometric factor λ in Equation (4.8), the following assumptions apply:

- $b = p_{\text{f}}$ for discontinuous strip reinforcement,
- $b = b_{\text{f}} = min(0.9d, h_{\text{w}}) \frac{sin(\theta+\beta)}{\sin(\theta)}$ for continuous reinforcement or adjacent strips.

(5) For U-wrap reinforcement with mechanical anchors at the free ends**,** if experimental evidence demonstrates that their contribution is at least equivalent to a fully wrapped system**,** the effective tensile strength may be obtained using Equation **(**4.84**).** Otherwise, it must be calculated using Equation (4.83).

(6) For continuous wrapping around circular sections (diameter D), with fibers oriented at $\beta = 90°$, the effective tensile strength of the FRP system is given by:

$$f_{\text{fed}} = E_{\text{f}} \cdot \varepsilon_{\text{f,max}} \tag{4.86}$$

where:

- E_{f} = elastic modulus of the FRP composite in the fiber direction,
- $\varepsilon_{\text{f,max}}$ = limiting strain in the FRP composite, assumed as 5×10^{-3} in the absence of more accurate data.

4.5 STRENGTHENING FOR TORSION

4.5.1 General Considerations

(1) Torsion strengthening is required for structural elements where the design torsional moment—potentially evaluated using capacity design principles—exceeds the corresponding design torsional resistance. The latter must be determined by considering both the contribution of concrete and any existing transverse steel reinforcement.

(2) Torsion strengthening is verified only for the Ultimate Limit States (ULS).

(3) In addition to the strengthening methods listed below, other techniques may be used, provided their effectiveness is demonstrated, and their contribution to torsional resistance is quantified.

Note:
To date, torsion strengthening of reinforced concrete (RC) and prestressed concrete (PC) elements using SFRP systems remains uncommon**.** Additionally, the scientific and technical literature on this topic is still limited**.**

4.5.2 Torsion Strengthening Configurations

(1) Externally Bonded Reinforcement (EBR) for torsion strengthening is applied by bonding one- or two-dimensional composite elements (typically fabrics) onto the external surface of the structural member (Figure 4-17). These elements consist of one or more layers of FRP material.

For one-dimensional reinforcement, composite strips can be placed:

- Adjacent to each other (continuous layout), or
- Discontinuously (spaced apart).

(2) The fibers must be oriented at an inclination of β=90° relative to the longitudinal axis.

(3) The only permitted configuration for torsion strengthening is complete wrapping (Figure 4-19).

(4) Torsion strengthening may also be achieved using Near-Surface Mounted (NSM) reinforcement, where composite bars or laminates are embedded into grooves cut into the external faces of the element. However, NSM torsion strengthening is not covered in these guidelines. If adopted, its effectiveness must be validated through experimental evidence**.**

4.5.3 Design Torsional Resistance of an FRP-Strengthened Element

(1) The following guidelines apply to prismatic elements where a fictitious resistant hollow section can be identified and where the insufficient torsional strength (to be supplemented with FRP) does not result from inadequate longitudinal steel reinforcement**.**

These elements must satisfy the following conditions:

$$T_{\mathrm{Rd,l}} > \min\left\{ T_{\mathrm{Rd,s}}, T_{\mathrm{Rd,c}} \right\} \tag{4.87}$$

where

- $T_{\mathrm{rd,s}}$, $T_{\mathrm{rd,l}}$, and $T_{\mathrm{rd,c}}$ represent the torsional resistances of the transverse steel reinforcement, longitudinal steel reinforcement, and the compressed concrete strut, respectively, evaluated in accordance with current standards.

4.5.3.1 Design Torsional Resistance

(1) The design torsional resistance of the FRP-strengthened element can be determined using the following equation:

$$T_{\mathrm{Rd}} = \min\left\{ T_{\mathrm{Rd,s}} + T_{\mathrm{Rd,f}}, T_{\mathrm{Rd,l}}, T_{\mathrm{Rd,c}} \right\} \tag{4.88}$$

where:

- $T_{\mathrm{Rd,s}}$, $T_{\mathrm{Rd,l}}$, $T_{\mathrm{Rd,c}}$ retain their previously defined meanings,
- $T_{\mathrm{Rd,f}}$ is the torsional resistance provided by the FRP reinforcement system, which is evaluated as follows.

(2) Provided that Equation 4.53 results in $T_{\mathrm{Rd}} = T_{\mathrm{Rd,s}}$, the torsional resistance contributed by the FRP reinforcement, $T_{\mathrm{Rd,f}}$ is given by:

$$T_{\mathrm{Rd,f}} = \frac{1}{\gamma_{\mathrm{Rd}}} \cdot 2 \cdot f_{\mathrm{fed}} \cdot t_{\mathrm{f}} \cdot b \cdot h \cdot \frac{b_{\mathrm{f}}}{p_{\mathrm{f}}} \cdot \cot\theta \tag{4.89}$$

where:

- $\gamma_{\mathrm{m}} = 1.20$ is the partial factor from Table 3-2, in Section § 3.4.2,
- f_{fed} = effective design strength of the FRP reinforcement, evaluated according to § 4.4.3.2,
- t_{f} = thickness of the FRP strip or sheet,
- b and h = width and height of the section, respectively,
- θ = angle of inclination of the compressed struts relative to the element's axis, within the range of 22° to 45° (default value: 45° if not specified),
- b_{f} and p_{f} = width and spacing of FRP strips, measured perpendicular to the fiber direction.
    - For adjacent strips or continuous reinforcement, assume $b_{\mathrm{f}}/t_{\mathrm{f}} = 1$.

(3) For composite strip reinforcement, the strip width b_{fb} and spacing p_{fp} (in mm, measured perpendicular to the fibers) must meet the following limits:

$$50mm \leq b_f \leq 250mm \quad \text{and} \quad b_f \leq p_f \leq min(0.5d, 3b_f, b_f + 200mm)$$

If the spacing exceeds the limit, i.e.,

$$p_f > min(0.5d, 3b_f, b_f + 200mm)$$

a different reinforcement system must be used, either by modifying the geometry or mechanical properties.

(4) For combined loading conditions of torsion, T_{Sd}, and shear, V_{Sd}, the following interaction equation must be satisfied:

$$\frac{T_{Sd}}{T_{Rd,c}} + \frac{V_{Sd}}{V_{Rd,c}} \leq 1 \tag{4.90}$$

where:

- $T_{Rd,c}$ and $V_{Rd,c}$ retain their previously defined meanings.

Torsion and shear strengthening with FRP must be designed independently.

- The total required FRP reinforcement area is the sum of the areas needed for torsion and shear strengthening.
- The inclination angle θ of the compressed struts must be the same for both torsion and shear design and should be assumed as 45°.

4.6 CONFINEMENT

4.6.1 General Considerations

(1) Adequate confinement of reinforced concrete elements can enhance structural performance, leading to increases in:

- Ultimate strength and corresponding ultimate strain in elements subjected to axial loads, whether concentrically applied or with small eccentricity.
- Ductility, and - when combined with longitudinal reinforcement (§ 4.3.2.4 and Appendix F) - the ultimate strength of compression-flexural elements.

(2) Confinement of reinforced concrete elements can be achieved using FRP fabrics or laminates, applied around the perimeter to form a continuous or discontinuous external wrapping.

Note:
To date, SFRP-based confinement of reinforced concrete columns is not widely used, and the scientific and technical literature on this topic remains limited.

(3) The increase in compressive strength and corresponding ultimate strain of FRP-confined concrete depends on the applied confinement pressure, which is a function of:

- The stiffness of the FRP reinforcement system, and
- The shape of the confined element's cross-section.

(4) Ductility enhancement cannot be relied upon for load redistribution in elements subjected to axial loads with small eccentricity.

(5) Unlike steel confinement (which follows an elastoplastic behavior), FRP confinement (which remains elastic until failure) applies an increasing lateral pressure as the transverse expansion of the confined element increases.

(6) A typical stress-strain "σ_c-ε_c" relationship for FRP-confined concrete specimens under compression is shown in Figure 4-22.

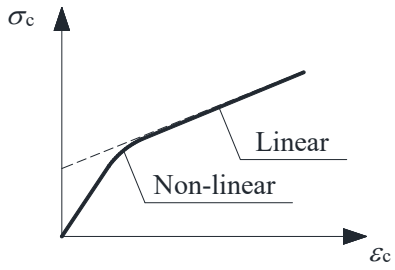

Figure 4-22 – Stress-Strain Behavior of FRP-Confined Concrete.

(7) For axial strains (ε_c) of 0.2%, the stress in confined concrete is only slightly higher than that of unconfined concrete, meaning it remains close to the design strength of unconfined concrete.

(8) For strains exceeding 0.2%, the stress-strain relationship becomes nonlinear, and the slope of the curve progressively decreases until reaching a nearly constant value in the final phase. In this last linear segment, the confined concrete progressively loses its integrity due to increasing crack formation.

(9) Failure of the confined element occurs when the FRP ruptures. However, beyond a certain axial strain, the confined element essentially loses its functionality, as it can no longer effectively resist transverse stresses. For this reason, failure is conventionally assumed to occur when the FRP strain reaches a limit value of 0.4%.

(10) Confined elements must be verified only for the Ultimate Limit States (ULS).

4.6.2 Design Compressive Strength of a Centrally Loaded or Slightly Eccentric Confinement System

(1) To achieve effective confinement, the FRP fibers should be oriented perpendicular to the element's longitudinal axis.

(2) For helical confinement arrangements, the effectiveness of confinement must be appropriately evaluated.

(3) In the absence of initial prestressing, the FRP reinforcement system provides passive confinement to the compressed member.

- The confinement effect becomes significant only after yielding and cracking occur in the concrete, which leads to increased transverse expansion of the confined element.

(4) The confined element is verified if the following inequality is satisfied:

$$N_{Sd} \leq N_{Rcc,d} \tag{4.91}$$

Where:

- N_{Sd} = design axial load,
- $N_{Rcc,d}$ = design compressive resistance of the confined element.

(5) In the absence of instability issues, the design compressive resistance, $N_{Rcc,d}$, is given by:

$$N_{Rcc,d} = A_c \cdot f_{ccd} + A_s \cdot f_{yd} \tag{4.92}$$

where:

- A_c and f_{ccd} are the cross-sectional area and design compressive strength of confined concrete, respectively (evaluated in the following section),
- A_s and f_{yd} are the area and design strength of the longitudinal steel reinforcement, respectively (evaluated according to § 3.3.3(6)).

(6) The design compressive strength of confined concrete, f_{cdd}, is determined as follows:

$$\frac{f_{ccd}}{f_{cd}} = 1 + \frac{2.6}{\gamma_{Rd}} \cdot \left(\frac{f_{l,eff}}{f_{cd}} \right)^{2/3} \tag{4.93}$$

where:

- γ_{rd} = partial safety factor, taken as 1.10 (Table 3-2, § 3.4.2),
- f_{cd} = design compressive strength of unconfined concrete, evaluated according to § 3.3.3(6),
- $f_{l,eff}$ = effective confinement pressure, defined in the following section.

Equation (4.93) can also be used to achieve the second objective stated in § 4.6.1 (1).

(7) Confinement is considered effective if:

$$\frac{f_{l,eff}}{f_{cd}} > 0.05.$$

4.6.2.1 Estimation of Lateral Confinement Pressure

(1) Of the total confinement pressure exerted by the FRP reinforcement system, f_l, only a portion - termed the "effective confinement pressure" ($f_{l,eff}$) - contributes to the strength of the confined element.

(2) The effective confinement pressure, $f_{l,eff}$, which depends on the cross-sectional shape and the specifics of the reinforcement application, is given by:

$$f_{l,eff} = k_{eff} \cdot f_l \tag{4.94}$$

where:

- k_{eff} is the efficiency coefficient (≤ 1), defined as the ratio between:
  - $V_{c,eff,}$ the volume of effectively confined concrete, and
  - $V_{c,}$ the total volume of the concrete element, excluding the volume occupied by longitudinal reinforcement (typically negligible).

(3) The confinement pressure (f_l) can be calculated using:

$$f_l = \frac{1}{2} \cdot \rho_f \cdot E_f \cdot \varepsilon_{fd,rid} \tag{4.95}$$

where:

- ρ_f = geometrical reinforcement ratio, which depends on:
  - The section shape and
  - The type of application (continuous or discontinuous confinement) as described in the following sections.
- E_f = elastic modulus of the FRP material in the fiber direction.
- $\varepsilon_{fd,rid}$ = reduced design strain of the fiber-reinforced composite, defined later in this section.

(4) The efficiency coefficient, k_{eff}, is expressed as the product of three factors:

- A horizontal efficiency coefficient (k_H),
- A vertical efficiency coefficient (k_V), and
- A coefficient related to the fiber inclination (k_α):

$$k_{eff} = k_H \cdot k_V \cdot k_\alpha \tag{4.96}$$

(5) The horizontal efficiency coefficient, k_H, depending on the shape of the section. The corresponding values for circular and rectangular sections are provided in the following sections.

(6) The vertical efficiency coefficient, k_V, depends on the distribution of confinement along the longitudinal axis of the strengthened element:

- For continuous wrapping, assume $k_V = 1$.

For discontinuous wrapping (Figure 4-23), where FRP strips are applied at a spacing p_f with a net gap p_f', net between them, the reduction in confinement effectiveness due to stress diffusion must be considered.

- Stress diffusion creates unconstrained regions between FRP wraps, which in a vertical section form approximately parabolic contours with an initial tangent inclined at 45°.

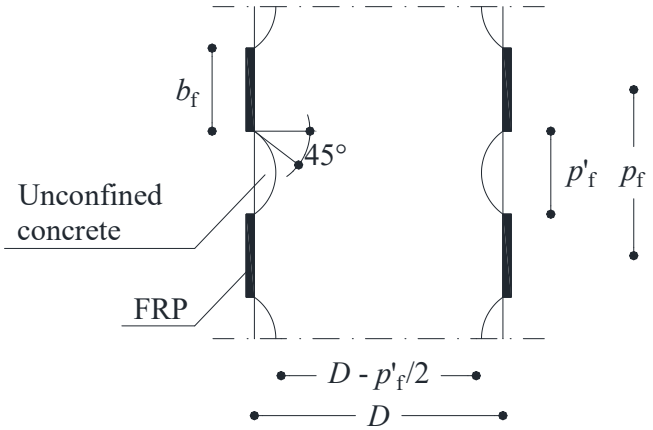

Figure 4-23 – Discontinuous Confinement on a Circular Section (Diameter DDD): Vertical Diametral Section.

or all section shapes, the vertical efficiency coefficient, k_V, can be taken as:

$$k_V = \left(1 - \frac{p'_f}{2 \cdot d_{min}}\right)^2 \tag{4.97}$$

where:
d_{min} = smallest cross-sectional dimension of the element.

(7) For discontinuous wrapping, the net gap between FRP strips should satisfy:

$$p'_f \leq d_{min}/2.$$

(8) Regardless of the section shape, the efficiency coefficient related to fiber inclination (k_α) is given as a function of the fiber inclination angle (α_{fl}):

$$k_\alpha = \frac{1}{1 + (\tan \alpha_{fl})^2} \tag{4.98}$$

(9) The reduced design strain of the fiber-reinforced composite ($\varepsilon_{fd,red}$), is defined as:

$$\varepsilon_{fd,red} = min\left\{\eta_a \frac{\varepsilon_{fk}}{\gamma_{f1}}, 0.004\right\} \tag{4.99}$$

where:

- η_a= environmental conversion factor,
- γ_{f1}= = partial safety factor for the composite material.

The values for η_a and γ_{f1} are provided in Table 3-3 and § 3.4.1 of these guidelines.

- The conventional strain limit of the composite is assumed to be 0.004, as stated in § 4.6.1(9).

4.6.2.1.1 Circular Sections

(1) FRP confinement is particularly effective for circular cross-sections subjected to axial compression (either concentrically loaded or with small eccentricity).

(2) When fibers are oriented transversely to the longitudinal axis of the element, the FRP reinforcement system induces a nearly uniform lateral pressure on the contact surface, opposing the radial expansion of the compressed element.

(3) The geometric reinforcement ratio (ρ_f), to be used in Equation 4.60 is given by:

$$\rho_f = \frac{4 \cdot t_f \cdot b_f}{D \cdot p_f} \tag{4.100}$$

where (Figure 4-23):

- t_f and b_f are the thickness and height of the generic FRP strip, respectively,
- p_f is the spacing between strips and
- D is the diameter of the circular section.

For continuous confinement, the expression for ρ_f simplifies to:

$$\rho_f = \frac{2t_f}{D}$$

(4) The horizontal efficiency coefficient, k_H, is equal to 1.0.

(5) For the calculation of the vertical efficiency coefficient (k_v) in Equation (4.62), the parameter d_{min}, should be interpreted as the section's diameter.

4.6.2.1.2 Square and Rectangular Sections

(1) FRP confinement of square or rectangular sections produces only marginal increases in compressive strength.

- As a result, such applications should be carefully evaluated and analyzed.

(2) The geometric reinforcement ratio (ρ_f) to be used in Equation (4.60a) is given by:

$$\rho_f = \frac{2 \cdot t_f \cdot (b+h) \cdot b_f}{b \cdot h \cdot p_f} \tag{4.101}$$

where:

- t_f and h_f are the thickness and height of the generic FRP strip, respectively,
- p_f is the spacing between strips and
- b and h are the cross-sectional dimensions of the rectangular section.

For continuous confinement, the expression for ρ_f simplifies to:

$$\rho_f = \frac{2t_f(b+h)}{b \cdot h}$$

(3) As shown in Figure 4-24 the effectively confined concrete area is only a fraction of the total section.
This behavior is due to the "arch effect," which occurs within the section and depends on the corner radius (r_c) (see § 4.9.2.2).

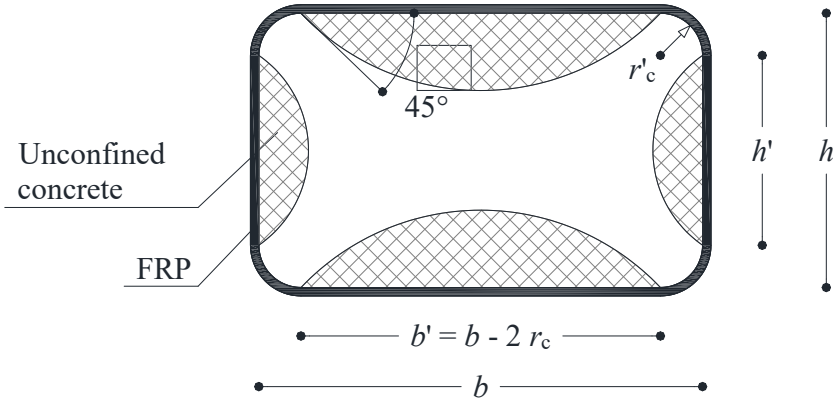

Figure 4-24 – Confinement of Rectangular Sections.

(4) The horizontal efficiency coefficient, k_H, is given by:

$$k_H = 1 - \frac{b'^2 + h'^2}{3 \cdot A_g} \tag{4.102}$$

where:

- *b'* and *h'* are the dimensions indicated in Figure 4-24, and
- A_g is the gross cross-sectional area of the confined element.

(5) In the absence of experimental data proving otherwise, confinement should not be considered effective for rectangular sections where *b/h*>2 or $max\{b,h\} > 900mm$, i.e., for sections with extreme aspect ratios or large sections.

4.6.3 Ductility of FRP-Confined Compression-Flexural Elements

(1) FRP confinement can also be applied to reinforced concrete elements subjected to compression-flexure (axial load with large eccentricity).

- This technique increases ductility but only slightly enhances the element's strength.

(2) In the absence of more precise calculations, the ultimate curvature of a compression-flexural section can be estimated using a classical parabolic-rectangular stress-strain model for confined concrete, amplifying the ultimate strain (ε_{ccu}), as follows:

$$\varepsilon_{ccu} = 0.0035 + 0.015 \cdot \sqrt{\frac{f_{l,eff}}{f_{cd}}} \tag{4.103}$$

where:

- f_{cd} = design compressive strength of unconfined concrete,
- $f_{l,eff}$ = effective confinement pressure.

The effective confinement pressure can be estimated using the reduced design strain of the fiber-reinforced composite:

$$\varepsilon_{fd,rid} = \eta_a \cdot \frac{\varepsilon_{fk}}{\gamma_{fl}} \leq 0.6 \cdot \varepsilon_{fk} \tag{4.104}$$

(3) More accurate estimations of the ultimate curvature and the corresponding increase in flexural strength can be obtained using appropriate constitutive models for FRP-confined concrete (Appendix F).

- These models better capture the behavior described in § 4.6.1 and Figure 4-22.

4.7 STRENGTHENING OF PRESTRESSED CONCRETE STRUCTURES

4.7.1 Use of FRP Composites for Pre-Tensioned and Post-Tensioned Concrete Elements

(1) The strength of pre-tensioned and post-tensioned reinforced concrete elements can be enhanced by using externally bonded FRP reinforcement without prestressing.

4.7.1.1 Ultimate limit state behavior analysis

(1) The determination of the ultimate flexural capacity of prestressed sections follows procedures similar to those described in § 4.3.2 for conventional reinforced concrete sections, with the following key differences:

- The strain in the prestressing tendons is given by the algebraic sum of:
  - The strain in the surrounding concrete, and
  - The decompression limit strain ($\bar{\varepsilon_p}$) is defined as the strain in the prestressing tendons when the surrounding concrete experiences zero stress due to an appropriate combination of internal forces (Figure 4-25.).
- Suppose the concrete has aged sufficiently for time-dependent effects to be considered negligible. In that case, the strain ε_0 coincides with the strain present on the concrete surface at the time of FRP installation, but with opposite sign.
  - In all cases, the evaluation of ε_0 should account for any redistributions caused by accidental factors (e.g., impact damage).
- If the time-dependent effects of concrete (creep and shrinkage) are still developing, the strain ε_0 is the algebraic sum of:

- The previously calculated value plus
- The additional strain that develops in the concrete (on the contact surface with the FRP laminate) after the reinforcement is applied.
- In this assessment, as well as in determining the long-term prestress losses, the presence of the FRP reinforcement may be neglected.

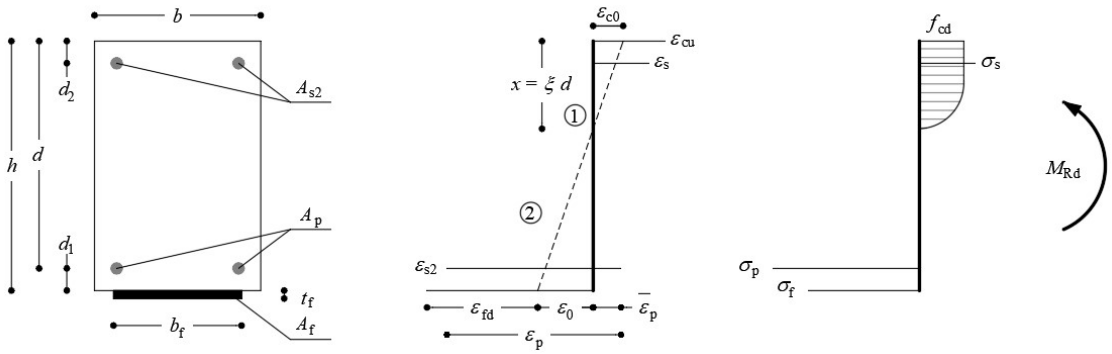

Figure 4-25 – Failure Modes of an Externally Strengthened Prestressed Concrete Section with FRP Composites.

(2) The yielding of the prestressing tendons must precede the attainment of the Ultimate Limit State (ULS).

(3) For verification against debonding failure, refer to §§ 4.1 and 4.2.

(4) For the determination of the shear and torsional strength of the strengthened element, as per the application rules (2) of § 4.4.3.1 and (1) of § 4.5.3.1, the angle θ may be evaluated by taking into account the axial pre-compression force acting on the element and may therefore be less than 45°.

4.7.1.2 Serviceability Limit State Analysis

(1) Under service conditions, the working stresses in concrete, steel, and FRP reinforcement must comply with the limitations set by current standards.

- For FRP reinforcement, the specific stress limitations introduced in §4.3.3.2 must be observed.

(2) As a general rule, the contribution of FRP reinforcement that is temporarily subjected to compression (e.g., due to the time-dependent deformation of concrete) should not be considered.

4.8 SEISMIC STRENGTHENING

4.8.1 General Considerations

(1) FRP reinforcement systems can be effectively used in seismic areas to strengthen reinforced concrete structures that do not meet the required safety criteria for one or more Ultimate Limit States (ULS).

These guidelines incorporate the requirements of the current Italian regulations, as well as key recommendations from scientific literature and international guidelines, covering:

- Seismic safety assessment
- Safety requirements (limit state verification)
- Levels of seismic protection (associated seismic action intensity)
- Analysis methods
- Verification criteria (distinction between "ductile" and "brittle" elements)
- Material properties

4.8.2 General Strengthening Principles

(1) The following principles must guide the strengthening strategy using FRP:

- Eliminating all brittle failure mechanisms (§ 4.8.2.1)
- Eliminating soft-story collapse mechanisms (§4.8.2.2)
- Improving the global deformation capacity of the structure can be achieved by one of the following methods (§ 4.8.2.3):
    - Increasing the rotational capacity of potential plastic hinges without changing their location (§4.8.2.3.1)
    - Relocating potential plastic hinges while respecting the capacity design principles (§4.8.2.3.2)

(2) The type, extent, and urgency of FRP interventions should be based on a preliminary seismic safety assessment, considering that:

- Severe structural irregularities (in terms of strength and/or stiffness) cannot be corrected solely by FRP strengthening.
- A more uniform strength distribution can be achieved by strengthening a limited number of structural elements.
- Local ductility improvements are always beneficial.
- The introduction of local strengthening should not reduce the overall ductility of the structure.

4.8.2.1 Eliminating Brittle Failure Mechanisms

(1) Failure mechanisms leading to the following failure modes must be eliminated:

- Shear failure
- Failure of columns due to loss of bond in overlapping splices
- Failure of columns due to buckling of compressed longitudinal bars
- Failure of beam-column joint panels due to tensile forces

4.8.2.1.1 Shear Failure

(1) Shear resistance can be increased by applying FRP reinforcement with fibers oriented perpendicular to the element's axis ($\beta = 90°$) and, if necessary, in additional directions.

(2) The shear strength of the strengthened element must be calculated by including the contribution of the fiber-reinforced material in the formula provided by current standards for reinforced concrete elements in existing structures. The contribution of the FRP reinforcement should be evaluated using equation (4.81) for rectangular sections or equation (4.82) for circular sections, assuming $\theta = 45°$.

4.8.2.1.2 Failure of Columns Due to Loss of Bond in Overlapping Splices

(1) The risk of bar slippage in column splice regions can be eliminated through FRP confinement.

(2) For circular sections with diameter D, the required confinement thickness can be calculated using the following equation:

$$t_f = \frac{D \cdot (f_l - \sigma_{sw})}{2 \cdot 0.001 \cdot E_f} \tag{4.105}$$

where:

- σ_{sw} = tensile stress in the stirrups corresponding to a strain of 1‰, or the injection pressure of grout between FRP and column (if present).
- f_l = confinement pressure in the overlapping splice region of length L_s, assumed as:

$$f_l = \frac{A_s \cdot f_{yd}}{\left[\frac{u_e}{2 \cdot n} + 2 \cdot (d_b + c)\right] \cdot L_s} \tag{4.106}$$

where:

- f_{yd} = design yield strength of the steel bars, evaluated according to § 3.3.3(6).
- u_e = perimeter of the section inside the polygon enclosing the longitudinal bars with an average diameter d_b.
- n = number of spliced bars along the length L_s.
- c = concrete cover thickness.

(3) For rectangular sections with dimensions *b* and *h*, the same equations can be used by substituting D with $max\{b, h\}$ and reducing the FRP confinement effectiveness using the factor k_H as defined in § 4.6.2.1.2.

4.8.2.1.3 Failure of Columns Due to Buckling of Longitudinal Bars

(1) The risk of buckling of longitudinal reinforcement bars can be eliminated through FRP confinement.

(2) The required confinement thickness (t_f) can be calculated using the following equation:

$$t_{\mathrm{f}} = \frac{0.45 \cdot n \cdot f_{\mathrm{yd}}^2 \cdot d}{4 \cdot E_{\mathrm{ds}} \cdot E_{\mathrm{f}}} \approx \frac{10 \cdot n \cdot d}{E_{\mathrm{f}}} \tag{4.107}$$

where:

- n = total number of longitudinal bars susceptible to buckling
- f_{yd} = design yield strength of the steel bars, as defined in § 3.3.3(6)
- d = effective depth of the flexural reinforcement
- E_{f} = elastic modulus of the FRP confinement in the direction of the longitudinal bars
- E_{ds} = "reduced modulus" of the longitudinal reinforcement bars, defined as follows:

$$E_{\mathrm{ds}} = \frac{4 \cdot E_{\mathrm{s}} \cdot E_{\mathrm{i}}}{\left(\sqrt{E_{\mathrm{s}}} + \sqrt{E_{\mathrm{i}}}\right)^2} \tag{4.108}$$

where:

- E_{s} = elastic modulus of the reinforcement bars
- E_{i} = initial tangent modulus in the plastic range.

4.8.2.1.4 Failure of Beam-Column Joints Due to Tensile Forces

(1) The tensile strength enhancement achievable in unconfined beam-column joint panels must be evaluated considering the contribution of the FRP composite in the direction of the principal tensile stresses.

- This reinforcement is effective only if the FRP ends are properly anchored using appropriate construction details.
- Without adequate anchorage, the FRP reinforcement is not considered effective.

(2) The design diagonal tensile resistance of the strengthened joint can be calculated using Equation (4.109):

$$\sigma_{\mathrm{nt,Rd}} = \sigma_{\mathrm{nt,Rd,c}} + \sigma_{\mathrm{nt,Rd,f}} \tag{4.109}$$

where:

- $\sigma_{\mathrm{nt,Rd,c}}$ = diagonal tensile strength of the concrete,
- $\sigma_{\mathrm{nt,Rd,f}}$ = diagonal tensile strength provided by the FRP reinforcement,

with the concrete tensile resistance determined according to the applicable standards.

(3) The diagonal tensile strength contributed by the FRP composite can be evaluated using Equation (4.110):

$$\sigma_{\mathrm{nt,Rd,f}} = \frac{A_{\mathrm{f}} E_{\mathrm{f}} \varepsilon_{\mathrm{fd}}}{b_{\mathrm{c}} (h_{\mathrm{c}} / sen\theta)} \tag{4.110}$$

where:

A_{f} = equivalent area of FRP reinforcement, calculated as described in point (4)
E_{f} = elastic modulus of the FRP reinforcement
$\varepsilon_{\mathrm{fd}}$ = design strain of the FRP reinforcement, as defined in point (5)
b_{c} and h_{c} = width and height of the lower column section (Figure 4-26)

(4) The equivalent area of FRP reinforcement, A_{f}, is calculated using Equation (4.111):

$$A_{\mathrm{f}} = \sum_{\mathrm{i=1}}^{\mathrm{n}} A_{\mathrm{f,i}} sen(\theta + \beta_{\mathrm{i}}) \tag{4.111}$$

where:

A_{fi} = Area of the FRP reinforcement oriented in the β_{i} direction (Figure 4-26).

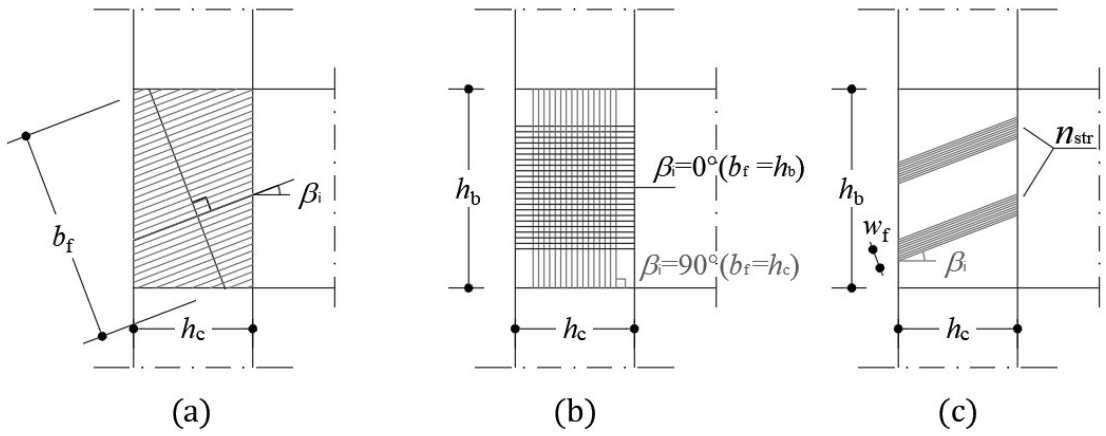

Figure 4-26 – Key Features of FRP Tensile Strengthening in Joint Panels: (a) Continuous fabric in a generic direction; (b) Continuous fabric in horizontal and vertical directions; (c) Discontinuous fabric in a generic direction.

.

For uni-axial, bi-axial, or quadri-axial FRP reinforcement schemes, the equivalent area, A_{f}, is determined from Equation (4.111) as follows:

- Uni-axial fabric – fibers oriented horizontally ($\beta = 0°$) or vertically ($\beta = 90°$):

$$\begin{aligned} A_{\mathrm{f}} &= n_{\mathrm{s}} t_{\mathrm{f}} h_{\mathrm{b}} \mathrm{sen}\theta \qquad \text{if } \beta = 0° \\ A_{\mathrm{f}} &= n_{\mathrm{s}} t_{\mathrm{f}} h_{\mathrm{c}} \cos\theta \qquad \text{if } \beta = 90° \end{aligned} \tag{4.112}$$

- Bi-axial fabric – fibers oriented horizontally and vertically (β=0° e β=90°)

$$A_f = n_s t_f h_c \cos\theta(1+\tan^2\theta) \tag{4.113}$$

- Quadri-axial fabric – fibers oriented horizontally, vertically, and diagonally ($\beta = 0°$, $\beta = 90°$ and $\beta = \pm 45°$)

$$A_f = n_s t_f h_c \cos\theta(1+\tan\theta+2\tan^2\theta) \tag{4.114}$$

where:

- β= angle of the fibers relative to the beam axis
- n_s = number of strengthened joint faces (1 or 2, Figure 4-27),
- θ = angle of the concrete compression strut relative to the beam axis**,** which can be taken as:

$$\theta = \arctan(h_b / h_c)$$

where:

- h_b = total height of the beam section.

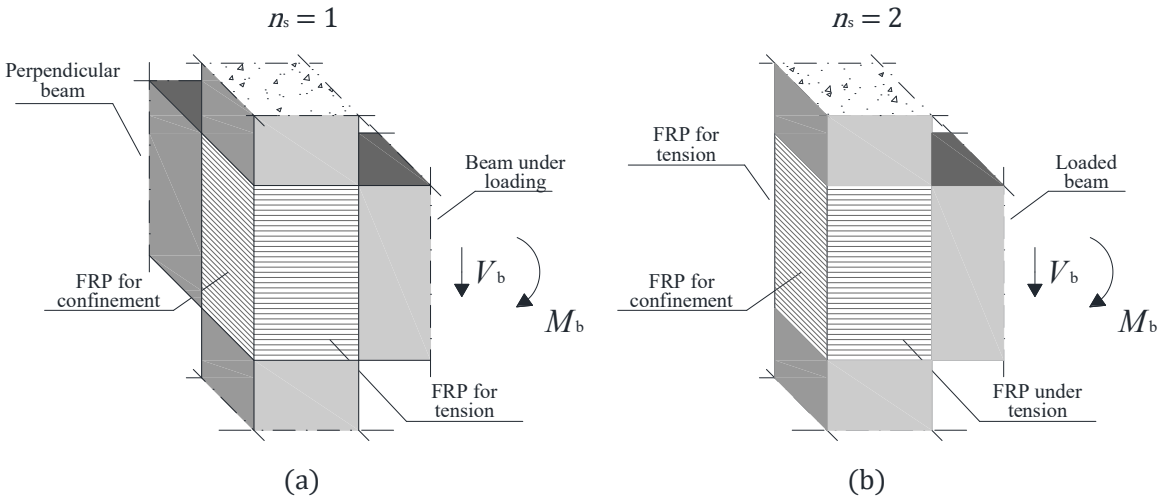

Figure 4-27 – FRP Strengthening of Joint Panels: (a) One face strengthened (n_s = 1), (b) Two faces strengthened (n_s = 2).

For discontinuous reinforcement, Equation (4.111) becomes:

$$A_{fi} = n_s t_f b_f$$

Where:

- b_f = equivalent width of the FRP strips, which is a function of the slope and number of strips applied on the panel, as follows:

$$b_f = \frac{(w_f n_{str})^2 \cos\beta}{h_b} \qquad \text{se } \beta = 0° \tag{4.115}$$

$$b_f = \frac{(w_f n_{str})^2 sen\beta}{h_c} \qquad \text{se } \beta = 90° \tag{4.116}$$

where:
w_f = width of a single strip
n_{str} = the number of FRP strips applied on the joint panel (Figure 4-26).

(5) The design strain of the FRP composite, ε_{fd}, can be calculated using Equation (4.117):

$$\varepsilon_{fd} = min\left\{\eta_a \frac{\varepsilon_{fk}}{\gamma_{f1}}; 34\left(\frac{f_{cm}^{2/3}}{A_f E_f}\right)^{0.6}\right\} \tag{4.117}$$

where:
f_{cm} = average compressive strength of the existing concrete.

For strengthening applied to a repaired joint panel, it is recommended to assume a design strain equal to 80% of the value attained from Equation (4.117).

4.8.2.2 Elimination of Soft-Story Collapse Mechanisms

(1) In the absence of shear walls, soft-story collapse mechanisms can be triggered when plastic hinges form at both the top and bottom of all the columns in a given story. Strengthening measures should aim to increase the flexural resistance of these zones to prevent hinge formation. In no case should interventions be implemented solely to increase the displacement capacity before collapse occurs.

4.8.2.3 Increasing the Global Deformation Capacity of a Structure

(1) The ultimate deformation capacity of a structure is a measure of its ability to withstand seismic action. It depends on the plastic deformation capacity of individual load-bearing elements (beams, columns, and walls).

4.8.2.3.1 Increasing the Local Deformation Capacity of Elements

(1) The deformation capacity of beams and columns can be measured using the rotation θ of the end section relative to the chord connecting it to the section with zero moments ("chord rotation") at a distance equal to the shear span:

$$L_v = \frac{M}{V}$$

The rotation θ is also equal to the relative displacement between the two sections and the shear span:

$$\theta = \text{atan}\left(\frac{\delta}{L_v}\right)$$

where δ is the relative displacement between the two sections, and L_v is the shear span.

(2) The crushing failure of compressed concrete generally limits the plastic deformation capacity of elements. FRP confinement in these elements (mainly columns) increases the ultimate strain of the compressed concrete, thereby improving the ductility of the elements.

4.8.2.3.2 Relocation of Potential Plastic Hinges

(1) The application of the capacity design approach requires measures to prevent the formation of plastic hinges in columns. In "weak column-strong beam" configurations—common in frame structures designed only for vertical loads—columns are often undersized and lack sufficient longitudinal reinforcement. In these cases, it is necessary to increase the flexural strength of the columns to shift the system toward a "strong column-weak beam" configuration.

(2) Applying the capacity design approach increases the flexural strength of columns, which also leads to an increase in the shear demand at ultimate conditions. This necessitates shear verification of the columns, and in some cases, additional strengthening may be required to ensure adequate shear capacity.

4.8.2.3.3 Ultimate Rotation of Strengthened Elements

(1) To evaluate the ultimate rotation θ_u of elements strengthened with FRP confinement, validated formulas can be used, assuming the ultimate strain of confined concrete ε_{ccu} is determined according to § 4.6.3.

4.9 INSTALLATION AND CONSTRUCTION DETAILS

(1) The optimal performance of a strengthening system depends on several factors. In addition to those previously discussed, substrate preparation and the proper application of the composite material play a crucial role.

4.9.1 Inspection and Preparation of the Substrate

(1) Before applying an FRP strengthening system, the condition of the substrate must be inspected and, if necessary, improved by removing and reconstructing deteriorated sections. If required, corroded steel reinforcement must be cleaned and passivated.

(2) Technological systems used for anchoring the ends of FRP laminates or fabrics must undergo standardized experimental testing to verify their performance. The installation protocol must consider the following:

- The materials used (adhesives and reinforcements),
- Surface preparation procedures,
- Execution timeframes,
- Environmental conditions,
- Sensitivity of results to variations in these parameters.

4.9.1.1 Assessment of Substrate Deterioration

(1) Before applying the bonded strengthening system, the designer and site inspector must verify substrate quality according to Chapter 6. The mean compressive strength of the concrete must not be less than 15 MPa. If this requirement is not met, the strengthening technique described in this document cannot be applied.

(2) Uniformity tests should be performed over the entire area to be strengthened.

4.9.1.2 Removal and Reconstruction of the Substrate & Steel Treatment

(1) Concrete deterioration can result from physical-chemical degradation, mechanical damage, or

impact. The damaged concrete must be removed from the affected area.

(2) Removing deteriorated concrete allows for an inspection of the reinforcement condition and the implementation of necessary measures to eliminate the causes of deterioration. If the steel reinforcement is corroded, it must be cleaned (wire brushing or sandblasting) and treated with corrosion inhibitors before concrete restoration.

(3) After deteriorated concrete has been removed and all corrosion control and water infiltration issues have been addressed, restoration can proceed using non-shrink repair mortars.

- Surface irregularities greater than 10 mm should be leveled using epoxy putty.
- If the voids exceed 20 mm, a suitable repair mortar should be used.
- If cracks wider than 0.5 mm are present, they must be injected and sealed before applying the strengthening system.

4.9.1.3 Substrate Preparation

(1) Once the substrate quality has been confirmed and necessary repairs completed, additional sandblasting may be performed to ensure a roughness of at least 0.3 mm (measurable using a laser profilometer or optical roughness gauge.

(2) If working on a low-quality but intact concrete surface, a consolidating treatment may be applied.

(3) If strengthening a new structure, any form-release agents must be removed before application. The surface must be free of dust, grease, hydrocarbons, or surfactants.

(4) For column confinement, shear, or torsional strengthening, and any application where FRP wraps around corners, the edges must be rounded to a minimum radius of 20 mm.

(5) For strengthening with NSM (Near-Surface Mounted) systems**,** the grooves must be thoroughly cleaned before filling. The reinforcements must also be surface-cleaned using solvents compatible with the FRP system being used. The reinforcement elements must be inserted into the groove-filling material in such a way that their **e**ntire surface is in perfect contact with the resin, without voids or cavities.

4.9.2 Best Practices for Proper Installation

(1) The quality of the FRP installation is directly influenced by the temperature and humidity of both the environment and substrate.

4.9.2.1 Environmental and Substrate Conditions

(1) FRP installation should not be performed in high humidity conditions, as excess moisture can delay resin curing and negatively affect bond performance in systems requiring in-situ polymerization.

(2) Composites must be installed following the temperature and humidity guidelines specified in their technical data sheets.

(3) Protective covers, tents, or temporary shelters should be used to prevent exposure to rain, excessive sunlight, thermal gradients, high humidity, or dust.

4.9.2.2 Construction Details & Installation Guidelines

(1) or shear, torsion, and confinement strengthening, corner rounding to at least 20 mm radius is required to prevent stress concentrations that could lead to premature FRP failure.

(2) In-situ installed FRP fibers must be aligned with the designed orientation and must not exhibit wrinkles or undulations.

(3) Carbon FRP (CFRP) strengthening should be isolated from direct contact with steel to prevent galvanic corrosion.

(4) Protection of SFRP Microstrands Against Corrosion
Ensuring the corrosion protection of microstrands in Steel-FRP (SFRP) systems is essential to maintaining the long-term effectiveness of the reinforcement system. Therefore, all procedures and quality control measures must be implemented to prevent degradation from occurring in the short term.

The microstrands used in SFRP systems are galvanized to provide corrosion protection for the steel. However, in cut zones (or areas with defects), this protection may be absent. Additionally, in aggressive environments (e.g., those classified as C4, C5, or CX for corrosivity), the zinc coating may not provide sufficient protection. For long-term durability, it is crucial that microstrands are fully embedded and coated with the resin used as the matrix.

Thus, it is critical to apply resin to cut areas or at the ends of the composite, ensuring that no strands are exposed to the atmosphere. At the end of the reinforcement installation process, a thorough inspection must be performed to confirm that adequate protection has been applied.

(5) Preparation of Test Specimens for Semi-Destructive Control Testing
In cases where semi-destructive control tests are anticipated, it is advisable to set up additional reinforcement test areas (“witness specimens”) in carefully selected parts of the structure. These areas should be divided into patches of at least 500 × 200 mm², with a total area of at least 0.1 m², but no less than 0.5% of the total reinforced area.

The witness patches must be installed at the same time as the reinforcement intervention, using the same materials and construction techniques. They should be located in zones where their removal will not affect collapse mechanisms and should be exposed to the same environmental conditions as the primary reinforcement. If multiple witness specimens are created, they must be evenly distributed across the reinforced structure.

(6) Installation of Fan-Shaped Anchors (Splay Anchors)
For the installation of fan-shaped anchors, the following guidelines should be followed to ensure that the execution matches the experimental conditions used for calibrating the design formulas in Section 4.1.5.
If different configurations are used, their effectiveness must be demonstrated through specific experimental tests. In particular, alternative strength values may be used instead of those calculated with the formulas in Section 4.1.5, provided they are evaluated using the "Design Assisted by Testing" approach described in EN 1990 – Annex D.

Manufacturing and Installation Process for Fan-Shaped Anchors:
Fan-shaped anchors can be made from fiber ropes or by rolling up strips of unidirectional fibers. In any case, they must be equipped at one end with a rigid tip, created using the same resin that will be used to secure the connectors. This rigid tip will facilitate the insertion of the anchor into the pre-

drilled hole in the structural element.

Step-by-Step Installation Procedure:

- Drill the necessary holes into the surface to be reinforced and clean both the holes and the surrounding surface.
- Fill the holes with resin and insert the connectors using a rigid rod, which will also help keep the loose fibers emerging from the hole perpendicular to the surface to be reinforced.
- Allow the connection resin to cure before proceeding.
- Apply the first layer of resin (which may include a primer) to the surface where the FRP reinforcement will be installed.
- Place the fiber strip on the resin-coated surface, spreading the fibers at the anchor locations to allow the fan-shaped strands to pass through the reinforcement strip.
- Impregnate the reinforcement fibers by rolling the fiber strip to ensure full saturation.
- Remove the rigid rods used to align the connectors, then spread the fibers of the fan-shaped anchors evenly in a fan-like pattern.
- Apply additional resin to impregnate the connectors and perform a final rolling operation to ensure proper bonding.

Complete the process by applying the final protective coating, ensuring that the reinforcement is fully cured and protected.

4.9.2.3 Protection of the Strengthening

(1) Outdoor FRP applications must be protected from direct sunlight to prevent chemical and physical degradation of the epoxy matrix.

- Protection of the FRP can be achieved using acrylic coatings or cement-based coatings applied over a quartz-sprinkled epoxy primer.

(2) Fire protection may be provided using:

- Gypsum board, calcium silicate panels, or fire-resistant coatings.
- Coatings must be certified for FRP application and adhesion-tested under high-temperature and load conditions.

(3) Fire Protection Measures for FRP Reinforcement.
Different fire protection techniques can be used, including:
Gypsum board panels,

- Calcium silicate panels,
- Similar protective materials, or
- Fire-resistant coatings and plasters.

In all cases, the selected materials must be appropriately certified to withstand fire exposure. Manufacturers must specify in their technical data sheets the level of protection achievable based on coating thickness.

Fire-resistant panels should be installed over the reinforcement using anchors that must never cut or pierce the FRP fibers.

For fire-resistant plasters, they must be certified specifically for FRP applications to ensure:

- Proper adhesion under both normal temperature conditions and during fire exposure,
- Adequate performance under static loading.

Additionally, fire-resistant plaster must be applied to the composite material following the manufacturer's guidelines provided in the technical documentation.

4.10 NUMERICAL EXAMPLES

Several numerical applications related to the strengthening of reinforced concrete structures with FRP are provided in Appendix H.

5 STRENGTHENING OF MASONRY STRUCTURES

5.1 GENERAL PRINCIPLES

5.1.1 Scope and Field of Application

(1) FRP strengthening systems can effectively consolidate masonry structures. This chapter provides guidelines for designing and verifying structural elements reinforced with these systems.

(2) The primary goal of the strengthening intervention is to enhance the resistance of individual structural elements and the entire building against applied loads. Additionally, when possible, the intervention should also increase the displacement capacity at failure.

Note:
To date, strengthening masonry structures with SFRP reinforcements is not a widely practiced approach, and the available technical and scientific literature on the subject remains limited.

5.1.2 Restoration Interventions on Historically and Monumentally Significant Structures

1) When structural reinforcement involves buildings of historical or monumental significance, a specific justification must be provided to demonstrate the necessity, urgency, and compatibility of the intervention with restoration principles (see § 3.1(3)).

5.1.3 Criteria for Structural Strengthening Design

(1) The strengthening interventions covered in these guidelines involve the application of FRP systems to structural elements of the building through adhesion or mechanical anchoring devices. The application can be performed on the external surfaces of the masonry (EBR systems) or within slots and grooves made inside the masonry (NSM systems).

(2) The objectives of these interventions may include:

- Increasing the strength of panels, arches, or vaults;
- Confining columns to enhance their compressive strength and ductility;
- Connecting elements that work together to resist external forces (e.g., vault and wall tie rods, connections between orthogonal walls, etc.);
- Converting non-structural elements into structural ones by improving stiffness and strength;
- Limiting crack openings.

(3) Strengthening interventions must always be evaluated within the context of an overall assessment of the mechanical behavior of the consolidated structure.

(4) Strengthening interventions are effective when the composite is subjected to tensile forces. FRP strengthening systems subjected to compression do not generally enhance the performance of masonry due to the geometric properties of the latter. Moreover, they may be prone to detachment from the substrate due to local instability phenomena.

(5) Cyclic tensile and compressive stresses, such as those induced by seismic events and thermal variations, can significantly degrade the adhesion between the masonry and the FRP. This issue

may be mitigated by embedding the reinforcement within grooves made on the masonry surface to prevent potential instability or to use mechanical connection devices.

(6) FRP strengthening systems must be applied only to structural elements with adequate mechanical properties. Suppose the masonry is damaged, heterogeneous, or affected by any defect that compromises the proper transmission of stresses at the masonry-FRP interface. In that case, the substrate must first be consolidated using traditional techniques. Additionally, the choice of the strengthening system should consider the physical and chemical properties of the composite in relation to the objectives of the intervention (further details are provided in § 5.9)

(7) It is essential to recognize the complete lack of breathability of composite materials. Consequently, FRP strengthening interventions should be installed at discrete intervals with gaps between individual strips and not cover the entire area of the masonry façade.

5.2 SAFETY ASSESSMENT

5.2.1 Structural Modeling

(1) The design of strengthening interventions must be based on a mechanical model that accurately represents the behavior of the structure under future service conditions.

(2) Proven nonlinear models capable of simulating the inelastic behavior of masonry, particularly its limited or even negligible tensile strength, may be used. With the necessary precautions outlined in the following points, linear elastic models may also be adopted. The structural analysis must aim to determine all the stress components required for subsequent verifications.

(3) In cases where stresses are determined using approximate yet equilibrium-compliant stress distributions that do not necessarily satisfy compatibility conditions, any tensile stresses must be fully absorbed by the FRP reinforcement, which must be designed appropriately and bonded for this purpose. These stress distributions must not lead to brittle failure of the strengthened masonry.

(4) In structures with regular or repetitive sections, it is possible to identify partial structural schemes within the construction that are still suitable for assessing the overall behavior of the strengthened structure.

(5) Safety checks against specific local failure mechanisms (some of which are described below) may be performed using simplified models, provided they are adequately justified. In this regard, limit states analysis methods are beneficial.

5.2.2 Verification Criteria

(1) The failure modes of masonry structures strengthened with FRP include:

- Tensile cracking of the masonry.
- Masonry crushing.
- Shear-sliding failure of the masonry.
- Failure of the FRP composite.
- Debonding of the FRP reinforcement from the masonry substrate.

The failure of strengthened structures generally results from the combined occurrence of multiple failure modes.

5.2.3 Safety Verification

(1) Masonry exhibits anisotropic and nonlinear behavior even at relatively small deformations. The stress-strain relationship can vary significantly depending on factors such as the masonry bond pattern, the type of masonry units (artificial or natural), and the type of mortar used.

(2) When subjected to uniaxial tensile testing, masonry displays brittle behavior, with tensile strength values significantly lower than those obtained from compression tests. A widely accepted constitutive assumption assigns a zero tensile strength to masonry. This assumption is particularly supported for existing (historic and monumental) constructions, where the tensile strength is highly variable and tends to degrade over time.

(3) Regarding uniaxial compression behavior, laboratory experiments indicate that the masonry's constitutive relationship is:

- Essentially linear for low strain values;
- Nonlinear with an increasing trend up to a peak compressive stress;
- Nonlinear with a decreasing trend beyond the peak stress (softening branch), where the material's strength progressively deteriorates, depending on the masonry type.

(4) Compression behavior is also influenced by lateral confinement: increasing the transverse compression enhances both strength and ductility.

(5) The shear strength of masonry depends on the applied compressive stress, as it results from both the internal cohesion of the material and friction effects.

(6) In situ masonry is characterized by average mechanical properties (§ 3.3.3(6)). For masonry with mortar joints, the following mechanical properties must be considered:

- Compressive strength perpendicular to the mortar joints, f_{mm};
- Compressive strength parallel to the mortar joints, f^{h}_{mm};
- Shear strength, f_{vm}.

As a general guideline, f^{h}_{mm} may be assumed as 50% of f_{mm}.

(7) The design values of masonry mechanical properties must be calculated in accordance with the guidelines provided in § 3.3.3.

(8) In most engineering applications, the σ-ε constitutive relationship of masonry under uniaxial stress conditions can be simplified as follows:

- Tension: Zero strength assumption;
- Compression:
    - Linear behavior up to the design strength, f_{md}, corresponding to a strain $\bar{\varepsilon}_m$;
    - Constant stress, equal to f_{md}, for strain values in the range $\bar{\varepsilon}_m \leq \varepsilon \leq \varepsilon_{mu}$.
    - Zero stress for strains greater than the ultimate strain, ε_{mu};

(9) In the absence of experimental data, the ultimate design strain, ε_{mu}, may be taken as 3.5‰.

(10) Alternatively, more comprehensive constitutive models that capture the various behaviors described in point (3) may be used, provided they are validated through suitable experimental investigations.

(11) The maximum strain of the FRP reinforcement considered in the design is:

$$\varepsilon_{fd} = \min\left\{\eta_a \cdot \frac{\varepsilon_{fk}}{\gamma_{f1}}, \varepsilon_{fdd}\right\} \tag{5.1}$$

where:

- ε_{fk} = characteristic strain at rupture;
- ε_{fdd} = maximum strain in the reinforcement at the onset of intermediate debonding from the masonry substrate (§5.3, equation (5.12)).
- η_a and γ_{f1} = conversion factor per Table 3-3 in § 3.4.1 of these guidelines.

For masonry exposed to high humidity levels, it is recommended to adopt particularly conservative values for the η_a conversion factor.

(12) Safety verification must be conducted exclusively for the ultimate limit state (ULS). Two possible cases are distinguished based on the type of structural analysis performed:

- If nonlinear models incorporating complete constitutive relationships and numerical solution techniques are used, the verification must ensure that the structure's capacity is not less than the applied demand. The demand must be evaluated using the load combinations prescribed by the applicable regulations. Additionally, particular care must be taken to demonstrate that the solution is objective, meaning it does not depend on the specific discretization adopted.
- Suppose the structural model is formulated within an elastic linear framework or employs simplified schemes with equilibrium-compliant stress distributions that may not necessarily satisfy compatibility conditions. In that case, verification must be performed with respect to the design stresses acting on individual structural elements. Specifically, the verification must ensure that the design shear and bending moments (or specific stress values for two-dimensional structures) do not exceed the corresponding resistance values. These resistance values must be determined as functions of the applied normal force, accounting for the nonlinear behavior of the materials comprising the structural elements, according to the adopted constitutive model.

5.3 ASSESSMENT OF ADHESION STRENGTH AND DEBONDING RESISTANCE FOR EBR SYSTEMS

(1) In the strengthening of masonry walls using externally bonded (EBR) laminates or fabric-reinforced composite materials, the bond between the masonry substrate and the composite plays a crucial role. Debonding failure is a brittle mechanism and, therefore, undesirable. In accordance with the capacity design principle, this failure mode should not occur before the inelastic crushing of the masonry.

(2) Given the wide variety of existing masonry compositions—such as masonry made of artificial clay or concrete blocks or natural stone masonry with regular or irregular units—the bonding surface is typically heterogeneous. In the case of irregular masonry surfaces, it is common practice to apply a leveling mortar layer before bonding the reinforcement, creating a suitable surface for adhesion. As a result, the same strengthening system may be bonded to different materials along its length, each with distinct interface properties.

(3) When the adhesive used for the reinforcement has a higher strength than the substrate material, the loss of adhesion between the composite and the masonry wall occurs through the cohesive failure of a superficial layer of brick, stone block, or mortar.

5.3.1 General Considerations and Failure Modes

(1) The debonding of laminates or fabric composites from the masonry substrate can occur through two different mechanisms: end debonding, which initiates at the reinforcement's extremities, and intermediate crack debonding, which originates from mortar joints or transverse cracks in the masonry. At both the reinforcement's extremities and in areas spanning mortar joints or cracks, the FRP-masonry interface is subjected to high shear and axial stresses, concentrated over lengths of approximately 150–200 mm from the discontinuity section.

(2) End debonding can be accompanied by the removal of a thin masonry layer (rip-off failure), particularly when high shear stresses at the extremities are combined with significant axial tensile forces (Figure 5-1).

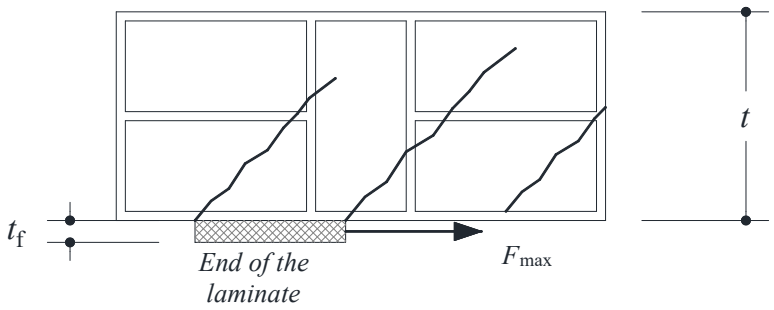

Figure 5-1 – Failure mechanism due to anchorage brick extraction.

(3) The debonding force at the substrate is reduced in cases of combined loading when the reinforcement system is also subjected to out-of-plane forces. In the case of reinforcements applied on concave surfaces (such as the intrados of arches or vaults) or when the flexural stiffness of the laminate is high, significant peeling forces perpendicular to the interface are mobilized, which contribute to reducing the debonding strength.

(4) The resistance of an FRP system to crack propagation in masonry is maximized when the fiber orientation is perpendicular to the cracks.

5.3.2 End Debonding Resistance

The following section adopts symbols already introduced for FRP reinforcement of concrete elements.

(1) The optimal anchorage length, ℓ_{ed}, can be estimated using the following equation:

$$\ell_{ed} = \max\left\{\ell_{ed,min};\ \gamma_{Rd}\frac{1}{f_{bm}}\sqrt{\frac{\pi^2 E_f t_f \Gamma_{Fm}}{2}}\right\} = \max\left\{\ell_{ed,min};\ \gamma_{Rd}\frac{\pi}{2}\sqrt{\frac{E_f t_f \cdot s_u}{f_{bm}}}\right\} \tag{5.2}$$

where:

- E_f = modulus of elasticity in the fiber direction
- t_f = thickness of the FRP reinforcement
- f_{bm} = mean value of the maximum bond stress at the substrate-reinforcement interface
- Γ_{Fm} = mean value of the specific fracture energy
- γ_{Rd} = 1.2 is a model partial factor
- $\ell_{ed,min}$ = is a minimum anchorage length set at 150 mm for all types of masonry substrate.

The mean value of the maximum bond stress, f_{bm}, is calculated as:

$$f_{bm} = k_{Gm} \cdot \frac{\sqrt{f_{bcm} \cdot f_{btm}}}{2 \cdot FC} \tag{5.3}$$

where:

- f_{bcm} = mean compressive strength of the masonry blocks
- f_{btm} = mean tensile strength of the masonry blocks; the tensile strength may be assumed as the minimum between the experimentally determined value (if available) and 0.10 times the compressive strength (0.10 f_{bcm}).
- k_{Gm} = is an empirical coefficient calibrated for different masonry substrates according to EN1990 – Annex D (*Design Assisted by Testing*), with the following values:
  - Brick masonry: k_{Gm} = 0.40;
  - Tuff masonry: k_{Gm} = 1.30;
  - Lecce stone masonry: k_{Gm} = 0.24;
  - Sicilian calcarenite masonry: k_{Gm} = 0.73.

The mean fracture energy, assuming a bilinear bond-slip relationship, is expressed as:

$$\Gamma_{Fm} = \frac{1}{2} f_{bm} s_u = \frac{k_{Gm} s_u}{4} \cdot \frac{\sqrt{f_{bcm} f_{btm}}}{FC} \tag{5.4}$$

where:

- s_u is the ultimate slip of the bond interface, with the following values based on different masonry substrates:
  - Brick masonry: s_u = 0.40 mm;

- Tuff masonry: s_u = 0.40 mm;
- Lecce stone masonry: s_u = 0.30 mm;
- Sicilian calcarenite masonry: s_u = 0.30 mm.

(3) For debonding failures involving the surface layer of masonry, the mean and design values of the maximum tensile force, $F_{max,m}$ and $F_{max,d}$, and consequently, the maximum tensile stresses, $f_{fdm,}$ and f_{fdd}, that the FRP can withstand without triggering end debonding, are given by:

$$F_{max,m} = k_b \cdot b_f \cdot \sqrt{2 \cdot E_f \cdot t_f \cdot \Gamma_{Fm}} \tag{5.5}$$

$$F_{max,d} = \frac{k_b \cdot b_f}{\gamma_{f2}} \cdot \sqrt{2 \cdot E_f \cdot t_f \cdot \Gamma_{Fk}} \tag{5.6}$$

$$f_{fdm} = k_b \cdot \sqrt{\frac{2 \cdot E_f \cdot \Gamma_{Fm}}{t_f}} \tag{5.7}$$

$$f_{fdd} = \frac{k_b}{\gamma_{f2}} \cdot \sqrt{\frac{2 \cdot E_f \cdot \Gamma_{Fk}}{t_f}} \tag{5.8}$$

where:

- $\gamma_{f2} = 1.3$ as specified in § 3.4.1 or ultimate limit state verification of debonding.
- k_b is a geometric correction factor, calculated as:

$$k_b = \sqrt{\frac{3 - b_f / b}{1 + b_f / b}} \tag{5.9}$$

where:
b_f = width of the stress diffusion zone at the bond interface
b = width of the FRP strip**.**
The value of b may be calculated by adding the width of the diffusion zone b_f to the width of the diffusion zone of the bond stresses, b_d.
For irregular masonry, b_d can be approximated as the mean diameter of the stone blocks (Figure 5-2).

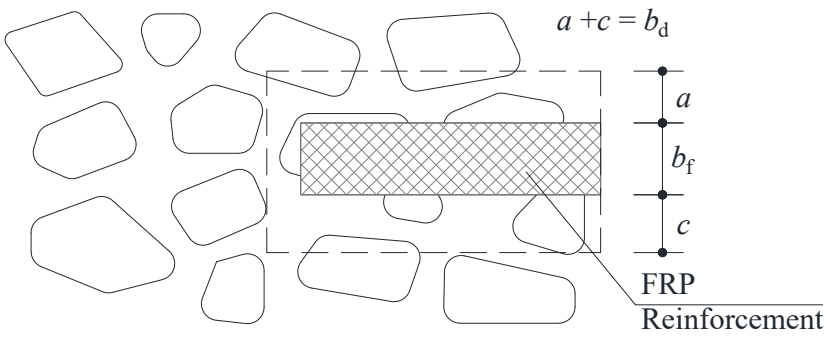

Figure 5-2 – Diffusion of the bond stresses.

Instead, in the case of regular masonry, the dimension b_d can be assumed to be equal to the width of the masonry block forming the substrate in the direction perpendicular to the reinforcement axis (Figure 5-3).

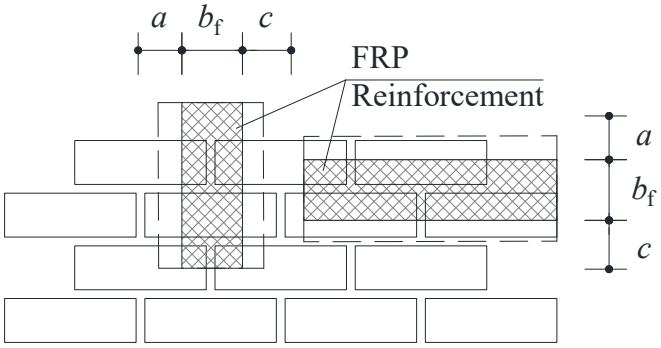

Figure 5-3 –Stress diffusion in the bond interface for regular masonry.

In Equation (5.5), the design value of the specific fracture energy, Γ_{Fk} is calculated as follows:

$$\Gamma_{Fk} = \frac{1}{2} f_{bk} \cdot s_u = \frac{k_{Gk}}{4} \frac{\sqrt{f_{bcm} f_{btm}}}{FC} \cdot s_u \tag{5.10}$$

where:

- k_{Gk} is the characteristic value (5% fractile) of the dimensionless coefficient calibrated based on experimental data in accordance with EN1990 – Annex D (*Design Assisted by Testing*, see Appendix D), with the following values:
  - Brick masonry: $k_{Gk} = 0.15$
  - Tuff masonry: $k_{Gk} = 0.60$
  - Sicilian calcarenite masonry: $k_{Gk} = 0.38$
  - Lecce stone masonry: $k_{Gk} = 0.12$
- s_u represents the ultimate slip value, which should be assumed as previously defined for the various masonry substrates.

If the reinforcement is bonded to masonry with mortar joints spaced closer than the optimal anchorage length, the design tensile stress in the reinforcement must be reduced to 85% of the value obtained from Equation (5.5).

or pultruded FRP applications, the k_G values must be determined through appropriate experimental testing using statistically sound procedures in accordance with EN1990 – Annex D (Design Assisted by Testing).

The formulas presented above are valid for resins with sufficiently low viscosity, ensuring proper penetration into the surface pores of masonry blocks. High-viscosity resins and low-porosity substrates should be treated with caution.

(4) Reduction of Design Tensile Stress for Shorter Anchorage Lengths
For anchorage lengths, l_b, shorter than the optimal length, l_{ed}, the design tensile stress must be appropriately reduced, following the relationship:

$$f_{\mathrm{fdd,rid}} = f_{\mathrm{fdd}} \cdot \frac{\ell_{\mathrm{b}}}{\ell_{\mathrm{ed}}} \cdot \left(2 - \frac{\ell_{\mathrm{b}}}{\ell_{\mathrm{ed}}} \right) \tag{5.11}$$

(5) Considerations for Anchoring Devices
When using special anchoring devices (see § 4.1.3), the design tensile stress at the ends of the FRP, denoted by f_{ffd}, must be determined through specific experimental investigations.

(6) Bond Verification in the Presence of a Leveling Layer
If the FRP reinforcement is not directly applied to the masonry surface but instead to a leveling layer (typically an epoxy-based mortar), the debonding verification must be conducted at the interface between the leveling layer and the underlying masonry. This is valid, provided that the epoxy resin in the mortar and the FRP impregnation resin cure simultaneously.

Unless a more detailed evaluation is available, Equations (5.2) and (5.11) can still be used for verification.

To facilitate this verification, defining, t_{r} and E_{r} as the average thickness and elastic modulus of the leveling layer, and, t_{h}, and E_{h}, as the thickness and elastic modulus of the homogenized system (which includes both the reinforcement and the leveling layer), these values can be estimated using the following relationships:

$$t_{\mathrm{h}} = t_{\mathrm{f}} + t_{\mathrm{r}}, \quad E_{\mathrm{h}} = \frac{E_{\mathrm{f}} \cdot t_{\mathrm{f}} + E_{\mathrm{r}} \cdot t_{\mathrm{r}}}{t_{\mathrm{h}}} \tag{5.12}$$

The thickness t_{r} of the leveling layer can be estimated based on the volume of material applied, assuming the layer is modeled as a cylindrical solid. The ultimate bond strength is determined using Equations (5.7), (5.8) and (5.11), considering the effective width b_{h} of the homogenized system as:

$$b_{\mathrm{h}} = b_{\mathrm{f}} + 2t_{\mathrm{r}}$$

5.3.3 Resistance to Intermediate Debonding

(1) In the absence of more precise determinations, verification against intermediate debonding is performed by limiting the tensile stress in the FRP reinforcement to the design value:

$$f_{\mathrm{fdd,2}} = k_{\mathrm{L}} \cdot f_{\mathrm{fdd}} \quad (1.0 \le k_{\mathrm{L}} \le 2.0). \tag{5.13}$$

Specifically, if the distance to the free end is less than $3\ell_{ed}$, it can be set to k_{L} =1.5.
By assuming in Equation (5.1):

$$\varepsilon_{\text{fdd}} = \varepsilon_{\text{fdd,2}} = \frac{f_{\text{fdd,2}}}{E_{\text{f}}}, \tag{5.14}$$

where E_f is the modulus of elasticity of the FRP composite in the fiber direction, verification against intermediate debonding is implicitly satisfied. However, verification against end debonding must still be performed according to the indications in § 5.3.2.

5.3.4 Resistance to Debonding Under Normal Action to the Adhesion Plane

(1) The debonding force due to an action normal to the adhesion plane is difficult to quantify. It should generally be determined through experimental tests conducted on the masonry surface where the reinforcement is applied.

(2) For reinforcements with slight curvature, the predictive formulas for flat reinforcements can continue to be used.

5.4 EVALUATION OF RESISTANCE TO DEBONDING FROM THE SUBSTRATE FOR REINFORCEMENTS APPLIED IN GROOVES

(1) The reinforcement of masonry structures can also be carried out using pultruded elements such as strips and bars embedded in grooves and anchored with resin (NSM). The grooves should be made in such a way as to minimize the exposed mortar areas, for example, by completely removing the thickness of horizontal joints or vertical mortar joints.

(2) The design of NSM reinforcements can be carried out based on the same principles outlined for concrete structures, using the mechanical parameters of the masonry blocks. Specifically, in equations (4.35), (4.41), (4.49), the average values of the compressive and tensile strength of the masonry blocks, denoted as f_{bcm} and f_{btm}, respectively, should be used. The average tensile strength of the blocks can be assumed as the lower value between the experimentally determined strength (if available) and $0.10\,f_{bcm}$.

5.5 VERIFICATION OF RECURRING STRUCTURAL ELEMENTS

The following section examines some FRP strengthening applications designed to counteract specific local collapse mechanisms that frequently occur in engineering practice.

5.5.1 Strengthening of Masonry Walls

(1) Masonry panels in buildings can be strengthened using FRP to increase either their load-bearing capacity or ductility against actions both in-plane and out-of-plane.
The following sections suggest some simplified verification methods to assess the safety of masonry panels. These verifications are not exhaustive and should be supplemented, if necessary, with additional checks appropriate to the complexity of the specific case under examination.

5.5.1.1 Verification for Out-of-Plane Actions

(1) Out-of-plane collapse of masonry panels is one of the most common local failure mechanisms. Various factors, including seismic actions, thrust from arches and vaults, or lack of verticality in the panels, can trigger this failure.

This failure mechanism can manifest in different forms:

- Simple overturning (§ 5.5.1.1.1);
- Vertical bending (§ 5.5.1.1.2);
- Horizontal bending (§ 5.5.1.1.3).

5.5.1.1.1 Verification for Simple Overturning

(1) The mechanism consists of the panel overturning around a cylindrical hinge that forms at its base due to the limited tensile strength of the masonry. Although the hinge has a finite width corresponding to the compressed masonry zone, it can be approximately assumed to be positioned at the outer edge of the masonry panel.

Overturning failure typically affects walls that are not anchored to perpendicular walls or walls that are not restrained at the top. The mechanism depends on various factors, such as boundary conditions, the slenderness of the wall, and the dimensions of the masonry section.

(2) A possible intervention with FRP reinforcement consists of inserting one or more horizontal elements bonded to the top of the exterior face of the wall, extended onto the orthogonal walls at the ends, and anchored to them. If pilasters are present on the perpendicular walls, shaping the FRP reinforcement to follow the pilaster profile can generate significant tensile stresses in the substrate, increasing the risk of debonding. It is, therefore, advisable to adopt appropriate measures, such as mechanical anchorages.
The most significant benefits and effectiveness against simple overturning are achieved when the entire masonry structure is fully wrapped with reinforcement, where possible. Special attention should be given to rounding corners to reduce stress concentrations in these areas, as specified in§ 5.9.2.2.
As an example, consider a masonry panel subjected to the following design actions:

- P Self-weight of the panel,
- N_{d} Axial force acting on the top of the panel,
- α_{s} The ratio between the intensity of horizontal and vertical loads,
- F_{d} Force in the FRP reinforcement.

Additional forces acting at the top of the panel, such as thrust from the roof slab, may also be considered.

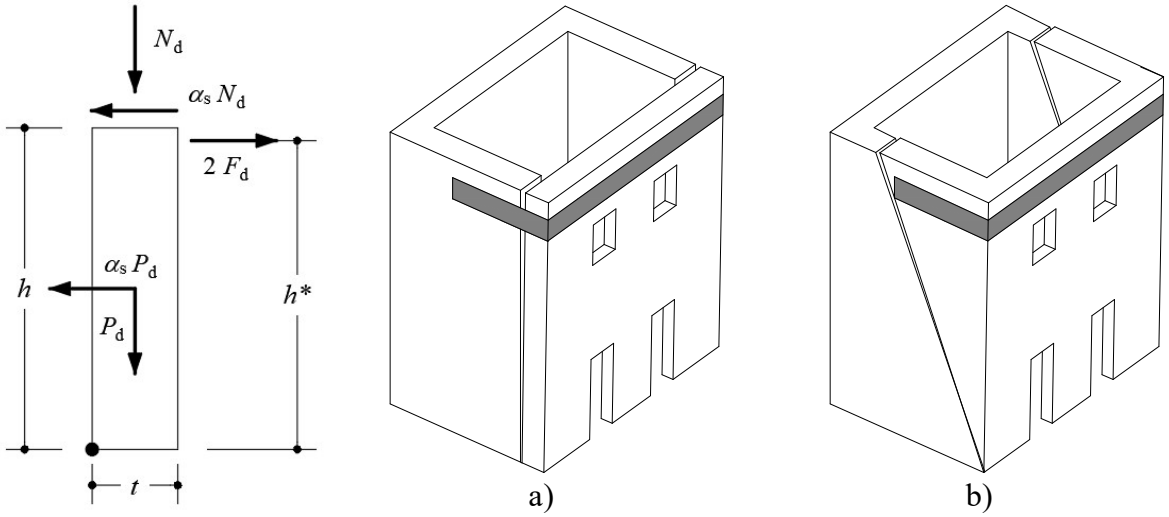

Figure 5-4 – Calculation scheme for the simple overturning collapse mechanism.

(3) Referring to mechanism (a) in Figure 5-4, assuming negligible constraints from floors and perpendicular walls, the tensile force in the reinforcement is determined by the rotational equilibrium equation around the base of the panel:

$$F_d = \frac{1}{2 \cdot h^*} \cdot \left[\alpha_s \cdot (P_d \cdot \frac{h}{2} + N_d \cdot h) - (P_d + N_d) \cdot t \right] \tag{5.15}$$

where h^* is the distance from the panel base to the application point of the FRP composite.
To prevent the simple overturning of the masonry panel, the following verifications must be performed:

- Tensile verification of the FRP reinforcement
  Considering A_f as the area of the FRP reinforcement and $f_{fd} = E_f \varepsilon_{fd}$ as its design tensile strength, the maximum force that can be developed is:

  $$F_{Rd} = A_f \cdot f_{fd}$$

  The verification is satisfied if:

  $$F_d \leq F_{Rd} \tag{5.16}$$

- Verification of FRP reinforcement debonding from the perpendicular walls
  Considering $F_{pd} = A_f \cdot f_{fdd}$ as the maximum anchoring force of the FRP composite applied to each of the two perpendicular walls, the verification is satisfied if:

  $$F_d \leq F_{pd} \tag{5.17}$$

In general, the second verification is more critical than the first. When full wrapping is applied with adequate overlap, this verification is unnecessary.

(4) In the absence of full wrapping, the FRP composite must extend sufficiently onto the perpendicular walls to prevent the formation of a wedge-type collapse mechanism, as illustrated in Figure 5-4 b) which would compromise the entire reinforcement system.
The verification can be performed using limit analysis while conservatively neglecting the contribution of cohesive stresses in the masonry.
The assumed collapse mechanism in Figure 5-4 b) identifies failure surfaces passing through the cylindrical hinge and the terminal sections of the reinforcement.

(5) The horizontal sections of the panel must be verified for combined bending and shear in accordance with the applicable regulations.

5.5.1.1.2 Verification for Vertical Bending of the Masonry Strip

(1) A masonry panel that is well restrained at both its base and top may collapse under horizontal actions due to the bending stresses that develop within it. This type of collapse occurs with the formation of three plastic hinges: one at the base, one at the top, and a third at an intermediate position. Panels that are particularly tall and/or are restrained by orthogonal masonry piers that are far apart are more susceptible to this failure mechanism.

(2) During seismic events, this type of collapse is particularly critical for panels supporting floor slabs at different levels on opposite sides due to variations in story heights. In such cases, applying FRP systems with vertically oriented fibers to the surfaces of the panel, adequately anchored, creates a “reinforced masonry” system in which compression forces due to bending are absorbed by the masonry. At the same time, the FRP reinforcement resists tensile forces.
As an example, consider (Figure 5-5) a unit-width strip of a masonry panel subjected to the following design actions:

- $P_{\mathrm{d}}^{(\mathrm{s})}$ = Self-weight of the upper portion of the panel,
- $P_{\mathrm{d}}^{(\mathrm{i})}$ = Self-weight of the lower portion of the panel,
- N_{d} = Axial force acting at the top of the panel,
- α_{s} = The ratio between the intensity of horizontal and vertical loads,
- Q_{d} = Additional horizontal thrust, if applicable.

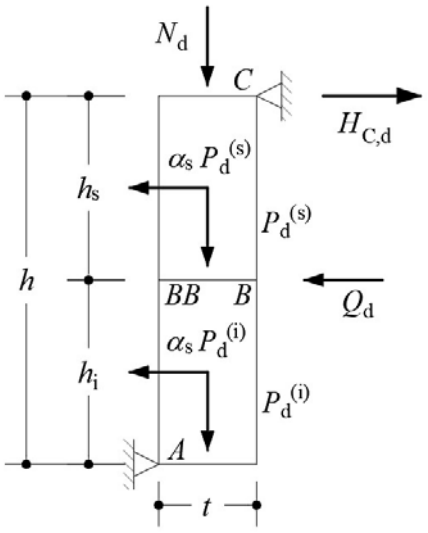

Figure 5-5 - Calculation scheme for the vertical bending collapse mechanism.

The design reaction force at restraint point C can be determined using the rotational equilibrium equation about hinge A:

$$H_{\mathrm{C,d}} = \frac{h_{\mathrm{i}} \cdot (2 \cdot Q_{\mathrm{d}} + \alpha_{\mathrm{s}} \cdot P_{\mathrm{d}}^{(\mathrm{i})}) + \alpha_{\mathrm{s}} \cdot P_{\mathrm{d}}^{(\mathrm{s})} \cdot (2 \cdot h - h_{\mathrm{s}}) - t \cdot (N_{\mathrm{d}} + P_{\mathrm{d}}^{(\mathrm{s})} + P_{\mathrm{d}}^{(\mathrm{i})})}{2 \cdot h} \tag{5.18}$$

The masonry cross-section at B-B, where the fiber-reinforced composite must be applied to prevent the formation of the plastic hinge, is subjected to a normal force and a bending moment, respectively, equal to:

$$\begin{aligned} N_{\mathrm{Sd}} &= N_{\mathrm{d}} + P_{\mathrm{d}}^{(\mathrm{s})}, \\ M_{\mathrm{Sd}} &= H_{\mathrm{C,d}} \cdot h_{\mathrm{s}} - \alpha_{\mathrm{s}} \cdot P_{\mathrm{d}}^{(\mathrm{s})} \cdot \frac{h_{\mathrm{s}}}{2}. \end{aligned} \tag{5.19}$$

The vertical bending verification is satisfied if:

$$M_{\mathrm{Sd}} \leq M_{\mathrm{Rd}} \tag{5.20}$$

The design bending moment capacity, M_{Rd}, of the strengthened masonry section can be expressed as a function of the mechanical properties of the masonry and the fiber-reinforced composite (§), the wall thickness, t, the value of the axial force acting on the section, and the relevant partial model coefficient, γ_{Rd}, which should be taken as (Table 3-2 in § 3.4.2).
For portions of the panel where the FRP composite does not contribute effectively, the bending moment capacity, M_{Rd}, should be calculated without considering the contribution of the reinforcement.

(3) As a simplified approach, the verification of the strengthened masonry section under combined axial and bending stresses can be conducted by assuming a constant compressive stress distribution equal to 0.85 f_{md}, extending over a portion of the cross-section with a depth of 0.6 ÷ 0.8 x, where x is the distance from the extreme compressed edge to the neutral axis.

(4) It must also be verified that the shear force, V_{Sd}, under the combined load condition does not exceed the shear resistance of any section:

$$V_{\mathrm{Rd,m}} = 1 \cdot x \cdot f_{\mathrm{vd}} \tag{5.21}$$

where f_{vd} is the design shear strength of the masonry, evaluated in accordance with current standards, based on the average normal stress calculated as the ratio between the resultant compressive forces and the area of the surface between the extreme compressed edge and the neutral axis.

(5) Additionally, the reinforcement must be verified against end debonding.

(6) Vertical reinforcements must be spaced at an interval, p_{f}, that meets the following requirements:

$$p_f \leq 3 \cdot t + b_f \tag{5.22}$$

where b_f is the width of the reinforcement strips used. Larger spacing distances should be carefully evaluated.

5.5.1.1.3 Verification for Horizontal Strip Bending

(1) In masonry panels that are effectively restrained by spine walls but not secured at the top by appropriate structures such as tie beams or reinforced slabs, mechanisms may develop that lead to the collapse of a portion of the wall, as exemplified in Figure 5-6.
In the scenario just described, resistance to horizontal forces is ensured by the arching action of the upper strip, as illustrated in Figure 5-7.
The ultimate value of the uniformly distributed horizontal load per unit area, q_d, that this arch can sustain can be evaluated using the following equation:

$$q_d = \frac{2 \cdot t^2}{3 \cdot L^2} \cdot f_{md}^h \tag{5.23}$$

Where

- L is the width of the panel, and
- f_{md}^h is the design compressive strength of the masonry in the horizontal direction.

The value of q_d can be increased by applying FRP strengthening systems.

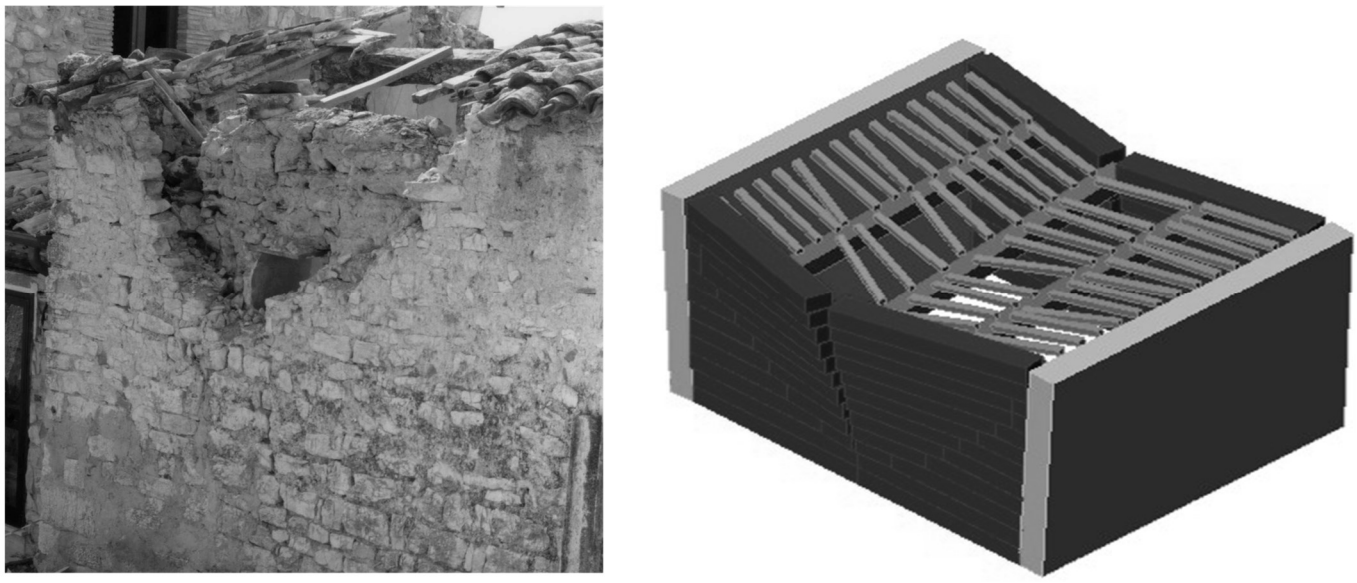

Figure 5-6 – Collapse due to horizontal bending.

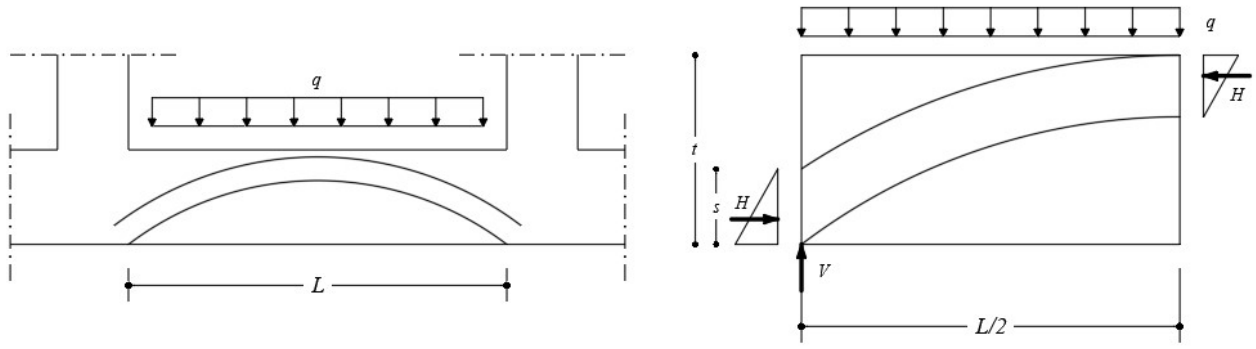

Figure 5-7 – Collapse due to horizontal flexure.

When properly anchored, composite materials help counteract this failure mechanism by providing flexural resistance to the upper strip of the panel, effectively transforming it into a "reinforced masonry beam."
Unless a more precise assessment of the required strengthening strip extension is made, it can generally be assumed that the reinforced strip should be half the panel's total height.
In this case, the design bending moment, M_{sd}, is determined considering the seismic action associated with the inertia of the wall itself or wind loads.

(2) An additional verification of the horizontal strip must be performed at locations where floor slabs interact with the wall or where thrusting roof structures are present. In such cases, the thickness of the horizontal strip resisting the applied forces from these structures can be determined by assuming a 45° stress diffusion pattern.

(3) The horizontal bending verification is satisfied if the inequality (5.20) is met, where the resisting moment, M_{Rd}, is determined based on:

- The mechanical properties of the masonry,
- The fiber-reinforced composite (FRP), and
- The thickness t of the masonry.

If a detailed evaluation of the horizontal normal force generated by the interaction with transverse walls is not available, this force must be assumed to be zero.

(4) Additionally, shear verification must be performed at the connection sections between the panel and the orthogonal walls.
This verification must follow the same procedure described in §5.5.1.1.2(3), assuming for f_{vd} the value corresponding to a zero compression force.

(5) The FRP composite must also be verified against end-debonding failure.

(6) Lastly, orthogonal walls must be verified against the tensile stress they experience near the connection to the panel.

5.5.1.2 Verifications for In-Plane Actions on the Panel

(1) he required verifications for masonry panels subjected to in-plane stresses, including:

- In-plane bending (flexure);
- Shear.

5.5.1.2.1 In-Plane Bending

(1) To enhance the in-plane bending capacity of masonry panels, vertically oriented FRP reinforcements can be applied symmetrically on both faces of the panel and adequately anchored.

(2) In a simplified approach, the in-plane bending verification can be conducted similarly to the method outlined in §5.5.1.1.2(2).

(3) In particular, the verification must also be performed on the end sections of the panel segments defined by the foundation and the first-floor slab or by two successive floor slabs.
In the absence of mechanical anchoring devices, the contribution of the composite should be disregarded in the verification.

5.5.1.2.2 Shear

(1) The shear capacity of a masonry panel reinforced for in-plane bending with vertically oriented FRP composites (applied symmetrically on both faces) can be further enhanced by additional FRP composites with fibers preferably aligned in the shear force direction, also applied symmetrically on both faces of the panel.
This method complements the classical shear resistance mechanism of masonry, which is based on friction, by enabling an additional truss action that enhances shear resistance through internal force equilibrium.

(2) If the formation of a resisting truss system is ensured, the design shear strength of the reinforced masonry panel, V_{Rd}, can be calculated as the sum of:

- The contribution from masonry frictional resistance, $V_{Rd,m}$,
- The contribution from the FRP reinforcement, $V_{Rd,f}$,

up to the ultimate shear strength, $V_{Rd,max}$, which corresponds to the failure of the compressed diagonal struts in the truss system:

$$V_{Rd} = \min\left\{ V_{Rd,m} + V_{Rd,f}; V_{Rd,max} \right\} \tag{5.24}$$

(3) If the shear reinforcement is aligned parallel to the mortar joints, the contributions defined above can be evaluated using the following expressions:

$$V_{Rd,m} = x \cdot t \cdot f_{vd} \tag{5.25}$$

$$V_{Rd,f} = \frac{1}{\gamma_{Rd}} \cdot 0.6 \cdot d \cdot (E_f \cdot \varepsilon_{fd}) \cdot 2 \cdot t_f \cdot \frac{b_f}{p_f} \tag{5.26}$$

where:

- x = distance from the neutral axis to the extreme compressed edge,
- t = wall thickness,
- f_{vd} = design shear strength of the masonry, evaluated per applicable codes based on the average normal stress (computed as the ratio of the total compressive force to the area, $x \cdot t$),
- E_f = elastic modulus of the FRP composite in the fiber direction,

- ε_{fd} = design strain of the FRP reinforcement from Equation (5.1),
- t_f = thickness of the FRP reinforcement,
- b_f and p_f = width and spacing of the FRP strips, measured perpendicular to the fiber direction (for adjacent strips, assume b_f/p_f =1.0).

The partial resistance model coefficient, γ_{Rd}, should be taken as 1.20 (per Table 3-2 in § 3.4.2).
If the friction angle, φ, of the mortar joints is less than 45°, the shear strength, $V_{Rd,f}$, given by Equation (5.26), must be reduced by a factor of $\tan^{-1}(90° - \varphi)$.

The friction angle φ can be evaluated based on the mortar's tensile and compressive strength values.

(4) To ensure the formation of a resisting truss system, FRP reinforcement must be provided in the vertical direction to resist the tensile force component acting as the tension tie in the truss mechanism.
In this regard, the usual moment equilibrium rules must be carefully considered.

(5) The maximum shear resistance of the masonry panel, $V_{Rd,max}$, corresponding to the ultimate compression failure of the diagonal struts in the truss, is given by:

$$V_{Rd,max} = 0.3 \cdot f_{md}^{h} \cdot t \cdot d \tag{5.27}$$

where

- f_{md}^{h} = design compressive strength of the masonry in the shear force direction (i.e., parallel to the mortar bed joints),
- d = effective height of the section.

(6) For walls strengthened only with vertically oriented FRP reinforcement (to resist bending-induced tension), the shear strength of the masonry is still enhanced.
This increase is a consequence of the higher compressive force acting on the masonry due to bending.
In this case, the shear resistance of the masonry is given by the following equation:

$$V_{Rd,m} = x \cdot t \cdot f_{vd} \tag{5.28}$$

where:

- f_{vd} = design shear stress of the masonry, evaluated per applicable codes, based on the average normal stress (computed as the ratio of the total compressive force to the area $x \cdot t$).

(7) Walls composed of multiple panels separated by structural floor slabs can be strengthened with diagonal FRP reinforcement instead of the previously described methods.
This approach is valid, provided that tie beams or steel ties are present at floor levels to ensure a substantially uniform horizontal displacement of the panel's top section.
Typically, a pair of diagonal FRP reinforcements is installed symmetrically on both faces of the panel.

(8) The shear strength of a rectangular masonry panel with width B and height H, reinforced with FRP strips oriented at an angle α to the horizontal (see Figure 5-8), can be evaluated as follows, neglecting the contribution of the compressed FRP component.

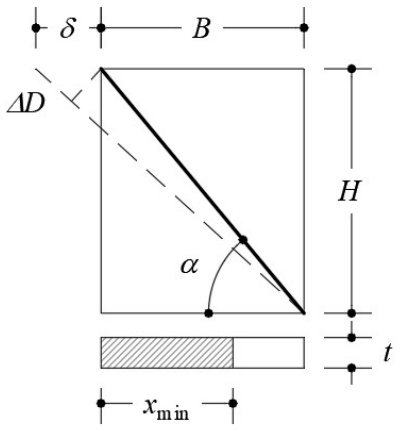

Figure 5-8 Masonry panel with shear reinforcement applied at an inclined angle α to the horizontal.

Based on Figure 5-8, the horizontal displacement at the top section of the strengthened panel can be approximated as:

$$\delta_{\mathrm{Rd},1} = 0.005 \cdot H \tag{5.29}$$

At this displacement level, the maximum shear force that the panel can sustain is:

$$V_{\mathrm{Rd,m}} = x_{\mathrm{min}} \cdot t \cdot f_{\mathrm{vd}} \tag{5.30}$$

where:

- x_{min} = minimum neutral axis depth from the extreme compressed edge,
- f_{vd} = design shear stress of the masonry, evaluated in accordance with applicable codes based on the average normal stress (computed as the ratio of the total compressive force to the minimum tensile stress, $x_{\mathrm{min}} \cdot t$).

On the other hand, the maximum horizontal displacement that can be reached at the panel's top section, considering the design strain of the FRP reinforcement at the onset of debonding, is:

$$\delta_{\mathrm{Rd},2} = \frac{\Delta D_{\mathrm{fdd}}}{\cos\alpha} = \varepsilon_{\mathrm{fdd}} \frac{H}{\sin\alpha\cos\alpha} = \frac{f_{\mathrm{fdd}} \cdot H}{E_{\mathrm{f}} \cdot \sin\alpha\cos\alpha}. \tag{5.31}$$

Thus, defining:

$$\frac{\delta_{\mathrm{Rd}}}{H} = \frac{1}{H} \min\left\{\delta_{\mathrm{Rd},1}, \delta_{\mathrm{Rd},2}\right\} = \min\left\{0.005, \frac{f_{\mathrm{fdd}}}{E_{\mathrm{f}} \cdot \sin\alpha\cos\alpha}\right\}, \tag{5.32}$$

The maximum shear force that the strengthened masonry panel can sustain is:

$$V_{\mathrm{Rd}} = \frac{\delta_{\mathrm{Rd}}}{H}\left(\frac{V_{\mathrm{Rd,m}}}{0.005} + \sin\alpha\cos^2\alpha \cdot E_{\mathrm{f}} \cdot A_{\mathrm{f}}\right) \tag{5.33}$$

where:

- $\frac{\delta_{\mathrm{Rd}}}{H}\left(\sin\alpha\cos^2\alpha \cdot E_{\mathrm{f}} \cdot A_{\mathrm{f}}\right)$ = horizontal component of the force exerted by the FRP reinforcement at the displacement level δ_{Rd}.

(9) If only diagonal FRP shear reinforcement is used, then bending verification of the horizontal sections of the panels must be performed in accordance with the applicable codes, neglecting the contribution of the composite material.

5.5.2 Lintels and Floor Bands

(1) The connection zones between masonry piers within a wall are referred to as floor bands. In addition to supporting the masonry above openings, these bands serve the function of restraining adjacent masonry piers, ensuring compatible deformations under horizontal forces.

(2) Due to the effect of vertical loads, two critical aspects must be considered in the masonry above openings:

- First, due to the low tensile strength of masonry, the zone above the opening cannot support its weight independently. It must be supported by a lintel capable of resisting shear and bending moments.
- Second, when the adjacent masonry piers are particularly slender, making them unable to withstand the horizontal thrust from the opening, the lintel must function as a tension tie, providing the necessary tensile force to ensure the overall stability of the wall.

(3) With reference to Figure 5-9, and considering the structural function of both lintels and floor bands, the following verification methods can be identified.

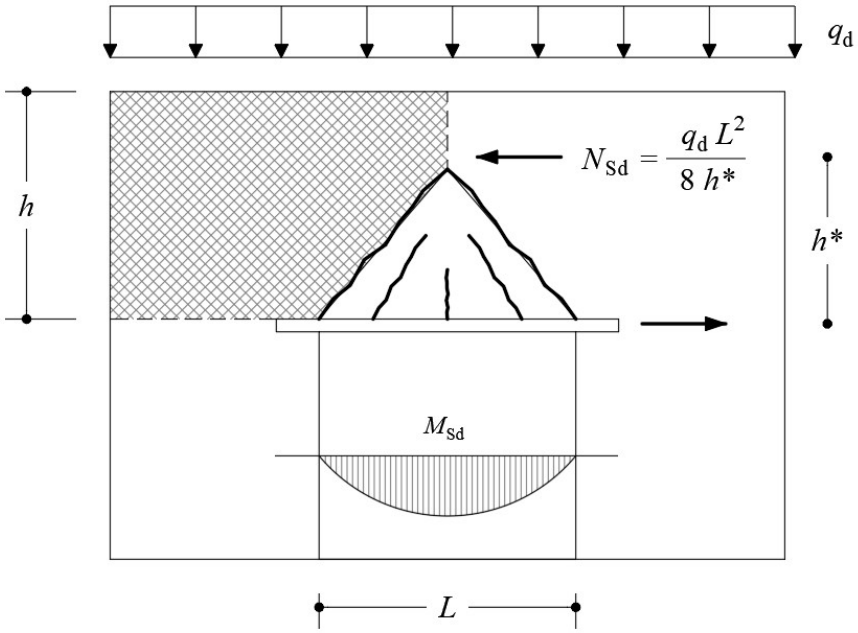

Figure 5-9 – Structural model for tension-bending lintels.

5.5.2.1 Verification of Lintel Action

(1) Lintels can be constructed using elements with both axial and flexural strength or elements providing only axial resistance.
In the first case, the member can act both as a beam and as a tie, ensuring both bending and tensile resistance.

(2) The dead load of the masonry above the opening must be supported by a reinforced masonry beam positioned above the opening, where tensile forces are absorbed by FRP reinforcement.
For the design of this reinforcement, the approach outlined in § 5.5.1.1.3, can be followed, considering the compressive strength of masonry, f^{h}_{md}, in the direction parallel to the mortar joints.

(3) The reinforced masonry section of the lintel must provide a design bending moment capacity, M_{Rd}, greater than the applied bending moment:

$$M_{Sd} = \gamma_G \cdot \frac{1}{24} \cdot g \cdot t \cdot L^3 \tag{5.34}$$

where:

- g = unit weight of masonry,
- t = masonry thickness,
- L = clear span of the opening,
- γ_G = partial safety factor for self-weight under ultimate limit state (ULS) conditions.

The applied reinforcement must also absorb a tensile force equal to:

$$N_{Sd} = \frac{q_d \cdot L^2}{8 \cdot h^*} \tag{5.35}$$

Where

- q_d = design vertical load at ULS transmitted to the lintel from the overlying portion of the building (sum of dead loads and live loads)
- h^* = internal lever arm, not exceeding the minimum value between the span L of the opening and the height h of the floor band.

5.5.2.2 Verification of Floor Band Action

(1) The performance of the floor band, when reinforced with FRP, must be verified against bending, shear, and axial forces acting at the connection sections with the masonry piers.
The resisting force values must be calculated using the same principles as masonry panels, considering the compressive strength of masonry, f^{h}_{md}, in the direction parallel to the mortar joints.

(2) The reinforcements can be installed parallel to the axis of the floor bands, either:

- At a level close to the floor slabs or
- In the upper and lower boundary zones of the floor bands.

They can be either continuous or discontinuous and should preferably be applied symmetrically on both the exterior and interior walls.
In particular, the reinforcement on exterior walls can be achieved using FRP systems designed for the perimeter confinement of the masonry structure.

(3) To ensure effective shear resistance, FRP reinforcements can also be applied diagonally across the masonry panels above openings.
In this case, it is recommended that the reinforcements be symmetrically applied relative to the mid-plane of the wall on both the exterior and interior surfaces of the floor bands.

5.6 STRENGTHENING OF SINGLE AND DOUBLE CURVATURE ELEMENTS

(1) Structural elements with single or double curvature collapse due to the formation of hinges, which occur because of the limited tensile strength of masonry.

(2) The use of FRP strengthening systems allows for the creation of a reinforced masonry system, improving the structural behavior of these elements.

The corresponding verifications can be conducted following the limit state approach.

(3) The design load effects, evaluated at the ultimate limit state (ULS), must be compared against the corresponding resistances, similar to the verifications for masonry panels (§ 5.5.1).
For two-dimensional structures, both load effects and resistances should be considered per unit length.

(4) The FRP reinforcement should be applied to the structure in a way that prevents the formation of hinges, which are responsible for potential failure mechanisms.
As a first approximation, these hinges can be assumed to form at the intrados (inner curve) or extrados (outer curve) of the structural element.
As a result, the normal force transmitted by these hinges is eccentric with respect to the mid-surface of the structure, with its eccentricity equal to half the thickness of the element.

(5) An adequately anchored FRP reinforcement system counteracts the rotational mechanism, thereby limiting crack opening.

Consequently, fiber-reinforced composites (FRP) can be used to prevent the formation of hinges on the opposite surface to the reinforcement application.

(6) The use of FRP strengthening systems is not particularly suitable for increasing shear strength or masonry compression strength unless, in the latter case, pultruded laminates are applied as intrados reinforcement arches, adequately anchored to the masonry.

(7) FRP strengthening systems applied to non-structural vaults (e.g., thin vaults, cane-reinforced vaults, etc.) enhance their structural integrity, improving both connection efficiency and overall stability performance.

5.6.1 Arches

(1) Regarding verifications related to the formation of collapse mechanisms, these guidelines provide specific recommendations for the following two structural schemes, which are common in practical applications:

- Arch scheme for arches resting on fixed supports;
- The arch-pier scheme, also known as the portal scheme, is for arches supported by piers.

(2) Generally, an arch or portal structure collapses due to the formation of at least four hinges.

(3) These hinges can be either proper or improper (double rocking hinges).
It is not uncommon for collapse mechanisms to arise from the formation of three proper hinges and one improper hinge, the latter being responsible for the shear-sliding failure of one portion of the arch relative to the other.

5.6.1.1 Arch Scheme

(1) In the arch scheme, to prevent the formation of hinges at the intrados (inner curve) or extrados (outer curve), FRP strengthening systems can be applied to the extrados (for intrados hinges) and to the intrados (for extrados hinges).

(2) Hinges can form both within the arch and at the supports.
Only specific strengthening interventions can effectively prevent hinge formation at the supports.

(3) Experimental evidence has shown that applying FRP reinforcement to the lateral surfaces of the arch does not significantly improve structural performance.
This is because the fiber-reinforced composite tends to debond prematurely from the masonry surface, with debonding starting in compressed areas due to local instability and progressively extending across the entire bonded surface.

(4) The technique of applying FRP reinforcement to both the extrados and intrados to prevent collapse mechanisms is less common and, in general, difficult to implement.

(5) Partial strengthening interventions, applied only to part of the extrados or intrados, do not completely eliminate collapse mechanisms.
However, if properly designed and executed, such interventions can significantly increase the collapse load capacity.

(6) As a general rule, it is preferable to:

- Apply full-surface strengthening on either the extrados or intrados;
- Ensure proper anchorage of the reinforcement to the vertical structures;
- Use FRP fabrics instead of laminates, particularly for extrados reinforcement on irregular masonry surfaces.

5.6.1.2 Portal Arch Scheme

(1) In the portal arch scheme, applying FRP reinforcement only to the extrados or intrados of the arch may not be sufficient to prevent the hinge-opening mechanism at the supports.
It may also be necessary to intervene on the piers.

(2) The verifications required are the same as those for the arch scheme but with additional consideration for failure mechanisms due to support settlements.

5.6.2 Single curvature vaults: barrel vaults

(1) In many cases, the structural analysis of barrel vaults, built with bricks arranged along the generator or orthogonal to it, can be reduced to that of a unit-depth arch whose profile corresponds to the vault's directrix curve.
As a result, barrel vaults can be strengthened using FRP composites applied along the directrix throughout the longitudinal span of the vault.
The spacing of the reinforcements, which depends on both the thickness and span of the vault, must be adequate to prevent the formation of failure mechanisms in this direction as well.
The recommended reinforcement spacing, $p_{f,}$ should satisfy the following inequalities:

$$p_f \leq 5 \cdot t + b_f \qquad b_f \leq 2 \cdot t \tag{5.36}$$

where t is the vault thickness, and b_f is the width of the applied reinforcements. For ribbed barrel vaults, the calculated thickness should be that of the vault shell, not the rib thickness.

(2) Longitudinal reinforcements, applied along the generators, serve as stitching elements between the ideal arches forming the barrel vault.
If properly positioned, they help prevent the formation of collapse mechanisms along the longitudinal span of the vault, particularly under horizontal actions.

(3) It is recommended to distribute reinforcement along the vault generators at a ratio of at least 10% of the reinforcement applied along the directrix.
This percentage should be increased to 25% in seismic zones.

(4) In the case of vaults located in cellular buildings with small spans, priority should be given to strengthening the surrounding masonry framework, as its integrity and stiffness allow the vault to balance vertical loads through membrane action with minimal or no tensile stress.
This type of strengthening often eliminates or reduces the need for interventions on the curved vault surface.

5.6.3 Double-Curvature Vaults: Domes

(1) Domes experience both membrane and flexural stress states.

5.6.3.1 Membrane Stress State

(1) In a dome subjected to vertical loads, a stress state develops with tensile forces acting along the parallels. This tensile stress is concentrated near the base of the dome and extends beyond the haunches.
Due to the very low tensile strength of masonry, domes frequently exhibit a typical cracking pattern: Cracks form along the meridians,

- Their apex is located roughly at the midpoint of the meridians,
- They extend from the apex to the base.

These meridional cracks alter the dome's equilibrium, significantly increasing thrust at the base, which may affect the underlying structure.

Applying FRP reinforcement circumferentially near the dome's base can help contain the cracked region and reduce the increase in base thrust.

To assess the structural safety of the strengthened dome, the following verifications must be performed:

- Tensile verification of the FRP composite;
- Debonding verification, as outlined in §5.3.4.

5.6.3.2 Flexural Stress State

(1) Flexural stresses are generally concentrated at the dome's base or along the edges of lantern openings.

- Flexural effects may cause the collapse of dome segments (meridional slices) bounded by meridional cracks.
- If the load-bearing capacity of these segments depends on a hinge-opening mechanism at the base, circumferential reinforcements at the base can effectively stabilize the dome.
- If the load-bearing mechanism relies on fixed supports, circumferential reinforcements at the base will be ineffective.
- In this case, FRP reinforcements should be applied along the meridians or at the parallels near the haunches.

To assess the safety of the strengthened dome, the following verifications must be performed:

- Flexural verification;
- Shear verification;
- Debonding verification.

(2) Flexural and shear verifications should be conducted in terms of specific design values per unit length, following the approach outlined in §§5.5.1.2.1 and 5.5.1.2.2.
It is essential to consider potential reductions in strength due to interactions between different stress components acting on all four faces within the thickness of a generic dome segment.
At a minimum, the interaction between the two flexural moments and the interaction between the two in-plane shear stresses should be accounted for.

(3) Regarding flexural stresses, special attention should be given when tensile and compressive zones in one direction are inverted compared to the other direction.

In such cases, a simplified approach—unless more rigorous determinations are available—assumes that:

- The sum of the absolute values of the two design flexural moments, each is divided by the corresponding absolute value of the design flexural resistance moment, should be ≤ 1 (considering the presence of a normal force).

If this condition is not met, the specific flexural strength in each of the two planes should be limited to the strength corresponding to a uniaxial stress state.

(4) Regarding in-plane shear stresses, the same approach applies as in the first case above.
The design flexural and shear resistances should be evaluated based on the appropriate masonry compressive strength values, considering differences between compression parallel and perpendicular to the bond courses (§ 5.2.3 (6)).

(5) For shear verification perpendicular to the dome segment plane, FRP reinforcement should not be considered, and the approach for unreinforced masonry should be followed, always in terms of specific design values and considering stress interaction effects.

(6) For debonding verification, the normal force acting at the adhesion plane must be accounted for, as outlined in § 5.3.4.

(7) To ensure proper functioning of the FRP reinforcement at the dome base, the reinforcement must be adequately extended and anchored to the underlying structure, possibly using mechanical devices.

5.6.4 Double-Curvature Vaults with Square Plans

(1) The strengthening of sail vaults (i.e., square-plan translation vaults), commonly found in cellular buildings with small spans, should primarily focus on reinforcing the surrounding masonry framework.

- The integrity and stiffness of the masonry framework allow the vaulted structure to balance vertical loads solely through compression stress states.
- If this condition cannot be fully achieved, reinforcement on the vault itself may be necessary. Still, it should be limited to the corner spandrels, where tensile forces develop perpendicular to the diagonal axes of the bay.

5.7 CONFINEMENT OF MASONRY COLUMNS

(1) The confinement of masonry structural elements subjected primarily to axial loading is achieved by implementing a system of tensile-resistant elements. These elements counteract the transverse expansion of the structural component, inducing a beneficial triaxial compression state in the masonry. Such interventions are carried out both for the repair of damaged or deteriorated elements and for strengthening intact elements to enhance the structural stability or seismic performance of the overall structure.

(2) Confinement can be achieved using FRP fabrics, laminates, and bars (also referred to as ties). Fabrics are applied around the perimeter as a continuous (wrapping) or discontinuous (hooping) external reinforcement, while bars are inserted within the column to create systematically distributed reinforced stitching.

(3) Internal stitching is performed by embedding FRP bars into holes drilled along two orthogonal directions of the column's cross-section. The set of bars placed at the same level in each of these directions forms a "layer" (Figure 5-10).

These stitched reinforcements counteract the transverse expansions that develop in the structural element due to axial compression. The stitching bars are bonded to the masonry by filling the drilled holes with adhesive material or by using mechanical anchoring systems at the ends.

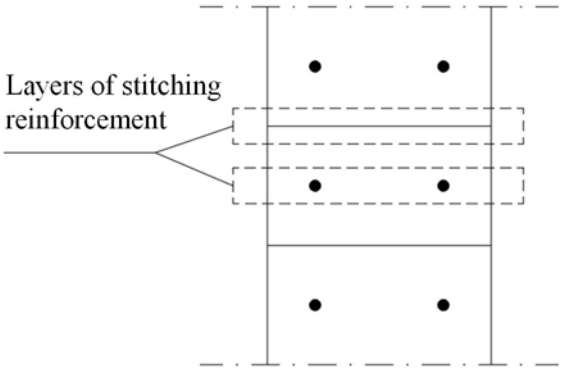

Figure 5-10 – Longitudinal section of a column with bars arranged in two orthogonal directions.

(4) When a confinement intervention includes both internal stitching and external wrapping, it is recommended to use bars and fabrics with similar mechanical properties.

(5) If columns exhibit vertical cracks, temporary forced confinement should be applied before inserting the transverse reinforcement bars.
For rectangular-section columns, reinforcement profiles (such as L-shaped profiles, possibly made of wood) can be installed at the corners and secured with temporary tensioning bands.

(6) The quantification of confinement effects on masonry elements under compression should be based on mechanical design parameters determined through experimental testing or defined by current regulations according to the properties of the constituent materials.

5.7.1 Design Compressive Strength of the Confined Element

(1) The verification of confined structural elements is carried out by assessing the action exerted by the wrapping and the ties based on the geometry and type of FRP reinforcement system used.

(2) To effectively evaluate the confining pressure, it is recommended to orient the fibers perpendicular to the element's axis. If a helical arrangement is used, its effectiveness should be assessed appropriately.

(3) The verification of the confined element consists of ensuring compliance with the following equation:

$$N_{\mathrm{Sd}} \leq N_{\mathrm{Rmc,d}} \tag{5.37}$$

where:

- N_{Sd} = design value of the axial load (evaluated for different load combinations as prescribed by current regulations)
- $N_{\mathrm{Rmc,d}}$ = design value of the strength of the confined column.

(4) The design axial strength, $N_{\mathrm{Rmc,d}}$, is defined as follows:

$$N_{\mathrm{Rmc,d}} = \frac{1}{\gamma_{\mathrm{Rd}}} \cdot A_{\mathrm{m}} \cdot f_{\mathrm{mcd}} \geq A_{\mathrm{m}} \cdot f_{\mathrm{md}} \tag{5.38}$$

where:

- γ_{Rd} = 1.1 partial factor (Table 3-2, § 3.4.2)
  - Note that γ_{Rd} = 1.25 for cases of internal confinement using only bars in non-circular columns.
- A_{m} = Cross-sectional area of the confined element
- f_{md} = Design compressive strength of the unconfined masonry element
- f_{mcd}= Design compressive strength of the confined masonry element.

(5) The design strength, f_{mcd}, of a confined element subjected to a confining pressure f_{l} (defined below as a function of the characteristics of the confining system) is influenced only by an effective portion of this pressure, $f_{\mathrm{l,eff}}$, known as the "effective confining pressure":

$$f_{\mathrm{mcd}} = f_{\mathrm{md}} \cdot \left[1 + k' \cdot \left(\frac{f_{\mathrm{l,eff}}}{f_{\mathrm{md}}} \right)^{\alpha_1} \right] \tag{5.39}$$

where:

- k' = is a dimensionless strength enhancement coefficient,
- α_1 = exponent that, in the absence of experimental results, can be assigned a value of 0.5.

(6) The strength enhancement coefficient k' can be determined based on experimental results obtained from masonry specimens with characteristics similar to those of the structure to be confined. Alternatively, the following equation may be used:

$$k' = \alpha_2 \cdot \left(\frac{g_m}{1000} \right)^{\alpha_3}, \tag{5.40}$$

where:

- g_{m} = is the masonry's mass density expressed in kg/m³,
- α_2 and α_3 = coefficients that, in the absence of experimental results justifying alternative assumptions, may conservatively be taken as 1.0.

(7) The effective confining pressure, $f_{\mathrm{l,eff}}$, depends on the cross-sectional shape and the type of confinement intervention. Defining V_{m} as the volume of the masonry element and $V_{\mathrm{c,eff}}$ as the volume of the effectively confined portion, the efficiency coefficient is introduced as:

$$k_{\text{eff}} = \frac{V_{\text{c,eff}}}{V_{\text{m}}} \tag{5.41}$$

The ratio $\frac{V_{c,eff}}{V_m}$ is used to define the effective confining pressure. The efficiency coefficient, k_{eff}, can be expressed as the product of a horizontal efficiency coefficient, k_{H}, and a vertical efficiency coefficient, k_{V}:

$$f_{\text{l,eff}} = k_{\text{eff}} \cdot f_{\text{l}} = k_{\text{H}} \cdot k_{\text{V}} \cdot f_{\text{l}} \tag{5.42}$$

(8) The helical arrangement of the external wrapping may also influence the effectiveness of the confinement intervention. If α_{f} is the fiber inclination angle relative to the plane of the element's cross-section, the following coefficient k_{α} is introduced:

$$k_{\alpha} = \frac{1}{1+\text{tg}^2\alpha_{\text{f}}} \tag{5.43}$$

This coefficient, applied as a multiplier to the confining pressure f_l, reduces the effective confining pressure $f_{\text{l,eff}}$ induced by the external wrapping due to its inclination. The contribution of ties placed perpendicular to the column's axis is not affected by this coefficient.

(9) To limit axial deformations and damage under service conditions, the stress increase in the confined element should be restricted to no more than 50% of the design stress f_{md} of the unconfined material

5.7.2 Confinement of circular columns

(1) The following dimensionless quantity is defined to represent the geometric percentage of the external wrapping (Figure 5-11):

$$\rho_{\text{f}} = \frac{4 \cdot t_{\text{f}} \cdot b_{\text{f}}}{D \cdot p_{\text{f}}} \tag{5.44}$$

where:

- t_{f} = thickness of the FRP reinforcement,
- b_{f} = height of the strips forming the discontinuous wrapping,
- D = external diameter of the cross-section,
- p_{f} = spacing of the strips (measured center-to-center).

For continuous wrapping, the ratio, ρ_{f}, simplifies to:

$$\rho_{\text{f}} = \frac{2t_{\text{f}}}{D}$$

(2) At the ultimate equilibrium condition, the confining pressure, f_l, can be calculated using the following equation:

$$f_l = \frac{1}{2} \cdot \rho_f \cdot E_f \cdot \varepsilon_{fd,rid} \tag{5.45}$$

Where:

- E_f = modulus of elasticity of the FRP reinforcement (in the fiber direction),
- $\varepsilon_{fd,rid}$ = reduced design strain of the reinforcement at the time of column collapse.

(3) The reduced design strain of the composite, $\varepsilon_{fd,rid}$, is calculated as:

$$\varepsilon_{fd,rid} = \min\{\eta_a \cdot \varepsilon_{fk} / \gamma_{f1};\ 0.004\} \tag{5.46}$$

where:

- η_a = environmental conversion factor (Table 3-3),
- ε_{fk} = ultimate strain of the FRP composite,
- γ_{f1} = partial factor of the FRP composite (§ 3.4.1);
- 0.004 = conventional strain limit of the composite (see § 4.6.1).

(4) The horizontal efficiency coefficient, k_H, equals 1. The same applies to the vertical efficiency coefficient, k_V, but only in the case of continuous wrapping.

(5) In the case of discontinuous wrapping, where strips of height b_f are placed at a spacing p_f, the confined volume is reduced due to stress diffusion, which can be approximated using a parabolic distribution with an engagement angle of 45° (Figure 5-11). The vertical efficiency coefficient, k_V, can be calculated as:

$$k_V = \left(1 - \frac{p'_f}{2 \cdot D}\right)^2 \tag{5.47}$$

where:

- $p'_f = p_f - b_f$ = net distance between the strips.

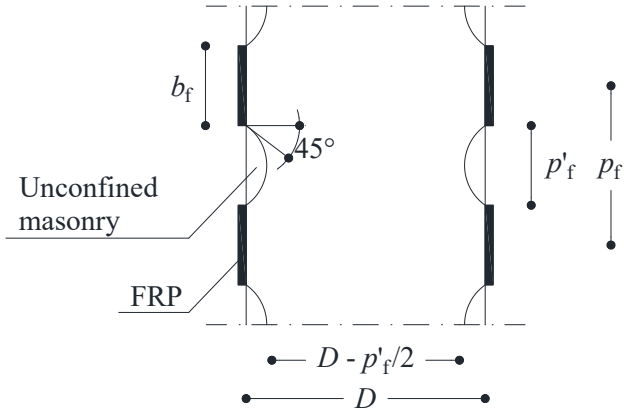

Figure 5-11 – Circular section confined with discontinuous wrapping.

(6) The strip spacing, $\boldsymbol{p_f}$, must not exceed $D/2$.

5.7.3 Confinement of square and rectangular columns

(1) The confinement of square or rectangular cross-section elements using FRP results in only modest increases in compressive strength. Therefore, such applications must be carefully evaluated and analyzed.

(2) In the absence of adequate experimental tests proving its effectiveness, external confinement should not be considered for rectangular sections where $b/h>2$, or the $\max\{b,h\} \geq 900mm$ (Figure 5-12).

(3) Using the symbols introduced in § **Errore. L'origine riferimento non è stata trovata.**(1), the confining pressure, f_l, exerted on a rectangular section of dimensions bxh, confined by an external discontinuous wrapping and internal stitching bars, can be calculated using the following equation:

$$f_l = \frac{1}{2} \cdot \min\left\{ \rho_{f,x} \cdot E_f + 2 \cdot \rho_{b,x} \cdot E_b \,;\; \rho_{f,y} \cdot E_f + 2 \cdot \rho_{b,y} \cdot E_b \right\} \cdot \varepsilon_{fd,rid} \tag{5.48}$$

where the dimensionless parameters $\rho_{f,x}$, $\rho_{f,y}$, $\rho_{b,x}$, $\rho_{b,y}$ are defined as follows (Figure 5-13):

$$\rho_{f,x} = \frac{4 \cdot t_f \cdot b_f}{h \cdot p_f}, \quad \rho_{f,y} = \frac{4 \cdot t_f \cdot b_f}{b \cdot p_f}, \quad \rho_{b,x} = \frac{n_{b,x} \cdot A_b}{p_b \cdot h}, \quad \rho_{b,y} = \frac{n_{b,y} \cdot A_b}{p_b \cdot b} \tag{5.49}$$

where:

- $n_{b,x}$ and $n_{b,y}$ = number of bars placed in layers arranged along the x and y directions, respectively,
- A_b = cross-sectional area of a single bar,
- p_b = spacing (measured center-to-center) between two consecutive layers of bars along the same direction.

(4) In the case of continuous wrapping, the expressions for ρ_{fx} and ρ_{fy} in Equations (5.49) simplify to:

$$\rho_{f,x} = \frac{4 \cdot t_f}{h}, \quad \rho_{f,y} = \frac{4 \cdot t_f}{b} \tag{5.50}$$

(5) For a rectangular section confined solely by external wrapping, whether continuous or discontinuous (see Figure 5-12), equation (5.48) simplifies to:

$$f_l = 2 \cdot \frac{t_f \cdot E_f}{\max\{b,h\}} \cdot \varepsilon_{fd,rid}, \quad f_l = \frac{2 t_f b_f E_f}{\max\{b,h\}\, p_f} \cdot \varepsilon_{fd,rid}. \tag{5.51}$$

(6) In the case of only internal bars, the confinement pressure is given by:

$$f_l = \min\left\{\rho_{b,x} \cdot E_b ; \rho_{b,y} \cdot E_b\right\} \cdot \varepsilon_{fd,rid} \tag{5.52}$$

(7) For a rectangular section confined only by an external wrapping (Figure 5-12, only a portion of the total masonry area is effectively confined due to an arch effect, which depends on the curvature radius of the rounded section corners.

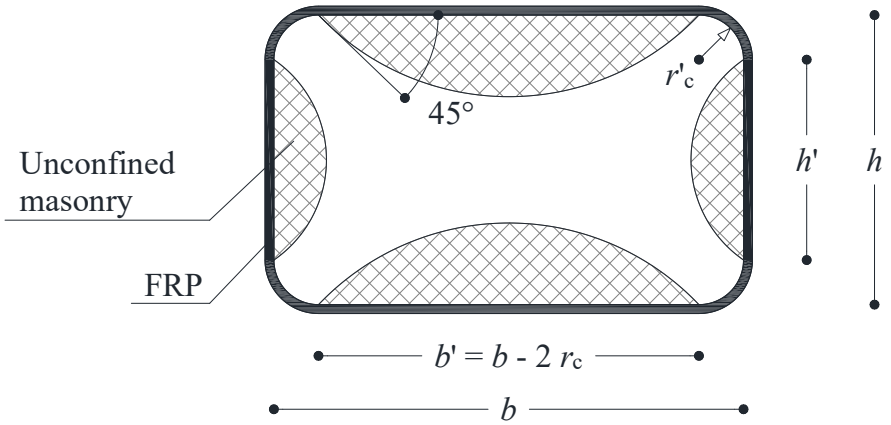

Figure 5-12 – Confinement of rectangular section with external wrapping.

The horizontal efficiency coefficient is given by the ratio between the confined area and the total area, A_m:

$$k_H = 1 - \frac{b'^2 + h'^2}{3 \cdot A_m} \tag{5.53}$$

where:

- *b'* and *h'* = dimensions indicated in Figure 5-12.

(8) If the wrapping is discontinuous, a similar vertical efficiency effect occurs (Figure 5-11). The vertical efficiency coefficient is given by:

$$k_{\mathrm{V}} = \left(1 - \frac{p_{\mathrm{f}}'}{2 \cdot \min\{b,h\}}\right)^2 \tag{5.54}$$

In contrast, for continuous wrapping, $k_{\mathrm{v}} = 1.0$.

(9) The strip spacing p_{f} must satisfy the following condition:

$$p_{\mathrm{f}} \leq \frac{1}{2} \cdot \min\{b,h\} \tag{5.55}$$

(10) In the absence of a detailed assessment of the effectively confined volume (Figure 5-13), the efficiency coefficient, k_{eff}, for internal ties only can be determined as follows:

$$k_{\mathrm{eff}} = k_{\mathrm{H}} \cdot k_{\mathrm{v}} = \left[1 - \frac{1}{3 \cdot b \cdot h} \cdot \left(c_{\mathrm{x}}^2 \cdot \left(n_{\mathrm{bx}} - 1\right) + c_{\mathrm{y}}^2 \cdot \left(n_{\mathrm{by}} - 1\right) + 6 \cdot c_{\mathrm{xs}} \cdot c_{\mathrm{ys}}\right)\right] \cdot \left(1 - \frac{p_{\mathrm{b}}}{2 \min\{b,h\}}\right)^2 \tag{5.56}$$

(11) For square sections of side b, equation (5.56) simplifies to:

$$k_{\mathrm{eff}} = k_{\mathrm{H}} \cdot k_{\mathrm{v}} = \left[1 - \frac{1}{3 \cdot b^2} \cdot \left(2 \cdot c_{\mathrm{b}}^2 \cdot \left(n_{\mathrm{b}} - 1\right) + 6 \cdot c_{\mathrm{bs}}^2\right)\right] \cdot \left(1 - \frac{p_{\mathrm{b}}}{2 \cdot b}\right)^2 \tag{5.57}$$

assuming:

- $n_{\mathrm{bx}} = n_{\mathrm{by}} = n_{\mathrm{b}}$,
- $c_{\mathrm{x}} = c_{\mathrm{y}} = c_{\mathrm{b}}$,
- $c_{\mathrm{xs}} = c_{\mathrm{ys}} = c_{\mathrm{bs}}$.

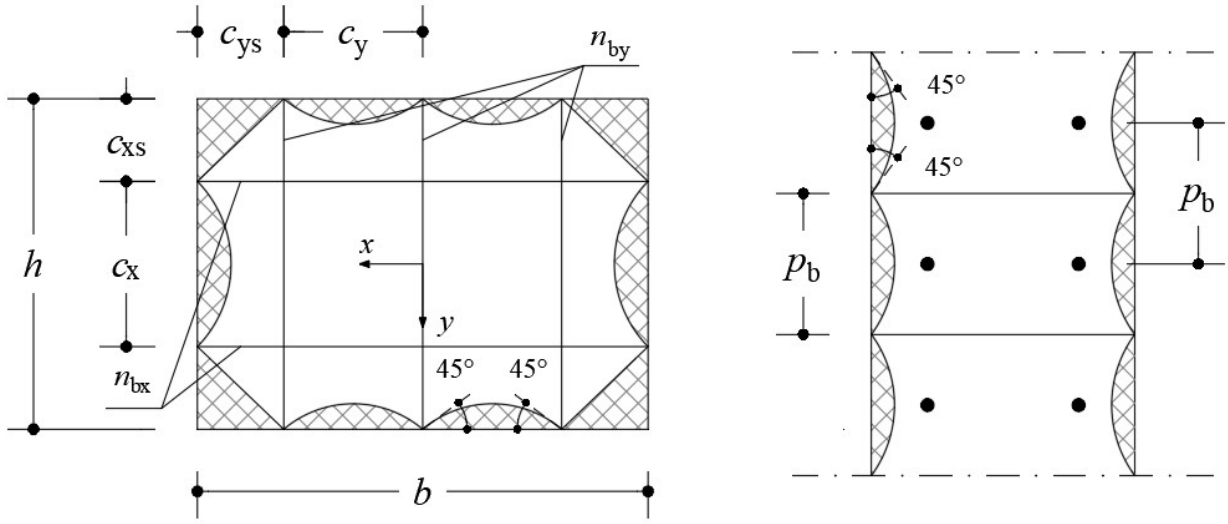

Figure 5-13 – Confined areas of ties in the cross-sectional and longitudinal directions.

(12) Among the bars placed in the same layer, the distance of the outermost bar from the side of the section parallel to the bars must not exceed 1/4 of the length of the side orthogonal to them. Additionally, the following conditions must be met:

$$c_x \leq \frac{h}{5},\ c_y \leq \frac{b}{5},\ p_b \leq max\{c_x, c_y\} \tag{5.58}$$

(13) To ensure that the confinement action of the bars extends to the column surface, the anchorage length must not exceed 10 times the bar diameter. If this length exceeds 1/5 of the bar length, an additional anchorage device must be provided.

(14)P Combining an external wrapping with internal stitching bars can increase the effectively confined section area in rectangular sections (Figure 5-14).

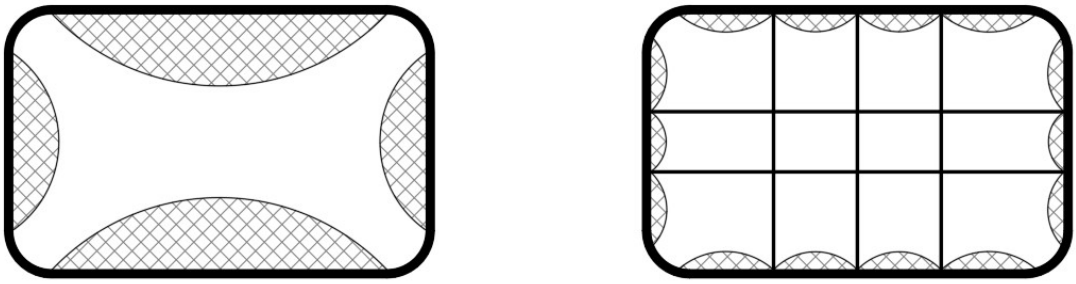

Figure 5-14 – Confinement of masonry elements using FRP fabrics, with and without bars.

(15) When continuous wrapping is combined with internal ties, the efficiency coefficient, k_{eff}, s used in equations (5.41) and (5.42), is given by:

$$k_{eff} = k_H \cdot k_v = \left[1 - \frac{1}{3 \cdot b \cdot h} \cdot \left(c_x^2 \cdot \left(n_{bx} - 1\right) + c_y^2 \cdot \left(n_{by} - 1\right) + 2 \cdot \left(c_{xs} - r_c\right)^2 + 2 \cdot \left(c_{ys} - r_c\right)^2\right)\right] \cdot 1 \tag{5.59}$$

For square sections of side b, the efficiency coefficient simplifies to:

$$k_{eff} = k_H \cdot k_v = \left[1 - \frac{1}{3 \cdot b \cdot h} \cdot \left(2 \cdot c_b^2 \cdot \left(n_b - 1\right) + 4 \cdot \left(c_{bs} - r_c\right)^2\right)\right] \cdot 1 \tag{5.60}$$

where:

- $n_{bx} = n_{by} = n_b$,
- $c_x = c_y = c_b$,
- $c_{xs} = c_{ys} = c_{bs}$
- r_c = curvature radius of the rounded corners.

5.8 INTERVENTIONS IN SEISMIC ZONES

5.8.1 General Considerations

(1) FRP strengthening systems can be effectively used in seismic zones to improve the performance of structures that do not meet the safety requirements for one or more Ultimate Limit States (ULS).

The specific guidelines provided below for interventions in seismic areas incorporate the current regulatory requirements, as well as recommendations from the latest scientific literature and international guidelines regarding:

- Seismic safety assessment
- Safety requirements (verification of limit states)
- Levels of seismic protection (intensity of associated seismic action)
- Analysis methods
- Verification criteria (distinction between “ductile” and “brittle” elements)
- Material properties.

5.8.2 General Intervention Principles

(1) The selection of the type and extent of FRP intervention is based on a careful evaluation of the seismic safety of the structure, taking into account the following aspects:

- Inadequate masonry that cannot withstand vertical and horizontal loads must be properly strengthened or replaced.
- Intersecting masonry walls forming corners or projections must be properly connected.
- Weak connections between floors and walls or roof and walls must be reinforced.
- Appropriate structural elements must resist thrust forces from roofs, arches, and vaults.
- Floors must be capable of:
    - Providing connections to vertical walls
    - Offering some degree of in-plane stiffness
    - Transferring horizontal loads to the walls aligned with the seismic action
    - Restraining out-of-plane movement of walls subjected to perpendicular seismic forces
- Highly vulnerable elements that cannot be strengthened should generally be removed.
- FRP strengthening alone cannot compensate for severe irregularities in stiffness or strength within a structure. However, targeted applications can help improve overall regularity and strength.
- FRP confinement to increase local ductility (e.g., wrapping of columns) is always beneficial.
- The introduction of localized FRP reinforcements should not reduce the overall global ductility of the structure.

(2) FRP interventions generally aim to:

- Strengthen, replace, or reconstruct certain elements partially or entirely (selective interventions).
- Improve structural connectivity, enhancing the overall behavior of the structure..

(3) The design of an FRP intervention must include the following steps:

- Justified selection of the intervention type

- Choice of techniques and materials
- Preliminary sizing of the reinforcements
- Structural analysis considering the post-intervention behavior
- Verification of the post-intervention structure, ensuring compliance for:
    - Existing elements
    - Modified elements
    - New elements
    - Verifications must be conducted in accordance with these guidelines to repair or strengthen existing elements.

5.9 INSTALLATION AND CONSTRUCTION DETAILS

(1) The optimal performance of a strengthening system depends on several factors. In addition to those previously discussed, the preliminary preparation of the substrate and the application process of the composite play a crucial role.

For SFRP system installation, steel fabrics are bonded to the surface of structural elements using a wet application process with epoxy or polyester resin, following the same procedures as other FRP systems, including:

- Restoration of the deteriorated substrate
- Leveling of irregular and uneven surfaces
- Surface preparation to achieve the required roughness
- Primer application to ensure adhesion of the polymeric matrix
- Steel fabric systems offer the same advantages as other FRP systems in terms of ease of application, curing time, and versatility.

Steel Fabric Bending Considerations:

- Steel fabric bending cannot be performed during application but requires a dedicated bending machine and must be prepared in advance.
- Bending is a delicate operation as it can compromise the zinc coating, exposing the steel fabric to corrosion risks.
- The work-hardening effects of bending can reduce the strength of the steel.
- Some manufacturers have developed bending systems that preserve mechanical and durability properties.

The importance of fabric bending (for applications that require it) is explicitly addressed in qualification standards, such as:

- Superior Council of Public Works (Consiglio Superiore dei Lavori Pubblici)
- Central Technical Service (Servizio Tecnico Centrale)
- Guidelines for the identification, qualification, and acceptance control of FRP composites for the structural strengthening of existing buildings

These standards include specific tests to ensure that bending does not significantly reduce mechanical properties, even under potentially aggressive environmental conditions. For example, mechanical tests are conducted on bent and straightened fabrics after 3,000 hours of exposure to a saline environment.

5.9.1 Inspection and Preliminary Preparation of the substrate

(1) The application of an FRP strengthening system requires a prior inspection to assess the deterioration of the substrate. Necessary measures must be taken to improve its condition, including:

- Removing and rebuilding degraded sections affected by:
    - Moisture

- Microvegetation growth
- Alteration of stone or brick materials.

(2) Anchoring technologies used for the ends of laminates or fabrics must undergo appropriate experimental investigations conducted under standardized criteria.

The application protocol must include:
- Material specifications (adhesives and reinforcements)
- Step-by-step preparation process as defined by the manufacturer
- Execution timeframes
- Environmental conditions
- Evaluation of sensitivity to these parameters

The investigation must assess the potential influence of these factors on the final performance of the strengthening system.

5.9.1.1 Assessment of Substrate Deterioration

(1) Before applying the reinforcement, the substrate characteristics must be evaluated by conducting homogeneity tests across the entire area to strengthen them and performing a structural survey of material degradation. This can be achieved, for example, using metal grids. The observation period should not be less than six months.

(2) Mechanical characterization tests of the masonry should be conducted at a minimum rate of one test per 100 m² of the area to be reinforced, with at least two tests per homogeneous zone, using at least one of the following methods:
- Compression test on masonry samples
- Shear test on masonry samples
- Flat-jack test
- Shear test with flat-jack
- Dilatometric test for cavity masonry
- Ultrasound testing.

(3) Homogeneity tests across the entire area to be reinforced, if performed, should follow a square grid layout with a 1 m spacing for areas smaller than 5 m² and proportionally larger spacing for larger areas, except in critical zones. These tests can be conducted using:
- Manual inspections by tapping
- Radiographic analysis
- Surface ultrasound velocity measurement
- Sonic pulse velocity measurement (with instrumented hammer and accelerometers)
- Penetrometer
- Thermography
- Tomography.

5.9.1.2 Removal and Reconstruction of the Substrate

(1) The masonry substrate may be damaged due to:
- Physical-chemical deterioration
- Physical-mechanical degradation
- Biological factors

- Impact damage

The deteriorated masonry must be removed entirely from the affected area.

(2) Removing damaged material allows for an assessment of the condition of the stone or brick material and mortar. This step enables the identification and mitigation of the causes of deterioration before reconstructing the removed masonry sections.

- If exfoliation, powdering, cracking, or chemical-physical attack is present, the deteriorated layer must be removed by brushing or sandblasting, followed by treatment with suitable inhibitors to halt further degradation.

(3) After removing the deteriorated substrate and implementing measures to prevent further degradation, such as:

- Stopping water infiltration
- Removing microvegetation
- Addressing other deterioration causes

The reconstruction of removed masonry sections can proceed using materials compatible with the existing masonry. Additionally:

- Surface irregularities greater than 10 mm should be leveled using a compatible epoxy putty.
- Cavities deeper than 20 mm should be filled with an appropriate repair material.
- Cracks wider than 0.5 mm should be sealed by injection before applying the reinforcement..

5.9.1.3 Substrate Preparation

(1) Once the substrate has been evaluated and repaired, a final sandblasting treatment may be required to enhance surface roughness.

- Minimum required roughness: 0.3 mm
- Measurement methods:
    - Laser profilometer
    - Optical roughness meter.

(2) If the masonry does not require repair but is of poor quality, a consolidating agent may be applied before priming.

(3) The surface must be perfectly clean before applying the FRP reinforcement:

- Remove all dust, grease, hydrocarbons, and surfactants.

5.9.2 Recommendations for proper execution

(1) The quality of composite reinforcement installation is highly dependent on:

- Ambient temperature and humidity conditions, and
- The condition of the substrate to which the reinforcement is applied.

5.9.2.1 Humidity and Temperature Conditions of the Environment and Substrate

(1) Avoid installing composite reinforcements in highly humid environments because:

- Excessive humidity can delay resin curing.
- In-situ polymerization of resin-based systems may be compromised.

(2) Composites must be applied within the hygrometric and thermal limits specified in the technical datasheets.

(3) In certain conditions, protective measures such as shielding sheets may be required, for example:

- Rain
- Excessive sunlight
- Strong thermal gradients
- High humidity
- Dust exposure.

5.9.2.2 Construction Details and Execution Norms

(1) Anchorage Length

- Minimum required anchorage length: 150 mm.
- Alternatively, mechanical connectors may be used.

(2) Rounding of Corners

- When reinforcement is applied to edges, the corners should be rounded beforehand to avoid stress concentrations that could cause premature failure.
- Minimum rounding radius (r_c): 20 mm.

(3) Fiber Alignment During Installation

- Fibers must be placed in the designed orientation.
- Fibers should be free of waviness.
- For SFRP systems, follow §4.9.2.2 (5).

(4) Semi-Destructive Testing Preparation

- For future quality control testing, installation should consider the provisions in § 4.9.2.2 (6)

(5) Splay Anchors Installation

- For the proper installation of spread-fiber connectors, follow §4.9.2.2 (7) for concrete substrates.

5.9.2.3 Protection of the Reinforcement System

(1) Protection Against UV Exposure

- For outdoor applications, the reinforcement system should be protected from direct solar radiation, which can cause chemical and physical degradation of the epoxy matrix.
- Protective coatings:
- Acrylic paints (water-based or solvent-based).
- Before application, clean the composite surface using a sponge soaked in soapy water.

(2) Higher Protection Levels

- Stronger protection can be achieved by applying plasters or mortars (preferably cement-based).
- Application process:
    - Prepare the composite surface by applying an epoxy resin primer.

  - Sprinkle quartz powder (“fresh-on-fresh” method) before applying the final protective layer.
- The manufacturer typically specifies the recommended thickness of protective layers.

(3) Fire Protection Measures

- Different techniques can be used to enhance fire resistance:
  - Gypsum boards, calcium silicate panels, or similar materials.
  - Fire-resistant protective plasters.
- All fire protection materials must be certified for fire resistance.
- Manufacturers must specify the level of protection provided by the coating based on its thickness.
- Panel installation:
  - Fixing panels should not cut or puncture FRP fibers.
- Fire-resistant plaster requirements:
  - Must be certified for FRP applications to ensure adhesion under normal and fire conditions, even under static load.
  - An application must follow the manufacturer’s technical documentation guidelines.

5.10 NUMERICAL EXAMPLES

Several numerical applications related to the FRP strengthening of masonry structures are provided in Appendix I.

6 INSPECTION AND MONITORING OF THE INTERVENTION

(1) Acceptance control of the strengthening systems is required.

(2) Once the strengthening intervention has been completed, post-installation inspections for acceptance testing and, subsequently, long-term monitoring, if necessary, must be conducted. In both cases, non-destructive testing (NDT) and semi-destructive testing (SDT) methods can be employed. Personnel performing these tests must hold specific qualifications, as outlined in § 6.3.

(3) If the configuration of the strengthening system allows, such as wrapping applications or systems with proper anchorage devices, some substrate-related inspections may be omitted.

6.1 ON-SITE ACCEPTANCE INSPECTIONS

(1) FRP strengthening systems must undergo a series of on-site inspections to ensure that their mechanical and physical properties meet the requirements specified by the Designer.

(2) On-site acceptance inspections are conducted through destructive testing on specimens. The number and type of tests must comply with the provisions outlined in the **"***Guidelines for the Identification, Qualification, and Acceptance Control of Fiber-Reinforced Polymer (FRP) Composites for the Structural Strengthening of Existing Buildings*"**.**

6.2 QUALITY CONTROL OF THE STRENGTHENING SYSTEM

(1) Semi-destructive tests (SDT) primarily serve as an indicative tool for the mechanical characterization of the installed strengthening system. In contrast, non-destructive tests (NDT) are helpful in detecting defects in the execution of the intervention.

(2) The type and number of tests to be conducted must be proportional to the importance of the intervention, taking into account the extent of the treated areas relative to the overall structure. Special attention should be given to public and strategically essential buildings, especially those relevant to Civil Protection operations in case of disasters.

6.2.1 Semi-Destructive Tests

(1) Semi-destructive tests can include both normal tensile pull-off tests and shear pull-off tests. These tests should be performed on designated test specimens (§§ 4.9, 5.9) and, where possible, in non-critical areas of the reinforcement. The recommended frequency for testing depends on the type of structure:

- For reinforced concrete (RC) structures: One test for every 30 m² of FRP application.
- For masonry structures: One test for every 50 m² of FRP application.

Regardless of the area being reinforced, there should be at least three tests of each relevant type to ensure reliable results.

(2) Normal Tensile Pull-Off Test.

The normal pull-off test is primarily used to evaluate the condition of the substrate. This test is typically conducted using circular steel plates with:

- A thickness of 20 mm
- A minimum diameter of 50 mm

Before the test, the FRP reinforcement must be cut along the edge of the steel plate. This can be done using a cylindrical milling cutter, with a maximum thickness of 3 mm, ensuring that:

- The composite material is not overheated

- The cut extends at least 2 mm into the substrate

Spherical joints or similar devices should be used to ensure that the pull-off force is applied perpendicularly to the reinforcement.

Acceptance Criteria
The substrate is considered suitable if at least 80% of the tests (at least two out of three, if only three tests are conducted) produce a peak pull-off stress of:

- At least 0.9 MPa for reinforced concrete
- At least 10% of the average compressive strength of the substrate for masonry

Additionally, the failure surface should occur within the substrate itself and not at the interface between the FRP and the substrate. If the failure occurs at the FRP-substrate interface, the acceptance of the test results is left to the discretion of the Site Supervisor.

(3) Shear Pull-Off Test.

Direct Method (Figure 6-1):

The shear pull-off test is primarily used to assess the quality of the bond between the FRP reinforcement and the substrate, as well as the effectiveness of the surface preparation.
One method for conducting this test is at a free edge of the structure where the FRP is bonded. In this case, a portion of the FRP reinforcement remains unbonded, allowing for the application of a shear force along the edge of the structure.

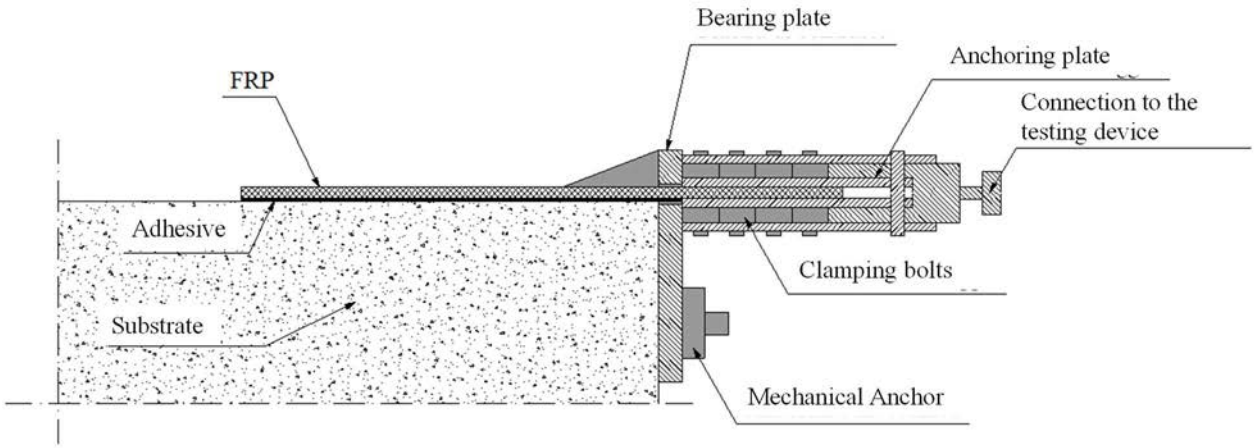

Figure 6-1 – Direct Shear Pull-Off Test

Indirect Method (Figure 6-2).

If test specimens are not available, an alternative method can be used on an installed FRP reinforcement. This requires a separate section of the FRP positioned near a structural edge. A metal plate is adhered to the exposed FRP, with a portion extending beyond the edge of the structure for gripping.

For optimal adhesion, the metal plate should have:

- Minimum width of 45 mm
- A maximum thickness of 6 mm
- Grooved surfaces to enhance bonding with the FRP

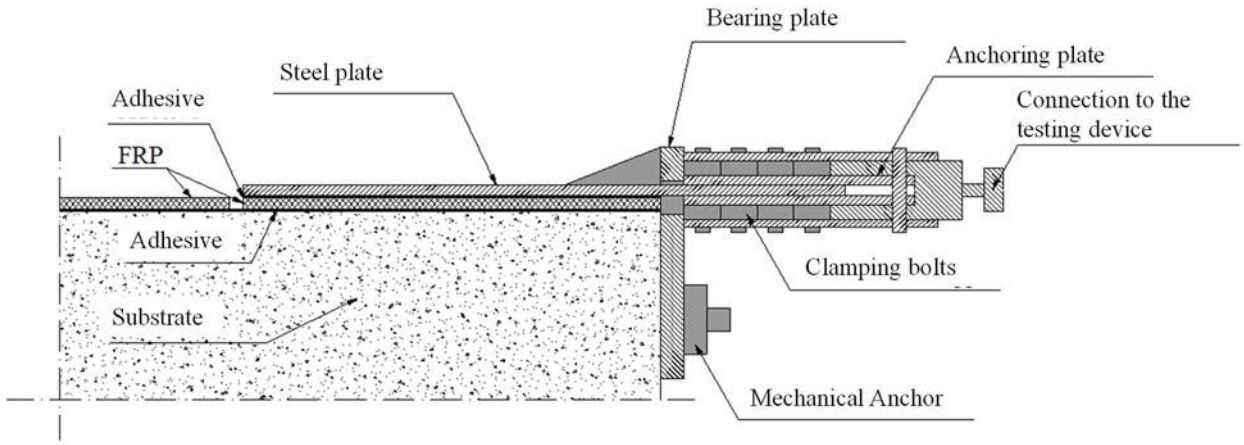

Figure 6-2 – Indirect Shear Pull-Off Test.

Testing Requirements

- The bonded FRP length should be:
  - At least 200 mm for reinforced concrete structures
  - At least 150 mm for masonry structures
  - At least 1.1 times the optimal bond length required for the FRP reinforcement (§§4.1.2, 5.3.2).
- For the indirect test method, the metal plate must fully overlap the FRP test sample.

Acceptance Criteria

The bonding and surface preparation are considered acceptable if at least 80% of the tests (at least two out of three, if only three tests are conducted) yield a shear force equal to or greater than 85% of the maximum design force, calculated using Equation (10.20) with a unitary k_b coefficient.

This testing process ensures that the reinforcement system is correctly installed, providing the expected strength and durability while verifying the quality of adhesion between the FRP and the substrate.

6.2.2 Non-Destructive Testing

(1) The strengthening intervention is considered non-compliant if bonding defects are detected, corresponding to cylindrical imperfections with a height and diameter exceeding 0.5 mm and 25 mm, respectively.

(2) Recommended Mapping Grid and Defect Detection Resolution

Table 6-1 provides suggested values for the mapping grid dimensions and the minimum detectable defect size for the most common scenarios.

Table 6-1 – Mapping Grid Dimensions and Testing Resolution.

Shear Stress Transfer at the Interface	Application Type	Non-Destructive Testing	Mapping Grid Dimensions (mm)	Minimum Detectable Defect Diameter (mm)
Absent	Confinement, except for overlap zones in single-layer applications	Optional	250	3
Weak	Central area of large-scale bidimensional reinforcements	Optional	250	3
Moderate or Potential	Central area of flexural unidimensional reinforcements	Recommended	100	0.5
Critical	Anchorage zones, overlap zones between layers,	Mandatory	50	0.1

	shear reinforcement, interface areas with connectors, areas with noticeable surface roughness or cracks

(3) Acoustic-Stimulated Testing – This method is based on the different vibrational behavior of the composite layer depending on whether it is bonded or detached from the underlying substrate. In its simplest form, the test can be conducted by an experienced technician tapping the composite surface with a rigid stick and listening to the resulting sound. More objective results can be obtained through automated systems.

(4) High-Frequency Ultrasonic Testing – This method requires the use of reflection-based techniques with frequencies not lower than 1.0 MHz and probes with a diameter not exceeding 25 mm. The preferred technique for locating defects involves analyzing variations in the amplitude of the first peak.

(5) Thermographic Testing – This technique is effective only when applied to reinforcement materials with low thermal conductivity, such as glass and aramid fibers. It is not suitable for carbon-fiber-reinforced composites unless specific precautions are taken. The heating applied during the test must not damage the reinforcement by exposing it to temperatures near the glass transition temperature of the matrix.

(6) Acoustic Emission Testing – This method detects the presence of bonding defects in a structural element under load by “listening” and recording the “noises” generated by the propagation of debonding between the substrate and the reinforcement.

(7) Electrical Continuity Testing for SFRP Systems – To verify the coverage of micro-wires within SFRP systems by the impregnation resin, a visual inspection can be supplemented with an electrical continuity test using a digital multimeter.

- Before sealing the composite ends, connect the exposed micro-wire ends to the tester's COM (black) terminal.
- Attach a copper or brass wire brush to the VΩ (red) terminal of the tester (ensuring that all brush wires are short-circuited together and connected to the tester).
- Set the multimeter to Continuity Test mode and, while maintaining contact with the micro-wire ends, gently brush the composite surface.
- If any micro-wires remain uncoated, the tester will emit a beep when the brush makes contact with an exposed wire.
- Any unimpregnated areas must be repaired with additional resin application before sealing the composite ends.

This procedure can be conducted both during the material qualification phase and, more importantly, as a quality control check in the field after installation.

6.3 QUALIFICATION OF OPERATORS FOR TEST EXECUTION

(1) Without prejudice to the mandatory requirements established by current laws or technical regulations, the professional profiles of operators responsible for testing may usefully refer to the three qualification levels specified below (Table 6-2), as outlined in the reference standards UNI EN 473 and UNI CEI EN ISO/IEC 17024.

Table 6-2 – Specialization Levels for Monitoring and Testing Procedures.

Level 1	• Set up the equipment. • Perform the tests. • Record and classify the results according to written criteria. • Prepare a report on the results.
Level 2	• Select the appropriate testing procedure. • Define the application limits of the test for which the Level 2 individual is qualified. • Understand the standards and test specifications and translate them into practical test instructions adapted to actual working conditions. • Adjust and calibrate the equipment. • Conduct and oversee the tests. • Interpret and evaluate the results according to the applicable standards, codes, or specifications. • Prepare written test instructions for Level 1 personnel. • Perform and supervise all tasks assigned to Level 1 personnel. • Train or guide personnel at levels below Level 2. • Organize the test results and compile the corresponding report.
Level 3	• Assume full responsibility for a testing laboratory and its personnel. • Establish and validate testing techniques and procedures. • Interpret standards, codes, specifications, and procedures. • Define the specific tests and procedures to be applied. • Possess the competence to evaluate and interpret results concerning existing standards, codes, and specifications. • Have sufficient practical knowledge of materials, manufacturing processes, and the technology of various related products to choose appropriate methods, establish techniques, and contribute to defining acceptance criteria when none are pre-established. • Have expertise in various fields of application. • Be capable of leading personnel at levels below Level 3.

6.4 MONITORING OF THE REINFORCEMENT INTERVENTION

(1) Given the currently limited availability of long-term data on the behavior of composite materials, it is advisable—particularly in cases of significant importance (considering the intended use of the structure, the number of reinforced elements, and the extent of the achieved strength increase)—to implement an appropriate monitoring system. This may involve periodic testing using non-destructive or semi-destructive methods, as well as tests performed with embedded sensors. The objective is to keep track of the following parameters, either entirely or selectively:

- Temperature of the reinforcement
- Environmental humidity
- Displacement and deformation trends
- Continuity and damage level of the fibers
- Extent of adhesive defects.

(2) The maintenance manual should also include the type and frequency of tests planned for monitoring.

7 APPENDIX A (CONSTITUENT PHASES OF FRP AND THEIR PHYSICAL-MECHANICAL PROPERTIES)

The content of Appendix A has been largely extracted from the book "Tecnologie e proprietà dei materiali compositi" (Amazon Publ., 2021, ISBN-13 979-8712973958), with the kind permission of the author, Professor Roberto Frassine.

7.1 GENERAL OVERVIEW

The development of composite materials for structural applications, along with their related production and design methodologies, has been one of the most significant advancements in modern materials science. Over the past 60 years, there has been an exponential increase in their applications, not only due to their exceptional structural properties but also because of their cost-effectiveness, flexibility in manufacturing processes, and durability. Recent advancements in nanotechnology and nanomaterials have further enhanced their range of properties and applications, making them fully-fledged multifunctional materials.

The definition of a composite material varies depending on the context. From a chemical perspective, a composite is defined as "a multi-component material comprising multiple phase domains, distinct (non-gaseous), in which at least one phase domain is a continuous phase" (IUPAC Gold Book, 2019).

In engineering, however, the most widely accepted definition describes a composite material (often simply called a "composite") as a material consisting of two or more distinct solid engineering materials with significantly different physical and/or chemical properties. When combined, these materials create a new material with characteristics different from those of the individual constituents, typically designed for a specific purpose.

Based on this definition, many materials we commonly use can be classified as composites, including reinforced concrete, masonry, wood, plywood, plastics with mineral fillers, ceramic or metal matrix composites, syntactic foams, laminated steel, bamboo, decorative plastic laminates, sandwich panels, multilayer films, and carbon-carbon composites.

However, the category of composite materials relevant to this document is that of reinforced composites, where the properties of a typically polymeric continuous phase (known as the matrix) are enhanced by a strong bond with a dispersed phase called reinforcement. This reinforcement can vary in nature but is always present in fiber form. For this reason, these materials are often referred to as fiber-reinforced composites and are commonly denoted by the acronym FRP (Fiber Reinforced Polymers).

Since polymeric matrices typically have elastic modulus values in the range of a few GPa and tensile strengths rarely exceeding 100 MPa, reinforcing fibers must exhibit significantly higher values for these properties. Examples of natural fibers include flax and hemp, while glass, carbon, and aramid fibers are considered high-performance reinforcements.

Recently, a new type of reinforcement system has been introduced, consisting of a polymer matrix combined with steel micro-strands (braids), identified by the acronym SFRP (Steel Fiber Reinforced Polymers).

Indicative values of the mechanical properties of these materials are presented in Table 7-1.

Table 7-1 – Comparison of the Properties of Common Reinforcing Fibers, Matrices, and Structural Steel (Indicative Values).

	Elastic Modulus E	Tensile Strength σ_r	Ultimate Strain ε_r	Thermal Expansion Coefficient α	Density ρ
	[GPa]	[MPa]	[%]	[10^{-6} °C^{-1}]	[g/cm^3]
E-glass fibers	70 – 80	2000 – 3500	3.5 – 4.5	5 – 5.4	2.5 – 2.6
S-glass fibers	85 – 90	3500 – 4800	4.5 – 5.5	1.6 – 2.9	2.46 – 2.49
Carbon fibers (high modulus)	390 – 760	2400 –3400	0.5 – 0.8	-1.45	1.85 – 1.9
Carbon fibers (high strength)	240 – 280	4100 – 5100	1.6 – 1.73	-0.6 – -0.9	1.75
Aramid fibers	62 – 180	3600 – 3800	1.9 – 5.5	-2	1.44 – 1.47
Polymer matrix	2.7 – 3.6	40 – 82	1.4 – 5.2	30 – 54	1.10 – 1.25
Structural steel	206	250 – 400 (yield) 350 – 600 (ultimate)	20 – 30	10.4	7.8

As seen in the table, carbon fibers exhibit significantly higher elastic modulus values than traditional construction materials, making them highly efficient for structural applications. However, their high stiffness may also create compatibility issues with other materials, a factor that designers must carefully evaluate.

In most cases, the matrix can be considered an isotropic continuous material. At the same time, the reinforcement phase, except for glass fibers, exhibits anisotropic behavior, meaning that its properties vary in different directions.

Volume Fractions of Fibers and Matrix

The mechanical properties of fiber-reinforced composites depend not only on the properties of the fibers but also on their volume fraction within the matrix. The volume fraction of fibers and matrix are defined as follows:

$$v_f = \frac{V_f}{V_{tot}}; v_m = \frac{V_m}{V_{tot}}, \tag{7.1}$$

where:

- v_f = volume fraction of the fibers
- v_m = volume fraction of the matrix
- V_f = Volume of fibers
- V_m = Volume of matrix
- $V_{tot} = V_f + V_m$

It is impossible to achieve a composite material with v_f=1 (100% fiber content) , as a finite volume cannot be filled with cylindrical fibers, even if perfectly aligned and packed. This packing limitation is one reason why composite properties are consistently lower than those of the reinforcement fibers themselves.

Fiber Orientation and Anisotropy

The effectiveness of reinforcement in a composite also depends heavily on fiber orientation. Fibers can be arranged in multiple directions within the matrix, and this has a significant impact on the mechanical behavior of the final material.

To describe fiber orientation, two coordinate systems are typically introduced:

- A global coordinate system (x, y, z) representing the structure
- A local coordinate system (1, 2, 3) representing the material microstructure

For unidirectional fiber-reinforced laminates, the fiber axis is assigned to direction 1, while direction 2 is orthogonal to the fibers within the laminate plane, and 3 is normal to the plane (thickness direction) (see Figure 7-1).
When fibers are arranged in a plane containing the x-direction, the fiber orientation angle (θ) is defined as the angle between the x-axis and the fiber direction (1) (Figure 7-2).

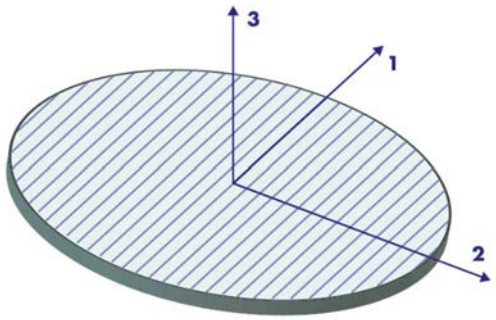

Figure 7-1 – Material Reference System for a Unidirectional Fiber Laminate.

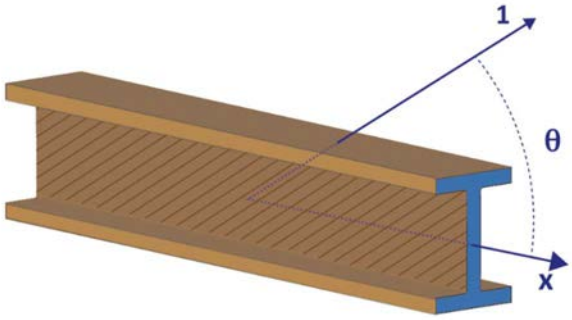

Figure 7-2 – Fiber Orientation Angle (θ) with Respect to the x-Direction.

Degree of Anisotropy in Composite Materials

The ratio between the values of a composite material's properties in different directions is referred to as the degree of anisotropy. In the case of unidirectional laminates, **Figure 7-2** provides indicative values of anisotropy for key properties relevant to design (E_i: elastic modulus; G_{ij}: shear modulus; σ_{ri}: ultimate strength; α_i: thermal expansion coefficient).

Table 7-2 – Degree of Anisotropy of Fiber-Reinforced Unidirectional Laminates (Indicative Values).

Material	E_1/E_2	E_1/G_{12}	σ_{r1}/σ_{r2}	α_1/α_2
Silicon carbide/ceramic	1.09	2.35	17.8	0.93
Boron/aluminum	1.71	5.01	11.6	0.30
Silicon carbide/aluminum	1.73	5.02	17.0	0.52
S-glass/epoxy	2.44	5.06	28.0	0.23
E-glass/epoxy	4.42	8.76	17.7	0.13
Boron/epoxy	9.27	37.40	24.6	0.20
Carbon/epoxy	13.60	19.10	41.4	-0.07
Aramid/epoxy	15.30	27.80	26.0	-0.07

Advantages of Composite Materials

Composite materials can exhibit higher strength and, at least in the case of carbon fiber composites, greater stiffness than traditional construction materials. As a result, when structural weight is a critical factor in a design, composites can be highly attractive due to their lower density.

- Composites' specific strength (strength-to-weight ratio) can be up to four times higher than that of traditional materials.
- Specific modulus (modulus-to-density ratio) can be up to twice as high.

This means that, for the exact stiffness requirements, a composite structure can weigh approximately half as much as a similar structure made from traditional construction materials.

Role of the Composite Phases in Material Properties

The final properties of a composite material are primarily determined by the nature of its constituent phases. However, to achieve a high-strength composite, it is not sufficient to use strong reinforcement fibers—it is also crucial to ensure a strong bond between the matrix and the reinforcement.

This adhesion is typically promoted through the use of a third component, which is applied as a thin layer on the fiber surface, making it compatible with the organic matrix. This surface treatment creates an intermediate interfacial phase between the matrix and the reinforcement, referred to as the interface or interphase (Figure 7-3).

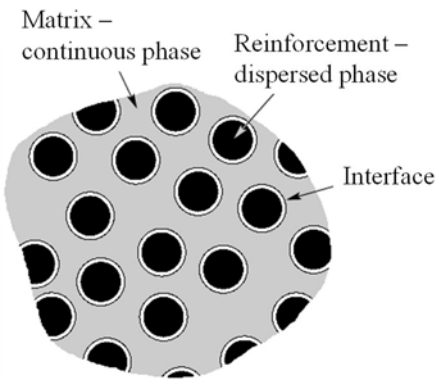

Figure 7-3 – Schematic Representation of Composite Phases.

Importance of the Interface in Composite Performance

The interface is usually an extremely thin layer (often monatomic) located at the reinforcement surface. While its properties do not directly contribute to the composite's global mechanical properties, they play a crucial role in the system's overall performance in structural applications.

Although the material supplier typically determines the specific chemical and physical mechanisms that govern fiber-matrix adhesion, it is essential to recognize that poor adhesion between fibers and the matrix is one of the primary causes of structural failure in composite materials.

7.2 REINFORCEMENT FIBERS

These guidelines cover the most commonly used fibers for the production of FRPs: glass, carbon, aramid, steel microfilaments, and braided steel strands.

In general, fibers tend to exhibit higher strength than the corresponding bulk material because their small cross-sectional dimensions reduce the presence of defects. As a result, fibers typically achieve strength values close to their theoretical maximum limit, which is about E/10 (where E is the elastic modulus).

Individual fibers are continuous, fragile filaments with diameters of approximately 10 μm, making them difficult to handle individually. For this reason, they are commercially available in bundles containing hundreds or even thousands of single filaments. The primary forms of fiber arrangements are summarized in Table 7-3.

Table 7-3 – Common Terminology in the Reinforcement Fiber Industry

Term	Definition
Fiber	An indivisible element of matter is characterized by having a length significantly greater than its diameter.
Filament	Synonym of fiber.
End/Strand	Set of glass filaments.
Tow	Like yarn, this term refers to a bundle of carbon fibers assembled without twist.
Roving	A set of yarns or bundles assembled without a twist.
Yarn	A set of yarns or bundles assembled with a twist.
Band	A set of overlapping tapes is used to produce composites using filament winding technology.
Tape	Set of parallel filaments sewn together or bound by an organic matrix.
Woven	The two-dimensional structure is obtained by assembling yarns, strands, or tapes using various types of weaving.

Due to this significant complexity, a specific technical designation is often required. This designation, given its clear analogy to textile applications for clothing and upholstery, follows a convention codified by ISO 1139 and ISO 2078 standards. It consists of the following elements:

1. A letter identifying the type of glass used.
2. A letter indicating the fiber type:
    - C - continuous (for filaments)
    - D - discontinuous (for chopped fibers)
3. A number indicating the nominal fiber diameter (in μm).
4. Another number (separated by a space) indicating the linear density of the fiber, expressed in tex.
5. The twist direction and rate (Figure 7-4), expressed in turns per meter (optional).
6. The number of twisted strands, including twist direction and rate (optional).

The tex unit is part of the International System of Units (SI) and describes yarn thickness based on length rather than volume (also known as linear density or "yarn count").

- A yarn of 1 tex weighs 1 gram per kilometer of length.
- A yarn of 50 tex weighs 50 grams per kilometer.
- The higher the tex value, the greater the number of fibers present in the yarn.

Textile yarns almost always undergo twisting operations to give them the required consistency and stability for weaving. However, for composite applications, excessive twisting is not recommended, as it can compromise the mechanical performance of the fabric and hinder resin impregnation. The typical twist rate for composite yarns is less than 50 turns per meter, which is significantly lower than that used for natural fiber yarns (e.g., cotton, which can exceed 600 turns per meter).

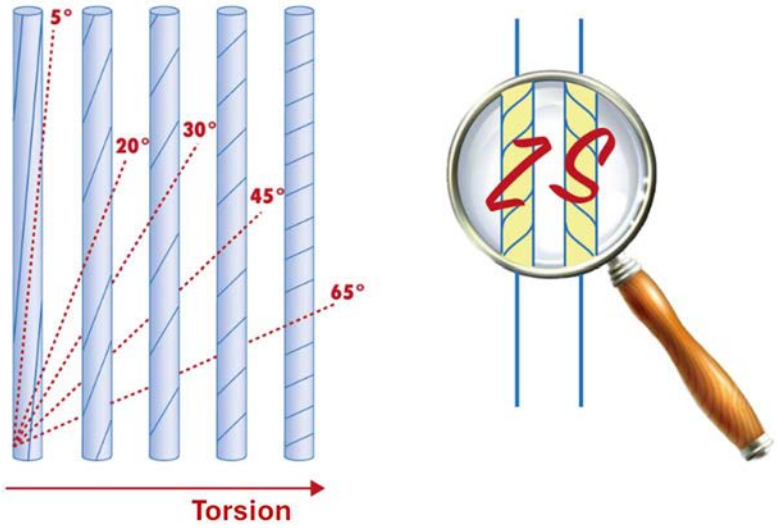

Figure 7-4 – Effect of Twist Direction and Rate on Yarn Appearance.

Examples of Fiber Designation and Interpretation

- EC10 40 → Continuous filament E-glass, 10 µm diameter, 40 tex linear mass.
- EC9 34 Z 40 → Continuous filament E-glass, 9 µm diameter, 34 tex linear mass, twisted at 40 turns/m. The letter Z indicates a positive twist direction according to ISO 1139 (S denotes a negative twist).
- EC9 34 Z 160 x 4 S 150 →
  - "x" indicates multiple strands.
  - The designation before "x" identifies the filament characteristics.
  - The number 4 specifies the number of filaments in the bundle.
  - The letter "S" indicates a negative twist applied at 150 turns/m.
  - EC9 x 4 S 150 → Simplified designation of the previous example.

Some commonly used yarns for structural composites include:

- EC5 10 x 2 → E-glass based
- SC5 4 x 2 → S-glass based (see Table 7-4).

For carbon fibers, the yarn classification is based on the "k" notation, where "k" stands for "thousands." For example:

- 1k yarn → Contains 1,000 filaments (66.6 tex).
- 3k yarn → Contains 3,000 filaments (200 tex).
- Other typical values: 0.5k, 1k, 3k, 6k, 12k, 18k, 24k, 48k.

In addition to yarns (yarn) or rovings, fibers are also commercially available in specialized arrangements to form a wide variety of fabrics. These woven configurations can enhance composite isotropy in the plane.

In woven fabrics, two primary fiber directions are defined:
- Warp → The main (longitudinal) fiber direction.
- Weft → The transverse (perpendicular) fiber direction.

7.2.1 Glass Fibers

Glass fibers were first produced in a laboratory by René-Félix-Antoine, comte de Réaumur, in the early 18th century. Still, the first glass fiber-based composite material was not used in the aerospace industry until World War II (1942). These fibers are highly versatile and are relatively easy to produce, as they are derived from raw materials available in virtually unlimited quantities.

Most high-performance glass fibers used in composite manufacturing are composed of a mixture of metal oxides, with silica being the primary component. They offer excellent structural and functional properties while maintaining the lowest cost among all reinforcement fibers. Glass fibers are highly resistant to fire and heat, and they retain approximately 25% of their initial strength up to temperatures slightly above 500°C.

Glass fibers also exhibit good chemical resistance, except in highly concentrated acidic and alkaline solutions. This factor must always be carefully considered when they come into direct contact with mortars and cement. Additionally, glass fibers are excellent materials for applications requiring:
- Good electrical insulation,
- Low thermal expansion coefficient, and
- High thermal conductivity.

Classification of Glass Fibers

Glass fibers are generally categorized into two main groups:
1. Low-cost fibers for general-purpose applications
2. Specialized high-performance fibers

Over 90% of commercially available glass fibers belong to the first category, designated by the letter "E" and characterized by a composition precisely defined by ASTM D578.

The remaining glass fibers fall into the high-performance or specialized category. Some of these fibers are designated by letters, usually associated with specific properties (as shown in Table 7-4), while commercial brand names identify others. However, not all specialized fibers are regulated under ASTM D578.

The chemical composition of the most commonly used glass fibers in structural applications is shown in Figure 7-5. As can be observed, the silica content in glass fibers is consistently above 50%.

In general terms:
- E-glass fibers → Suitable for applications where exposure to aggressive environments is not expected.
- ECR-glass fibers → Suitable for moderately aggressive alkaline environments.
- AR-glass fibers → The best choice for highly aggressive alkaline environments.

Table 7-4 – Designation of common glass fibers and glass fibers for special applications

Designation	Property
A	High alkali content
C	Resistant to chemical agents
D	Low dielectric constant
ECR	High chemical and electrical resistance
AR	Resistant to alkaline environments
R	High tensile strength
S	High elastic modulus and strength

Oxide (Chemical Composition)	Oxide	AR (%)	ECR (%)	E (%)
SiO_2	Silica	65%	60%	55%
Al_2O_3	Alumina	1%	12%	14%
B_2O_3	Boron trioxide	–	–	7%
CaO	Lime (Calcium oxide)	3%	21%	21%
MgO	Magnesia	–	2%	3%
ZnO	Zinc oxide	–	3%	–
Na_2O/K_2O	Sodium/Potassium oxide	1%	1%	1%
ZrO_2	Zirconium dioxide	14%	–	–
TiO_2	Titanium dioxide	5%	–	–

Figure 7-5 – Indicative Chemical Composition of Major Glass Fibers for Civil Engineering Applications.

The different compositions of various types of glass fibers are generally designed to achieve specific properties while ensuring suitability for fiber spinning. The spinning process used is known as melt spinning, where the melting temperature of the mixtures ranges from approximately 1160°C for E-glass to over 1500°C for S-glass.

During fiber formation, the molten mass is rapidly cooled to prevent crystallization. The molten glass is then gravity-fed through platinum alloy bushings equipped with a large number of small holes (typically ranging from 400 to 8000, with diameters between 0.8 and 3 mm). This process results in glass filaments with typical diameters ranging from 3 to 25 μm. These individual filaments are then combined into multifilament strands, which are wound—typically without twisting—onto spools at speeds exceeding 60 meters per second.

Protection and Surface Treatment of Glass Filaments

Glass filaments are highly abrasive, and friction between them during handling can irreversibly damage their surface, compromising their mechanical properties. To prevent this, newly formed filaments are coated with special sizing agents immediately before collection. These sizing agents serve two primary purposes:

- Protection against abrasion, and
- Improved adhesion to the polymer matrix.

Some sizing agents are temporary - such as starch-oil emulsions - and can be easily removed through processes like heating.

Processing and Commercial Forms of Glass Fibers

Once the filaments are produced, they are gathered into a strand before being wound onto a collection spool. The strand can then undergo further processing to be converted into different commercial products, depending on the intended application. The primary commercially available glass fiber products include:

- Roving (bundled continuous fibers),
- Chopped strands (short, discontinuous fibers),
- Yarn (used in textiles, but rarely in composites),
- Non-woven fabric (mat).

Direct Roving and Direct Chopped Strand

In recent years, new processes have been developed to manufacture roving or chopped fibers directly during filament formation. These products are referred to as:

- Direct roving, and
- Direct chopped strand.

Non-Woven Mat (Mat)

The mat, sometimes referred to in Italian as "materassino" (mattress in English) is a non-woven fabric that comes in two main types (Figure 7-6):

1. Continuous strand mat, and
2. Chopped strand mat.

In both cases, the fibers are randomly arranged within the mat and held together by a chemical binder, usually thermoplastic. The binder's solubility in the polymer resin used for composite manufacturing can range from low to high, depending on the specific application.

Glass Fiber-Based FRPs (GFRP)

As previously mentioned, glass fiber-reinforced polymers (FRP) are commonly known by the acronym GFRP (Glass Fiber Reinforced Polymers).

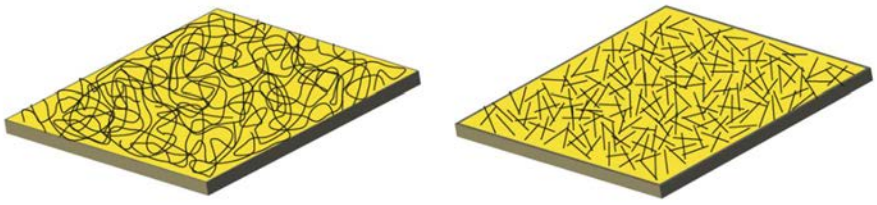

Figure 7-6 – Different Type of Mat.

7.2.2 Carbon Fibers

The first known industrial application of carbon fibers dates back to Thomas Alva Edison, who obtained them in 1879, during his work on incandescent light bulbs, through the pyrolysis of cotton threads or bamboo strips. However, the first process for producing carbon fibers for composites from polyacrylonitrile (PAN) filaments was patented by Akio Shindo in Japan in 1960. Even today, carbon fibers produced with a PAN-based precursor represent more than 95% of the market, although processes utilizing other precursors, such as pitch or rayon, have been developed since 1964. More recently, materials such as lignin and polyethylene (PE) have also been used to reduce the cost of carbon fibers, albeit with some difficulties and significantly lower mechanical properties.

Carbon fiber is a unique reinforcement material, as its properties span a wide range of thermo-physical characteristics, which can be easily adjusted depending on the intended application. This results in a broad variety of properties for the composite materials derived from it. In addition to having intrinsically high strength-to-weight and stiffness-to-weight ratios, carbon fiber is thermally and electrically conductive, possesses a very low coefficient of thermal expansion, and provides excellent fatigue resistance to structural composite elements.

Manufacturing Process of PAN-Based Carbon Fibers

The production of PAN-based carbon fibers occurs in two distinct phases:

1. Polymerization of the PAN-based copolymer, starting from the selected monomers, which is then processed into a fiber through solvent spinning.
    a. The PAN fiber is classified as acrylic if it contains at least 85% acrylonitrile by weight or modacrylic if it contains between 35% and 85% acrylonitrile by weight.
    b. The most commonly used comonomers in the manufacture of carbon fiber precursors include acrylic acid, methacrylic acid (MAA), itaconic acid, methacrylate, acrylamide, vinyl acetate, vinyl bromide, and quaternary ammonium salts.
2. Heat treatment processes:
    a. The stabilization phase occurs in air under tension at 200°C to 300°C for 30 to 120 minutes. During this phase, the fibers absorb oxygen molecules, leading to a rearrangement of atomic bonds.
    b. After stabilization, the carbonization phase occurs through pyrolysis in an inert atmosphere at temperatures ranging between 1000°C and 1700°C.
    c. c. For a more advanced degree of carbonization, a subsequent heat treatment can be applied at temperatures up to 3000°C, also in an inert atmosphere.
    d. During pyrolysis, the fibers lose various atoms - primarily nitrogen, hydrogen, oxygen, and even some carbon - which form gases such as water vapor, ammonia, carbon monoxide, carbon dioxide, hydrogen, nitrogen, and others (Figure 7-7).

Structural Characteristics of Carbon Fibers

Due to the pyrolysis process, carbon fibers are composed of more or less pure graphite planes, which vary in extent and organization depending on the precursor material and manufacturing processes.

- These graphite planes primarily develop along the fiber length, resulting in extremely high modulus of elasticity and tensile strength in the longitudinal direction.
- However, these properties are significantly lower in the transverse direction, resulting in anisotropic behavior.

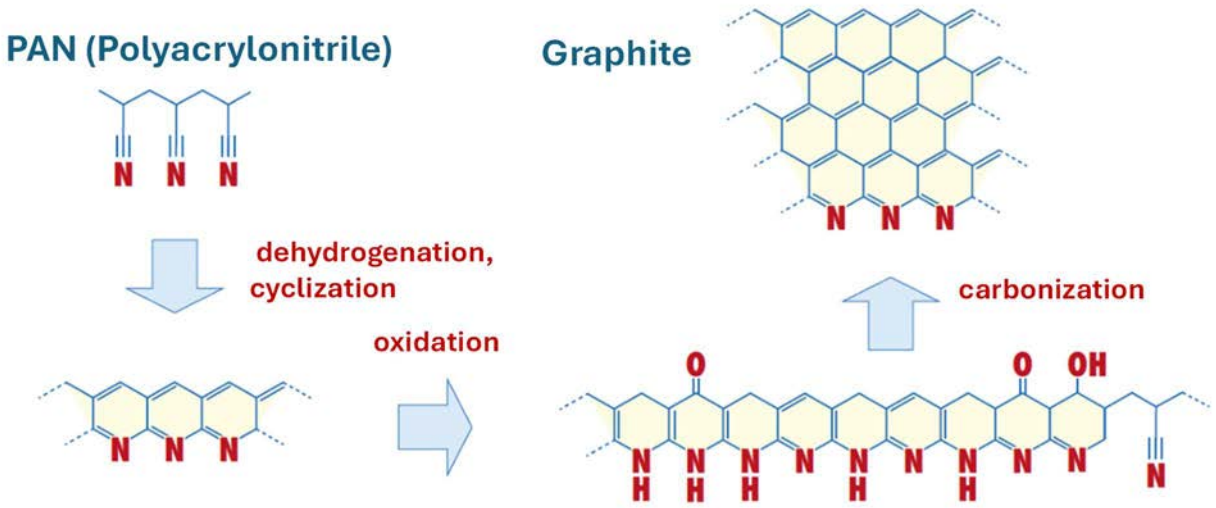

Figure 7-7 – Decomposition reactions of PAN for the production of carbon fibers.

Once produced, carbon fibers are wound onto a spool, following a process very similar to that used for glass fibers. The types of commercial products are also analogous, including:

- Tows (bundles of filaments)
- Twisted yarns for textiles
- Mats
- Fabrics

Designation of Carbon Fibers

The designation system used for carbon fiber products differs from that of glass fibers and follows conventional naming schemes and commercial labels used by major suppliers.

Common Naming Convention: "k" Notation

The size of the tow, yarn, or filament is typically identified using a number followed by the letter "k", where "k" stands for "thousands". It represents the number of individual filaments in the product:

- 1k → 1000 filaments
- 3k → 3000 filaments
- 6k → 6000 filaments
- 12k, 18k, 24k, etc.

The most common fiber counts used in composite materials range from 1k to 24k.

ISO 13002 Standardized Designation

There is also an internationally standardized designation system, outlined in ISO 13002, which consists of three sections separated by hyphens:

1. First section (optional): Identifies the product type (e.g., "reinforcing fiber").
2. Second section: Indicates the ISO standard designation.
3. Third section: Describes the specific product properties, including:
    a. Fiber precursor and product form
    b. Mechanical properties (e.g., tensile modulus, strength)
    c. Additional information (optional, such as twist direction or sizing type)

Example:

"ISO 13002-CF-AC,450-45-1400,,"

This designates a carbon fiber (CF) produced from a PAN precursor (AC) with:

- Nominal elastic modulus = 450 GPa
- Nominal tensile strength = 4.5 GPa
- Nominal tex value = 1400 tex
- The double comma at the end indicates that no additional information is included.

Carbon fiber-based FRPs are commonly referred to as CFRP (Carbon Fiber Reinforced Polymers)..

7.2.3 Aramid Fibers

Aramid fibers (sometimes referred to as "aramidic fibers" based on the corresponding English term) are synthetic organic fibers whose name is derived from the contraction of the words "aromatic polyamide." These fibers consist of a special type of polyamide, in which at least 85% of the amide groups in the molecular structure are bonded to two aromatic rings.

The development of aramid fibers began in 1938 when DuPont commercialized the first synthetic polyamide fiber, nylon.

The first significant advances toward fibers with high mechanical properties were achieved in 1962, again by DuPont, with the introduction of the first meta-aramid fiber based on metaphenylene diamine (MPD), known as Nomex. However, it was only in 1965 that Stephanie Kwolek, a researcher at DuPont, discovered a new method for producing highly oriented aramid molecules: a polymer based on para-phenylenediamine (PPD). Thanks to the formation of hydrogen bonds between the molecules, this new polymer enabled them to self-organize into a liquid-crystalline structure (Figure 7-8).

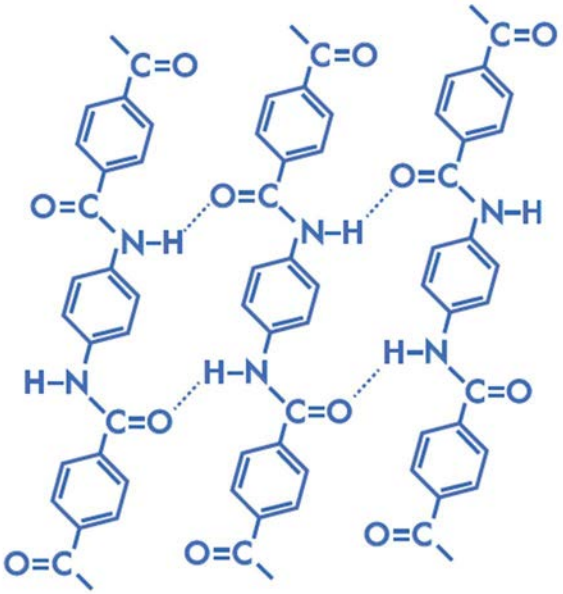

Figure 7-8 – Chemical structure of para-aramid fibers.

The PPD-based fibers were later commercialized under the name "Kevlar," which is still commonly used today as a synonym for aramid fibers. In 1971, DuPont further developed a poly-para-phenylene terephthalamide (PPTA) fiber, which was introduced to the market under the name high-strength Kevlar.

In conclusion, the history of aramid fiber development has been almost exclusively dominated by DuPont. DuPont remains the world’s largest manufacturer of aramid fibers, controlling nearly 70% of the global market. The Japanese company Teijin is the second-largest producer.

Manufacturing Process of Aramid Fibers
The manufacturing process involves the synthesis of the polymer, starting from PPD and aromatic diacid chloride (TCl) in a hexamethylphosphoramide (HPT) solution through two successive reaction stages at relatively low temperatures (below 100°C).

After washing, filtration, and drying, the polymer undergoes solution spinning, either dry or wet spinning, depending on the product type, using sulfuric acid as the solvent.

- The crystalline structure, already present in the liquid phase, aligns along the fiber length due to shear forces acting during extrusion.
- After coagulation, the fibers maintain a highly oriented molecular structure, as illustrated in Figure 7-9.
- Following spinning, aramid fibers undergo thermal stretching treatments at temperatures between 360°C and 550°C to enhance their properties.
- This process enables them to achieve modulus values exceeding 140 GPa and tensile strength values exceeding 4 GPa.

Applications of Aramid Fibers
Thanks to their outstanding mechanical properties, high thermal resistance, and low weight, para-aramid fibers (Kevlar) are widely used in military and civilian aerospace applications, as well as in various industrial sectors. Their applications include:

- Personal ballistic protection and lightweight armor
- Pressure tanks
- Brake and clutch discs
- Tire reinforcements
- Protective gloves
- Electrical insulation
- Printed circuit boards

Use in Hybrid Laminates
Aramid fibers are often incorporated into hybrid laminates, where their unique properties are synergistically combined with those of other reinforcement fibers. This is particularly advantageous for structural components subjected to impacts (e.g., protective panels) or dynamic loads, as aramid fibers have an exceptional ability to dampen vibrations.

Classification and Designation of Aramid Fibers
The designation of aramid fibers follows a conventional naming system, where a numerical value is added after the commercial name to indicate the fiber's specific properties. Some of the most commonly used Kevlar grades include:

- Kevlar 29 → Used in ballistic protection and electrical cables
- Kevlar 149 → High modulus fiber
- Kevlar 49 → The most commonly used aramid fiber in composites, with a strength similar to Kevlar 29 but a 50% higher modulus
- Kevlar 149 → 40% higher modulus and 70% lower moisture absorption than Kevlar 49
- Kevlar 129 → High Tenacity (HT)
- Kevlar 119 → High elongation at break (HE)
- Kevlar 68 → Intermediate performance (HP)

Other commercial names for aramid fibers include:

- Twaron and Technora (produced by Teijin)
- Vectran (developed by Celanese)
- Staramid

Limitations of Aramid Fibers
Despite their numerous advantages, aramid fibers have some limitations, including:

- High moisture absorption, which can affect their properties
- Degradation from prolonged exposure to sunlight, leading to significant reductions in mechanical strength

Durability and Commercial Availability
Despite these limitations, aramid fibers remain highly durable in various applications, including non-composite uses, such as coating for submarine cables.

Aramid fibers are commercially available in the form of:

- Yarns
- Rovings
- Fabrics

Aramid fiber-reinforced composites are commonly referred to as AFRP (Aramid Fiber Reinforced Polymers).

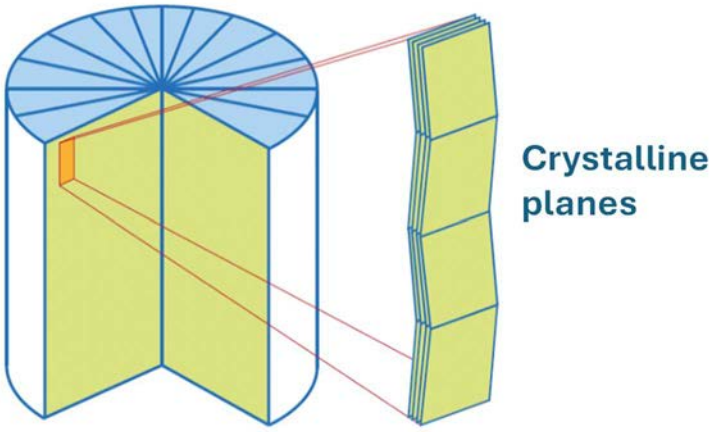

Figure 7-9 – Crystalline structure of aramid fibers.

7.2.4 Basalt Fibers

In recent years, fibers derived from basalt have found numerous applications as a replacement for glass fibers, particularly in situations requiring high fire resistance.

These fibers were first developed by the Research Institute for Glass and Plastics in Moscow in 1953. As a result, they represent a high-tech fiber initially developed in the former Soviet Union. The first commercial applications emerged after 30 years of research and development. The first industrial production furnace was launched in 1985 in Ukraine.

Basalt is a natural material found in volcanic rocks, formed from rapidly cooled lava with a melting temperature ranging from 1,500 °C to 1,700 °C. Approximately 80% of basaltic rocks consist of two primary minerals: plagioclase and pyroxene, which are primarily composed of silica (SiO_2) and alumina (Al_2O_3). The manufacturing process of basalt fibers is very similar to that of glass fibers. Still,

due to lower energy consumption and the absence of chemical additives, it is generally more cost-effective.

Basalt fibers exhibit mechanical properties similar to those of glass fibers, along with excellent chemical stability and good resistance to various environmental agents, including atmospheric conditions, alkaline environments, and acid exposure. Their thermal stability depends on the composition of the raw material but is generally better than that of glass fibers. This is primarily due to the presence of micropores, which limit air convection and radiation, making basalt fiber fabrics widely used for thermal insulation and passive fire protection.

FRPs made with basalt fibers are commonly referred to as BFRP (Basalt Fiber Reinforced Polymers).

7.2.5 Micro-Cables and Steel Braids

The micro cables and braids used in SFRP systems are made of various types of steel wires. In general, ultra-high tensile strength steel (UHTSS) is initially developed for the tire industry. The steel wires typically have a diameter ranging from 0.10 to 0.50 mm and are twisted together to form micro-cables or braids, with a cross-sectional area between 0.30 and 0.60 mm². Various configurations exist, including:

- Micro-cables composed of five twisted filaments (Figure 7-10),
- Micro-cables with three straight filaments and two additional filaments wrapped around them (Figure 7-10b),
- Micro-cables consisting of 12 twisted steel filaments with an extra filament wrapped around them at a tighter twist angle (Figure 7-10c),
- Braids made up of small twisted filaments (Figure 7-10d).

Figure 7-10 – Common types of steel micro-cables (a-c) and braids (d) used in SFRP systems.

The twisted arrangement slightly reduces the strength and stiffness of the cable compared to a single steel wire. Still, it improves adhesion to the matrix and provides the fabric with greater geometric stability during installation. The steel wires must be protected against corrosion either by zinc galvanization (Figure 7-11) or by being made from stainless steel. Tensile tests conducted after artificial accelerated aging in aggressive environments have shown that a zinc coating of at least 22 g/kg achieves adequate corrosion protection of the filaments.

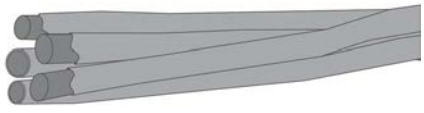

Figure 7-11 – UHTSS steel cable with galvanized wires.

Micro-cables or braids are arranged in parallel to form unidirectional fabrics, which are then wound into rolls for commercial distribution. Their mechanical properties are defined only in the longitudinal direction of the micro-cables/braids, while they are non-existent in the transverse direction. Transverse connectivity can be achieved using:

- Thin metallic filaments (which have no structural function) create a fabric that holds the micro-cables/braids in place during installation or

- Heat-welding to a plastic or glass fiber mesh that does not have a structural role but facilitates storage and installation.

The spacing of the micro-cables/braids varies between 1.1 mm (23 per inch) and 6.35 mm (4 per inch). Depending on the wire cross-sectional area, their quantity, and the density of the micro-cables/braids, the equivalent thickness of the fabrics ranges from 0.075 mm to 0.440 mm. Based on this equivalent thickness ($\boldsymbol{t_f}$), fabrics can be classified as follows:.

- Low density: $t_f \leq 0.1$ mm
- Medium density: 0.1 mm < $t_f \leq 0.3$ mm
- High density: $t_f > 0.3$ mm

The corresponding values expressed as surface mass density are:

- 600-1500 g/m² (low density)
- 1500-2500 g/m² (medium density)
- 2500-3300 g/m² (high density)

The steel fabric primarily governs the tensile mechanical behavior of SFRP systems, while the resin matrix's contribution is negligible, except in low-density fabrics, where it provides a small additional contribution to stiffness.

The tensile behavior of UHTSS steel is comparable to that of high-carbon steel commonly used in prestressed concrete structures. It exhibits a linear elastic phase up to 60-70% of its ultimate strength, followed by a gradual reduction in stiffness until the ultimate stress is reached. To account for this stiffness reduction before the peak strength, qualification protocols and strength classifications for SFRP systems refer to the yield limit stress, which is defined as the stress corresponding to a residual strain of 0.1% after unloading rather than the ultimate strength.

As with other FRP systems, the mechanical properties are based on the net cross-sectional area of the fabric, excluding the resin. Available test data in the literature indicate the following values for steel fabrics:

- Tensile strength: 2000-3300 MPa
- Ultimate strain: 1.6% – 2.2%
- Elastic modulus: 180 – 220 GPa
- Conventional yield stress: 1600 – 2600 MPa

Currently, available stainless steel fabrics exhibit a tensile strength of approximately 1500 MPa and an elastic modulus of about 180 GPa.

7.2.6 Natural Fibers

Driven by the growing awareness of the need to reduce the environmental impact of human activities and encourage the use of sustainable materials, the use of natural fibers as a substitute for glass fibers in composites for structural and semi-structural applications has become increasingly common in recent years. Today, natural fibers account for approximately 15% of the European composite market.

Natural fibers can exhibit mechanical properties similar to those of glass fibers but have lower density, are biodegradable, and are non-abrasive. Additionally, they are typically more cost-effective than other reinforcement fibers.

Among natural fibers used for structural applications, flax (Linum usitatissimum) is the most widely employed, making up about 20% of the market, followed by kenaf (8%), hemp (5%), and jute. Europe is currently the largest producer and exporter of flax globally, with France, Belgium, and the Netherlands being the central producing countries.

Flax has a short growth cycle, requiring only 100 days from sowing in March to harvesting in July. Long, uniform flax fibers are primarily used to produce textile yarns for clothing and home furnishings. In contrast, lower-quality flax fibers are mainly used to manufacture panels for automotive interiors.

Structure and Properties of Flax Fibers
Flax fibers are extracted from the bast (the vascular subcortical layer found between the bark and xylem) in the stem of the plant. A cross-section of a flax stem reveals about twenty fiber bundles, each containing ten to forty individual fibers bonded together by pectin lamellae.

Similar to cotton fibers, flax fibers are primarily composed of cellulose, but their crystalline structure makes them stronger and stiffer. These fibers can reach several dozen centimeters in length, with an average diameter between 10 and 20 μm.

Flax fibers can absorb significant amounts of moisture from the environment, up to 12% of their weight. A high moisture content can pose significant challenges during composite manufacturing, necessitating strict humidity control. Additionally, the waxy substances on the fiber surface can affect the wettability and adhesion characteristics of the fiber with composite matrices. Therefore, before being used in composite fabrication, flax fibers should undergo appropriate chemical and physical treatments.

Other Natural Fibers
Beyond flax, other natural fibers used in composites include:

- Sisal
- Hemp
- Coconut fibers
- Cotton
- Abaca (Manila hemp)
- Banana leaf fibers
- Bamboo fibers
- Wheat straw
- Other fibrous natural materials

Although the range of available natural fibers and their possible combinations is virtually endless, the bast fibers—flax, hemp, and jute—remain the most relevant for structural composite materials.

7.2.7 Fibers Properties

The application of reinforcement fibers in the production of structural composite materials necessitates a thorough examination of their mechanical behavior and primary mechanical properties, including elastic modulus, strength, and strain at failure.

In general, all fibers exhibit an elastic-brittle behavior characterized by a linear elastic response to applied stress, followed by sudden fracture, as shown in Figure 7-12.

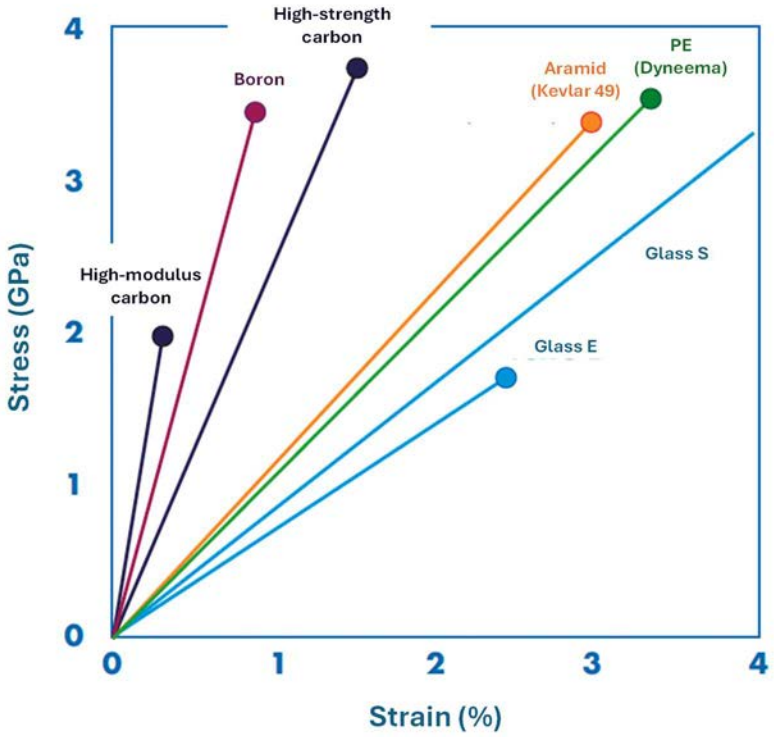

Figure 7-12 – Stress-strain curves of primary reinforcement fibers.

A comparison of the characteristic values of key properties for the most commonly used reinforcement fibers is presented in Figure 7-13.

Material	E (GPa)	σ_{RT} (GPa)	σ_{RC} (GPa)	ρ (kg/dm³)	α (10^{-6} °C^{-1})
E-glass	75	1.5	1.5	2.5	8
S-glass	85	4.5	2	2.5	3.5
Aramid (Kevlar 49)	70	3.5	0.3	1.45	≈0
Carbon (high strength)	210	4.5	1.5	1.8	0
Boron (Boron)	240	2	3	2.4	5
PE (Dyneema)	140	3.5	0.3	0.97	6

Figure 7-13 – Comparison of some properties of the primary reinforcement fibers.

Regarding elastic modulus, three distinct groups can be identified:

- Glass fibers, with modulus values ranging from 75 to 85 GPa,
- Aramid fibers, with modulus values up to 140 GPa,
- Carbon fibers, with values exceeding 200 GPa.

Carbon fibers exhibit a wide range of elastic modulus values depending on the type of precursor and the carbonization/graphitization process, as illustrated in Figure 7-14.

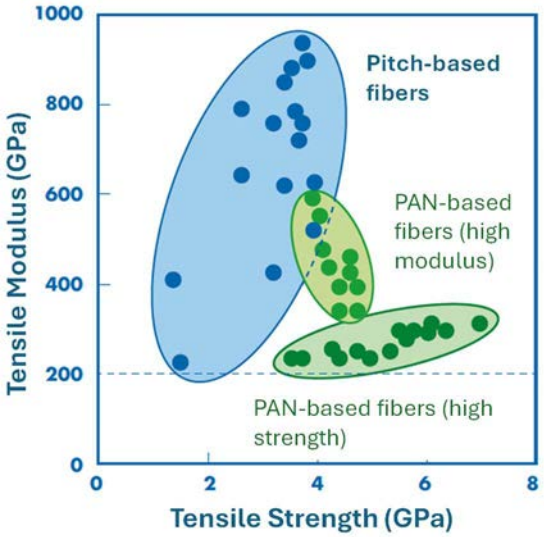

Figure 7-14 – Mechanical properties of the main types of carbon fibers.

Carbon fibers derived from pitch account for less than 5% of the total carbon fiber market. They are primarily used in specialized applications, often in the military sector, due to their ability to achieve maximum elastic modulus values close to 1000 GPa. Depending on the final heat treatment temperature, PAN-based carbon fibers are classified as high-strength or high-modulus fibers. Higher heat treatment temperatures result in fibers with increased microstructural order, provided sufficient pretensioning is applied, allowing elastic modulus values to reach up to 600 GPa.

However, unlike pitch-based carbon fibers or most other reinforcement fibers, PAN-based carbon fibers cannot simultaneously achieve high modulus and high strength.

Regarding Poisson's ratio,

- Glass fibers typically have values between 0.16 and 0.2,
- Carbon fibers exhibit slightly higher values (0.26 to 0.3) due to their anisotropic structure,
- Aramid fibers have even higher values (0.37).

It should be noted that, with the sole exception of glass fibers, reinforcement fibers are inherently anisotropic. Consequently, their properties in the longitudinal direction (as discussed so far) can differ significantly from those in the radial direction. Although this difference is often negligible for most fiber-reinforced composite applications—where the primary stresses are predominantly aligned with the fiber direction—certain cases require consideration of this factor.

For instance:

- Polyethylene fibers have a transverse elastic modulus about 40 times lower than their longitudinal modulus and a transverse tensile strength two orders of magnitude lower than their longitudinal strength.
- Carbon fibers, both PAN- and pitch-based, exhibit much lower radial elastic modulus values compared to their longitudinal values, ranging from 10 to 20 GPa.
- Shear modulus (G12) in carbon fibers is also significantly lower, with typical values around 15 GPa.

The highest density values are observed in glass fibers (~2.5 kg/dm³), while carbon and aramid fibers have lower values (1.8 kg/dm³ and 1.4 kg/dm³, respectively).

Regarding the coefficient of linear thermal expansion:

1. Glass fibers exhibit positive values between 3 and 6 × 10^{-6} °C^{-1},
2. Carbon and aramid fibers, on the other hand, show negative values (with a minimum of -2 × 10^{-6} °C^{-1} for aramid fibers) due to structural reorganization occurring at elevated temperatures.

Negative thermal expansion coefficients are highly desirable in applications involving significant temperature variations, such as space applications, where maintaining tight dimensional tolerances is crucial. By carefully selecting the stacking sequence of laminates, composite materials can be designed with near-zero overall thermal expansion.

Other Functional Properties

Beyond mechanical behavior, reinforcement fibers also exhibit additional functional properties, such as thermal/electrical conductivity, moisture absorption, and magnetic characteristics.

Regarding electrical resistance:

- Polymer fibers have very high resistivity (> 10^{14} Ω·cm), making them excellent insulators.
- Glass fibers also exhibit high resistivity (~ 4 × 10^{12} Ω·cm) and are considered insulating materials.
- Carbon fibers, however, have much lower resistivity (~30 Ω·cm), making them electrically conductive and suitable for applications such as electrostatic painting, electromagnetic shielding, and thermal resistors.

Regarding thermal conductivity:

- Aramid fibers have a very low conductivity (~4 × 10^{-2} W/m·K).
- Glass fibers exhibit values about two orders of magnitude higher (~1.3 W/m·K).
- PAN-based carbon fibers range from 5 to 15 W/m·K.
- Pitch-based carbon fibers can reach up to 800 W/m·K, exceeding even aluminum (205 W/m·K).

7.2.8 Physical and Dimensional Characteristics of Yarns

Yarns are not marketed as materials for structural reinforcement, as they serve as the raw material for fabric production. However, manufacturers may provide the mechanical properties of the yarn upon request. The relevant international standard for yarns is ISO 2113.

To determine or verify the linear density (tex) of a yarn, the procedure outlined in ISO 1889 can be followed. This involves extracting a defined length of yarn from the fabric and weighing it. The linear density (title) is then calculated using the following formula:

$$T_x = \frac{P \cdot 1000}{L} \tag{7.2}$$

where:

- T_x is the linear density (yarn count) of the yarn, expressed in tex (g/km),
- P is the mass of the sample, expressed in grams,
- L is the length of the sample, expressed in meters.

The cross-sectional area (A) of a yarn or bundle (yarn, tow, or roving) in mm² can be determined from the linear density and mass density of the yarn using the following equation:

$$A = \frac{T_x}{\rho \cdot 1000} \tag{7.3}$$

where:

- ρ is the mass density of the yarn, expressed in g/cm³,
- T_x is the linear density (yarn count) expressed in tex.

Assessing these parameters can be valuable for quality control of the supplied product, ensuring consistency and compliance with specifications.

7.2.9 Fabrics

Fabrics are almost always used in the applications covered in this document to facilitate the rapid application of reinforcement during installation. Traditional textile looms with a "shuttle" can weave fabrics with interwoven fibers, or specialized looms can produce unidirectional or multi-axial fabrics with non-interwoven fibers. Knitting or braiding machines may also be employed for special applications. Fabrics that are not impregnated with resin are commonly referred to as "dry" fabrics.

The most common fabrics are those woven on traditional looms with a plain or twill weave, which have very similar characteristics in both the warp and weft directions (symmetric fabrics). Unidirectional fabrics provide good properties in a single direction, while multiaxial fabrics, on the other hand, have balanced properties in multiple directions.

The main characteristics of a fabric include the type and yarn count used in both the warp and weft, the type of weave pattern, the thread count, and the weight per unit area. The thread count of the fabric refers to the number of warp and weft threads per unit length (usually the number of threads per centimeter), which determines how "tight" or "dense" a fabric is. The most commonly used weave patterns in the field of composite materials are plain, basket (Panama), twill (diagonal), and satin, as shown in Figure 7-15. The choice of weave pattern determines several key properties, such as formability (also called "drapeability") and the final performance of the composite.

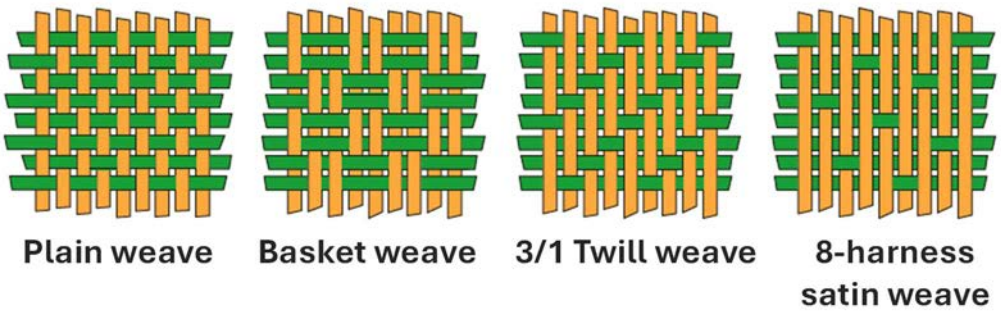

Figure 7-15 – Main types of traditional woven fabrics.

The combination of all a fabric's characteristics can be encoded in its fabric style, a designation first introduced in the military aerospace sector in the 1950s (MIL-C-9084 standards, now AMS-C-9084). Over time, this classification evolved, often taking on different names depending on the supplier. For example, a style 7781 fabric is made of fiberglass with an 8-harness satin weave and is widely used in the aerospace industry for aircraft cabin interiors.

The plain weave is the simplest weave type, in which the warp threads pass alternately over and under the weft threads. The basket weave is similar to a plain weave. Still, it involves two or more warp threads interlacing (binding) over and under an equal number of weft threads, producing a characteristic checkerboard effect, with the size of the squares depending on the number of threads grouped.

In the twill weave, one or more warp threads separate two binding points with the weft (as in plain weave), but in this case, the points are staggered, creating a diagonal structure at a 45° angle. A specific type of twill weave is Batavia.

Finally, in the satin weave, the number of binding points is minimized to make them almost invisible, allowing the warp threads to remain much straighter than in previous cases. For instance, in an eight-harness satin weave, only one warp thread out of eight binds with the weft. As shown in Figure 7-15, the total surface area of warp threads (colored orange) that remain continuously visible over the weft (colored green) increases from left to right, indicating greater warp thread straightness due to fewer interlacing points compared to a plain weave.

From a composite manufacturing standpoint, satin weaves conform best to complex surfaces because, for the exact yarn count and thread density, they are "softer" due to fewer binding points per unit area. Satin weaves also provide the best mechanical properties in the composite because fiber waviness (crimp) caused by interlacing is minimized.

The descending order of flexibility and mechanical performance among fabric types is satin, twill, basket, and plain weave. However, regardless of weave type, the fibers in a woven fabric will always be more wavy in both the warp and weft directions compared to a unidirectional or multi-axial fabric.

On the downside, satin fabrics are the least stable during handling. Therefore, they must be treated with care when manufacturing thick laminates with relatively simple curvatures, where the reduction in mechanical properties due to fiber waviness is not critical. Plain or twill weaves are preferred, as they are more stable and widely used in the industry.

A solution to the compromise between fiber straightness (mechanical performance) and ease of processing (weaving stability) is multi-axial fabrics, where unidirectional fibers are stacked at various angles - not just orthogonal to each other (Figure 7-16). The layers are then stitched together using tack stitches, which pass through all the layers to maintain fabric stability during handling. The ultimate form of multi-axial fabric is the unidirectional fabric, which consists of a single layer of fibers.

Since multi-axial fabrics have no interwoven fibers, all fibers remain perfectly straight, making them known as "non-crimp fabrics" (NCF).

In addition to higher mechanical properties (due to the elimination of fiber waviness), NCFs also conform better to highly complex surfaces - for example, double-curved surfaces - without creating wrinkles, which commonly occur when using traditional woven fabrics or prepreg tapes. This is because the fibers in NCFs can slide relative to each other, as there are no interwoven points restricting movement.

For these reasons, NCFs are rapidly becoming the preferred choice in industries requiring complex structural components.

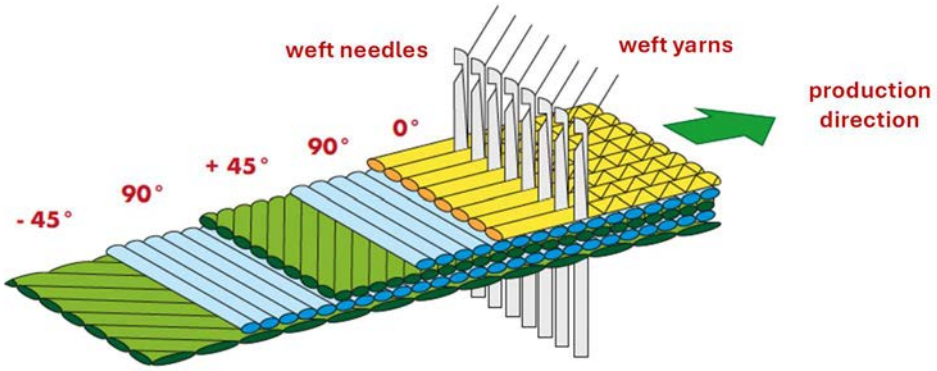

Figure 7-16 – Example of a multi-axial fabric.

7.2.10 Physical and Dimensional Characteristics of Fabrics

Structural reinforcement fabrics are commonly supplied in dry form and in rolls, intended for on-site impregnation with specialized resins. They can be classified into three main types:

- Unidirectional fabrics, where all fibers are aligned along the fabric's length and held together by a lightweight, non-structural weft.
- Bidirectional fabrics, woven with an orthogonal warp-weft structure, typically balanced (i.e., with an equal percentage of fibers in both directions).
- Multi-axial fabrics, where fibers are oriented in multiple in-plane directions.

The general reference standard for these fabrics is UNI 8099:1980.

For multi-axial fabrics, in addition to the standard information regarding yarn type and other fabric characteristics, the fiber orientation of each layer must also be specified.

The following section presents examples of methods for determining key fabric properties used in structural reinforcement.

If only the yarn count (tex) and fabric geometry are provided, the mass per unit area of fibers (areal weight) in a given direction can be determined using the following equation:

$$\rho_x = \frac{T_x \cdot N_f}{10} \tag{7.4}$$

Where:
ρ_x = mass per unit area of the fabric or fabric component in the considered direction, expressed in g/m^2,
T_x = yarn count in the considered direction, expressed in tex (g/km).
N_f = number of threads per unit width in the considered direction [n$_o$/cm].

For example, considering a unidirectional fabric with 3.8 threads/cm and a yarn count of 800 tex, the areal weight is calculated as:

$$\rho_x = \frac{800[tex] \cdot 3.8[fili/cm]}{10} = 304\,g/m^2 \tag{7.5}$$

If it is necessary to determine the number of fibers per unit length in a given direction orthogonal to the fibers, the ISO 4602 standard can be followed. This involves counting the number of fibers arranged in the orthogonal direction over a predefined width of the fabric (e.g., 10 cm) and then scaling this number proportionally to the selected unit length.

7.3 MATRICES OF FRP COMPOSITES

The matrix is a fundamental component of composite materials, playing a crucial role in both manufacturing technologies and the final properties of the components. Its primary functions are to ensure material continuity (essentially filling all the gaps between the fibers), protect the fibers from external environmental and mechanical agents (e.g., abrasion), and uniformly distribute external mechanical loads among the different fibers to optimize the composite material's strength. The matrix must be free of voids or discontinuities and capable of developing and maintaining strong adhesion to the fibers throughout the composite's service life.

The matrices covered in this document are the so-called polymeric matrices, which are composed of long and highly flexible molecules known as macromolecules formed through the repeated combination of relatively simple molecules called monomers. The names of polymers are derived from the monomer name, preceded by the prefix "poly-": for example, polyethylene is a macromolecule derived from ethylene monomers, polypropylene from propylene monomers, and so on. In the field of composite materials, synthetic polymers are commonly referred to as synthetic resins or simply resins.

Synthetic polymers can be classified into two main categories:

- Thermoplastics, in which individual polymer chains are held together only by weak interactions (such as van der Waals forces, dipole-dipole interactions, or hydrogen bonds), allow the material to be liquefied by heating.
- Thermosetting resins are more commonly used in fiber-reinforced composites.

Thermosetting resins are available in a partially polymerized state and typically appear as liquids or pastes at room temperature. When mixed with a suitable curing agent, they undergo polymerization (cross-linking) and solidify into a glassy material. The reaction can be accelerated by increasing the temperature. These resins offer several advantages, including:

- Low viscosity in the liquid state, allowing easy fiber impregnation
- Excellent adhesive properties
- The ability to cure at room temperature
- Good resistance to chemical agents
- The absence of a melting temperature, meaning they do not soften when heated

However, they also present some drawbacks, such as:

- A limited operating temperature range, constrained by the glass transition temperature
- Brittle behavior with low fracture toughness
- Sensitivity to moisture during application on structures

The most commonly used thermosetting resins in the civil engineering sector are epoxy resins, while polyester and vinyl ester resins are also employed.

Fiber-reinforced composites with thermoplastic polymer matrices are also available and may require different application techniques. For example, composite rebars with a thermoplastic matrix are being studied, offering the advantage of being bendable at any time by applying heat—unlike thermoset-based rebars.

Additionally, fiber-reinforced composites with elastomeric resins as the matrix are available. These materials exhibit an elastic and non-brittle behavior, characterized by high toughness and high elongation at break.

7.3.1 Epoxy resins

Epoxy resins are known for their good resistance to moisture and chemical agents, as well as their excellent adhesive properties. These characteristics make them particularly well-suited for the production of composites used in civil engineering applications.

The maximum service temperature of an epoxy resin depends on its specific formulation and the curing temperature. For service temperatures exceeding 60°C, the resin must be carefully selected, considering the resulting variations in its mechanical properties. On the other hand, there are generally no significant limitations for the minimum service temperature.

The term "epoxy" refers to a chemical group consisting of an oxygen atom bonded to two carbon atoms, which are, in turn, connected to the polymer chain in some manner. The most straightforward epoxy resin features three-membered ring structures along its chain, known as alpha-epoxy (or ethylene oxide). The most commonly used epoxy resin in composite materials is diglycidyl ether of bisphenol A (DGEBA), whose chemical structure is shown in Figure 7-17.

In its uncrosslinked state, epoxy resin is a low-viscosity liquid that is easy to process and can be cured quickly and efficiently at any temperature by adding a curing agent. This curing agent must be added immediately before application in a stoichiometric ratio (a precise dosage established by the manufacturer). Additionally, thorough mixing is essential to ensure a high-quality application.

Figure 7-17 – Chemical structure of an epoxy oligomer based on diglycidyl ether of bisphenol A (DGEBA).

7.3.2 Polyester Resins

Polyester resins are characterized by lower viscosity compared to epoxy resins and exhibit remarkable versatility and high reactivity. However, their mechanical strength and adhesive properties are generally inferior to those of epoxy resins. In civil engineering applications, polyester resins are primarily used in pultruded profiles and partition and/or insulating panels, almost exclusively in combination with glass fiber reinforcements.

The synthesis reaction of these resins is the organic equivalent of the inorganic reaction in which a base and an acid produce a salt. Similarly, in organic chemistry, the reaction of an alcohol with an organic acid produces an ester and water as a byproduct. Unsaturated polyester resin is produced using dihydric alcohols (glycols) that react with saturated and unsaturated dicarboxylic acids; as a result, there is an entire range of polyester formulations, each with different properties. The specific

polyester resins used in composite materials are classified as "unsaturated," meaning they contain double atomic bonds along the molecular chain that allow them to undergo a curing reaction.

The two main types of polyester resins used for impregnation in the composites industry are orthophthalic polyester resins and isophthalic polyester resins. The former is a standard resin used in most applications. At the same time, the latter is slightly more expensive and widely utilized—particularly in the marine sector—due to its superior water resistance (Figure 7-18). The resin is available as a clear, viscous liquid consisting of a polyester solution in a solvent (styrene), which also acts as a crosslinking agent. From a chemical reaction standpoint, the styrene does not necessarily need to be present in stoichiometric amounts. It is typically used to adjust the resin's viscosity based on the specific application and environmental conditions.

With the addition of a catalyst, the crosslinking reaction is activated, leading to the formation of a rigid, infusible, and chemically resistant solid. However, this solid is also relatively brittle, particularly in terms of impact resistance.

Another type of polyester resin often used in structural applications is epoxy vinyl ester. While it follows the same curing reaction with styrene as traditional polyester, vinyl ester resin possesses properties that are intermediate between those of polyester and epoxy resins, offering improved chemical and mechanical resistance, especially in terms of impact resistance.

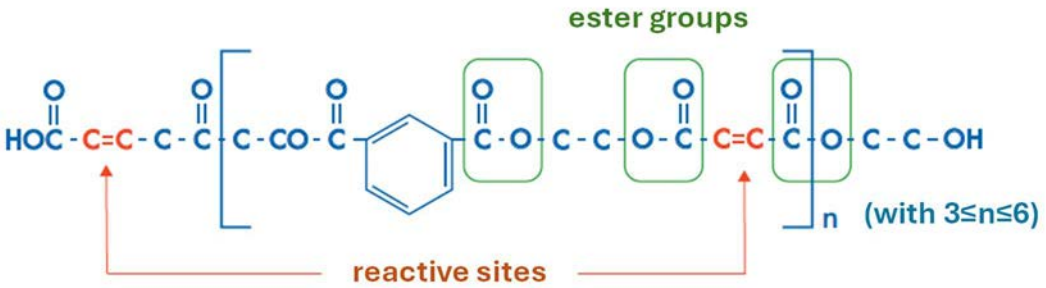

Figure 7-18 – Chemical structure of an isophthalic polyester resin.

7.3.3 Other Types of Resins

The intrinsic limitations of thermosetting resins, as outlined above—particularly their low toughness, relatively low service temperatures, and tendency to absorb moisture from the environment—have led, in recent years, to the development of thermoplastic matrix composites. Their market share is rapidly expanding within the global structural composite materials industry. This growth is primarily driven by the automotive sector, which, in its pursuit of low-environmental-impact vehicles, requires lightweight structural materials that can be manufactured using high-productivity technologies.

Thermoplastic resins are characterized by their ability to flow when heated to a sufficiently high temperature, precisely above T_g (glass transition temperature) for amorphous materials and T_m (melting temperature) for semi-crystalline materials. This property allows the shape of components to be modified at will simply by reheating the material to the appropriate temperature (hot forming). Additionally, thermoplastic components can be assembled using thermal welding, a process that is not possible with crosslinked resins, which are infusible.

These resins also offer better durability in aggressive environments - especially in their semi-crystalline forms - and have a much longer shelf life compared to thermosetting resins, as they are non-reactive systems.

The most commonly used thermoplastic matrices for composite materials are shown in Table 7-5. Most of them are semi-crystalline, with melting temperatures (T_m) starting at 130°C, which defines their upper operating temperature limit. Polyetherimide (PEI), being an amorphous polymer, has its upper service temperature determined by its T_g instead.

Only the three resins with melting temperatures above 300°C (PPS, PEKK, and PEEK) fall into the category of high-temperature thermoplastics. The monomeric units of some of the thermoplastic resins listed in Table 7-5 are shown in Figure 7-19.

Although their current use in civil engineering is relatively limited, research is ongoing into high-potential applications, such as reinforcement bars for reinforced concrete. Compared to thermosetting resins, thermoplastic resins tend to be tougher and, in some cases, offer higher service temperatures. They also exhibit better resistance to environmental factors.

The primary limitation to their use is their high viscosity, which makes fiber impregnation challenging and necessitates the use of complex and costly processing equipment.

Lastly, inorganic matrices, such as cement-based, metallic, and ceramic matrices, are also noteworthy. Their use in fiber-reinforced composites for civil applications—particularly cement-based composites—is gradually increasing. While they are not covered in this document, their use may be considered viable, provided that it is supported by adequate technical documentation and experimental validation, which demonstrates performance at least equivalent to that of the organic matrices discussed here.

Table 7-5 – Transition Temperatures of Major Thermoplastic Resins for Composites

Polymer	Morphology	T_g (°C)	T_m (°C)	Relative Cost
PBT	Semicrystalline	56	223	Medium
PA6	Semicrystalline	48	219	Low
PA12	Semicrystalline	52	176	Low
PP	Semicrystalline	-20	165	Low
PE	Semicrystalline	-120	130	Low
PEI	Amorphous	217	–	Medium
PPS	Semicrystalline	89	307	Low
PEKK	Semicrystalline	156	306	Medium
PEEK	Semicrystalline	143	343	High

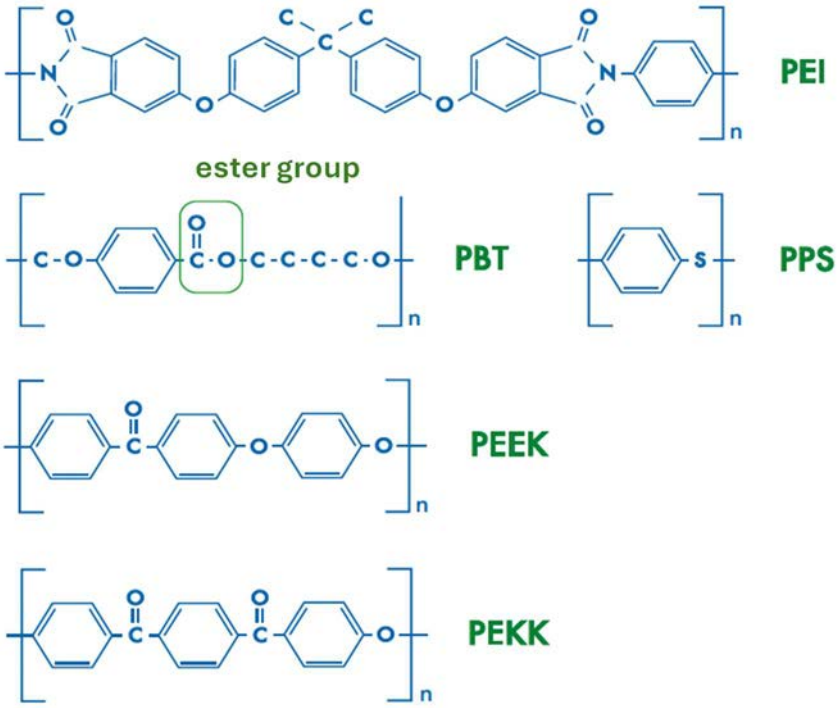

Figure 7-19 – Chemical Structure of Monomeric Units of Selected Thermoplastic Resins for Composites.

7.4 ADHESIVES

The installation of certain types of FRP-based structural reinforcements, such as pultruded laminates, requires the use of adhesives. The appropriate selection of both the adhesive and the surface treatment to be performed before application depends on the nature of the substrate of the structure being repaired and the reinforcement material.

A detailed analytical discussion of this topic would be complex, as it would first require distinguishing between various structural cases (steel, reinforced concrete, masonry, or wood), an approach that exceeds the scope of this document.

Typically, technical data sheets for reinforcement materials provide guidelines on the type of adhesive to use based on the nature of the structure to be strengthened. Even the application of dry fabrics, which are impregnated on-site, can broadly be considered a form of adhesive bonding, as the same resin used for impregnation also serves as an adhesive.

For the proper use of adhesives, the surface treatment performed before application is critical. Therefore, this section focuses primarily on why proper substrate preparation is essential, providing an overview of the physical, chemical, and mechanical mechanisms that underlie adhesion.

For a more in-depth discussion, reference should be made to specialized texts on the subject.

An adhesive is defined as a material, almost always polymer-based, capable of bonding at least two surfaces and transmitting significant forces (structural bonding). There are many types of natural and synthetic adhesives (elastomers, thermoplastic and thermosetting resins, single-component and two-component systems). Still, epoxy-based adhesives are the most suitable for composite materials.

Epoxy adhesives are typically two-component viscous mixtures that, upon curing, undergo a chemical crosslinking reaction, forming a structural bond.

The advantages of adhesive bonding over mechanical connections are numerous, including:

- The ability to bond different materials
- Greater stiffness
- More uniform load distribution
- Strengthening of connected parts
- No need for drilled holes, which can cause stress concentrations
- Improved fatigue resistance
- Lower intervention costs.

7.5 TRANSITION TEMPERATURES

Impregnation resins and adhesives undergo thermal transitions that significantly influence their application fields.

One inherent transition is the so-called glass transition temperature (T_g), at which a substantial reduction in elastic modulus (E) occurs, sometimes by several orders of magnitude. As a result, T_g defines the upper-temperature limit for all thermosetting resins as well as amorphous thermoplastic polymers (such as PEI, listed in Table 7-5).

For semi-crystalline polymers (which include all other polymers in Table 7-5), the upper application temperature is instead the melting temperature (Tm).

These transition temperatures are determined by measuring changes in mechanical properties with temperature variations through Dynamic Mechanical Analysis (DMA) or Differential Scanning Calorimetry (DSC). Due to its simplicity and rapid execution, DSC is by far the most commonly used method for measuring impregnation resins and adhesives.

The test is conducted following ISO 11357-2, which provides detailed guidelines. However, it is essential to note that since this standard is primarily designed for thermoplastic resins, its application to thermosetting resins requires adherence to the special procedure for reactive systems outlined in paragraph 9.4.2, third sub-section of the standard.

This procedure mandates explicitly that:

- The test specimen must be preconditioned.
- The measurement must be conducted exclusively during the first heating cycle to prevent the resin from reacting while performing the test.

8 APPENDIX B (MANUFACTURING TECHNIQUES)

The content of Appendix B has been largely extracted from the book "Technologies and Properties of Composite Materials" Amazon Publ. (2021) ISBN-13 979-8712973958, with the kind permission of the Author, Prof. Roberto Frassine.

8.1 MANUFACTURING TECHNIQUES

This appendix describes the manufacturing techniques of preformed FRP composites relevant to Civil Engineering applications.

8.1.1 Pultrusion

Pultrusion is the first continuous manufacturing process developed for producing reinforced composite materials. It was first introduced in the United States in the 1950s and, by the 1960s, a wide range of pultruded profiles with various dimensions and cross-sectional shapes were already available on the American market. Today, the European market alone accounts for approximately 50,000 tons of pultruded products per year.

The name pultrusion is rather unusual and is, in fact, a compound word derived from the combination of the English terms pull and extrusion: unlike extrusion, where the material is pushed through the equipment, pultrusion pulls it using the reinforcing fibers.

Pultrusion is a widely used technology in the civil engineering field, primarily for producing laminates and structural profiles. The process is continuous and consists of three main stages:

- Forming
- Impregnation
- Consolidation

In its most common form, designed for thermosetting matrices, the components (resin and fibers) are fed separately into a machine that grips and pulls the fibers through various processing stages.

A widely adopted version of this process involves resin bath impregnation, as illustrated in Figure 8-1. The fibers are drawn from a set of spools and guided through racks that ensure uniform alignment before entering a resin bath for impregnation.

Upon exiting the resin bath, the fiber bundle—mainly composed of fibers aligned along the profile's longitudinal axis—can be coated with additional reinforcing materials such as rovings, mats, and fabrics. *Continuous filament mats* are used primarily to reinforce the outer surfaces of profiles that require a high-quality finish. Typical basis weights range from 300, 450, and 600 g/m². *Polyester or glass veils* are often applied to improve surface quality, enhance weather and UV resistance, and provide color stability and chemical resistance, with basis weights ranging from 30 to 100 g/m².

Fabrics and mats can also be used to increase transverse strength. Various fiber combinations in 0°, 45°, and 90° orientations, as well as hybrid fabrics, can be applied in successive layers to achieve the desired final properties. *Flame-retardant mats* may also be applied to the surface, producing a protective foam layer that acts as an oxygen barrier in the event of a fire, thereby slowing combustion.

The impregnated fiber bundle is preformed into the desired profile shape and then enters a heated mold (*die*), where the material is consolidated under pressure. Heat is typically supplied through electrical resistance heaters, and the temperature profile inside the mold is monitored using strategically placed thermocouples. The production speed controls the residence time of the profile within the mold. The curing reaction begins once the decomposition temperature of the radical initiator (*peroxide*) is reached, initiating polymerization at the mold surfaces before propagating to the profile's core.

Upon exiting the mold, the matrix has solidified, and the composite is gripped by a pulling device that drags it forward at a constant speed. This device consists of caterpillar tracks or hydraulic clamps, which can be operated individually, jointly, or in parallel. A circular saw then cuts the product into bars of the desired length (usually no more than 15 meters) or, if flexibility allows, winds it onto large-diameter reels.

The traditional pultrusion process is suitable only for producing straight profiles with a constant cross-section. However, there are variations in which the mold is not fixed but moves back and forth along the profile being produced. This modified process, known as "Radius-Pultrusion," enables the production of two-dimensional and three-dimensional curved profiles, such as wave-shaped or spiral profiles. By combining pultrusion technology with compression molding, it is also possible to produce profiles with moderately variable cross-sections.

Pultruded profiles weigh between 30% and 80% less than equivalent aluminum and steel profiles, respectively. They are also more cost-effective, highly durable even without maintenance - being immune to corrosion - and have significantly lower electrical conductivity.

For these reasons, pultruded profiles are used in a wide range of industrial applications, from construction to the transportation industry, including cable trays, tie rods, ladder uprights, fishing rods, tool handles, lighting and signage supports, risers for the oil industry, and more.

.

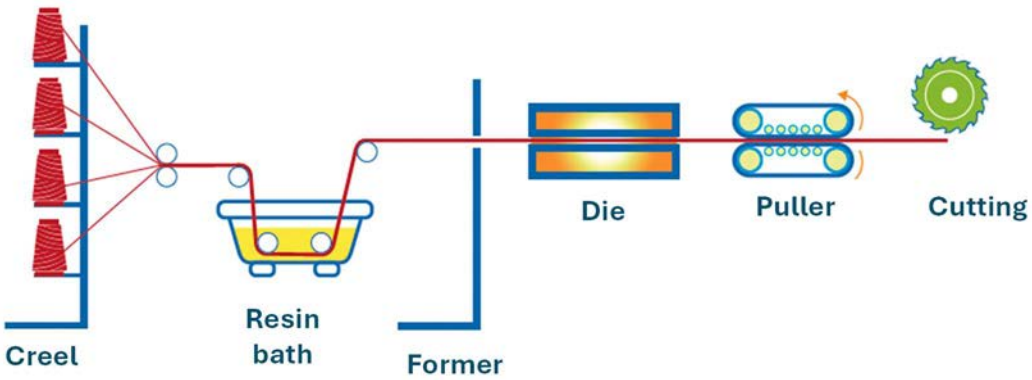

Figure 8-1 – Pultrusion technology.

8.1.2 Vacuum Bagging Lamination

Vacuum bagging lamination is used almost exclusively for manufacturing high-performance composites.

This is a batch process, which allows for the production of laminates with thicknesses of up to several centimeters and highly complex lay-up sequences. Compared to pultrusion, it offers almost absolute freedom in fiber orientation across different laminas and in shaping curved components. However,

the main limitation lies in its slow production cycle, with an output rate of approximately 0.5 kg/h for relatively simple components.

The typical production of a laminate involves the following fundamental steps:

a) Preparation (of the mold and materials);
b) Lamination (cutting the material, layering, and compacting the plies);
c) Vacuum bagging setup;
d) Curing of the material (at room temperature, in an oven, or in an autoclave);
e) Inspection (visual, ultrasonic, and X-ray analysis);
f) Finishing (trimming edges with a milling machine or high-pressure water jet).

The lamination process (lay-up) can be carried out using dry fibers, which must be impregnated with resin during application, or using prepregs—unidirectional or woven continuous fiber reinforcements that are pre-impregnated with resin.

The next step (step c) involves preparing the vacuum bag. A typical vacuum bag assembly, along with its various components, is illustrated in Figure 8-2.

A vacuum is created inside the bag through a valve connected to a vacuum pump. The vacuum primarily serves to quickly extract solvents and trapped air from the laminate, compacting the layers together before the resin fully cures. Additionally, the vacuum bag serves several essential functions that facilitate the curing process (step d), though it is not strictly essential.

Advantages and Applications

The primary advantage of this technique is its extreme versatility, enabling the manufacture of highly complex components without the need for expensive molds.

Key applications include aerospace and aeronautics, motorsports, shipbuilding, and the broader transportation sector.

An example of manual lamination in civil engineering is the confinement of columns or shear strengthening of beams by applying a dry fabric (or prepreg) onto the surface of structural members, followed by resin impregnation using a roller.

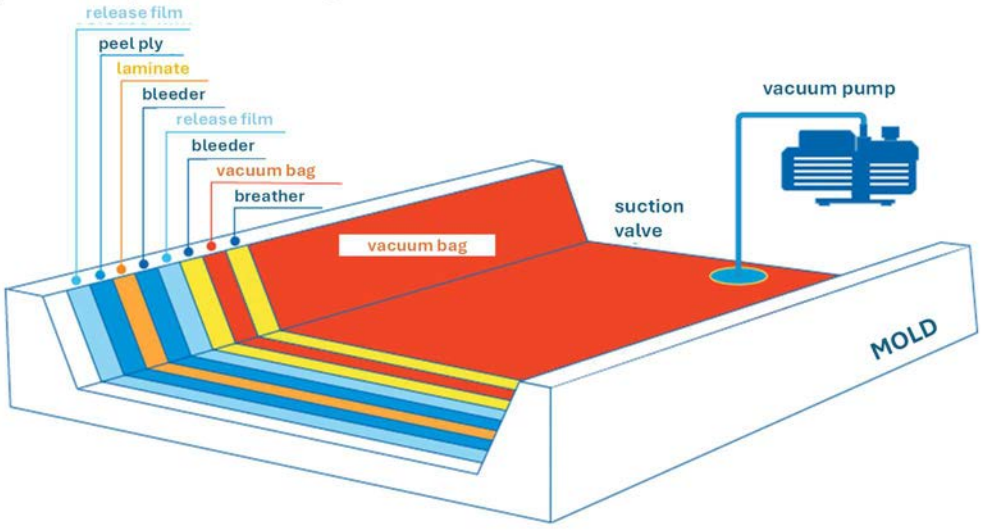

Figure 8-2 – Vacuum bag molding of prepregs.

8.1.3 Wet lay-up

Wet lay-up is one of the most straightforward and most traditional techniques used for the on-site fabrication of composite materials.

This process consists of two main phases:

- Lamination (lay-up)
- Curing (polymerization)

In detail, the first phase involves manually placing a layer of fabric onto a specific surface, which is then impregnated with a resin that has been pre-mixed with a catalyst (Figure 8-3).

Impregnation is performed manually using rollers or brushes, followed by careful rolling to compact the material and eliminate trapped air bubbles.

This procedure can be repeated for each additional fabric layer, applied individually, until the desired thickness is reached.

The curing phase follows the lay-up and occurs at room temperature, within a relatively short period, without the need for external heating of the composite surface.

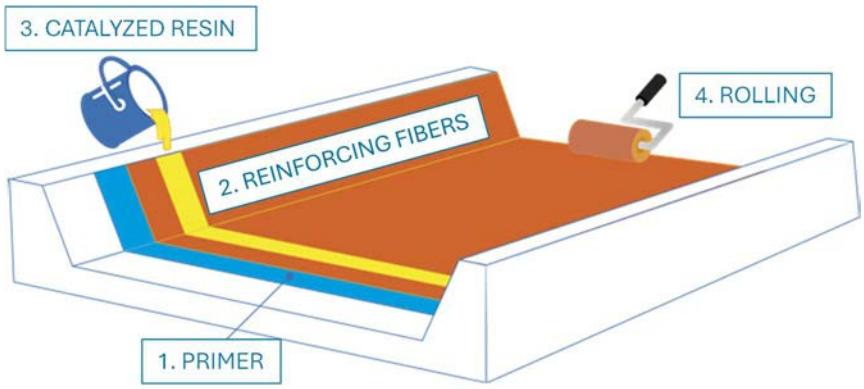

Figure 8-3 – Manual impregnation (also known as wet lay-up) of reinforcement fabrics in situ.

9 APPENDIX C (CONSTITUTIVE RELATIONSHIP OF FRP AND FAILURE CRITERIA)

9.1 CONSTITUTIVE RELATIONSHIPS

Fiber-reinforced composite materials are heterogeneous (i.e., composed of different materials) and anisotropic (i.e., exhibiting different properties in different directions). Since the scale of applications relevant to civil engineering is significantly larger than the microstructural scale of the material, its heterogeneity can be neglected by representing the actual material as a homogeneous continuum.

As is well known, if the stress and strain state at a given point within the continuum can be represented by the components of the stress tensor ($\underline{\sigma}$ in Figure 9-1) and the corresponding components of the strain tensor (ε), then the mechanical behavior of a homogeneous, elastic, and anisotropic solid can be defined by 21 independent elastic constants through a matrix relationship of the form:

$$\underline{\sigma} = [C]\underline{\varepsilon} \quad \Leftrightarrow \quad \begin{bmatrix} \sigma_1 \\ \sigma_2 \\ \sigma_3 \\ \tau_{23} \\ \tau_{31} \\ \tau_{12} \end{bmatrix} = \begin{bmatrix} C_{11} & C_{12} & C_{13} & C_{14} & C_{15} & C_{16} \\ C_{12} & C_{22} & C_{23} & C_{24} & C_{25} & C_{26} \\ C_{13} & C_{23} & C_{33} & C_{34} & C_{35} & C_{36} \\ C_{14} & C_{24} & C_{34} & C_{44} & C_{45} & C_{46} \\ C_{15} & C_{25} & C_{35} & C_{45} & C_{55} & C_{56} \\ C_{16} & C_{26} & C_{36} & C_{46} & C_{56} & C_{66} \end{bmatrix} \begin{bmatrix} \varepsilon_1 \\ \varepsilon_2 \\ \varepsilon_3 \\ \gamma_{23} \\ \gamma_{31} \\ \gamma_{12} \end{bmatrix} \tag{9.1}$$

where [C] is the stiffness matrix.

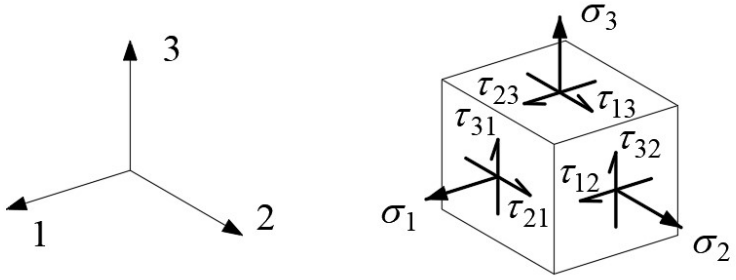

Figure 9-1 – Representation of the stress state acting on an infinitesimal element.

A complete characterization of the stiffness matrix would therefore require evaluating these 21 constants through appropriate combinations of tensile and shear tests. However, the number of required tests can be significantly reduced if the material exhibits some form of symmetry, which is the case for nearly all composite materials used in engineering applications.

Many unidirectional composites, consisting of fibers aligned in a single direction, can be considered transversely isotropic—as in Figure 9-2, where the 2-3 plane (perpendicular to the fibers) represents the plane of isotropy. In this case, the number of independent elastic constants is reduced to five, and the stiffness matrix takes the following form:

$$[C]=\begin{bmatrix} C_{11} & C_{12} & C_{12} & 0 & 0 & 0 \\ C_{12} & C_{22} & C_{23} & 0 & 0 & 0 \\ C_{12} & C_{23} & C_{22} & 0 & 0 & 0 \\ 0 & 0 & 0 & \frac{1}{2}(C_{22}-C_{23}) & 0 & 0 \\ 0 & 0 & 0 & 0 & C_{66} & 0 \\ 0 & 0 & 0 & 0 & 0 & C_{66} \end{bmatrix} \tag{9.2}$$

In practice, it is often convenient to refer to the so-called engineering constants:

- E (Normal elastic modulus or Young's modulus),
- ν (Transverse contraction coefficient or Poisson's ratio)
- G (modulo di elasticità tangenziale).

These constants have distinct values in different directions. For example, it is reasonable to expect that the longitudinal Young's modulus in the fiber direction **(**E_1**)** is greater than the transverse Young's modulus (E_2), which in turn may differ from the out-of-plane modulus **(**E_3**)**. The same considerations apply to the shear moduli G_{12}, G_{13}, and G_{23} (the 1, 2, and 3 directions are defined in Figure 9-2).

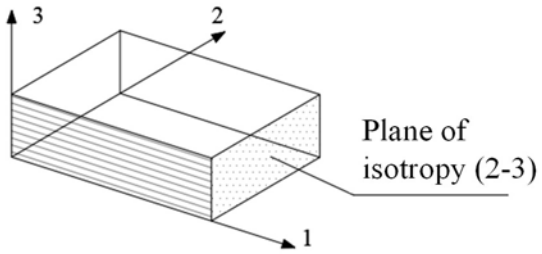

Figure 9-2 – Unidirectional composite with a plane of transverse isotropy.

Using these engineering constants, the compliance matrix [S]**,** which is the inverse of the stiffness matrix [C], can be expressed as:

$$[S]=\begin{bmatrix} \frac{1}{E_1} & -\frac{\nu_{12}}{E_1} & -\frac{\nu_{12}}{E_1} & 0 & 0 & 0 \\ -\frac{\nu_{12}}{E_1} & \frac{1}{E_2} & -\frac{\nu_{23}}{E_2} & 0 & 0 & 0 \\ -\frac{\nu_{12}}{E_1} & -\frac{\nu_{23}}{E_2} & \frac{1}{E_2} & 0 & 0 & 0 \\ 0 & 0 & 0 & \frac{2\cdot(1+\nu_{23})}{E_2} & 0 & 0 \\ 0 & 0 & 0 & 0 & \frac{1}{G_{12}} & 0 \\ 0 & 0 & 0 & 0 & 0 & \frac{1}{G_{12}} \end{bmatrix} \tag{9.3}$$

The five independent engineering constants in this case are:

- E_1 (Longitudinal modulus),
- E_2 (Transverse modulus),
- ν_{12} (Poisson's ratio in the fiber plane),
- ν_{23} (Poisson's ratio in the transverse plane),
- G_{12} (In-plane shear modulus).

9.2 PLANE STRESS STATES

In the specific case of a thin unidirectional laminate under plane stress conditions, the compliance matrix takes the following form:

$$\begin{bmatrix} \varepsilon_1 \\ \varepsilon_2 \\ \gamma_{12} \end{bmatrix} = \begin{bmatrix} \frac{1}{E_1} & -\frac{\nu_{12}}{E_1} & 0 \\ -\frac{\nu_{12}}{E_1} & \frac{1}{E_2} & 0 \\ 0 & 0 & \frac{1}{G_{12}} \end{bmatrix} \begin{bmatrix} \sigma_1 \\ \sigma_2 \\ \tau_{12} \end{bmatrix} \tag{9.4}$$

In this case, the mechanical behavior of the unidirectional laminate can be characterized by four independent elastic constants. The uniaxial tensile tests are typically performed with the fibers inclined at a predefined angle, θ, relative to the direction of the applied load. By setting $\theta = 0°$, meaning the fibers are parallel to the loading direction, E_1 and ν_{12} can be determined. When $\theta = 90°$ (fibers perpendicular to the load direction), E_2 is evaluated. The choice of the angle θ for determining G_{12} depends on the specific reinforcement geometry.

It is also possible to estimate some elastic constants with good accuracy using simple micromechanical models based on the properties of the individual constituents (fiber and matrix) and their volume fractions. In particular, for unidirectional laminates, the properties in the longitudinal direction can be approximated using a relationship known as the "rule of mixtures." This model, derived from a basic micromechanical approach (Slab Model), assumes that fibers and matrix "work" in parallel. It provides a good approximation for the elastic modulus in the fiber direction E_1 and the Poisson's ratio ν_{12}:

$$\begin{aligned} E_1 &= V_{\text{fib}} \cdot E_{\text{fib}} + (1 - V_{\text{fib}}) \cdot E_{\text{mat}}, \\ \nu_{12} &= V_{\text{fib}} \cdot \nu_{\text{fib}} + (1 - V_{\text{fib}}) \cdot \nu_{\text{mat}}, \end{aligned} \tag{9.5}$$

where:

- V_{fib} = fiber volume fraction (ratio of fiber volume to total composite volume),
- E_{fib} and E_{mat}, = axial elastic moduli of the fibers and the matrix, respectively,
- ν_{fib} and ν_{mat} = Poisson's ratios of the fibers and the matrix.

Often, weight fractions of the fibers and matrix are known instead of volume fractions. These are represented as P_{fib} and P_{mat}. Given the densities ρ_{fib} and ρ_{mat} of the fiber and matrix, the volume fraction can be determined using:

$$V_{\text{fib}} = \frac{P_{\text{fib}}/\rho_{\text{fib}}}{P_{\text{fib}}/\rho_{\text{fib}} + P_{\text{mat}}/\rho_{\text{mat}}}, \qquad P_{\text{fib}} + P_{\text{mat}} = 1. \tag{9.6}$$

For example, consider a composite with glass fibers, where the fiber weight fraction is 60%. The properties of the components are shown in Table 9-1.

Table 9-1 – Example of Glass Fiber Reinforced Polymer

	Weight Fraction	Density [g/cm^3]
Fiber	0.60	2.5
Matrix	0.40	1.2

Applying Equation (9.6), the resulting fiber volume fraction for glass fibers is 42%. Finally, knowing the mechanical properties of the fibers (E_{fib} = 80 GPa, ν_{fib} = 0.3) and the matrix (E_{mat} = 3 GPa, ν_{mat} = 0.34), the elastic constants of the composite are calculated as:

$$E_1 = 35.2 \text{ GPa},$$

$$\nu_{12} = 0.32.$$

For further details on micromechanical models, refer to specialized publications.

9.2.1 Effect of Loads Acting in Directions Different from the Material's Symmetry Axes

Once the elastic constants of the material are known, the behavior of the fiber-reinforced composite is entirely determined for any loading direction, regardless of its orientation relative to the material's symmetry axes. These symmetry axes do not necessarily coincide with the symmetry axes of the body or the loading system.

For example, considering the case shown in Figure 9-3, which refers to a unidirectional, continuous-fiber laminate, it is possible to calculate the *equivalent* elastic constants, E_x , E_y , G_{xy} e ν_{xy}, with respect to the reference axes x and **y** of the loading system, which are rotated by an angle θ relative to the material's symmetry axes 1 and 2. These equivalent constants depend on θ and the material's elastic constants E_1, E_2, G_{12}, and ν_{12}.

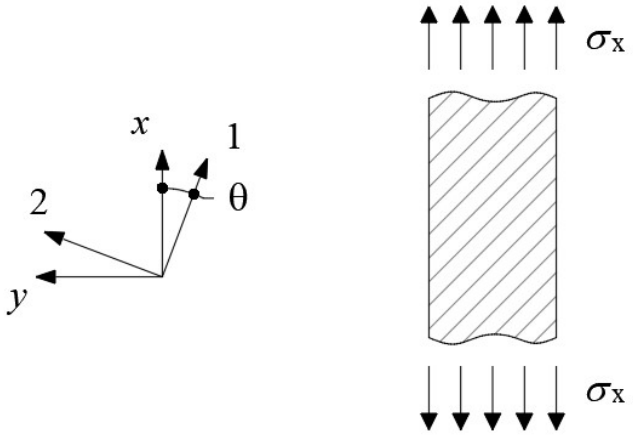

Figure 9-3 – Definition of reference systems x, y, and 1, 2.

Figure 9-4 and Figure 9-5 illustrate the variations of the normal modulus of elasticity E_x and the shear modulus $G_{x\gamma}$ as the fiber orientation angle θ changes relative to the loading direction for different values of E_1.

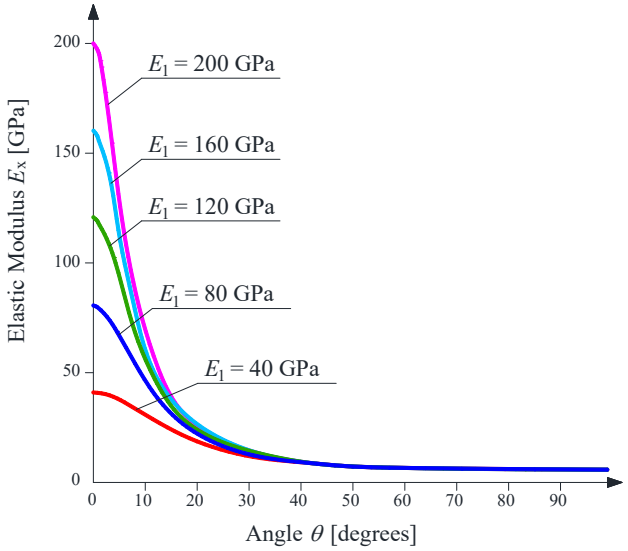

Figure 9-4 – Normal modulus of elasticity E_x as a function of the rotation angle θ *(For fiber-reinforced composites with different values of normal elastic modulus E_1, with E_2 = 5 GPa, G_{12} = 3 GPa, and ν_{12} = 0.35)*.

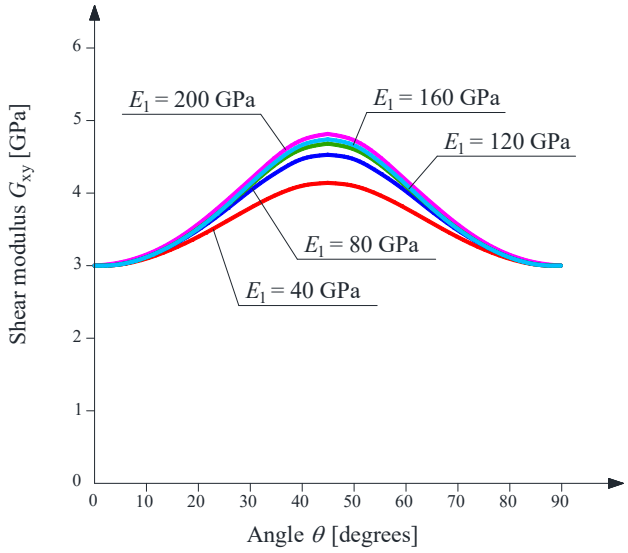

Figure 9-5 – Shear modulus $G_{x\gamma}$ as a function of the rotation angle θ (*For fiber-reinforced composites with different values of normal elastic modulus* E_1, *with* $E_2 = 5$ *GPa,* $G_{12} = 3$ *GPa, and* $\nu_{12} = 0.35$).

Significant variations in the E_x and $G_{x\gamma}$ moduli as a function of θ are clearly evident.

In the case of fabrics, it is necessary to consider that fibers are arranged in two or more directions (multi-axial fabrics). Neglecting the crimping effect of the yarn due to weaving and assuming the fabric consists of two superimposed layers of unidirectional fibers oriented at 90°, the normal modulus of elasticity E_x can be estimated using approximate methods based on the assumption that there is no relative sliding between the layers.

For a balanced plain weave fabric, meaning an equal percentage of fibers in both directions, the variation of E_x as a function of θ is shown in Figure 9-6.

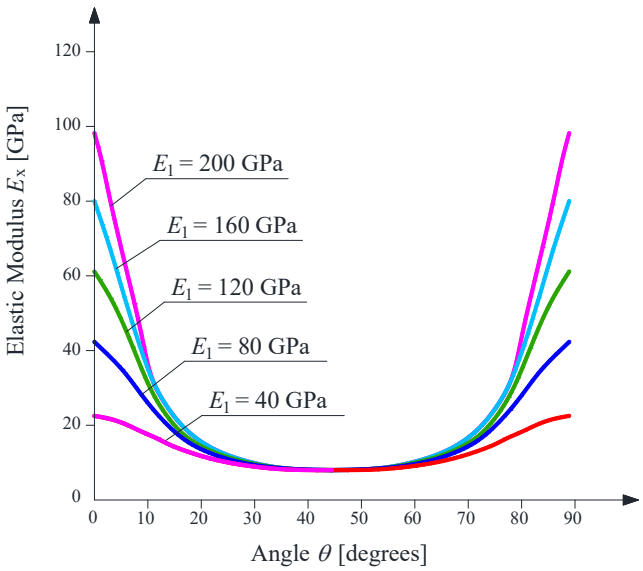

Figure 9-6 – Longitudinal modulus of elasticity E_x as a function of the rotation angle θ for a plain balanced fabric with different values of the principal modulus of elasticity E_1
($E_2 = E_1$; $G_{12} = 3$ GPa; $\nu_{12} = 0.35$)

9.3 FAILURE CRITERIA

The failure behavior of fiber-reinforced composites is a remarkably complex phenomenon at the micromechanical level, as it depends on various factors such as loading type and constituent material properties (fiber, matrix, and interface). For this reason, failure criteria for composite materials are preferably formulated at a macro mechanical scale, assuming material homogeneity. Additionally, a linear elastic behavior up to failure is typically assumed.

In the case of a laminate subjected to a plane stress state, one of the most straightforward failure criteria is the maximum stress criterion.

By denoting:

- $\sigma_{1u,t}$ ($\sigma_{1u,c}$) as the tensile (compressive) failure stress along the fiber direction,
- $\sigma_{2u,t}$ ($\sigma_{2u,c}$), as the tensile (compressive) failure stress perpendicular to the fiber direction
- τ_{12u} as the shear failure stress,

the maximum stress criterion can be analytically expressed as follows:

$$\begin{aligned} \sigma_1 &\quad \begin{cases} \leq \sigma_{1u,t} \text{ per } \sigma_1 > 0, \\ \geq \sigma_{1u,c} \text{ per } \sigma_1 < 0, \end{cases} \\ \sigma_2 &\quad \begin{cases} \leq \sigma_{2u,t} \text{ per } \sigma_2 > 0, \\ \geq \sigma_{2u,c} \text{ per } \sigma_2 < 0, \end{cases} \\ |\tau_{12}| &\quad \leq \quad \tau_{12u}. \end{aligned} \tag{9.7}$$

Observations:

- The criterion is independent of the sign of the shear stress.
- It does not account for interaction effects between different failure modes, meaning they can occur independently of one another.

Referring to the Figure 9-3 scenario, the minimum of the following values gives the maximum allowable stress for the laminate:

$$\sigma_{max} = min\left\{\frac{\sigma_{1u}}{(cos\,\theta)^2}, \frac{\sigma_{2u}}{(sin\,\theta)^2}, \frac{\tau_{12u}}{sin\,\theta\,cos\,\theta}\right\} \tag{9.8}$$

The variation of the maximum stress σ_{max}, is a function of the fiber orientation angle θ is shown in Figure 9-7.

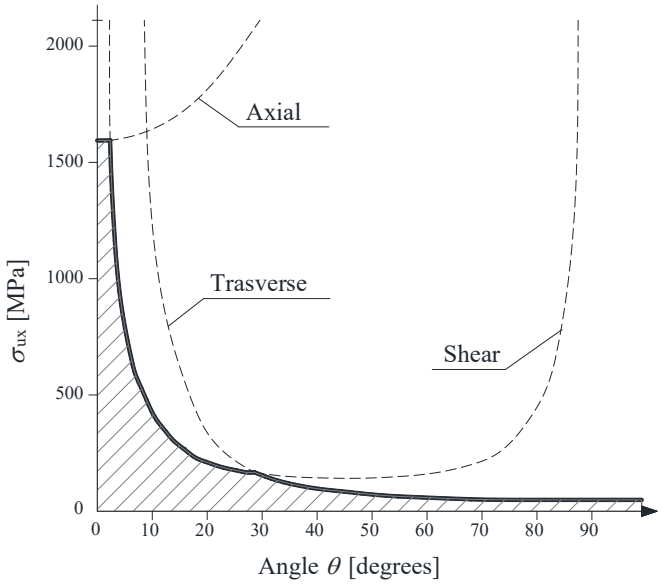

Figure 9-7 – Maximum stress criterion: Tensile failure stress as a function of rotation angle θ (*For a unidirectional laminate with* $\sigma_{1u} = 1600$ *MPa;* $\sigma_{2u} = 40$ *MPa;* $\tau_{12u} = 70$ *MPa*).

In general, the maximum stress criterion aligns reasonably well with experimental data for tensile tests conducted at fiber angles below 15° and above 45°. However, measured compressive strengths tend to be significantly higher than predicted.

A more accurate failure prediction criterion is the Tsai-Hill criterion, which accounts for interactions between stress components. It is expressed as:

$$\left(\frac{\sigma_1}{\sigma_{1u}}\right)^2 + \left(\frac{\sigma_2}{\sigma_{2u}}\right)^2 - \frac{\sigma_1 \cdot \sigma_2}{\sigma_{1u}^2} + \left(\frac{\tau_{12}}{\tau_{12u}}\right)^2 \leq 1 \tag{9.9}$$

With reference to Figure 9-3, the failure stress as a function of angle θ is given by:

$$\sigma_{xu} = \left[\frac{\cos^4\theta}{\sigma_{1u}^2} + \left(\frac{1}{\tau_{12u}^2} - \frac{1}{\sigma_{1u}^2}\right)\cos^2\theta \cdot \sin^2\theta + \frac{\sin^4\theta}{\sigma_{2u}^2}\right]^{-1/2} \tag{9.10}$$

The variation of failure stress as a function of θ is plotted in Figure 9-8.

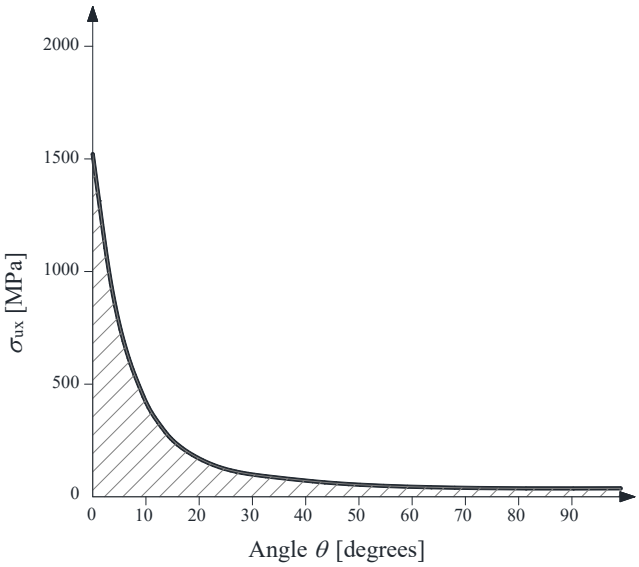

Figure 9-8 – Tsai-Hill criterion: Tensile failure stress as a function of rotation angle θ (*For a unidirectional laminate wit* σ_{1u} *= 1600 MPa;* σ_{2u} *= 40 MPa;* τ_{12u} *= 70 MPa*).

The observations presented highlight the strong variability in the elastic and strength properties of fiber-reinforced composites depending on fiber orientation relative to the loading direction.

10 APPENDIX D (DEBONDING OF EBR AND NSM REINFORCEMENTS FROM THE SUBSTRATE)

10.1 FAILURE MODES DUE TO DEBONDING OF EBR REINFORCEMENTS FROM A CONCRETE SUBSTRATE

The primary failure modes of structural elements reinforced with EBR-type FRP systems due to debonding from the substrate are as follows:

- Mode 1 (End Debonding) (Figure 10-1).
  The terminal zones of the reinforcement, which serve to anchor the composite to the substrate, are subjected to high interfacial shear stresses. Typically, these zones have a length of about 100–200 mm.
  In the specific case of laminate reinforcements, their flexural stiffness may also induce significant tensile stresses perpendicular to the interface (peeling stresses) (Figure 10.2(a)). These stresses can considerably reduce the maximum allowable shear stress, as indicated by the fracture Mode II resistance domain shown in Figure 10-2(b).
  End debonding failure is particularly brittle.

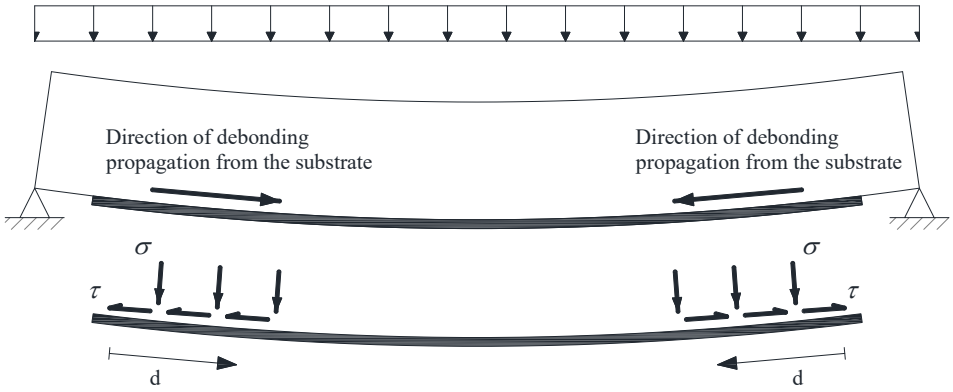

Figure 10-1 – End debonding of the reinforcement.

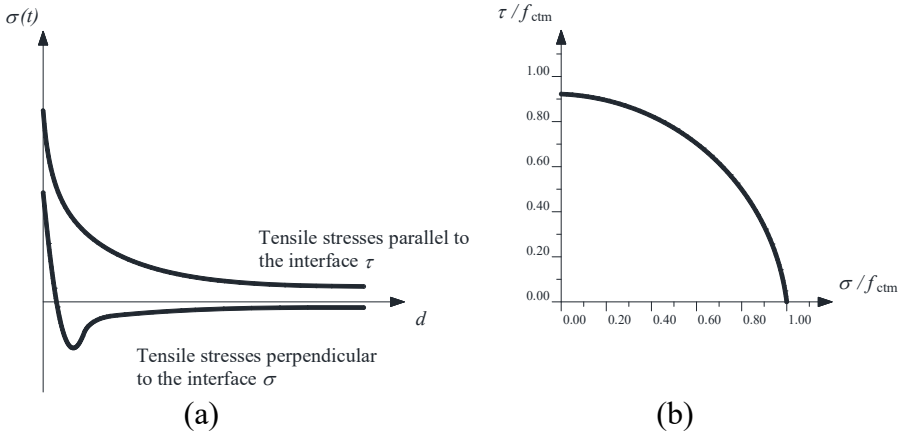

(a) (b)

Figure 10-2 – (a) Concentration of tangential and normal stresses at the interface near the reinforcement end (obtained through an elastic-linear calculation);
(b) Resistance domain in terms of tangential and normal interface stresses.

- Mode 2 (Debonding due to flexural cracks in the beam) (Figure 10-3).
  Discontinuities in the substrate caused by transverse cracks in the tensioned concrete generate stress concentrations at the concrete-FRP interface, which can trigger complete or partial debonding of the reinforcement.
  The cracks may be orthogonal to the beam axis if flexural stress is predominant or inclined in cases of combined flexural and shear stress.

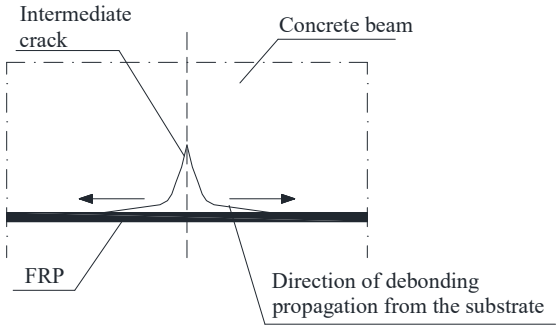

Figure 10-3 – Debonding initiated by transverse cracks in concrete.

- Mode 3 (Debonding due to diagonal shear cracks) (Figure 10-4).
  When shear stress is predominant over flexural stress, a relative displacement occurs between the faces of the inclined cracks. The vertical component of this displacement induces high tensile stresses at the concrete-FRP interface, which may trigger reinforcement debonding.
  Experimental studies have shown that this failure mode occurs even in the presence of stirrups, whether they are working in the elastic or plastic phase.
  This failure mode is typical of four-point bending laboratory tests but is less frequent under distributed transverse loads.
  For beams with low shear reinforcement but heavily strengthened with FRP (e.g., laminates with a width comparable to the beam width), debonding typically initiates at the end section of the reinforcement due to peeling stresses.

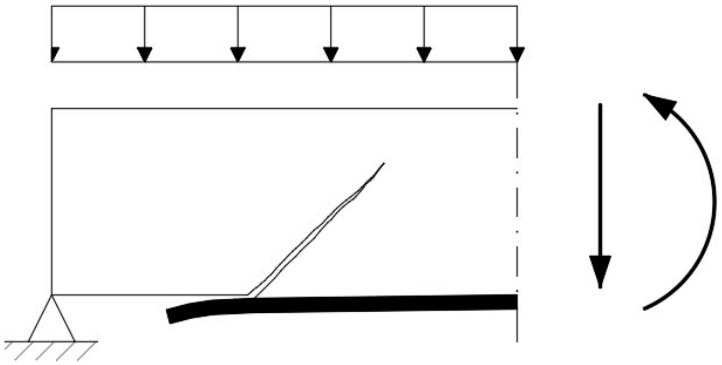

Figure 10-4 – Debonding due to diagonal shear cracks.

- Mode 4 (Debonding due to surface irregularities and roughness of the concrete substrate).
  Localized debonding caused by surface irregularities in the concrete substrate may propagate and lead to the complete detachment of the reinforcement.
  This failure mode can be prevented by applying proper surface treatments before installing the reinforcement and/or using techniques to regularize the surface.

10.2 MODELING THE BOND BEHAVIOR BETWEEN REINFORCEMENT AND CONCRETE FOR EBR SYSTEMS

Below are some additional details on modeling the bond behavior between the reinforcement and concrete for EBR systems and on calculating debonding forces from the substrate.

10.2.1 Bond Behavior

The bond between an EBR-type FRP reinforcement and a concrete substrate can be modeled through a relationship between the tangential stress at the interface (assumed constant across the width, b_f) and the corresponding slip ($\tau - s$ relationship).
This bond behavior depends on both:

- The mechanical properties of the materials in contact.
- The geometry of both the reinforced element and the reinforcement influences the stress distribution phenomenon.

The bond-slip relationship is typically nonlinear, featuring a softening branch. It can be approximated using a bilinear model, as illustrated in Figure 10-5. The graph of this model consists of:

- An initial linear segment, increasing with the slip "s" up to the peak tangential stress at the interface, f_b.
- A descending linear branch reflects progressive damage in the concrete at the interface, leading to complete debonding at the ultimate slip value, s_u, where the tangential stress reaches zero.

At s_u, complete detachment of the reinforcement from the substrate is assumed. The area under the $\tau - s$ curve represents the specific fracture energy, $\Gamma_F = \frac{1}{2} f_b s_u$, associated with "Mode II" debonding of the reinforcement from the substrate.

he peak tangential stress f_b can be assumed equal to the cohesion strength of the substrate:

$$f_b = \frac{\sqrt{f_c \cdot f_t}}{2} \tag{10.1}$$

where:

- f_c = compressive strength of the concrete substrate.
- f_t = tensile strength of the concrete substrate.

The first branch of the bilinear model is determined by considering:

- The deformability of the adhesive layer (typically a millimeter-thick layer).
- The deformability of a superficial concrete layer of appropriate thickness.

In the absence of specific experimental data, the mechanical parameters defining the bilinear τ – s bond relationship can be estimated using the following expressions.

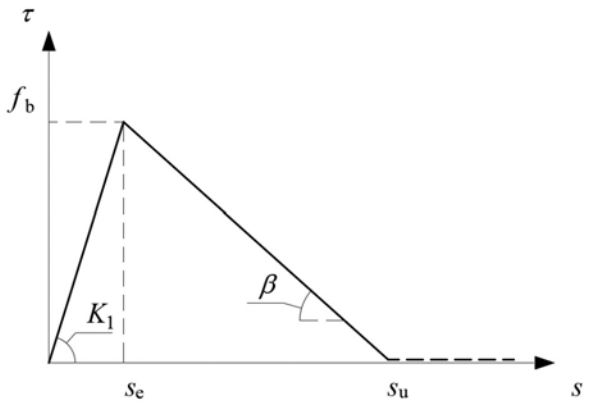

Figure 10-5 – Examples of bond-slip "τ – s" relationship.

Slip at Complete Debonding
The ultimate slip value corresponding to full detachment is widely accepted in the literature and can be estimated as:

$$s_u = 0.25\,\text{mm} \tag{10.2}$$

Initial Stiffness of the Bond-Slip Curve
The slope of the initial linear branch, K_1, can be calculated as:

$$K_1 = \frac{c_1}{t_a/G_a + t_c/G_c} \tag{10.3}$$

where:

- G_a = shear modulus of the adhesive.
- G_c = shear modulus of the concrete.
- t_a = nominal thickness of the adhesive layer.
- t_c = thickness of the concrete layer contributing to the interface deformability (*if experimental data is unavailable, assume* $t_c = 20 \div 30$ mm, $c_1 = 0.5 \div 0.7$).
- c_1 = coefficient ranging from 0.5 to 0.7.

Application in Serviceability Limit State (SLS) Checks
For stress calculations in SLS verifications, the τ – s bond relationship is simplified to include only the initial linear segment. In this case, the slope K_1 is computed using Equation (10.2) with $c_1 = 1$.

10.2.2 Bond-Slip Relationship with a Rigid-Softening Model

The expression for the design value of the optimal anchorage length, adopted in these guidelines, derives from the assumption of a "$\tau - s$" rigid-softening bond-slip relationship ($K_1 \rightarrow \infty$). This assumption is justified at the Ultimate Limit State (ULS) since the extent of the elastic-linear portion is negligible compared to the subsequent softening phase.

Below, we outline the application of this bond-slip model, represented in Figure 10-6, to derive this expression. Furthermore, it will be shown how its use allows for the determination of the maximum force transferable to the FRP reinforcement and thus justifies the expression for the ULS resistance due to end debonding (4.1.3). As illustrated in Figure 10-6, it is assumed that $\beta = \frac{f_{\mathrm{b}}}{s_{\mathrm{u}}}$; therefore, the bond-slip relationship in the softening phase can be expressed as $\tau = \beta \cdot \left(s_u - s\right)$.

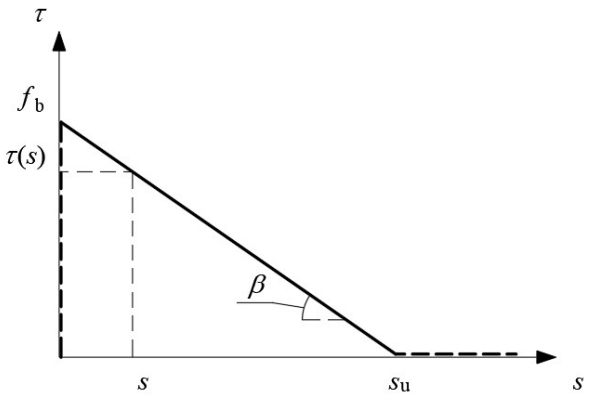

Figure 10-6 – Rigid-Softening Bond-Slip Relationship "$\tau - s$".

o this end, we refer to the simplified scheme in Figure 10-7, where, compared to Figure 4-3, the cantilevered segment of the reinforcement extending beyond the support is omitted as it is irrelevant to the proposed objective. The symbols used are those already introduced in § 4.1.

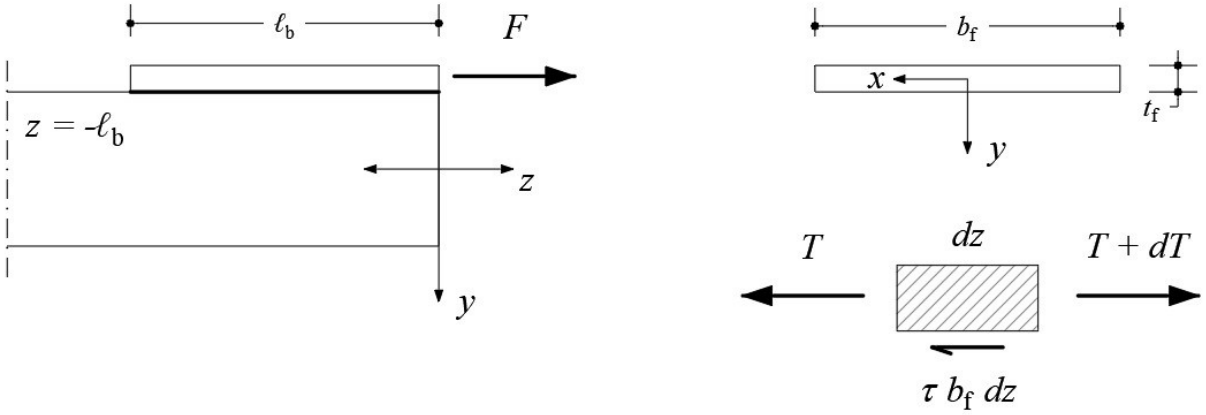

Figure 10-7 – Geometric Parameters for Determining the Optimal Anchorage Length.

t is assumed that the substrate can be considered infinitely rigid relative to the FRP reinforcement so that the strain at the interface is $\frac{ds}{dz} = \varepsilon_{\mathrm{f}}$, where "$s$" is the interface slip previously introduced. The strain ε_f is the axial strain in the reinforcement. Additionally, the cross-section of the FRP reinforcement is assumed to be rigid within its plane, making the equilibrium problem one-dimensional. The analysis of this problem, for which a solution is not always guaranteed, is restricted to cases where the condition $s_{\mathrm{u}} - s \leq 0$, is satisfied at all contact points between the substrate and reinforcement. Under this constraint, which will be justified below, a unique solution to the problem exists.

The governing equations are as follows:

- Differential equation of equilibrium in the z-direction:

$$\frac{dT}{dz} - \tau(s) b_{\mathrm{f}} = 0 \tag{10.4}$$

where T represents the tensile force in the reinforcement at a generic section z, and b_{f} is the width of the FRP reinforcement.

- Compatibility equation:

$$\frac{ds}{dz} = \frac{T}{E_{\mathrm{f}} b_{\mathrm{f}} t_{\mathrm{f}}} \tag{10.5}$$

Substituting the compatibility equation (10.5) into the equilibrium equation (10.4), and considering the bond-slip relationship, we obtain the following second-order differential equation in $s(z)$:

$$\frac{d^2 s}{dz^2} + \omega^2 s - \omega^2 s_{\mathrm{u}} = 0 \tag{10.6}$$

where:

$$\omega^2 = \frac{\beta}{E_{\mathrm{f}} t_{\mathrm{f}}} \tag{10.7}$$

where E_{f} is the elastic modulus of the FRP reinforcement in the longitudinal direction.
The boundary conditions based on the Equation (10.5) are:

$$\begin{aligned} E_{\mathrm{f}} b_{\mathrm{f}} t_{\mathrm{f}} \left.\frac{ds}{dz}\right|_{z=0} &= T(z=0) = F \\ E_{\mathrm{f}} b_{\mathrm{f}} t_{\mathrm{f}} \left.\frac{ds}{dz}\right|_{z=-\ell_{\mathrm{b}}} &= 0 \Leftrightarrow \left.\frac{ds}{dz}\right|_{z=-\ell_{\mathrm{b}}} = 0 \end{aligned} \tag{10.8}$$

where F is the applied force at the reinforcement's end (z = 0).

The equilibrium solution is:

$$s(z) = -\frac{F}{\omega E_{\mathrm{f}} b_{\mathrm{f}} t_{\mathrm{f}}} \frac{1}{\sin(\omega \ell_{\mathrm{b}})} \cos\left(\omega\left(z + \ell_{\mathrm{b}}\right)\right) + s_{\mathrm{u}} \tag{10.9}$$

A condition sufficient to ensure $s_u - s \geq 0$ for each $z \in [-\ell_b, 0]$ is that $\cos(\omega(z+\ell_b)) \geq 0$, which occurs $\omega(z+\ell_b) \leq \frac{\pi}{2}$, or $\ell_b \leq \frac{\pi}{2\omega}$.

The limit bonded length is given by:

$$\ell_e = \frac{\pi}{2\omega} \tag{10.10}$$

This is called the "optimal anchorage length" as for $\ell_b = \ell_e$, we have:

$$s(z) = -\frac{F}{\omega E_f b_f t_f}\cos(\omega(z+\ell_e)) + s_u \tag{10.11}$$

By evaluating the slip at $z = 0$, in Equation (10.9), we obtain that $s(0) = s_u$, which corresponds to $\tau(0) = 0$ and indicates that the bond-slip relationship is fully developed for $l_b = l_e$.
Furthermore, for $z = -l_e$, we also have $\tau(-l_e) = 0$ meaning that the terminal section of the reinforcement does not experience displacement, so from (10.11) we obtain:

$$s_u = \frac{F}{\omega E_f b_f t_f}.$$

Since $s(-l_e) = 0$, from the bond-slip relationship, we obtain $\tau(-l_e) = 0$, which corresponds to the maximum force, F, for which equilibrium is possible and, therefore, represents the maximum force that can be transferred through the bond, and it is equal to:

$$F_{max} = \omega E_f b_f t_f s_u \tag{10.12}$$

For $\ell_b < \ell_e$ and for $z = 0$, substituting $\omega = \frac{\pi}{2\ell_e}$ in equation (10.10), equation (10.11) provides:

$$s(0) = -\frac{F}{\omega E_f b_f t_f}\frac{1}{\sin\left(\frac{\pi}{2}\frac{\ell_b}{\ell_e}\right)}\cos\left(\frac{\pi}{2}\frac{\ell_b}{\ell_e}\right) + s_u \tag{10.13}$$

And therefore, since $s(0) < s_u$, we obtain that $\tau(0) > 0$.

Furthermore, for $z = -\ell_b$, as in the previous case, we must have $s(-\ell_b) = 0$, since the terminal section of the reinforcement does not undergo displacement. Therefore, from the equation (10.9) we obtain: $s_u = \frac{F}{\omega E_f b_f t_f} \cdot \frac{1}{\sin(\omega \ell_b)}$, which means that for $\ell_b < \ell_e$ the maximum force F for which equilibrium is ensured is:

$$F_{\max}\left(\ell_{\mathrm{b}}\right)=\omega E_{\mathrm{f}} b_{\mathrm{f}} t_{\mathrm{f}} s_{\mathrm{u}} \sin\left(\frac{\pi}{2}\frac{\ell_{\mathrm{b}}}{\ell_{\mathrm{e}}}\right)=\sin\left(\frac{\pi}{2}\frac{\ell_{\mathrm{b}}}{\ell_{\mathrm{e}}}\right)F_{\max} \tag{10.14}$$

It can be verified that, since $\frac{\ell_{\mathrm{b}}}{\ell_{\mathrm{e}}}<1$, $F_{\max}(\ell_b)<F_{\max}$ Therefore, the optimal anchorage length, l_{b}, is the minimum length required to ensure the transmission of the maximum bond stress.

10.2.3 Determination of Equations 4.1, 4.4, and 4.5

Starting from equation (10.10) in §10.2.2, squaring both sides results in:

$$\ell_{\mathrm{e}}{}^{2}=\left(\frac{\pi}{2}\right)^{2}\frac{1}{\omega^{2}}=\left(\frac{\pi}{2}\right)^{2}\frac{E_{\mathrm{f}} t_{\mathrm{f}}}{\beta}=\left(\frac{\pi}{2}\right)^{2}\frac{E_{\mathrm{f}} t_{\mathrm{f}} s_{\mathrm{u}}}{f_{\mathrm{b}}}=\left(\frac{\pi}{2}\right)^{2}\frac{E_{\mathrm{f}} t_{\mathrm{f}} f_{\mathrm{b}} s_{\mathrm{u}}}{f_{\mathrm{b}}{}^{2}} \tag{10.15}$$

from which it follows:

$$\ell_{\mathrm{e}}=\frac{1}{f_{\mathrm{b}}}\sqrt{\frac{\pi^{2}}{4}E_{\mathrm{f}} t_{\mathrm{f}} f_{\mathrm{b}} s_{\mathrm{u}}}=\frac{1}{f_{\mathrm{b}}}\sqrt{\frac{\pi^{2}}{2}E_{\mathrm{f}} \Gamma_{\mathrm{F}} t_{\mathrm{f}}} \tag{10.16}$$

where $\Gamma_{\mathrm{F}}=\frac{1}{2}f_{\mathrm{b}} s_{\mathrm{u}}$.

Additionally, considering the equation (10.7), we have:

$$\omega^{2}=\frac{\beta}{E_{\mathrm{f}} t_{\mathrm{f}}}\Rightarrow \omega E_{\mathrm{f}} t_{\mathrm{f}}=\frac{\beta}{\omega} \tag{10.17}$$

Thus, considering the equation (10.12), it follows that:

$$F_{\max}=\frac{\beta}{\omega}b_{\mathrm{f}} s_{\mathrm{u}}=\frac{f_{\mathrm{b}} b_{\mathrm{f}}}{\omega} \tag{10.18}$$

or, equivalently, using equation (10.10):

$$F_{\max}=\frac{2}{\pi}f_{\mathrm{b}} b_{\mathrm{f}} \ell_{\mathrm{e}} \tag{10.19}$$

Ultimately, using the equation (10.16); we obtain:

$$F_{\max}=b_{\mathrm{f}}\sqrt{E_{\mathrm{f}} t_{\mathrm{f}} f_{\mathrm{b}} s_{\mathrm{u}}}=b_{\mathrm{f}}\sqrt{2E_{\mathrm{f}} \Gamma_{\mathrm{F}} t_{\mathrm{f}}} \tag{10.20}$$

where, as previously noted, $\Gamma_F = \frac{1}{2} f_b s_u$.

Equations (10.16) and (10.20) allow for the direct derivation of equations (4.1), (4.4) and (4.5), introducing the appropriate partial material factors (FC, γ_{f2}) and correction coefficients (k_G, k_b). Additionally, as can be easily verified, the equation (4.11) represents a good parabolic approximation of (10.14), which is more practical for technical applications.

10.2.4 Calibration of the k_G coefficient

Based on numerous experimental data available in national and international literature concerning bond tests of various FRP strengthening systems applied to concrete substrates, it was deemed appropriate, compared to the R1 version of the Guidelines, to introduce a new calibration of equation (10.20). This was achieved by incorporating the k_G coefficient, which allows obtaining both the mean and characteristic values of the specific fracture energy Γ, as defined in 10.2.1.
The experimental database includes results from composite-to-concrete bond tests conducted as part of Task WP1—Polymer Matrix Composites (FRP) of the ReLUIS-DPC 2019-2021 Project. The mean and characteristic values of the k_G coefficient were calibrated by comparing the collected experimental data following the approach suggested in EN1990 - Annex D (Design assisted by testing).
The experimental database comprises 280 bond tests for in situ-impregnated composites (glass and carbon fiber fabrics, as well as steel micro-strands) and 100 bond tests for preformed composites (carbon fiber laminates). The main characteristics of the tested specimens fall within the following ranges:

For in situ-impregnated composite systems

- Mean compressive strength of concrete: f_{cm} = 14.6-70.0 MPa;
- Elastic modulus of FRP reinforcements: E_f = 73-409 GPa;
- Thickness of FRP reinforcement: t_f = 0.083-0.600 mm (1 to 3 reinforcement layers);
- Width ratio of FRP reinforcement to concrete element: b_f/b = 0.20-1.00;
- Width of FRP reinforcement: b_f = 30-150 mm;
- Bonded length of FRP reinforcement: ℓ_b = 85 – 500 mm.

For preformed composite systems

- Mean compressive strength of concrete: f_{cm} = 15.0-66.0 MPa;
- Elastic modulus of FRP reinforcements: E_f = 150-400 GPa;
- Thickness of FRP reinforcement: t_f = 1.2-1.6 mm (1 reinforcement layer);
- Width ratio of FRP reinforcement to concrete element: b_f/b = 0.15-1.00;
- Width of FRP reinforcement: b_f = 50-100 mm;
- Bonded length of FRP reinforcement: ℓ_b = 150 – 400 mm.

The calibration procedure was carried out separately for preformed composites (§ 2.2.2) and in situ-impregnated composites (§2.2.3), yielding the following results:

- **For preformed composites:**
  - Mean value: k_{Gm} = 0.80
  - Characteristic value (5% fractile): k_{Gk} = 0.35.
- For in situ-impregnated composites:
  - Mean value: k_{Gm} = 1.25
  - Characteristic value (5% fractile):k_{Gk} = 0.60.

In Figure 10-8, the experimental values of the debonding force, extracted from the extensive bond test database used for calibrating the k_G coefficient, are compared with the design values of the debonding force obtained from the following equation (10.21):

$$F_{\mathrm{max,d}} = \frac{k_{\mathrm{b}} \cdot b_{\mathrm{f}}}{\gamma_{\mathrm{f2}}} \sqrt{2 E_{\mathrm{f}} t_{\mathrm{f}} \Gamma_{\mathrm{Fk}}} \tag{10.21}$$

where:

$$\Gamma_{\mathrm{Fk}} = \frac{1}{2} f_{bk} \cdot s_{\mathrm{u}} = \frac{k_{\mathrm{Gk}}}{4} \frac{\sqrt{f_{\mathrm{cm}} f_{\mathrm{ctm}}}}{FC} \cdot s_{\mathrm{u}} \tag{10.22}$$

In cases where the mean tensile strength of the concrete substrate, f_{ctm}, was unavailable, it was calculated following the guidelines of the current regulations. The values $FC = 1$ and $\gamma_{\mathrm{f2}} = 1.3$ were assumed, and the ultimate slip of the interface bond was taken as $s_{\mathrm{u}} = 0.25$ mm.
For real applications, FC represents the confidence factor associated with the level of knowledge of the substrate to which the reinforcement is applied and should be evaluated according to validated standards.

In Figure 10-8, the experimental values of the maximum delamination force are also compared with the characteristic and mean debonding force values, calculated using the following formulations:

$$F_{\mathrm{max},k} = k_{\mathrm{b}} \cdot b_{\mathrm{f}} \cdot \sqrt{2 E_{\mathrm{f}} t_{\mathrm{f}} \Gamma_{\mathrm{Fk}}} \tag{10.23}$$

$$F_{\mathrm{max,m}} = k_{\mathrm{b}} \cdot b_{\mathrm{f}} \cdot \sqrt{2 E_{\mathrm{f}} t_{\mathrm{f}} \Gamma_{\mathrm{Fm}}} \tag{10.24}$$

where:

$$\Gamma_{\mathrm{Fm}} = \frac{1}{2} f_{\mathrm{bm}} s_{\mathrm{u}} = \frac{k_{\mathrm{Gm}} s_{\mathrm{u}}}{4} \frac{\sqrt{f_{\mathrm{cm}} f_{\mathrm{ctm}}}}{FC} \tag{10.25}$$

considering the same assumptions as in equations (10.21) and (10.22).

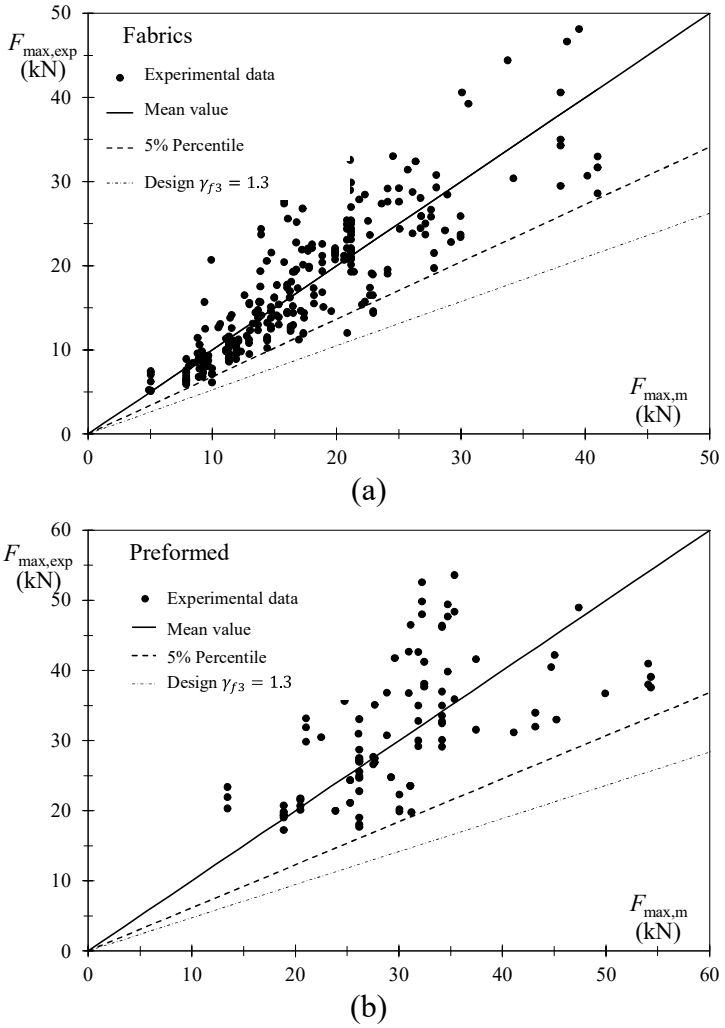

Figure 10-8 – Experimental calibration results of mean, characteristic, and design values of F_{max} for concrete substrates: (a) In situ-impregnated composites (b) Preformed composites.

10.2.5 Bond Failure Resistance at Flexural Cracks

The calibration of the mean and characteristic values of the coefficient $k_{G,2}$ in equation (4.12) was also conducted based on a statistical analysis of numerous experimental results available in national and international literature. These results pertain to reinforced concrete beams and slabs strengthened with FRP laminates or fabrics that failed due to intermediate debonding (Mode 2 failure).

As in previous cases, the calibration procedure followed the approach suggested in EN1990 – Annex D (Design assisted by testing), considering the mechanical properties of materials as random variables.

The statistical analysis of the results provided:

- A mean value of $k_{G,2}$ = 5.1
- A 5% fractile characteristic value of 1.6
- These values were found to be independent of the type of reinforcement.

The introduction of the additional correction coefficient k_q is justified based on experimental test results and numerical analyses, which distinguish between:

- Distributed loading conditions (k_q = 1.25)
- Concentrated loading conditions (k_q = 1.00)

This distinction accounts for the evident beneficial effect of distributed loading compared to concentrated loading.

The value $k_q = 1.25$ represents a conservative choice, given the limited number of available experimental tests on distributed loading conditions.

10.3 MODELING THE BOND BEHAVIOR BETWEEN EBR REINFORCEMENT AND MASONRY

Similar considerations to those already presented in this Appendix for concrete substrates apply to masonry substrates. Therefore, only details on the calibration of the coefficient k_G for different masonry supports are provided.

10.3.1 Calibration of the Coefficient k_G

Based on numerous experimental data available in national and international literature, which include bond tests of various FRP reinforcement systems applied to different masonry substrates (brickwork and natural stone blocks), it was deemed appropriate to conduct a new calibration of the coefficient k_G. his coefficient allows for obtaining the mean and characteristic values of the specific fracture energy (as defined in 10.2.1), with specific adjustments for different masonry materials.

For natural stone masonry, the availability of a significant number of experimental results allowed for separate calibrations of the coefficient k_G for three different types of stone:

- Campanian tuff
- Sicilian calcarenite
- Lecce stone

A portion of the experimental database includes the results of composite-to-concrete bond tests conducted as part of Task WP1—Fiber-Reinforced Polymer (FRP) Composites within the ReLUIS-DPC 2019-2021 Project. The calibration of the mean and characteristic values of k_G was performed by comparing experimental data, following the approach suggested in EN1990 - Annex D (Design assisted by testing).

The calibration procedure was conducted only for in-situ impregnated composites (§ 2.2.3) since there are no experimental bond test data available for preformed composites applied to masonry substrates.

The compressive strength ranges of the bricks and natural stone blocks used in the bond tests for the calibration are:

- Brick masonry (377 tests): 12.0-30.0 MPa
- Campanian tuff blocks (39 tests): 2.0-6.0 MPa
- Sicilian calcarenite blocks (68 tests): 2.0-11.0 MPa
- Lecce stone blocks (35 tests): 21.0-31.0 MPa

The calibration results for the coefficient k_G are as follows:

- Brick masonry:
  - Mean value: $k_{Gm} = 0.40$
  - Characteristic value (5% fractile): $k_{Gk} = 0.15$

- Campanian tuff blocks:
  - Mean value: $k_{Gm} = 1.30$
  - Characteristic value (5% fractile): $k_{Gk} = 0.6$
- Lecce stone blocks:
  - Mean value: $k_{Gm} = 0.24$
  - Characteristic value (5% fractile): $k_{Gk} = 0.12$
- Sicilian calcarenite blocks:
  - Mean value: $k_{Gm} = 0.73$
  - Characteristic value (5% fractile): $k_{Gk} = 0.38$

For masonry types different from those listed above, appropriate experimental tests should be conducted using statistically valid procedures in accordance with EN1990 – Annex D (Design assisted by testing).

In Figure 10-9, he experimental bond strength values obtained from the adhesion tests used for calibrating the coefficient k_G (distinguished by brick masonry and natural stone supports such as Campanian tuff, Sicilian calcarenite, and Lecce stone) are compared with the design bond strength values calculated using the following equation (10.26).

$$F_{max,d} = \frac{k_b b_f}{\gamma_{f2}} \cdot \sqrt{2 E_f t_f \Gamma_{Fk}} \quad \text{with} \quad \Gamma_{Fk} = \frac{1}{2} f_{bk} s_u = \frac{k_{Gk}}{4} \frac{\sqrt{f_{bcm} f_{btm}}}{FC} \cdot s_u \tag{10.26}$$

where:

- The confidence factor is assumed as $FC = 1$
- The partial material safety factor is $\gamma_{f2} = 1.3$
- The mean tensile strength of the masonry substrate f_{btm}, if unavailable, was calculated as:
$$f_{btm} = 0.10 f_{bcm}$$
- The mean compressive strength of the masonry substrate, f_{bcm}, was assumed to be the experimentally measured compressive strength of the brick or stone block as provided by the researchers.

The ultimate slip, s_u, of the bond interface in Equation (10.26) is differentiated based on the type of masonry substrate as follows:

- Brick masonry: $s_u = 0.40$ mm;
- Campanian tuff blocks: $s_u = 0.40$ mm;
- Lecce stone blocks: $s_u = 0.30$ mm;
- Sicilian calcarenite blocks: $s_u = 0.30$ mm.

In Figure 10-9, the experimental maximum delamination force values are also compared with the characteristic and mean values of the bond strength, calculated using the following equations, assuming FC = 1 and the previously mentioned ultimate slip values (s_u):

$$F_{max,k} = k_b b_f \sqrt{2 E_f t_f \Gamma_{Fk}} \tag{10.27}$$

$$F_{max,m} = k_b b_f \sqrt{2 E_f t_f \Gamma_{Fm}} \tag{10.28}$$

where:

$$\Gamma_{\mathrm{Fm}} = \frac{1}{2} f_{\mathrm{bm}} s_{\mathrm{u}} = \frac{k_{\mathrm{Gm}} s_{\mathrm{u}}}{4} \cdot \frac{\sqrt{f_{\mathrm{bcm}} f_{\mathrm{btm}}}}{FC} \tag{10.29}$$

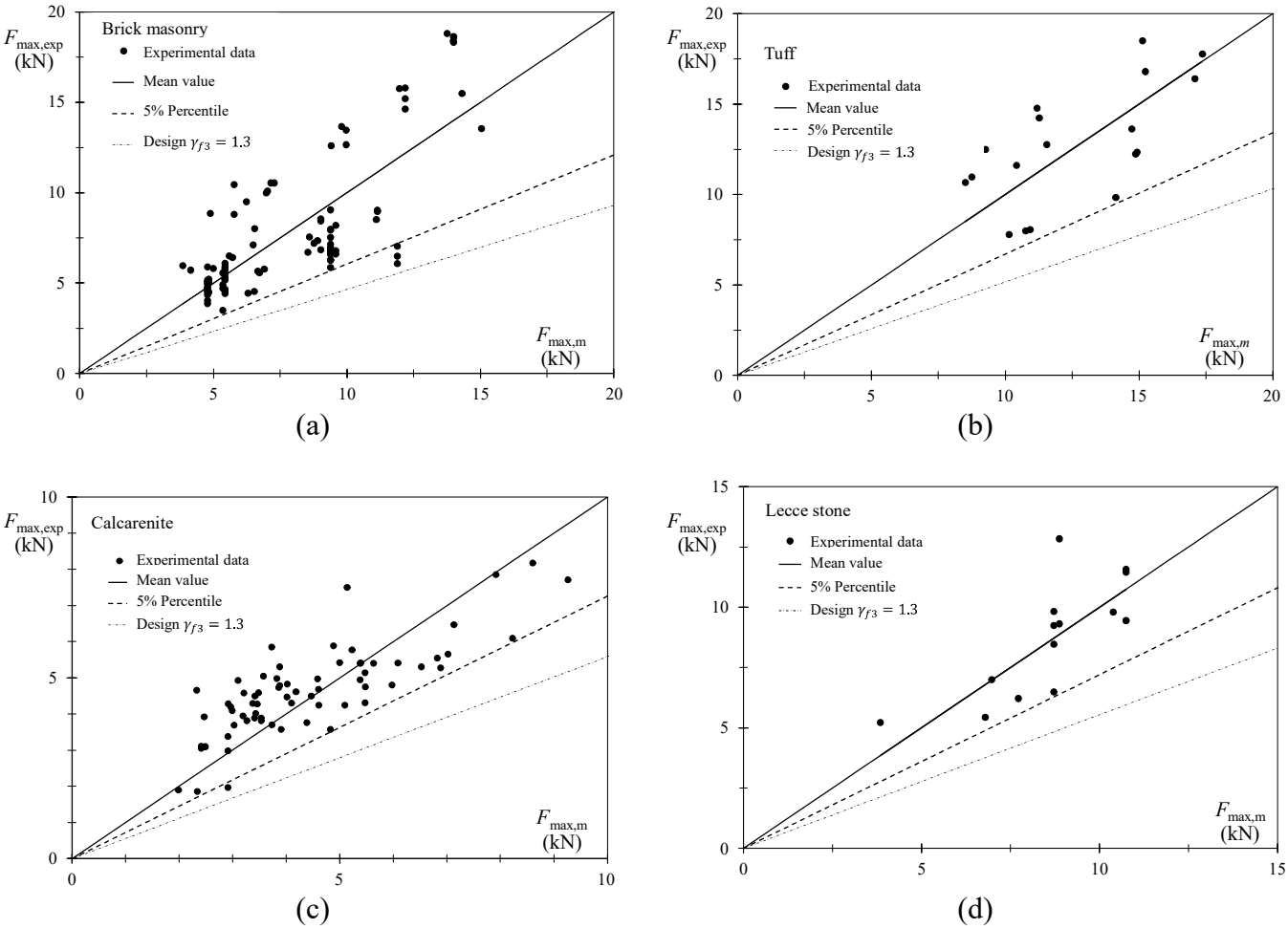

Figure 10-9 – Experimental calibration results for mean, characteristic, and design values of the maximum bond force (F_{max}) for masonry substrates: (a) Brick masonry, (b) Campanian tuff, (c) Sicilian calcarenite, (d) Lecce stone.

10.4 MODELING THE BOND BEHAVIOR BETWEEN NSM REINFORCEMENT AND CONCRETE OR MASONRY

10.4.1 Introduction

Below, a simple mechanical model is presented to evaluate the bond failure resistance of FRP reinforcements in the form of bars or strips embedded in grooves (NSM FRP reinforcement). This model is a generalization of the rigid-softening model presented earlier in Appendix 10 for FRP reinforcement applied using the EBR technique.

To this end, the equilibrium problem depicted in Figure 10-10 is analyzed concerning the determination of the maximum force that can be transmitted by an FRP reinforcement embedded in a groove of dimensions w_{G} and d_{G} within a prismatic solid.

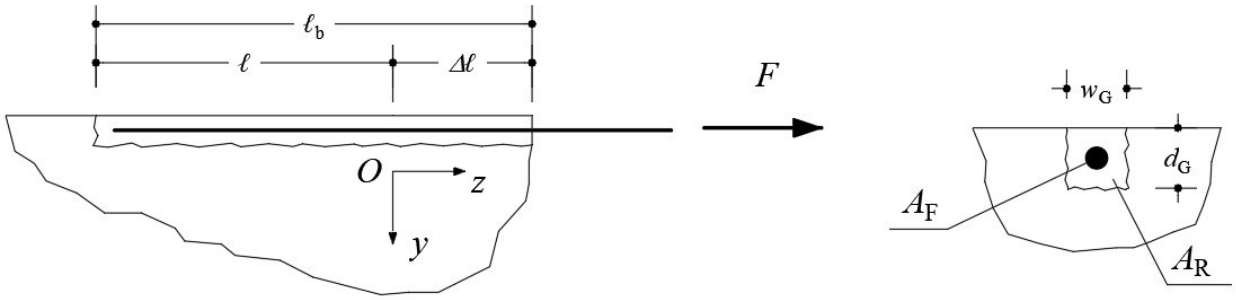

Figure 10-10 – Geometry of an FRP element embedded in a groove.

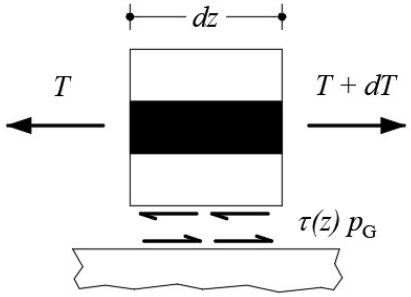

Figure 10-11 – Equilibrium problem of an FRP element embedded in a groove.

It is assumed that the substrate is infinitely rigid compared to the FRP reinforcement.

Let E_F e the longitudinal elastic modulus of the fiber and E_R the modulus of the resin; both assumed constant along the longitudinal axis of the reinforcement. The cross-section of the strip is assumed to be rigid within its plane, so the examined equilibrium problem is one-dimensional. The following homogenized quantities are introduced:

$$A_H = A_F + A_R = w_G d_G \quad , \quad p_G = 2d_G + w_G \quad , \quad E_H = \frac{E_F A_F + E_R A_R}{A_H} \tag{10.30}$$

where w_G and d_G are the dimensions defined in Figure 10-10.

A bilinear bond model is assumed, characterized by:

- A peak bond stress f_b, followed by
- A constant frictional branch, identified by the residual bond strength f_{bR} and the maximum slip smax, as illustrated in Figure 10-12.

Here, s and τ denote the slip of the reinforcement and the tangential stress at the reinforcement-substrate interface, respectively.

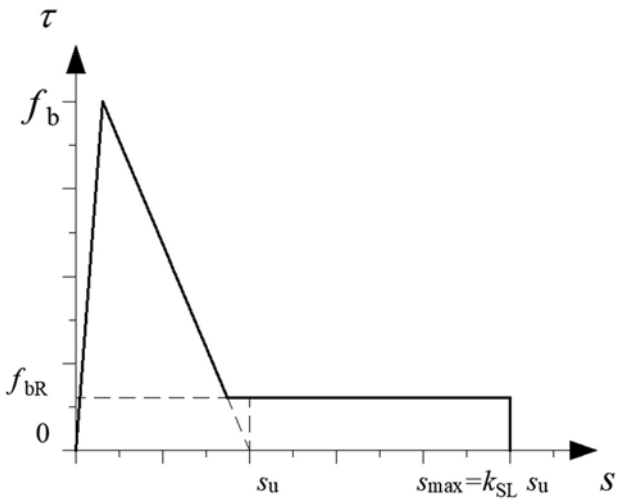

Figure 10-12 – Bond-slip model with residual friction.

For technical purposes, similar to the FRP EBR systems, the rising branch of the bilinear law can be neglected, reducing it to the softening branch only.

This softening branch extends until its intersection s_u with the slip axis, followed by a constant frictional branch for slip values between s_u and s_{max}, where $s_{max} = k_{SL} \cdot s_u$, as represented in Figure 10-13.

This bond-slip model introduces a first-order discontinuity at the abscissa s_u. However, as will be shown later, this simplification enables the efficient analysis of NSM reinforcements, leveraging results already presented in Appendix 10 for EBR FRP reinforcements when studied using a rigid-softening bond-slip model without the frictional branch.

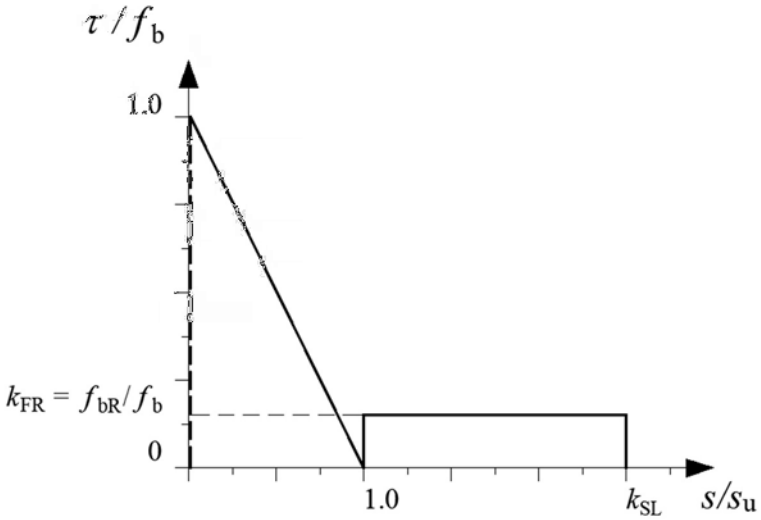

Figure 10-13 – Rigid-softening bond-slip model with residual friction.

Analytical Representation of the Bond-Slip Model

In analytical terms, the adopted bond-slip model is described by the following equations:

- For the rigid-softening branch

$$\tau = \beta(s_u - s) \qquad \forall s \in [0, s_u] \tag{10.31}$$

- For the frictional branch

$$\tau = f_{bR} = k_{FR} f_b \qquad \forall s \in [s_u, s_{max}] \tag{10.32}$$

- For slip beyond the maximum value

$$\tau = 0 \qquad \forall s > s_{max} = k_{SL} s_u \tag{10.33}$$

It is noteworthy that the parameter $\beta = f_b / s_u$ has the dimensions of a force per unit cubic length.

Numerous experimental tests and numerical studies have demonstrated that this bond-slip model is particularly suitable for modeling the bond failure behavior of NSM FRP reinforcements.

The peak bond stress f_b can be assumed to be equal to the substrate's cohesion, given by:

$$f_b = \frac{\sqrt{f_c \cdot f_t}}{2} \tag{10.34}$$

where f_c and f_t, are the compressive and tensile strengths of the substrate, respectively.

10.4.2 The Equilibrium Problem

To study the ultimate limit state, it is convenient to assume that the origin of the reference system is at point O, where the slip exhibited by the reinforcement equals the previously defined value, s_u. This condition identifies the length $\ell_b = \ell + \Delta\ell$ **.** This assumption is certainly valid if the problem admits a solution, ℓ_b, at equilibrium at the SLU. In the following discussion, a method to identify this origin will be presented.

With this premise, the problem is governed by the following field equations, explicitly formulated for the two sections of the reinforcement, corresponding respectively to the intervals $[-\ell, 0]$ and $[0, \Delta\ell]$.

The symbol T denotes the current tensile force in the reinforcement, which varies along the length with the slip s.

To distinguish quantities related to these two intervals, the subscripts 1 and 2 are used, respectively.

For Section 1 (Problem "1", valid for $z \in [-\ell, 0]$), the field equations are:

$$\frac{dT_1}{dz} - \tau p_G = 0 \text{ (Equilibrium Equation)} \tag{10.35}$$

$$\frac{ds_1}{dz} - \frac{T_1}{E_H A_H} = 0 \text{ (Congruence Equation)} \tag{10.36}$$

$$\tau = \beta(s_u - s_1) \text{ (Bond-Slip Equation for the Softening Branch)} \tag{10.37}$$

where:

- The product $E_H A_H$ represents the homogenized axial stiffness of the reinforcement.
- The parameter p_G indicates the perimeter of the groove, which also corresponds to the interface surface between the structural element and the reinforcement, referred to per unit length.

By applying simple transformations, the equations reduce to the following second-order equilibrium differential equation, with s_1 as the unknown:

$$\frac{d^2 s_1}{dz^2} - \frac{f_b p_G}{E_H A_H s_u}\left(s_u - s_1\right) = 0 \tag{10.38}$$

Or, introducing an analogy with the Equation (10.7) (already assumed for FRP EBR reinforcements):

$$\omega^2 = \frac{f_b p_G}{E_H A_H s_u} = \frac{\beta p_G}{E_H A_H} \tag{10.39}$$

$$\frac{d^2 s_1}{dz^2} + \omega^2 s_1 - \omega^2 s_u = 0 \tag{10.40}$$

Equation (10.40) is analogous to Equation (10.6), which is valid for EBR FRP reinforcements.

For Section 2 (Problem "2", valid for $z \in [0, \Delta\ell]$), the field equations are:

$$\frac{dT_e}{dz} - \tau p_G = 0 \text{ (Equilibrium Equation)} \tag{10.41}$$

$$\frac{ds_2}{dz} - \frac{T_2}{E_H A_H} = 0 \text{ (Congruence Equation)} \tag{10.42}$$

$$\tau = f_{br} = k_{FR} f_b \text{ (Equation for the Friction Branch)} \tag{10.43}$$

By applying simple transformations, the equations reduce to the following equilibrium differential equation, with s_2 as the unknown:

$$\frac{d^2 s_2}{dz^2} - \frac{k_{FR} f_b \cdot p_G}{E_H A_H} = 0 \tag{10.44}$$

10.4.3 Discussion of equilibrium problem “1”

For the discussion of equilibrium problem "1," it is possible to refer to the reasoning already presented in Appendix 10 regarding the end debonding of an EBR reinforcement when a rigid-softening bond model is used.

It has been demonstrated how this leads to the definition of the so-called optimal anchorage length, which is now applied to NSM FRP reinforcements by replacing the term ω^2 with the equation (10.39):

$$\ell_{e1} = \frac{\pi}{2\omega} = \frac{1}{f_b}\sqrt{\frac{\pi^2 E_H A_H \Gamma_{F_1}}{2 p_G}} = \frac{\pi}{2}\sqrt{\frac{E_H A_H s_u}{f_b p_G}} \tag{10.45}$$

In this case, the fracture energy, corresponding to the area under the rigid-softening segment of the bond-slip relationship, is defined as follows:

$$\Gamma_{F1} = \frac{f_b \cdot s_u}{2} \tag{10.46}$$

By assigning to ℓ_{e1} the length ℓ of the first segment of the reinforcement, thus assuming $\ell_b \geq \ell_{e1}$ in

Figure 10-10, the following two conditions are satisfied at section z = 0 (point O, origin of the reference system):

i) $s_1(z=0)=s_u$;

ii) The maximum tensile force, $F_{1,max} = T_1(\ell_{e1})$, that the reinforcement can resist while respecting the bond-slip relationship given by the equation (10.31) in segment 1 $z \in [-\ell_{e1}, 0]$ is reached and can be expressed as follows:

$$T_1(\ell_{e1}) = F_{1,\max} = \sqrt{2\,p_G E_H A_H \Gamma_{F1}} = \sqrt{E_H A_H p_G f_b s_u} \tag{10.47}$$

where the expression (10.46) for fracture energy, Γ_{F1}, has been considered. Equation (10.47), in fact, was obtained similarly to (10.20) by adopting the perimeter of the groove, p_g instead of b_f, and replacing the cross-sectional area and elastic modulus of the FRP EBR reinforcement fibers with the homogenized parameters E_H and A_H, defined in equations (10.30).

The condition $\ell = \ell_{e1}$ therefore allows for the immediate identification of point O with the required property: point O is located at a distance ℓ_{e1} from the opposite edge of the reinforcement where the force F is applied.

10.4.4 Discussion of Equilibrium Problem "2"

The existence of an additional reinforcement segment of length $\Delta\ell$, exceeding the length ℓ_{e1}, indicates that the reinforcement can transfer a force to the substrate greater than the maximum tensile force**,** F_1, that can be sustained by the segment of length ℓ_{e1}.
To determine the maximum increase in the transferable force and the length of the additional segment, $\Delta\ell_{e,max}$, at which the maximum transferable force is reached, it is necessary to solve equilibrium problem "2", defined in the interval $0 \le z \le \Delta\ell_e$.

The solution of equation (10.44) is easily derived as::

$$s_2(z) = \frac{1}{2}\frac{k_{FR} f_b \cdot p_G}{E_H A_H} z^2 + Cz + D \tag{10.48}$$

where *C* and *D* are integration constants to be determined using the boundary conditions. These conditions include both kinematic and static constraints and must be imposed at coordinate *z* = 0:

$$s_2(0) = s_u \qquad \Rightarrow \; D = s_u \tag{10.49}$$

$$E_H A_H \left.\frac{ds_2}{dz}\right|_{z=0} = T_2(z=0) = F_{1,\max} \;\Rightarrow\; C = \frac{F_{1,\max}}{E_H A_H} \tag{10.50}$$

Ultimately, the particular integral of the equation (10.44) that satisfies both the kinematic and static boundary conditions is:

$$s_2(z) = \frac{1}{2}\frac{k_{FR} f_b \cdot p_G}{E_H A_H} z^2 + \frac{F_{1,\max}}{E_H A_H} z + s_u \tag{10.51}$$

Equation (10.51) is valid as long as the slip s_2 does not reach the maximum slip s_{max} defined by the

bond-slip model. For $s_2 = s_{\max}$, equation (10.51) provides the following equation to compute the maximum value for $\Delta\ell_e$, $\Delta\ell_{e,\max}$:

$$s_2\left(\Delta\ell_{e,\max}\right) = s_{\max} = \frac{1}{2}\frac{k_{FR} f_b \cdot p_G}{E_H A_H}\Delta\ell_{e,\max}^2 + \frac{F_{1,\max}}{E_H A_H}\Delta\ell_{e,\max} + s_u \tag{10.52}$$

Equation (10.52) is a second-degree algebraic equation that has one negative and one positive root, with only the positive root being physically meaningful. The positive root provides the upper limit for $\Delta\ell_e$; and it is also the root with the smallest absolute value. It is given by:

$$\Delta\ell_{e,\max} = \frac{-F_1 + \sqrt{F_1^2 + 2k_{FR} f_b \cdot p_G E_H A_H (s_{\max} - s_u)}}{k_{FR} f_b \cdot p_G} \tag{10.53}$$

A more compact form of the equation (10.53) can be obtained by introducing the notation $s_{\max} = k_{SL} s_u$, and recalling the value of $F_{1,\max}$ in equation (10.47):

$$\Delta\ell_{e,\max} = \frac{F_{1,\max}}{k_{FR} f_b p_G}\left[\sqrt{1 + 2k_{FR} \cdot (k_{SL} - 1)} - 1\right] \tag{10.54}$$

Ultimately, the maximum force, $F_{2,\max}$, that a reinforcement of length, $\ell_{e2} = \ell_{e1} + \Delta\ell_{e,\max}$ can transfer to the substrate can be estimated using the equation (10.42) evaluated at $z = \Delta\ell_{e,\max}$, where $\Delta\ell_{e,\max}$ is given by equation (10.54):

$$E_H A_H \left.\frac{ds_2}{dz}\right|_{z=\Delta\ell_{e,\max}} = T_2(z = \Delta\ell_{e,\max}) = F_{2,\max} = F_{1,\max} + k_{FR} f_b p_G \cdot \Delta\ell_{e,\max} \tag{10.55}$$

$$\begin{aligned} F_{2,\max} &= F_{1,\max} + k_{FR} f_b p_G \cdot \left(\frac{F_{1,\max}}{k_{FR} f_b p_G}\left[\sqrt{1 + 2k_{FR} \cdot (k_{SL} - 1)} - 1\right]\right) \\ F_{2,\max} &= F_{1,\max} \cdot \sqrt{1 + 2k_{FR} \cdot (k_{SL} - 1)} \end{aligned} \tag{10.56}$$

Equation (10.58) explicitly highlights the frictional contribution to the maximum force that the NSM reinforcement can transfer to the substrate.

10.4.4.1 Evaluation of the Debonding Force for $\ell_{e1} < \ell_b < \ell_{e2}$

Equations (10.54) allow for a closed-form evaluation of the debonding force when the bonding length is equal to ℓ_{e2} that is, equal to the sum of length ℓ_{e1} plus an additional segment of maximum length $\Delta\ell_{e,\max}$. The length ℓ_{e2} is therefore the minimum necessary for the FRP-NSM reinforcement to transmit the maximum debonding force, and by analogy, it takes on the role of "optimal anchorage length" for an FRP-NSM reinforcement.

If the additional segment has a smaller length, $\Delta\ell_e < \Delta\ell_{e,\max}$, and hence, $\ell_{e1} < \ell_b = \ell_{e1} + \Delta l_e < \ell_{e2}$ it follows directly, starting from equations (10.54) and (10.50), that the reinforcement can only transmit a reduced force, linearly dependent on the bonded length, $F_2(\ell_b)$, equal to:

$$F_2(\ell_b) = F_{1,\max} + \frac{\Delta\ell_e}{\Delta\ell_{e,\max}} \cdot k_{FR} f_b p_G \cdot \Delta\ell_{e,\max} = F_{1,\max} + k_{FR} f_b p_G \cdot \Delta\ell_e$$
$$F_2(\ell_b) = F_{1,\max} + k_{FR} f_b p_G \cdot (\ell_b - \ell_{e1}) \tag{10.57}$$

10.4.4.2 Evaluation of the Debonding Force for $\ell_b < \ell_{e1}$

In the case where the reinforcement has a total length $\ell_b < \ell_{b1}$, equation (10.13) allows us to state that at no point along the reinforcement can the slip reach the value s_u; therefore, the frictional part of the bond-slip law cannot be activated. The corresponding value of the debonding force, $F_1(\ell_b)$, can thus be determined based on equation (10.14), already demonstrated for FRP-EBR systems:

$$F_1(\ell_b) = F_{1,\max} \cdot \sin\left(\frac{\pi}{2}\frac{\ell_b}{\ell_{e1}}\right) \tag{10.58}$$

With $F_{1,max}$ given by (10.46). Equation (10.55) is well approximated by the following rational function, which is easier to apply:

$$F(\ell_b) = \frac{2\ell_b}{\ell_b + \ell_{e1}} \cdot F_1 = k_{l_b} \cdot F_1, \quad k_{l_b} = \frac{2\ell_b}{\ell_b + \ell_{e1}} < 1 \tag{10.59}$$

Figure 10.14 illustrates the trend of the maximum force in the FRP-NSM reinforcement as a function of bonded length, based on Equations (10.56), (10.57), (10.58) and (10.59).

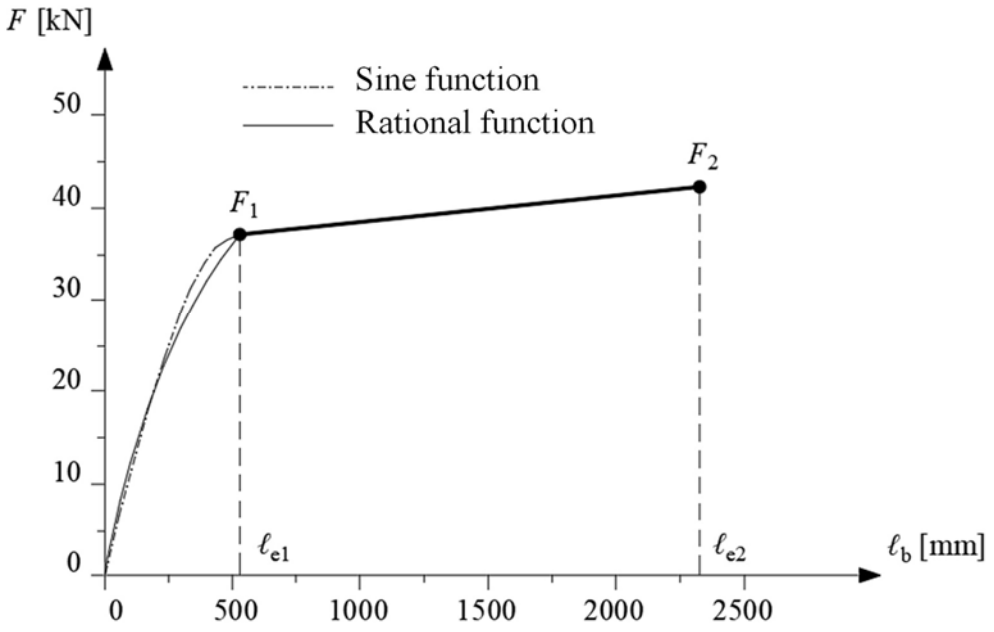

Figure 10-14 – Relationship between the maximum force in the FRP-NSM reinforcement and the bonded length.

10.4.5 Calibration Based on Experimental Data

Given the extensive experimental data available in both national and international literature regarding bond tests on various NSM reinforcement systems applied to concrete and masonry substrates, the equations for the maximum load have been calibrated by comparing the collected data following the methodology outlined in EN1990 – Annex D (Design assisted by testing).

In total, 350 experimental tests were collected for concrete substrates and 150 for masonry substrates.

Since in experimental tests, the bonded length ℓ_b is always less than or comparable to the effective anchorage length ℓ_{e1}, given by equation (10.45), the comparison with experimental data was conducted using Equation (10.60) in terms of mean values.

Mean Maximum Force for Calibration

The experimental data were compared with the following expression for the mean maximum force $F_{1,m}(\ell_b)$ corrected by the intensification coefficient k_l and expressed as a function of ℓ_b through the coefficient k_{l_b}:

$$F_{lm}(\ell_b) = k_{l_b} \cdot k_I \sqrt{E_H A_H \cdot p_G \cdot f_{bm} \cdot s_u} \quad , \quad k_{l_b} = \frac{2\ell_b}{\ell_b + \ell_{el}} \tag{10.60}$$

where:

- **For concrete substrates**:

$$f_{bm} = \frac{1}{2}\frac{\sqrt{f_{cm} f_{ctm}}}{FC}$$

with f_{cm} and f_{ctm} being the mean compressive and tensile strength values of the concrete substrate, respectively, assuming FC = 1. If the mean tensile strength f_{ctm} is not available, it was calculated based on current regulations.

- **For masonry substrates**:

$$f_{bm} = \frac{1}{2}\frac{\sqrt{f_{bcm} f_{btm}}}{FC}$$

with f_{bcm} and f_{btm} being the mean compressive and tensile strength values of the masonry elements, assuming FC = 1. If the mean tensile strength f_{btm} is not available, it was calculated as:

$$f_{btm} = 0.1 f_{bcm}$$

where f_{bcm} was taken as the measured compressive strength of the stone or brick material provided by the experimental studies.

In real-world applications, *FC* represents the confidence factor associated with the level of knowledge of the substrate where the reinforcement is applied and should be evaluated in accordance with recognized regulations.

Calibration Results and Experimental Comparison

The comparison of Equation (10.60) with experimental data, shown in Figure 10-15, for both concrete and masonry supports, enabled the calibration of:

- s_u = 1.2 mm for both concrete and masonry substrates.

- The intensification coefficient k_I was selected as:

$$\text{For concrete substrates: } k_I = 0.95\left(\frac{f_{Rm}}{f_{cm}}\right)^{nf} \cdot \left(\frac{p_F}{p_G}\right)^{np} \tag{10.61}$$

$$\text{For masonry substrates: } k_I = 1.05 \cdot \left(\frac{f_{Rm}}{f_{bcm}}\right)^{nf} \cdot \left(\frac{p_F}{p_G}\right)^{np} \tag{10.62}$$

where:

- f_{Rm} is the mean compressive strength of the resin,
- p_F and p_G are the perimeters of the NSM reinforcement and groove wetted by the resin,
- f_{cm} and f_{bcm} are the compressive strengths of the substrates as introduced earlier..

The best approximation of the experimental results provided values of $n_f = 0.5$ and $n_p = 0.25$, which can be used for design purposes unless more precise experimental data are available for specific reinforcement systems.

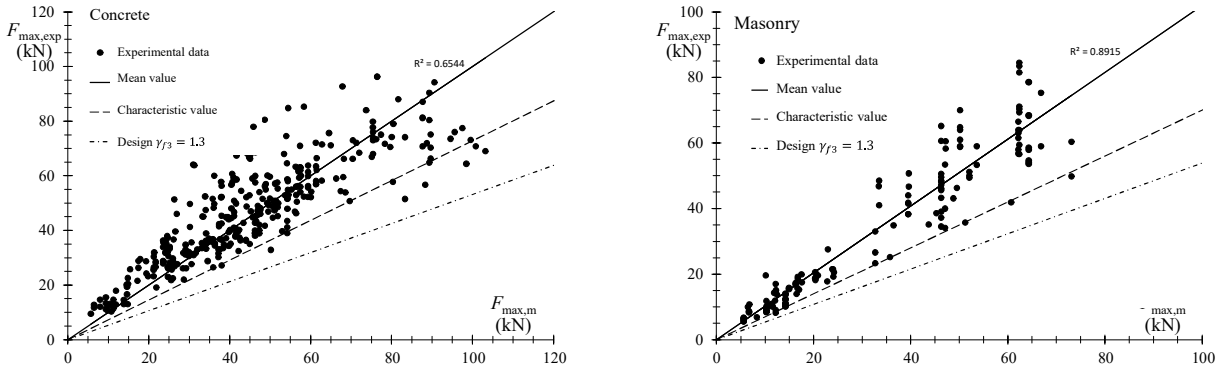

Figure 10-15 – Calibration Results Based on Experimental Data. (a) FRP NSM systems on concrete supports; (b) FRP NSM systems on masonry supports.

For $\ell_b = l_{e1}$ equation (10.58) becomes:

$$F_{1,max,m} = k_I \sqrt{E_H A_H \cdot p_G \cdot f_{bm} \cdot s_u} \tag{10.63}$$

In the case $\ell_b < l_{e1}$, and in the absence of specific experimental data, the theoretical values of the maximum force in the reinforcement, calculated with equations (10.55) and (10.56), must still be corrected using the intensification coefficient k_I by referring to the value $F_{1max,m}$ given in equation (10.64), as follows:

$$\ell_{e1} < \ell_b < \ell_{e2} \quad F_{2,m}(\ell_b) = F_{1,max,m} + k_{FR} f_b p_G \cdot (\ell_b - \ell_{e1}) \tag{10.64}$$

Similarly, for $\ell_b \geq l_{e2}$, the following applies:

$$\ell_b \geq \ell_{e2} \qquad F_{2,max,m} = F_{1,max,m} \cdot \sqrt{1 + 2k_{FR} \cdot (k_{SL} - 1)} \tag{10.65}$$

In which the value $F_{1max,m}$ is given in the equation (10.64).

Characteristic Values and Design Strength Estimation

The statistical analysis of data using the methodology outlined in EN1990 – Annex D (Design assisted by testing) allowed the estimation of the characteristic value (5th percentile fractile) for theoretical predictions:

$$F_{1k}(\ell_b) = k_{l_b} \cdot k_{k,NSM} \cdot k_I \cdot \sqrt{E_H A_H \cdot p_G \cdot f_{bm} \cdot s_u} \tag{10.66}$$

with $k_{k,NSM} = 0.7$.

Finally, following EN1990 recommendations, the design value of the debonding force can be calculated as:

$$F_{1,d}(\ell_b) = \frac{F_{1,k}(\ell_b)}{\gamma_f} = \frac{k_{l_b} \cdot k_I \cdot k_{k,NSM}}{\gamma_f} \sqrt{E_H \cdot A_H \cdot p_G \cdot f_{bm} \cdot s_u} \tag{10.67}$$

Where γ_f is the partial safety factor for the FRP material, which was estimated as:

- γ_f = 1.30 for NSM systems with rough, deformed, or sand-coated surfaces.
- γ_f = 1.70 for smooth-surfaced laminates or bars.

In Figure 10-15, the experimental values of maximum delamination force are compared with:

- Mean values (Equation (10.60)),
- Characteristic values (Equation (10.66)),
- Design values (Equation (10.67)).

assuming FC = 1 in all expressions and γ_f = 1.30 in Equation (10.67).

For design purposes, design values are also defined for optimal anchorage lengths by introducing a model factor γ_{Rd} = 1.20, in analogy to what is done for FRP-EBR systems:

$$\ell_{e1,d} = \gamma_{Rd} \cdot \ell_{e1,m} \tag{10.68}$$

$$\ell_{e2,d} = \gamma_{Rd} \cdot \ell_{e2,m} \tag{10.69}$$

Therefore, if $\ell_b < \ell_{e1,d}$, the design value of the force in the FRP-NSM reinforcement that causes debonding is given by equation (10.67), while the design value of the force $F_{1,max,d}$, corresponding to $\ell_b = \ell_{e1,d}$, is:

$$F_{1,max,d} = \frac{k_I \cdot k_{k,NSM}}{\gamma_f} \sqrt{E_H A_H \cdot p_G \cdot f_{bm} \cdot s_u} \tag{10.70}$$

If $\ell_b \geq \ell_{e2,d}$, the design value of the maximum force in the FRP-NSM reinforcement $F_{2,max,d}$ can be calculated as follows using equation (10.56), adopting the design value $F_{1,max,d}$:

$$F_{2,max,d} = F_{1,max,d} \cdot \sqrt{1 + 2k_{FR} \cdot (k_{SL} - 1)} \tag{10.71}$$

Finally, if $\ell_{e1,d} < \ell_b < \ell_{e2,d}$, the design value of the maximum force in the FRP-NSM reinforcement can be calculated as a function of the bonded length ℓ_b using equation (10.57), as follows:

$$F_{2,d}(\ell_b) = F_{1,max,d} + \left(\ell_b - \ell_{e1,d}\right) \cdot \left(\frac{F_{2,max,d} - F_{1,max,d}}{\ell_{e2,d} - \ell_{e1,d}} \right) \tag{10.72}$$

10.5 MODELING OF FAN-SHAPED CONNECTORS FOR CONCRETE SUBSTRATES

The equations presented in Section 4.1.5 are based on a statistical analysis of experimental data available in the literature, specifically regarding bond tests on inclined and in-line fan-shaped connectors.

Equations (4.18) and (4.19), used to calculate the terms N_{PO} and N_S, are intended to provide a mean prediction of the force associated with the failure mechanism. Therefore, they must include the mean values of the concrete substrate properties appropriately divided by the confidence factor *FC*.

Equations (4.20)-(4.24), used to calculate the terms N_{FD} and N_{FR}, provide characteristic values of the force associated with the failure mechanism. This is because they depend on the characteristic values of the reinforcement material properties (resins and fibers) provided by manufacturers.

Validation of the Pull-Out Resistance Formula

Equation (4.18), which estimates the pull-out failure resistance for in-line fan connectors ($\psi = 180°$), has been validated by comparing it with experimental pull-out tests available in the literature. These tests were conducted on in-line fan-shaped connectors, where failure was observed due to the detachment of a concrete cone.

Figure 10-16 presents a comparison between the experimental data from the literature and the mean predictions provided by Equation (4.18).

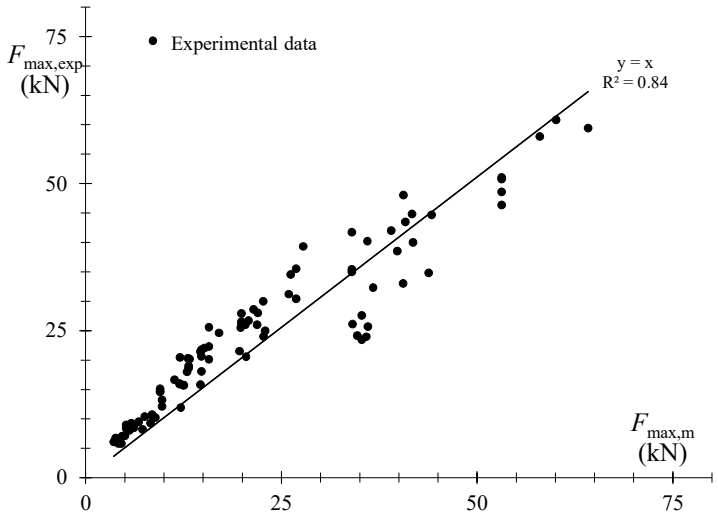

Figure 10-16 – Comparison Between Experimental Data and Mean Maximum Force Predictions of Equation (4.18) (for pull-out failure in in-line fan-shaped connectors, $\psi = 180°$)

Validation for Inclined Fan-Shaped Connectors

For inclined fan-shaped connectors ($\psi \neq 180°$), Figure 10-17, compares the experimental results from the literature with the Equation (4.15) in terms of:

- Mean values,
- Characteristic values,
- Design values (obtained using the calibration coefficients $k_k = 0.7$ and $\gamma_{f2} = 1.3$, in accordance with EN1990 – Annex D (Design assisted by testing)).

For all comparisons, *FC* = 1.0 was assumed.

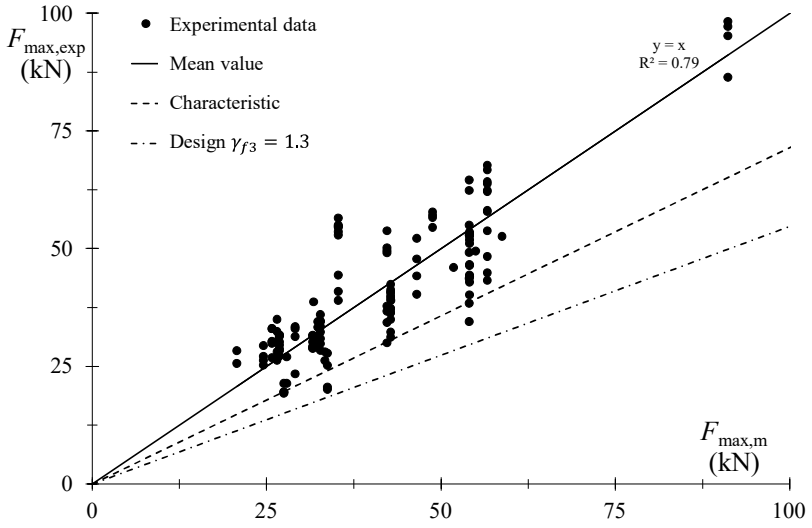

Figure 10-17 – Comparison Between Experimental Data and Mean, Characteristic, and Design Values from Equation (4.15) (for inclined fan-shaped connectors, $\psi \neq 180°$).

11 APPENDIX E (STRENGTHENING OF REINFORCED CONCRETE ELEMENTS UNDER COMBINED COMPRESSION AND BENDING)

11.1 EVALUATION OF THE DESIGN FLEXURAL STRENGTH OF ELEMENTS STRENGTHENED WITH FRP UNDER AXIAL FORCE (COMPRESSION-BENDING)

In sections subjected to combined compression and bending, the Ultimate Limit State (ULS) design requires sizing the FRP strengthening to ensure compliance with the following inequality:

$$M_{\mathrm{Sd}} \leq M_{\mathrm{Rd}}(N_{\mathrm{Sd}}) \tag{11.1}$$

where M_{Sd} is the design bending moment, and M_{Rd} is the design flexural strength of the strengthened section in the presence of the design axial force N_{Sd}.

A possible design procedure is described below.

First, the mechanical reinforcement ratio of the tensile steel reinforcement, μ_{s}, and that of the tensile FRP reinforcement, , μ_{f}, , are calculated using the following equations, respectively:

$$\mu_{\mathrm{s}} = \frac{A_{\mathrm{s1}} \cdot f_{\mathrm{yd}}}{f_{\mathrm{ccd}} \cdot b \cdot d} \tag{11.2}$$

$$\mu_{\mathrm{f}} = \frac{b_{\mathrm{f}} \cdot t_{\mathrm{f}} \cdot f_{\mathrm{fd}}}{f_{\mathrm{ccd}} \cdot b \cdot d} \tag{11.3}$$

where:

- A_{s1} and f_{yd} are the area and the design yield strength of the steel tensile reinforcement;
- f_{ccd} is the design compressive strength of the confined concrete;
- b and d are the width of the section and the effective depth of the mild reinforcement;
- b_{f} and t_{f} are the width and thickness of the FRP reinforcement;
- f_{fd} is the design tensile strength of the FRP reinforcement, evaluated according to the provisions given in § 4.3.2.4(2)P.

The design strength properties of existing materials must be determined:

- For non-seismic applications, according to the provisions of § 3.3.3;
- For seismic applications based on in-situ testing of existing materials.

In the latter case, if an adequate level of knowledge of the structural details and material properties is not available, these strength characteristics must be divided by a confidence factor greater than one.

Additionally, the following dimensionless parameters related to loading conditions are introduced:

$$n_{Sd} = \frac{N_{Sd}}{f_{ccd} \cdot b \cdot d} \tag{11.4}$$

$$m_{Sd} = \frac{M_{Sd}}{f_{ccd} \cdot b \cdot d^2} \tag{11.5}$$

Assuming the width and mechanical properties of the FRP reinforcement are known, the thickness t_f remains the only design variable to be determined.

Starting with an initial trial value for t_f and, consequently, for the reinforcement mechanical ratio μ_f, the following iterative procedure is applied:

Step 1
Calculate the η parameter, defined as:

$$\eta = n_{Sd} + \mu_s \cdot (1-u) + \mu_f \tag{11.6}$$

Step 2
Determine the η limit values (η_i, where i = 0,1,2,3) using the following equations:

$$\eta_0 = -\mu_s \cdot u, \quad \eta_1 = \frac{2}{3} \cdot \frac{r}{r+1}, \quad \eta_2 = 0.8 \cdot \frac{1.75 \cdot r}{1.75 \cdot r + 1}, \quad \eta_3 = 0.51 + \mu_f \cdot (1-r) \tag{11.7}$$

where:

- u = Ratio between the compression reinforcement, A_{s2}, to the area of the tensile reinforcement, A_{s1};
- $r = \frac{2/1000}{\varepsilon_{fd}}$.

Step 3

Using Table 11-1 compare the η parameter with the η limit values from Step 2 to determine the failure mode of the strengthened section (Figure 4-14, 4.3.2.3) and compute the corresponding $m_{(mr)}(\eta)$ parameter.

Table 11-1 – Comparison between

Failure Mode	η	$W_{(mr)}(\eta)$
1a	$\eta_0 \le \eta \le \eta_1$	$W_{(1a)}(\eta) = \frac{1}{2} \cdot \left\{ \eta_0 + \frac{\eta_1 \cdot (1-\eta_1) - \eta_0}{\eta_1 - \eta_0} \cdot (\eta - \eta_0) \right\}$
1b	$\eta_1 \le \eta \le \eta_2$	$W_{(1b)}(\eta) = \frac{1}{2} \cdot \left\{ \eta_1 \cdot \eta_2 + \left[1 - (\eta_1 + \eta_2)\right] \cdot \eta \right\}$
2	$\eta_2 \le \eta \le \eta_3$	$W_{(2)}(\eta) = \frac{1}{2} \cdot \left\{ \eta_2 \cdot (1-\eta_2) + \frac{(0.75-\eta_3) - \eta_2 \cdot (1-\eta_2)}{\eta_3 - \eta_2} \cdot (\eta - \eta_2) \right\}$

Step 4

Evaluate the dimensionless design flexural strength of the strengthened section, $m_{Rd}(n_{Sd})$, using the following equation:

$$m_{Rd}(n_{Sd}) = W_{(mr)}(\eta) + \frac{1}{2} \cdot \left[\mu_s \cdot (1+u) + \mu_f \right] \tag{11.8}$$

Step 5

Verify compliance with the following design requirements:

$$m_{Rd}(n_{Sd}) \geq m_{Sd} \tag{11.9}$$

If the inequality is not satisfied, increase the FRP thickness, t_f, and thus the reinforcement ratio, μ_f, and repeat the procedure from Step 1.

Conversely, if the required FRP thickness is excessive, the design can be optimized by increasing the concrete compressive strength through confinement, which enhances the flexural capacity.

12 APPENDIX F (CONSTITUTIVE RELATIONSHIP OF CONFINED CONCRETE)

12.1 CONSTITUTIVE RELATIONSHIP OF CONFINED CONCRETE

The modeling of the mechanical behavior of reinforced concrete elements confined with FRP requires the prior definition of an appropriate constitutive relationship $\sigma(\varepsilon)$, describing the uniaxial compression behavior (σ representing axial compressive stress as positive and ε representing the corresponding strain, also considered positive).
For this purpose, as an alternative to the parabola-rectangle model proposed in § 4.6.3, a nonlinear relationship of the type represented in Figure 12-1, can be adopted. This model consists of an initial parabolic segment followed by a linear increasing segment. At the transition point between the parabolic and linear portions, continuity of the first derivative of the function $\sigma(\varepsilon)$ is assumed.

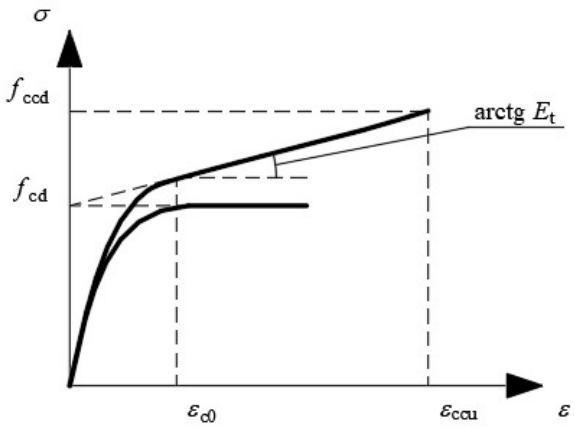

Figure 12-1 – Stress-strain model of FRP-confined concrete.

In analytical terms, the proposed relationship can be expressed as follows:

- *(Parabolic segment)* $\dfrac{\sigma}{f_{cd}} = a \cdot \overline{\varepsilon} - \overline{\varepsilon}^2 \quad \text{per} \quad 0 \le \overline{\varepsilon} \le 1$ (12.1)

- *(Linear segment)* $\dfrac{\sigma}{f_{cd}} = 1 + b \cdot \overline{\varepsilon} \quad \text{per} \quad 1 \le \overline{\varepsilon} \le \dfrac{\varepsilon_{ccu}}{\varepsilon_{c0}}$ (12.2)

In Equations (12.1) and (12.2), the introduced symbols have the following meanings:

- $\overline{\varepsilon}$ is the dimensionless coefficient:

$$\overline{\varepsilon} = \frac{\varepsilon}{\varepsilon_{c0}} \tag{12.3}$$

- f_{cd} and ε_{c0} are, respectively, the design strength of unconfined concrete and its corresponding strain (generally assumed to be 0.002);
- ε_{ccu} is the ultimate design strain of confined concrete corresponding to the design strength f_{ccd} (Chapter 4);

- The coefficients *a* and *b* are:

$$a = 1 + \gamma \,, \quad b = \gamma - 1 \tag{12.4}$$

Additionally (see Figure 12-1):

$$\gamma = \frac{f_{cd} + E_t \cdot \varepsilon_{c0}}{f_{cd}} \tag{12.5}$$

$$E_t = \frac{f_{ccd} - f_{cd}}{\varepsilon_{ccu}} \tag{12.6}$$

13 APPENDIX G (DERIVATION OF THE FORMULA FOR CRACK WIDTH IN RC ELEMENTS STRENGTHENED WITH FRP MATERIALS)

The formula for calculating crack width depends on two terms: the maximum crack spacing $s_{r,max}$ and the difference between the average strain in the steel reinforcement and the average strain in the tensile concrete $\left(\varepsilon_{sm}-\varepsilon_{cm}\right)$ computed between two consecutive cracks. The equations provided in Chapter 4 were obtained through simple steps based on force equilibrium equations and adopting some simplifying assumptions.

13.1 CALCULATION OF THE MAXIMUM CRACK SPACING

In reinforced concrete elements externally strengthened with FRP systems, the transfer length l_E can be defined as the distance between an already cracked section and the section (hereafter referred to as section E) where there is no slip between the tensile concrete and the internal steel reinforcement or between the tensile concrete and the external FRP reinforcement. A simplifying assumption is made that the transfer length is the same for both the internal steel reinforcement and the external FRP reinforcement (Figure 13-1). Within the transfer length between the cracked section and section E, the shear stresses at the steel-concrete and FRP-concrete interfaces are assumed to be constant and equal to τ_{sm} and τ_{fm}, respectively.

The theoretical value of the transfer length can be obtained by writing equilibrium equations for translational forces along the interfaces and ensuring the equality of normal tensile force along the axis of the element. To correlate the transfer length with the crack spacing, it is assumed that at section E, the tensile strength of the concrete in the vicinity of the reinforcements is reached due to the double transfer of shear stresses, τ_{sm} and τ_{fm}, induced by the internal reinforcement and the external strengthening system (Figure 13-1.b).

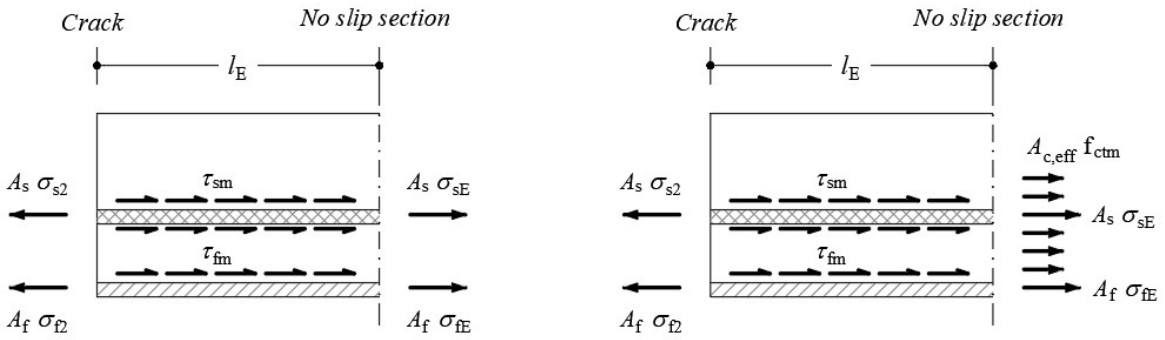

Figure 13-1 – (a) Translational equilibrium along the interfaces; (b) Forces acting in the cracked section (Type 2 section) and in the incipient cracking section at a distance l_E (section E, 'no slip' section).

Translational equilibrium along the steel reinforcement gives:

$$A_s \cdot \sigma_{s2} = A_s \cdot \sigma_{sE} + \tau_{bsm} \cdot l_E \cdot u_s \tag{13.1}$$

Translational equilibrium along the external FRP reinforcement gives:

$$A_{\mathrm{f}} \cdot \sigma_{\mathrm{f2}} = A_{\mathrm{f}} \cdot \sigma_{\mathrm{fE}} + \tau_{\mathrm{bfm}} \cdot l_{\mathrm{E}} \cdot u_{\mathrm{f}} \tag{13.2}$$

By writing the equality of normal force in the cracked section (Section 2) and in Section E, we obtain:

$$\begin{aligned} A_{\mathrm{s}} \cdot \sigma_{\mathrm{s2}} + A_{\mathrm{f}} \cdot \sigma_{\mathrm{f2}} &= A_{\mathrm{s}} \cdot \sigma_{\mathrm{sE}} + A_{\mathrm{f}} \cdot \sigma_{\mathrm{fE}} + A_{\mathrm{c,ef}} \cdot f_{\mathrm{ctm}} \\ A_{\mathrm{s}} \cdot \left(\sigma_{\mathrm{s2}} - \sigma_{\mathrm{sE}}\right) + A_{\mathrm{f}} \cdot \left(\sigma_{\mathrm{f2}} - \sigma_{\mathrm{fE}}\right) &= A_{\mathrm{c,ef}} \cdot f_{\mathrm{ctm}} \end{aligned} \tag{13.3}$$

In Equation (13.3), it is assumed that in Section 2 (cracked), the concrete does not contribute to the tensile force, while in Section E, its contribution is a function of the effective area, $A_{\mathrm{c,ef}}$, affected by the shear stress transfer. It is computed considering an incipient cracking condition, assuming the tensile stress to be equal to f_{ctm}.
By substituting Equations (13.1) and (13.2) in (13.3) the following expression for the transfer length is obtained:

$$\begin{aligned} l_{\mathrm{e}} &= \frac{f_{\mathrm{ctm}} \cdot A_{\mathrm{ct,ef}}}{\tau_{\mathrm{bms}} \cdot u_{\mathrm{s}} + \tau_{\mathrm{bmf}} \cdot u_{\mathrm{f}}} = \frac{f_{\mathrm{ctm}}}{\tau_{\mathrm{bms}}} \cdot \frac{A_{\mathrm{ct,ef}}}{u_{\mathrm{s}} \cdot \left(1 + \frac{\tau_{\mathrm{bmf}}}{\tau_{\mathrm{bms}}} \cdot \frac{u_{\mathrm{f}}}{u_{\mathrm{s}}}\right)} \\ &= \frac{f_{\mathrm{ctm}}}{\tau_{\mathrm{bms}}} \cdot \frac{A_{\mathrm{s}}}{u_{\mathrm{s}}} \cdot \frac{A_{\mathrm{ct,ef}}}{A_{\mathrm{s}} \cdot \left(1 + \frac{\tau_{\mathrm{bmf}}}{\tau_{\mathrm{bms}}} \cdot \frac{u_{\mathrm{f}}}{u_{\mathrm{s}}}\right)} = \frac{f_{\mathrm{ctm}}}{\tau_{\mathrm{bms}}} \cdot \frac{\phi_{\mathrm{s}}}{4} \cdot \frac{1}{\rho_{\mathrm{s+FRP,ef}}} \end{aligned} \tag{13.4}$$

In Equation (13.4) it was set $\frac{A_{\mathrm{s}}}{u_{\mathrm{s}}} = \frac{\phi_{\mathrm{s}}}{4}$, and an equivalent reinforcement ratio is introduced:

$$\rho_{\mathrm{s+FRP,ef}} = \frac{A_{\mathrm{s}}}{A_{\mathrm{ct,ef}}} \left(1 + \frac{\tau_{\mathrm{bmf}}}{\tau_{\mathrm{bms}}} \cdot \frac{u_{\mathrm{f}}}{u_{\mathrm{s}}}\right) = \frac{A_{\mathrm{s}} + \xi_1^2 \cdot A_{\mathrm{f}}}{A_{\mathrm{ct,ef}}} \tag{13.5}$$

where:
A_s is the area of the internal steel reinforcement,
A_{f} is the area of the external FRP reinforcement,
ξ_1^2 is a dimensionless coefficient defined as:

$$\xi_1^2 = \frac{\tau_{\mathrm{bmf}}}{\tau_{\mathrm{bms}}} \cdot \frac{A_{\mathrm{s}}}{u_{\mathrm{s}}} \cdot \frac{u_{\mathrm{f}}}{A_{\mathrm{f}}} \tag{13.6}$$

where u_{s} and u_{f} are the perimeters of the internal steel reinforcement and the external FRP reinforcement, respectively.
Using Equation (13.4), the maximum crack spacing can be expressed following the same approach used in Model Code 2020 for reinforced concrete elements:

$$s_{r,max} = \beta_w \cdot \left(k_c \cdot c + k_{\phi/\rho} \cdot k_{fl} \cdot k_b \frac{f_{ctm} \cdot \phi_s}{\tau_{bms} \cdot \rho_{s+FRP,ef}} \right) \tag{13.7}$$

In Equation (13.7):

- The first term accounts for the geometrical concrete cover effect,
- The second term, a function of l_e, incorporates the same correction factors used for reinforced concrete elements to model the transfer of shear stresses at the interface.

For Equation (13.6), in the absence of more precise evaluations:

- By analogy with internal steel reinforcement, where $\tau_{bms} = 1.8 f_{ctm}$, for NSM strengthening systems, it can be assumed that $\tau_{bmf} = 1.8 f_{ctm}$.
- For EBR strengthening systems, it can be assumed that $\tau_{bmf} = f_{ctm}$.

The symbols in Equation (13.7) are described in §4.3.3.4.

13.2 CALCULATION OF THE DIFFERENCE BETWEEN AVERAGE STRAINS IN THE REGION BETWEEN TWO CRACKS

By adopting a constant distribution of shear stress at the steel-concrete interface, leading to a linear variation of stresses and strains in the steel reinforcement and tensile concrete, we can write, with reference to Section 2 (cracked) and Section E (incipient cracking, no slip) Figure 13-1.b:

$$\varepsilon_{sm} = \varepsilon_{s2} - \beta \cdot \left(\varepsilon_{s2} - \varepsilon_{sE} \right) = \frac{\sigma_{s2} - \beta \cdot \left(\sigma_{s2} - \sigma_{sE} \right)}{E_s} \tag{13.8}$$

$$\varepsilon_{cm} = \beta \cdot \varepsilon_{cE} = \beta \cdot \frac{f_{ctm}}{E_c} \tag{13.9}$$

$$\varepsilon_{sm} - \varepsilon_{cm} = \frac{\sigma_{s2} - \beta \cdot \left(\sigma_{s2} - \sigma_{sE} \right)}{E_s} - \beta \cdot \frac{f_{ctm}}{E_c} = \frac{\sigma_{s2} - \beta \cdot \left(\sigma_{s2} - \sigma_{sE} \right) - \beta \cdot \alpha_s f_{ctm}}{E_s} \tag{13.10}$$

where:

- $\alpha_s = \frac{E_s}{E_c}$.
- β is a coefficient that depends on the strain variation between two consecutive cracks (equal to 0.5 for a linear variation).

Using Equations (13.1) and (13.2) for translational equilibrium, we obtain:

$$l_{\mathrm{E}} = \frac{A_{\mathrm{s}} \cdot (\sigma_{\mathrm{s2}} - \sigma_{\mathrm{sE}})}{\tau_{\mathrm{bsm}} \cdot u_{\mathrm{s}}} \tag{13.11}$$

$$(\sigma_{\mathrm{f2}} - \sigma_{\mathrm{fE}}) = \tau_{\mathrm{bfm}} \cdot l_{\mathrm{E}} \cdot \frac{u_{\mathrm{f}}}{A_{\mathrm{f}}} \tag{13.12}$$

By substituting Equation (13.11) into (13.12) and assuming the same transfer length for both reinforcements and recalling that $\xi_1^2 = \frac{\tau_{\mathrm{bmf}}}{\tau_{\mathrm{bms}}} \cdot \frac{A_{\mathrm{s}}}{u_{\mathrm{s}}} \cdot \frac{u_{\mathrm{f}}}{A_{\mathrm{f}}}$, we obtain:

$$(\sigma_{\mathrm{f2}} - \sigma_{\mathrm{fE}}) = \frac{\tau_{\mathrm{bfm}}}{\tau_{\mathrm{bsm}}} \cdot \frac{A_{\mathrm{s}} \cdot (\sigma_{\mathrm{s2}} - \sigma_{\mathrm{sE}})}{A_{\mathrm{f}}} \cdot \frac{u_{\mathrm{f}}}{u_{\mathrm{s}}} = \xi_1^2 \cdot (\sigma_{\mathrm{s2}} - \sigma_{\mathrm{sE}}) \tag{13.13}$$

Substituting $(\sigma_{\mathrm{f2}} - \sigma_{\mathrm{fE}})$ given by Equation (13.13) into (13.3), it is obtained:

$$A_{\mathrm{s}} \cdot \left(\sigma_{\mathrm{s2}} - \sigma_{\mathrm{sE}}\right) + A_{\mathrm{f}} \cdot \left(\sigma_{\mathrm{f2}} - \sigma_{\mathrm{fE}}\right) = A_{\mathrm{c,ef}} \cdot f_{\mathrm{ctm}} = A_{\mathrm{s}} \cdot \left(\sigma_{\mathrm{s2}} - \sigma_{\mathrm{sE}}\right) + A_{\mathrm{f}} \cdot \xi_1^2 \cdot (\sigma_{\mathrm{s2}} - \sigma_{\mathrm{sE}}) \tag{13.14}$$

which leads to:

$$\left(\sigma_{\mathrm{s2}} - \sigma_{\mathrm{sE}}\right) = \frac{A_{\mathrm{c,ef}} \cdot f_{\mathrm{ctm}}}{A_{\mathrm{s}} + A_{\mathrm{f}} \cdot \xi_1^2} = \frac{f_{\mathrm{ctm}}}{\rho_{\mathrm{s+FRP,ef}}} \tag{13.15}$$

The difference in average strains between the internal steel reinforcement and the concrete between two consecutive cracks can, therefore, be obtained by substituting Equation (13.15) into Equation (13.10):

$$\varepsilon_{\mathrm{sm}} - \varepsilon_{\mathrm{cm}} = \frac{\sigma_{\mathrm{s2}} - \beta \cdot \frac{f_{\mathrm{ctm}}}{\rho_{\mathrm{s+FRP,ef}}} - \beta \cdot \alpha_{\mathrm{s}} f_{\mathrm{ctm}}}{E_{\mathrm{s}}} = \frac{\sigma_{\mathrm{s2}} - \beta \cdot \frac{f_{\mathrm{ctm}}}{\rho_{\mathrm{s+FRP,ef}}} (1 - \alpha_{\mathrm{s}} \cdot \rho_{\mathrm{s+FRP,ef}})}{E_{\mathrm{s}}} \tag{13.16}$$

Equation (13.16) coincides with the formula for RC elements, except that the effective reinforcement ratio is modified to account for the presence of external FRP reinforcement**.**

The symbols in Equation (13.16) are described in §4.3.3.4 except that the coefficient β replaces the previous coefficient k_{t} as it is a function of load duration.

14 APPENDIX H (EXAMPLES OF FRP STRENGTHENING DESIGN ON RC STRUCTURES)

This appendix presents several numerical examples related to FRP strengthening interventions using EBR and NSM systems on structural elements of a residential reinforced concrete (RC) building located in a non-seismic zone.

The interventions are assumed to be necessary due to a change in the building's intended use, leading to an increase in live loads. The strengthening design is limited to the Ultimate Limit State (ULS).

14.1 EXAMPLE 1 – STRENGTHENING OF RC ELEMENTS WITH DIFFERENT FRP SYSTEMS

14.1.1 Geometric, Mechanical, and Load Data of the Structure

The building structure is schematically represented in Figure 14-1. The geometric and mechanical data are derived from the original design documents and in-situ tests.

The structure consists of:

- Primary beams with a rectangular cross-section of 30.0 cm x 50.0 cm (cover $d_1 = d_2 = 3$ cm);
- Secondary beams, parallel to the slab direction, with a rectangular cross-section of 30.0 cm x 40.0 cm (concrete cover $d_1 = d_2 = 3.0$ cm);
- Columns with a rectangular cross-section of 30.0 cm x 30.0 cm (cover $d_1 = d_2 = 3.0$ cm)..

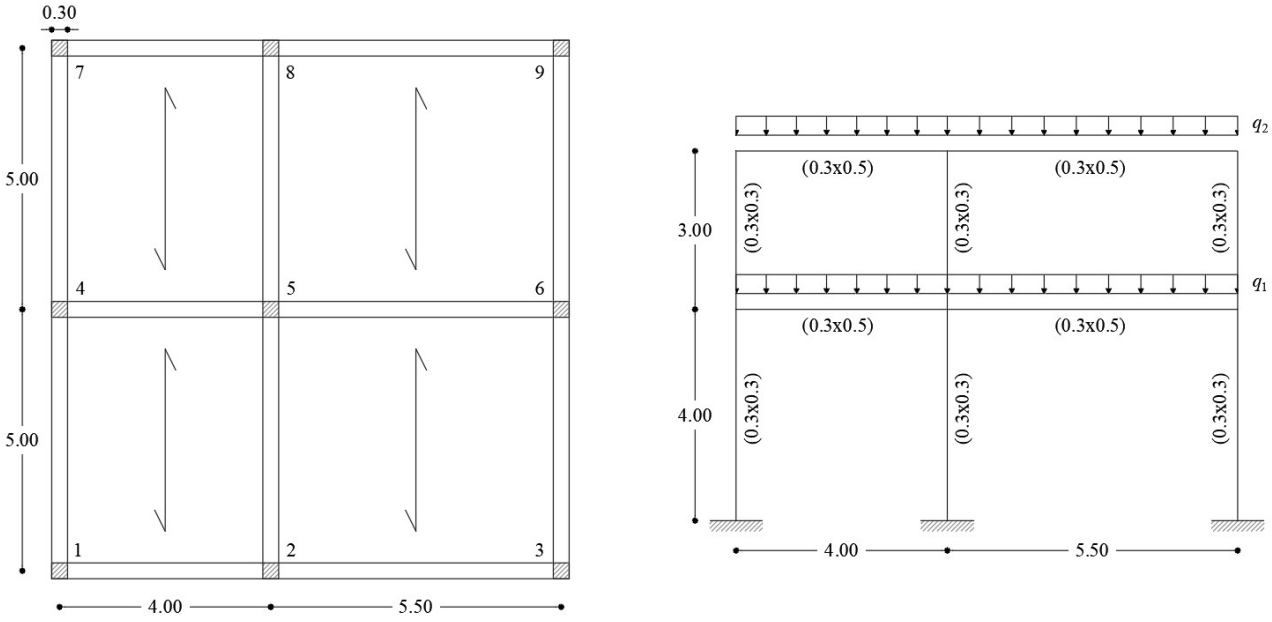

Figure 14-1 – Geometry of the RC structure (dimensions in meters).

The material properties are:

- Concrete strength: f_{cm} = 20.00 MPa;
- Steel reinforcement: FeB38k (Characteristic values for yield and ultimate strength are $f_{yk} = 375MPa$ and $f_{uk} = 450MPa$, respectively).

The structure is assumed to have a knowledge level of 2, so a confidence factor (FC) of 1.20 will be applied.

The slabs are subjected to the following unit loads:

- Variable load at level 1 (residential use): $q_{k1,1} = 2.00$ kN/m^2;
- Variable load at level 2 (non-accessible roof): $q_{k1,2} = 0.50$ kN/m^2;
- Snow load at level 2 (zone III, altitude $a_s < 200$ m): $q_{k2,2} = 0.75$ kN/m^2;
- Permanent structural load transmitted by the slab at each level: $g_{1,1} = g_{1,2} = 4.00$ kN/m^2;
- Permanent non-structural load transmitted by the slab at each level: $g_{2,1} = g_{2,2} = 1.40$ kN/m^2.

Next, the total loads, including self-weight, acting on the beams of the central frame at the Ultimate Limit State (ULS) are evaluated:

- Level 1: $q_{d,1} = 56.4$ kN/m;
- Level 2: $q_{d,2} = 47.9$ kN/m.

The reinforcement schedule for the main beams at the first and second levels, as well as for the columns, is shown in Figure 14-2.

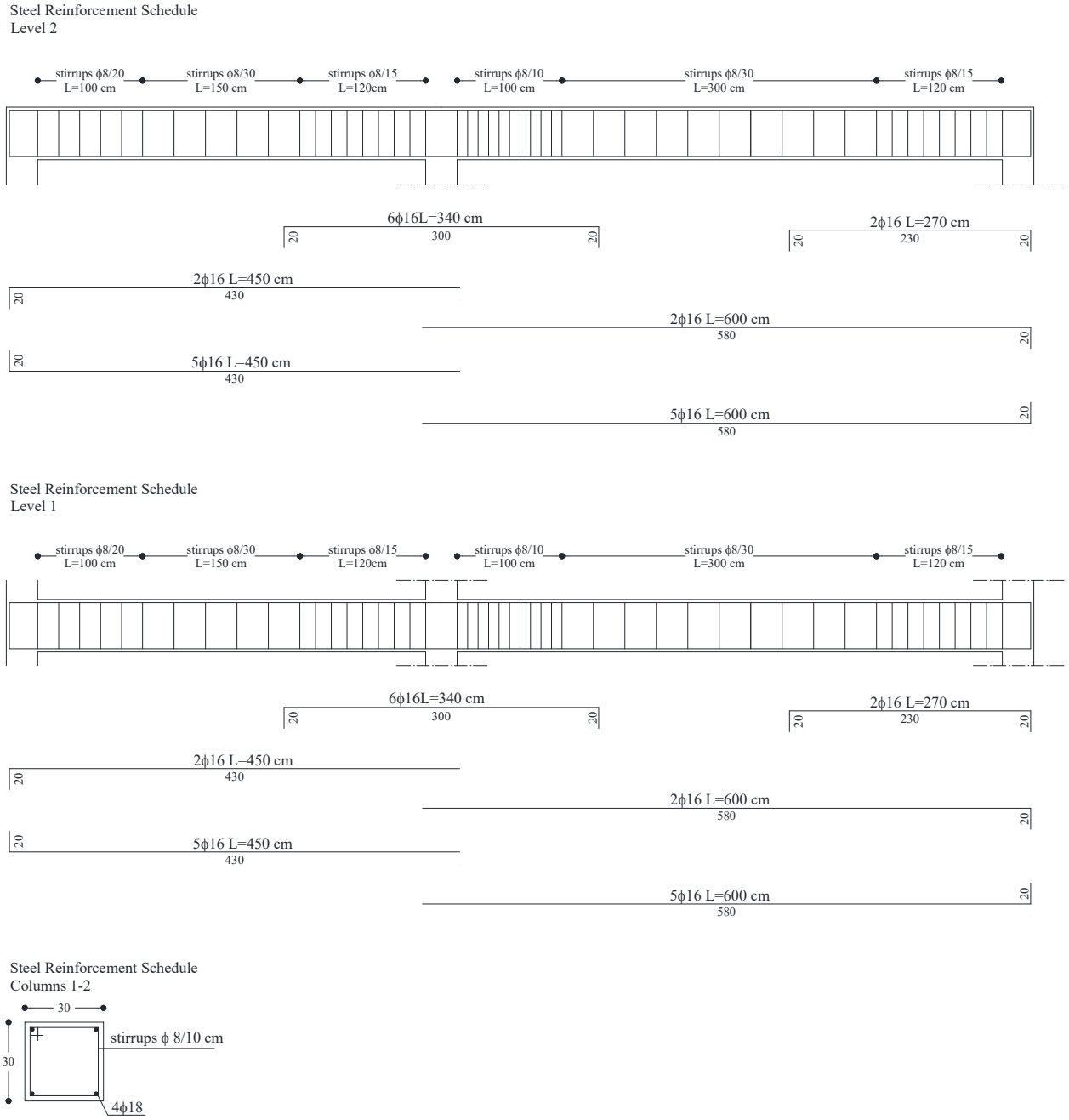

Figure 14-2 – Reinforcement schedule of structural elements.

14.1.2 Scenario of Change in Intended Use

It is assumed that the structure under analysis will undergo a change in use, from residential to museum, and that the roof will become accessible.

The corresponding unit live loads are reported below:

- Variable load at level 1 (museum use): $q_{k1,1} = 5.00$ kN/m^2;
- Variable load at level 2 (accessible roof): $q_{k1,2} = 4.00$ kN/m^2.
- Snow load at level 2 (zone III, altitude $a_s < 200$ m): $q_{k2,2} = 0.75$ kN/m^2;
- Permanent structural load transmitted by the slab at each level: $g_{1,1} = g_{1,2} = 4.00$ kN/m^2;

- Permanent non-structural load transmitted by the slab at each level: $g_{2,1} = g_{2,2} = 1.40$ kN/m^2.

Consequently, the total loads per unit length acting on the beams of the central frame in the ultimate limit state (ULS) fundamental combination (including the self-weight of the beams) are:

- Level 1: $q_{d,1} = 78.90$ kN/m;
- Level 2: $q_{d,2} = 74.20$ kN/m.

Table 14-1 presents the maximum positive and negative bending moments (M_{Sd}) acting on the frame beams under the fundamental ULS combination, along with their respective locations. The maximum shear forces (T_{Sd}) for the same combination are also provided.

Additionally, Table 14-1 includes the bending moments (M_0) acting in the same sections, considering only the non-amplified permanent structural and non-structural loads ($q_{d0,1} = q_{d0,2} = 30.80$ kN/m). This load combination accounts for the load condition of the beams at the time of reinforcement application, assuming the removal of variable loads.

14.1.3 Flexural Strengthening

By assuming the following resistance values for the existing materials, the design resistant moments, M_{Rd}, for each section of interest are calculated and reported in Table 14-1:

- Concrete: $f_{cm} = 20.00$ MPa, γ_c=1, FC=1.20, f_{cd}=16.67 MPa;
- Steel: $f_{ym} = 380.00$ MPa, $\gamma_s = 1$, FC =1.20, $f_{yd} = 316.67$ MPa.

Table 14-1 also reports the values of the existing steel reinforcement, where A_{s1} always represents the reinforcement present on the bottom flange of the section, and A_{s2} represents the reinforcement on the top flange.

It is observed that the inequality:

$$M_{Sd} \leq M_{Rd} \tag{14.1}$$

is not satisfied near the midspan of the two 5.5 m span beams located on levels 1 and 2 (beam 2.1 and beam 2.2).

In particular, an increase in the resistant moment of 20% and 22% is required for beam 2.1 and beam 2.2, respectively.

Table 14-1 - Bending and Shear Capacity Assessment of Beams After Change in Building Use.

Floor	Beam	Span [m]	Section	M_0 [kNm]	M_{Sd} [kNm]	A_{s1} [cm²]	A_{s2} [cm²]	M_{Rd} [kNm]	Verification Satisfied?
1	1.1	4.0	Left support	-17.10	-41.40	10.05	4.02	-58.10	YES
		4.0	Span (1.83 m)	22.50	90.20	10.05	4.02	141.90	YES
		4.0	Right support	-64.30	-178.80	10.05	16.08	-225.80	YES
	2.1	5.5	Left support	-80.60	-214.00	10.05	16.08	-225.80	YES
		5.5	Span (3.00 m)	60.20	170.10	10.05	4.02	141.90	NO
		5.5	Right support	-34.20	-79.80	10.05	8.04	-114.20	SI
2	1.2	4.0	Left support	-12.70	-27.90	10.05	4.02	-58.10	YES
		4.0	Span (1.78 m)	23.50	90.80	10.05	4.02	141.90	YES
		4.0	Right support	-68.00	-175.30	10.05	16.08	-225.80	YES
	2.2	5.5	Left support	-80.00	-198.70	10.05	16.08	-225.80	YES
		5.5	Span (3.00 m)	65.60	173.80	10.05	4.02	141.90	NO
		5.5	Right support	-24.90	-53.10	10.05	8.04	-114.20	YES

Legend:

- M_0 (kNm): Bending moment considering only permanent structural and non-structural loads (non-amplified).
- M_{Sd} (kNm): Design bending moment under the Ultimate Limit State (ULS).
- A_{s1} (cm²): Area of tensile reinforcement.
- A_{s2} (cm²): Area of compressive reinforcement.
- M_{Rd} (kNm): Flexural capacity of the section.
- Verification Satisfied?: Indicates whether the section meets the design requirements.

14.1.3.1 Case 1 - Strengthening with the FRP-EBR System

It was decided to strengthen beams 2.1 and 2.2 by applying a wet-lay-up unidirectional CFRP fabric in the tension zone with the following geometric and mechanical properties:

- Equivalent layer thickness: $t_{f,1}$= 0.167 mm;
- Layer width: b_f = 30.0 cm (corresponding to the width b of the beam)
- Elastic modulus in the fiber direction (beam axis): E_f = 270000 MPa;
- Characteristic strength: f_{fk} = 2700 MPa;
- FRP system classification: C210C (according to the Guidelines for the Identification, Qualification, and Acceptance Control of Fiber-Reinforced Polymer (FRP) Composites Used for the Structural Strengthening of Existing Constructions).

Two layers of CFRP fabric are assumed (n_f = 2), and verification is performed to check whether this configuration satisfies inequality (14.1) for the two beams under consideration.

The design maximum strain of the composite, ε_{fd}, is evaluated using equation (4.51):

$$\varepsilon_{fd} = \min\left\{\eta_a \cdot \frac{\varepsilon_{fk}}{\gamma_f}, \varepsilon_{fdd,2}\right\} = \varepsilon_{fdd,2} = 3.14‰ \tag{14.2}$$

where:

$$\eta_a \cdot \frac{\varepsilon_{fk}}{\gamma_f} = \eta_a \cdot \frac{f_{fk}}{\gamma_f}\frac{1}{E_f} = 0.95 \cdot \frac{2700}{1.3} \cdot \frac{1}{270000} = 7.31‰ \tag{14.3}$$

where the partial safety factors were assumed as follows:

- Partial safety factor at the Ultimate Limit State, $\gamma_f = 1.30$ (Table 3-1, §3.4.1)
- Enviromental conversion factor, $\eta_a = 0.95$ (Table 3-3, §3.5.1).

For the resistance of the composite against Mode 2 debonding, $f_{fdd,2}$, the following value was obtained:

$$f_{\mathrm{fdd,2}} = \frac{k_{\mathrm{q}} k_{\mathrm{b}}}{\gamma_{\mathrm{f2}}} \sqrt{\frac{2E_{\mathrm{f}} \frac{k_{\mathrm{Gk,2}}}{4FC} \sqrt{f_{\mathrm{cm}} f_{\mathrm{ctm}}} \cdot s_{\mathrm{u}}}{t_{\mathrm{f}}}} = 847.02\mathrm{MPa} \tag{14.4}$$

which results in:

$$\varepsilon_{\mathrm{fdd,2}} = \frac{f_{\mathrm{fdd,2}}}{E_{\mathrm{f}}} = \frac{847.02}{270000} = 3.14‰ \tag{14.5}$$

where:

- $k_{\mathrm{Gk,2}} = 1.60$
- $k_{\mathrm{q}} = 1.25$
- $s_{\mathrm{u}} = 0.25$ mm
- $k_{\mathrm{b}} = \max\left(1, \sqrt{\frac{2 - b_{\mathrm{f}}/b}{1 + b_{\mathrm{f}}/b}}\right) = \max(1, 0.7) = 1$
- $t_{\mathrm{f}} = n_{\mathrm{f}} \cdot t_{\mathrm{f,1}} = 2 \cdot 0.167$ mm $= 0.334$ mm
- $f_{\mathrm{cm}} =$ 20.00 MPa
- $f_{\mathrm{ctm}} = 0.3 \cdot \left(f_{\mathrm{ck}}\right)^{2/3} = 0.3 \cdot \left(f_{\mathrm{cm}} - k\right)^{2/3} = 1.66\mathrm{MPa}$
- in which k was assumed to be seven (7) based on the Guidelines for the assessment of in-situ concrete properties (assuming that the number of tests conducted to characterize the compressive strength of concrete was between 4 and 6). $\gamma_{\mathrm{f2}} = 1.3$ (Table 3-1, §3.4.1)
- $FC = 1.2$.

Failure Mechanism

The flexural failure mechanism can occur in two ways, depending on whether the maximum tensile strain in the FRP reinforcement (zone 1) or the maximum compressive strain in concrete ($\varepsilon_{\mathrm{cu}}$) (zone 2) is reached (Figure 14-3).

It is assumed that failure occurs in the FRP reinforcement. Thus, setting $\varepsilon_{\mathrm{fd}} = \varepsilon_{\mathrm{fdd}} = 3.14$ ‰, the strain values in other materials can be calculated as follows:

- Concrete at the compressed edge: $\varepsilon_{\mathrm{c}} = (\varepsilon_{\mathrm{fd}} + \varepsilon_0) \cdot \frac{x}{(h - x)} \le \varepsilon_{\mathrm{cu}}$ (14.6)
- Steel in compression: $\varepsilon_{\mathrm{s2}} = (\varepsilon_{\mathrm{fd}} + \varepsilon_0) \cdot \frac{x - d_2}{(h - x)}$ (14.7)
- Steel in tension: $\varepsilon_{\mathrm{s1}} = (\varepsilon_{\mathrm{fd}} + \varepsilon_0) \cdot \frac{d - x}{(h - x)}$ (14.8)

At this stage, the initial strain ε_0 at the time of FRP application is neglected. It is assumed that the tensile steel is yielded ($\sigma_{s1} = f_{yd} = 316.67$ MPa) while the compressed steel remains elastic ($\sigma_{s2} = E_s \varepsilon_{s2}$, assuming $E_s = 200000$ MPa).

Equilibrium Equations
The equilibrium equation for translational forces is::

$$\psi \cdot b \cdot x \cdot f_{cd} + A_{s2} \cdot \sigma_{s2} - A_{s1} \cdot f_{yd} - A_f \cdot f_{fdd,2} = 0 \tag{14.9}$$

where the dimensionless coefficient ψ represents the intensity of the resultant compression force relative to $b \cdot x \cdot f_{cd}$ and is expressed as:

$$\psi = \begin{cases} 1000\varepsilon_c \left(0.5 - \dfrac{1000}{12}\varepsilon_c\right) & \text{per } \varepsilon_c \le 2.00‰ \\ 1 - \dfrac{2}{3000\varepsilon_c} & \text{per } 2.00‰ \le \varepsilon_c \le 3.50‰ \end{cases} \tag{14.10}$$

The equation is solved iteratively by assuming trial values for the position of the neutral axis x, which allows for the calculation of the corresponding value of ψ and the stress in the compressed steel reinforcement. When the initially assumed value of x matches the one calculated from equation (14.9), convergence is achieved.

The following results were obtained: $\psi = 0.477$ and $x = 13.7$ cm, along with the following strain values in the materials, which confirm the initial assumptions:

- $\varepsilon_f = \varepsilon_{fdd} = 3.14$ ‰
- $\varepsilon_c = 1.19$ ‰ < 3.50 ‰,
- $\varepsilon_{s1} = 2.88$ ‰ > $\varepsilon_{yd} = f_{yd} / E_s = 316.7 / 200000 = 1.58$ ‰,
- $\varepsilon_{s2} = 0.93$ ‰ < $\varepsilon_{yd} = 1.58$ ‰.

Verification of the Strengthened Section
The moment equilibrium equation around the tensile reinforcement is:

$$M_{Rd} = \left[\psi \cdot b \cdot x \cdot f_{cd} \cdot (d - \lambda \cdot x) + A_{s2} \cdot E_s \cdot \varepsilon_{s2} \cdot (d - d_2) + A_f \cdot f_{fdd,2} \cdot d_1\right] = 173.80 \text{kNm} \tag{14.11}$$

where λ is the distance of the resultant compression force from the compressed edge, given by:

$$\lambda = \begin{cases} \dfrac{8 - 1000\varepsilon_c}{4\left(6 - 1000\varepsilon_c\right)} & \text{if } \varepsilon_c \le 2.00‰ \\ \dfrac{1000\varepsilon_c\left(3000\varepsilon_c - 4\right) + 2}{2000\varepsilon_c\left(3000\varepsilon_c - 2\right)} & \text{if } 2.00‰ \le \varepsilon_c \le 3.50‰ \end{cases} \tag{14.12}$$

The final result is $\lambda = 0.354$.

The design moment capacity, M_{Rd}, is then greater than or equal to the applied moment, $M_{Sd,}$ in the right span of the frame at levels 1 and 2 (170.10 kNm for beam 2.1 and 173.80 kNm for beam 2.2). Table 14-2 provides a comparison of design bending moments and the resistant moments for the beams receiving FRP flexural strengthening.

It is important to note that, for both beams, the effect of the pre-existing deformation state in the section prior to the application of the reinforcement was neglected in the calculations of the resistant moment. This assumption is generally on the safe side, as will be demonstrated later.

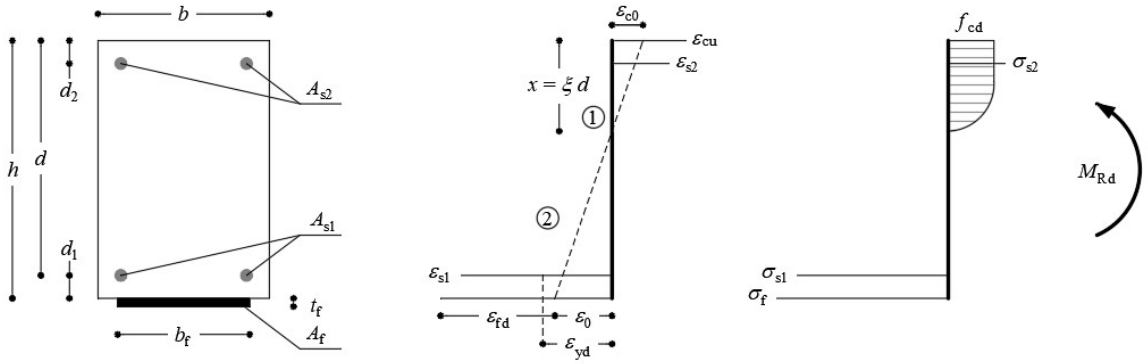

Figure 14-3 – Failure modes for a rectangular section subject to flexure.

Table 14-2 - Comparison of Design and Resistant Moments for Reinforced Beams

Level	Beam	Section	M_{Sd} [kNm]	M_{Rd} [kNm]
1	2.1	Span 3.00 m	170.10	173.80
2	2.2	Span 3.00 m	173.80	173.80

Anchorage Verification

The verification of reinforcement anchorage must be conducted concerning the following maximum applicable stress in the reinforcement at the anchorage section:

$$f_{fdd} = \frac{k_b}{\gamma_{f2}} \cdot \sqrt{\frac{2E_f \Gamma_{Fk}}{t_f}} = 415.00\text{MPa} \tag{14.13}$$

where:

$$\Gamma_{Fk} = \frac{k_{Gk}}{4} \frac{\sqrt{f_{cm} f_{ctm}}}{FC} \cdot s_u = 0.18\text{N/mm} \tag{14.14}$$

In addition to the previously defined symbols, it has been assumed that k_{Gk} = 0.60 for wet lay-up systems.

The optimal anchorage length, ℓ_{ed}, is given by equation (4.1):

$$\ell_{ed} = \max\left\{\ell_{ed,min};\ \gamma_{Rd} \frac{1}{f_{bm}} \sqrt{\frac{\pi^2 E_f t_f \Gamma_{Fm}}{2}}\right\} \tag{14.15}$$

which, assuming $\Gamma_{\mathrm{FM}} = \frac{1}{2} f_{\mathrm{bm}} s_{\mathrm{u}}$, becomes:

$$\ell_{\mathrm{ed}} = \max\left\{100\,\mathrm{mm};\ \gamma_{\mathrm{Rd}} \frac{\pi}{2}\sqrt{\frac{E_{\mathrm{f}} t_{\mathrm{f}} \cdot s_u}{f_{\mathrm{bm}}}}\right\} = \max\left\{100\,\mathrm{mm};163\,\mathrm{mm}\right\} = 163\,\mathrm{mm} \tag{14.16}$$

where:

- γ_{Rd} = 1.20 (model coefficient)
- $f_{\mathrm{bm}} = \frac{k_{\mathrm{Gm}}}{2}\frac{\sqrt{f_{\mathrm{cm}} f_{\mathrm{ctm}}}}{FC} = 3.00\mathrm{MPa}$ (14.17)
- k_{Gm} = 1.25 for wet lay-up systems.

Using $f_{\mathrm{fd}} = 415MPa$ as the stress acting in the FRP reinforcement in equations (14.9) and (14.11), a design moment of 136.00 kNm is obtained.

Table 14-3 reports the distances from the left and right supports of each beam where the design moment for the considered ultimate limit state (ULS) combination equals 136.00 kNm.
End anchorage failure is prevented if the reinforcement is extended at least 163 mm beyond the sections indicated in Table 14-3, according to the reinforcement scheme shown in Figure 14-4 for beam 2.1, where the anchorage length has been rounded up to 170 mm. The total length of the beam requiring reinforcement is 1.90 m, plus the two anchorage lengths.
t is noted that, in the anchorage sections of the reinforcement (defined based on the verification of end debonding), the design flexural capacity of the unreinforced concrete section (M_{Rd} =141.90 kNm) exceeds the applied moment (M_{Sd} = 136.00 kNm). The sections where the applied moment equals the flexural resistance of the unreinforced section are located 2.15 m and 1.65 m from the left and right supports for beam 2.1, respectively. This indicates that the reinforcement length (1.90 m, excluding anchorage lengths) slightly exceeds the strictly necessary length (1.70 m) required for reinforcement.

Although the anchorage section of the reinforcement is not located in the maximum shear zone, the moment diagram is shifted by 0.9d = 330 mm, resulting in the reinforcement ends being extended by an additional 0.33 m toward the beam supports.
Finally, for practical implementation, it is suggested to stagger the starting sections of the two reinforcement strips on both sides by $\ell_{\mathrm{ed}} = 170mm$. Figure 14-4 illustrates the final configuration of the two reinforcement layers for beam 2.1.

Table 14-3 - Anchorage Section Locations for Reinforced Beams

Level	Beam	Distance from left support [m]	Distance from right support [m]	M_{Sd} [kNm]	f_{fdd} [MPa]
1	2.1	2.05	1.55	136.00	415.00
2	2.2	2.00	1.45	136.00	415.00

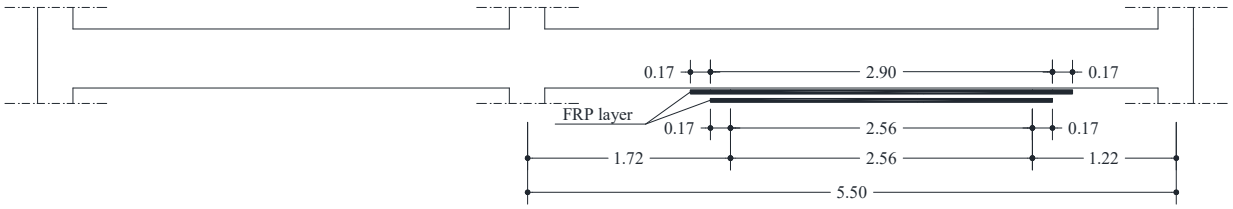

Figure 14-4 – Configuration of CFRP-EBR Reinforcement for Beam 2.1.

Since for beam 2.2, the flexural strength of the strengthened section was found to be exactly equal to the applied moment, the effect of the pre-existing deformation in the section before applying the reinforcement is evaluated at the moments M_0 = 60.20 kNm for beam 2.1 and M_0 = 65.60 kNm for beam 2.2. The deformation at the bottom fiber of the section, ε_0, is calculated using the following simplified formula:

$$\varepsilon_0 = \frac{M_0}{0.9 \cdot d \cdot E_s \cdot A_{s1}} \cdot \frac{h}{d} \tag{14.18}$$

The resulting deformations at the bottom fiber are ε_0 = 0.75 ‰ and ε_0 = 0.82 ‰ for the two beams, respectively. Introducing these values into equations (14.18), (14.19), (14.20) and solving equations (14.9) and (14.10), again, the flexural strengths of the FRP-strengthened sections are found to be slightly higher than those previously calculated while neglecting ε_0: 175.20 kNm for beam 2.1 and 175.30 kNm for beam 2.2.

These results confirm that neglecting the initial deformation ε_0 is a conservative assumption when calculating the flexural strength of the FRP-strengthened section. In this case, accounting for ε_0 allows beam 2.2 to achieve a flexural strength greater than the applied moment (173.80 kNm).

14.1.3.2 Case 2 – Strengthening with SFRP-EBR System

The same beams 2.1 and 2.2 analyzed previously are strengthened by implementing, as an alternative to the solution designed in section 14.3.1, a reinforcement system consisting of a unidirectional SFRP fabric with the following geometric and mechanical characteristics:

- Equivalent layer thickness:: $t_{f,1}$= 0.254 mm;
- Layer width: b_f = 30.0 cm (corrispondente alla larghezza della trave b;);
- Normal modulus of elasticity in the fiber direction (beam axis): E_f = 190000 MPa;
- Characteristic strength: f_{fk} = 2200 MPa;
- SFRP system classification: 190S (according to the Guidelines for the Identification, Qualification, and Acceptance Control of Fiber-Reinforced Polymer (FRP) Composites for Structural Strengthening of Existing Buildings).

Two layers of SFRP fabric are assumed, thus n_f = 2, and a verification is conducted to check whether they are sufficient to satisfy inequality (14.1) for the two beams under analysis. The design and verification procedure for the SFRP reinforcement follows the same methodology as the CFRP reinforcement described previously. Therefore, only the summarized calculation results are provided below.

The maximum design strain that the SFRP system can withstand is:

$$\varepsilon_{fd} = \min\left\{\eta_a \cdot \frac{\varepsilon_{fk}}{\gamma_f}, \varepsilon_{fdd}\right\} = \min\left\{0.0085; 0.00299\right\} = \varepsilon_{fdd} = 2.99‰$$

The composite's resistance against intermediate debonding from the substrate is:

$$f_{fdd,2} = E_f \cdot \varepsilon_{fdd,2} = 576.10\text{MPa}$$

assuming, as in the example from section 14.3.1, $k_{Gk,2}$ = 1.60; k_q = 1.25; s_u = 0.25 mm; k_b = 1; $t_f = t_{f,1} \cdot n_f$ = 0.508 mm; f_{cm} = 20 MPa; f_{ctm} = 1.66 MPa; γ_{f2} = 1.30; FC = 1.20.

The flexural strength of the strengthened section, applying equations (14.9) and (14.11) and disregarding the pre-existing deformation state before the application of the reinforcement is equal to M_{Rd} = 174.90 kNm, which is greater than both the maximum acting moment on beam 2.1 (M_{Sd}=170.10 kNm) and on beam 2.2 (M_{Sd}=173.80 kNm).
If instead, ε_0 = 0.75 ‰ and ε_0 = 0.82 ‰ are considered for the two beams, as calculated in the previous example, the flexural strength results in M_{Rd}=176.30 kNm for beam 2.1 and M_{Rd}=176.40 kNm for beam 2.2, once again confirming that disregarding ε_0 is a conservative approach for the calculation of the flexural strength of the section strengthened with SFRP..

The anchorage verification of the reinforcement is now performed, referring to the following maximum stress in the reinforcement against end debonding from the substrate:

$$f_{fdd} = \frac{k_b}{\gamma_{f2}} \cdot \sqrt{\frac{2E_f \Gamma_{Fk}}{t_f}} = 282.30\text{MPa}$$

where, as in the previous example, k_{Gk} = 0.60; k_b = 1.00; γ_{f2} = 1.30; Γ_{fk} = 0.180 N/mm.

The design value of the optimal anchorage length is calculated as:

$$\ell_{ed} = \max\left\{100\,\text{mm};\ \gamma_{Rd}\frac{\pi}{2}\sqrt{\frac{E_f t_f \cdot s_u}{f_{bm}}}\right\} = \max\left\{100\,\text{mm};169\,\text{mm}\right\} = 169\text{mm}$$

assuming $\gamma_{Rd} = 1.20$, $f_{bm} = \frac{k_{Gm}}{2}\frac{\sqrt{f_{cm} f_{ctm}}}{FC} = 3.00$ MPa with $k_{Gm} = 1.25$ and $s_u = 0.25$ mm. The anchorage length is rounded up to 170 mm.

The acting moment corresponding to an SFRP reinforcement stress of $f_{fdd} = 282.30$ MPa is $M_{Sd} = 92.50$ kNm. The distances from the left and right supports of the sections where the acting moment, for the considered ULS combination, is equal to 92.50 kNm are 1.60 m and 1.10 m for beam 2.1 and 1.55 m and 1.00 for beam 2.2 (Table 14-4). To satisfy the end debonding verification, the reinforcement must extend at least 170 mm beyond these sections. Net of the anchorage lengths, the total reinforcement length is 2.80 m for beam 2.1 and 2.95 m for beam 2.2.

Finally, it is noted that $M_{Sd} = 92.50$ kNm is lower than the flexural strength of the RC section without FRP reinforcement ($M_{Rd} = 141.90$ kNm); this means that to satisfy the end debonding verification, the reinforcement must be applied over a longer length than strictly necessary.

Although the anchorage section of the reinforcement is not located in the maximum shear region, the bending moment diagram is still shifted by 0.9d = 330 mm, meaning that the reinforcement ends are shifted by an additional 0.33 m towards the beam ends.

For practical application, it is recommended to stagger the starting sections of the two SFRP reinforcement strips by $\ell_{ed} = 170mm$ on both sides (Figure 14-5).

Table 14-4 - Distances of Sections from Beam Supports where $M_{Sd} = 92.5kNm$

Level	Beam	Distance from Left Support [m]	Distance from Right Support [m]	M_{Sd} [kNm]	f_{fdd} [MPa]
1	2.1	1.60	1.10	92.50	282.30
2	2.2	1.55	1.00	92.50	282.30

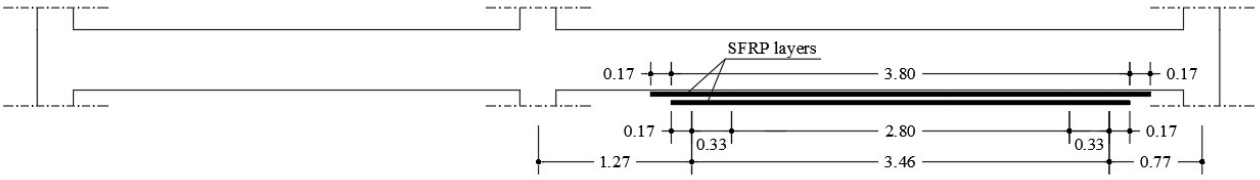

Figure 14-5 – SFRP-EBR Strengthening Configuration for Beam 2.1.

14.1.3.3 Case 3 – Strengthening with the FRP-NSM System

As an alternative to the unidirectional CFRP or SFRP wet-lay-up fabric designed in the previous sections, a strengthening intervention using the NSM (Near-Surface Mounted) technique is designed below, with the following geometric and mechanical characteristics:

- Type of reinforcement: Carbon Fiber Reinforced Polymer (CFRP) bars
- Bar diameter: 8 mm, corresponding to a single bar area of A_F = 50.2 mm^2;
- Normal elastic modulus of the bar in the fiber direction: E_f = 150000 MPa;
- Characteristic tensile strength of the bar: f_{ftk} = 2800 MPa;
- Groove dimensions: w_G = 18 mm, d_G = 18 mm
- Tensile strength of the resin: f_{Rm} = 70.00 MPa.

Two bars are assumed $n_f = 2$, and verification is carried out to determine whether they are sufficient to satisfy inequality (14.1) for the two beams under consideration..
The maximum design strain supported by the composite in the section of maximum moment,, ε_{fd}, is evaluated using equation (4.51):

$$\varepsilon_{fd} = \min\left(\frac{F_{max,d}(\ell_b)}{E_F \cdot A_F}; \eta_a \frac{f_{ftk}}{E_F \cdot \gamma_{f1}}\right) \tag{14.19}$$

For $\ell_b < \ell_{ed2}$, the force $F_{max,d}$ depends on the distance from the reinforcement end section, z, according to the following expression:

$$F_{max,d}(l_b) = \frac{a_F \ell_b}{b_L + \ell_b} \quad , \quad a_F = \frac{\ell_{ed2} - \ell_{ed1}}{\frac{\ell_{ed2}}{F_{2d}} - \frac{\ell_{ed1}}{F_{1d}}} \quad , \quad b_L = \frac{F_{2,d} - F_{1d}}{\frac{F_{1d}}{\ell_{ed1}} - \frac{F_{2d}}{\ell_{ed2}}} \tag{14.20}$$

While $\ell_b \geq \ell_{ed2}$, it s assumed $F_{max,d} = F_{2,d}$.
The terms in equation (14.18) are expressed as follows:

$$\ell_{e1d} = \gamma_{Rd} \cdot \ell_{e1m} = \gamma_{Rd} \cdot \frac{\pi}{2}\sqrt{\frac{E_H A_H s_u}{p_G f_{bm}}} \tag{14.21}$$

$$\ell_{e2d} = \gamma_{Rd} \cdot \ell_{e2m} = \gamma_{Rd} \cdot \left(\ell_{e1m} + \frac{F_{1,m}}{f_{bm} \cdot p_G \cdot k_{FR}}\left[\sqrt{1 + 2k_{FR}(k_{SL} - 1)} - 1\right]\right) \tag{14.22}$$

$$F_{1d} = \frac{k_{k,NSM}}{\gamma_{f3}} \cdot F_{1m} = \frac{k_{k,NSM} \cdot k_I}{\gamma_{f3}}\sqrt{2E_H \cdot A_H \cdot p_G \cdot \Gamma_{F1m}} \tag{14.23}$$

$$F_{2d} = F_{1d}\sqrt{1 + 2k_{FR}(k_{SL} - 1)} \tag{14.24}$$

he calculation of the length l_{ed2}, is carried out with the following assumptions:

- k_{FR} = 0.05
- k_{SL} = 4.00
- s_u = 1.20 mm
- p_G is the perimeter of the groove wetted by the resin = $w_G + 2d_G$ = 54.00 mm

- $f_{bm} = \frac{\sqrt{f_{cm} f_{ctm}}}{2 \cdot FC} = 2.40\text{MPa}$ is the peak stress of the bond law, obtained by assuming FC=1.2, $f_{cm} = 20.00\text{MPa}$, $f_{ctm} = 0.3 \cdot (f_{ck})^{2/3} = 0.3 \cdot (f_{cm} - 8)^{2/3} = 1.57\text{MPa}$
- $\Gamma_{F1m} = \frac{1}{2} \cdot s_u f_{bm} = 1.44\,\text{N/mm}$
- E_H is the homogenized elastic modulus of the bar + resin system, calculated as:

$$E_H = \frac{E_F A_F + E_R A_R}{w_G d_G} = 26217 \text{ MPa}$$

where $E_R = 50 f_{Rm} = 3500$ MPa, $E_f = 150000$ MPa, $A_H = w_G d_G = 324.0$ mm^2, $A_F = 50.20$ mm^2, $A_R = w_G d_G - A_F = 273.80$ mm^2.

- The intensification coefficient k_I is equal to:

$k_I = 0.95 \cdot \left(\frac{p_F}{p_G}\right)^{0.25} \left(\frac{f_{Rm}}{f_{cm}}\right)^{0.5} = 1.47$, where $p_F = 25.10$ mm, $f_{Rm} = 70.00$ MPa.

Using equations (14.21), (4.20) and (4.21), the following values are obtained:

- $\ell_{e1m} = \frac{\pi}{2} \sqrt{\frac{E_H A_H s_u}{p_G f_{bm}}} = 440$ mm
- $F_{1m} = k_I \sqrt{2 E_H \cdot A_H \cdot p_G \cdot \Gamma_{F1m}} = 68.87\text{kN}$
- $\ell_{e2m} = \left(\ell_{e1m} + \frac{F_{1,m}}{f_{bm} \cdot p_G \cdot k_{FR}} \left[\sqrt{1 + 2 k_{FR} (k_{SL} - 1)} - 1 \right] \right) = 1.90\text{m}$
- $\ell_{e2d} = \gamma_{Rd} \cdot \ell_{e2m} = 2.30\text{m}$, essendo $\gamma_{Rd} = 1.2$.

The sections of the maximum applied moment are located 3.00 m from the left support for both beams (see Table 14-1) and 2.50 m from the right support. Therefore, since both are greater than $l_{ed2} = 2.30m$, it is possible to apply the FRP bars over a total length of 2 x 2.30 m = 4.60 m so that, at the sections of the maximum moment, the tensile force that each FRP bar can carry is equal to F_{2d}, which is calculated using equation (14.22) as follows:

$$F_{2d} = F_{1d} \cdot \sqrt{1 + 2 k_{FR} (k_{SL} - 1)} = 42.30\text{kN}$$

where:

- $k_{k,NSM} = 0.70$;
- γ_{f3} is the partial factor for the NSM reinforcement at the Ultimate Limit State (ULS) for debonding failure, assumed to be 1.30 for NSM systems with rough, deformed, or resin-and-sand-coated surfaces;
- $F_{1d} = \frac{k_{k,NSM}}{\gamma_{f3}} F_{1m} = 37.10kN$

The force F_{2d} corresponds to a stress of:

$$f_{max,d}(\ell_{e2d}) = \frac{F_{2d}}{A_F} = 841.60 \text{ MPa}$$

and a strain of:

$$\varepsilon_{\mathrm{fdd}} = \frac{f_{\max,\mathrm{d}}(\ell_{\mathrm{e2d}})}{E_F} = \frac{F_{2\mathrm{d}}}{A_{\mathrm{F}} E_F} = \frac{841.60}{150000} = 0.00561.$$

The maximum strain in each FRP bar is then calculated as:

$$\varepsilon_{\mathrm{fd}} = \min\left(\varepsilon_{\mathrm{fdd}}; \eta_{\mathrm{a}} \frac{f_{\mathrm{ftk}}}{\gamma_{\mathrm{f1}} \cdot E_{\mathrm{F}}}\right) = \min\left(0.00561; 0.95 \frac{2800}{1.25 \cdot 150000}\right) = \left(0.00561; 0.0142\right) = 5.61‰$$

The partial factor applied to the tensile strength of the fibers at the ULS, $\gamma_{\mathrm{f}} = 1.25$, has been defined based on the guidelines provided in the CNR DT 203 document.

The environmental conversion factor, $\eta_{\mathrm{a}} = 0.95$, has been assumed to be the same as that used for the CFRP-EBR system considered as an alternative reinforcement in Example 14.1.3.2. This choice is more conservative compared to the value (1.00) provided for CFRP bars in the CNR DT 203 document. Since this is an external reinforcement application, it is deemed more appropriate to adopt the environmental conversion factor estimated for this type of application.

Even in the case of NSM reinforcement, the flexural failure mechanism can be of two types, depending on whether the maximum tensile strain, $\varepsilon_{\mathrm{fd}}$, s reached in the NSM reinforcement (Zone 1) or the maximum compressive strain, $\varepsilon_{\mathrm{cu}}$, is reached in the concrete (Zone 2) (Figure 14-3).

It is assumed that the section's failure occurs in the NSM reinforcement. Thus, fixing the strain in the reinforcement at $\varepsilon_{\mathrm{fd}} = 5.61‰$, the strains in the other materials can be calculated using the same expressions seen previously (Equations Eq. (14.19), (14.20), (14.21)).

The strain ε_0 present at the time of reinforcement application is neglected, and it is assumed that the strain in the tensile steel reinforcement exceeds the elastic limit (yielded steel reinforcement, so $\sigma_{\mathrm{s1}} = f_{\mathrm{yd}} = 316.67$ MPa) and that the compressed steel remains in the elastic phase ($\sigma_{\mathrm{s2}} = E_{\mathrm{s}}\, \varepsilon_{\mathrm{s2}}$, assuming $E_{\mathrm{s}} = 200000$ MPa). Under these assumptions, the equilibrium equation for section translation is written as follows:

$$\psi \cdot b \cdot x \cdot f_{\mathrm{cd}} + A_{\mathrm{s2}} \cdot \sigma_{\mathrm{s2}} - A_{\mathrm{s1}} \cdot f_{\mathrm{yd}} - n_{\mathrm{f}} \cdot A_{\mathrm{F}} \cdot f_{\mathrm{fdd}} = 0 \qquad (14.25)$$

where the dimensionless coefficient ψ represents the intensity of the resultant compressive stresses relative to $b \cdot x \cdot f_{cd}$ and n_{f} is the number of applied FRP bars.

The equation was solved iteratively by assuming trial values for the position of the neutral axis x, which allows calculating the corresponding value of ψ and solving the equation: when the initial trial value of xxx matches the one calculated from the equation, convergence is achieved. For this case, the following values were obtained:

- $\psi = 0.448$
- $x = 127$ mm

The resulting strain values in the materials confirm the initial assumptions:

- $\varepsilon_{\mathrm{c}} = 1.92$ ‰ < 3.50 ‰,
- $\varepsilon_{\mathrm{s1}} = 5.61$ ‰ > $\varepsilon_{\mathrm{yd}} = f_{\mathrm{yd}} / E_{\mathrm{s}} = 316.67 / 200000 = 1.58$ ‰
- $\varepsilon_{\mathrm{s2}} = 1.46$ ‰ < $\varepsilon_{\mathrm{yd}} = 1.58$ ‰.

The equilibrium equation for rotation relative to the tensile reinforcement is then written as follows:

$$M_{\mathrm{Rd}} = \left[\psi \cdot b \cdot x \cdot f_{\mathrm{cd}} \cdot (d - \lambda \cdot x) + A_{\mathrm{s2}} \cdot E_{\mathrm{s}} \cdot \varepsilon_{\mathrm{s2}} \cdot (d - d_2) + n_{\mathrm{f}} \cdot A_{\mathrm{F}} \cdot f_{\mathrm{fdd}} \cdot (d_1 - 0.5 d_{\mathrm{G}})\right] = 174.83 \mathrm{kNm} \qquad (14.26)$$

where the dimensionless coefficient λ represents the distance of the neutral axis from the extreme compressed fiber of the resultant compressive stresses relative to x, and it was found to be $\lambda = 0.352$.

Therefore, the ultimate moment capacity, M_{Rd} = 174.83 kNm, is greater than the applied moment M_{Sd} for both beams 2.1 and 2.2 (170.10 kNm e 173.80 kNm, respectively).

At this point, it is evaluated whether it is necessary to apply the NSM reinforcement along the entire beam or whether it is sufficient to terminate the bars at the zero-moment sections. For beam 2.1, the zero-moment points are located 0.90 m from the left support and 0.45 m from the right support. Therefore, the distances of the maximum moment section (which is 3.00 m from the left support and 2.50 m from the right support) from the zero-moment sections are 2.10 m and 2.05 m.
Considering the smaller of these two distances as the bond length ℓ_{b} to be used in Equation (14.20) for the calculation of $F_{\mathrm{max,d}}$, a value very close to $F_{2,d}$ (42.05 kN vs 42.30 kN), is obtained, corresponding to a maximum strain in the reinforcement of $\varepsilon_{\mathrm{fd}}$ = 5.58 ‰, slightly lower than the previously calculated value, so the ultimate moment remains essentially unchanged (174.55 kNm) and is greater than the applied moment for beam 2.1 (M_{Sd} = 170.10 kNm).

For beam 2.1, therefore, the solution of applying the NSM reinforcement starting from the zero-moment sections, with a total length of 2.10 m + 2.05 m = 4.15 m (Figure 14-6) is feasible as it ensures compliance with condition (14.1) at the most stressed section.

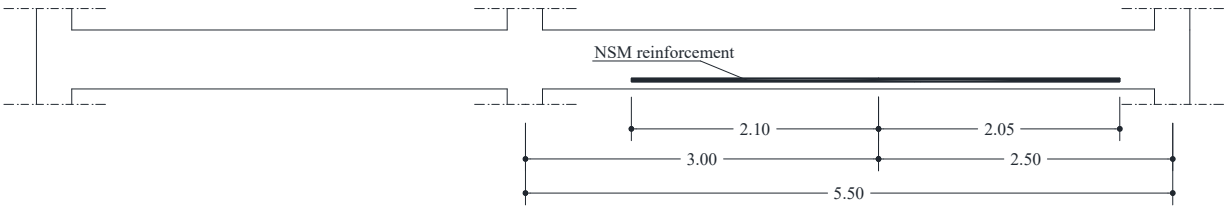

Figure 14-6 – Configuration of the NSM reinforcement for beam 2.1.

Finally, considering the translation of the moment diagram by $0.9d$ = 0.33 m, the same translation is applied to the zero-moment points. Approximating the translation to 0.35 m, the total length of the NSM reinforcement becomes 4.85 m = 4.15m + 0.70m.

Alternatively, if the reinforcement is not to be terminated at the zero-moment sections to reduce the bar length, it is necessary to calculate the maximum design stress in the reinforcement as $f_{\mathrm{max,d}}(\ell_{\mathrm{b}}) = \dfrac{F_{\mathrm{max,d}}(\ell_{\mathrm{b}})}{A_{\mathrm{F}}}$, where ℓ_{b} is the distance of the verification section from the end of the reinforcement.

Figure 14-7, shows the variation of the maximum stress $f_{max,d}(\ell_b)$ in the NSM reinforcement as the bond length ℓ_b increases.

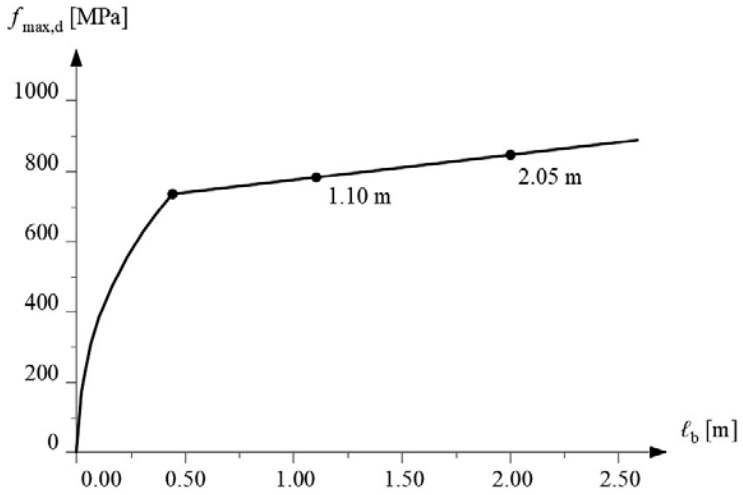

Figure 14-7 – Variation of the maximum stress in the NSM reinforcement with bond length ℓ_b .

For beam 2.1, as already seen in previous examples, the sections where the ultimate moment capacity of the unreinforced beam equals the applied moment are located 0.85 m from the maximum moment section (positioned 3.00 m from the left support). Thus, the minimum length of the NSM reinforcement must be at least 1.70 m = 0.85m + 0.85m.

Based on the trend shown in Figure 14-7, if an additional reinforcement length of 0.25 m beyond these sections is assumed, then at midspan, ℓ_b=1.10m (0.85m + 0.25 m) corresponding to $f_{max,d}$ = 805 MPa and an ultimate moment capacity of 173.3 kNm, which is greater than the midspan applied moment (170.1 kNm).

Thus, the solution of terminating the reinforcement 0.25 m beyond the sections where the ultimate moment capacity of the unreinforced beam equals the applied moment is also valid, and in this case, the total length of the bars would be 2.20m = 1.70m + 0.25m + 0.25m.

Additionally, it is noted that in the sections where ℓ_b = 0.25m, the stress is $f_{max,d}$ =474MPa, and the ultimate moment capacity is 157.3 kNm, which is already about 10% greater than the applied moment.

Even in this reinforcement configuration, considering the translation of the moment diagram by 0.9*d* = 0.33 m, the same translation applies to the reinforcement termination points. Approximating the translation to 0.35 m, the total length of the NSM reinforcement becomes 2.90m = 2.20m + 0.70m.

For beam 2.2, the zero-moment points in the moment diagram are located 0.85 m from the left support and 0.30 m from the right support. Consequently, the distances of the maximum moment section (which is at 3.00 m from the left support and 2.50 m from the right support) from the zero-moment sections are 2.70 m and 2.20 m.

Considering the smaller of these two distances as the bond length ℓ_b to be used in equation (14.20) for calculating $F_{max,d}$, the result is again $F_{max,d}$ = 42.20 kN ≈ $F_{2,d}$, meaning that the ultimate moment capacity coincides with that calculated using equation (14.23), M_{Rd} = 174.60 kNm, which is slightly greater than the maximum applied moment (173.80 kNm). However, it should be noted that the ultimate moment capacity was calculated while neglecting the strain state present in the section before applying the reinforcement, making it a slightly conservative estimate of the actual ultimate moment capacity.

For beam 2.2, if it is decided to apply NSM reinforcement starting from the zero moment sections, the total length is 2.70 m + 2.20 m = 4.90 m. Similarly, for beam 2.2, considering the translation of the moment diagram by 0.9d = 0.33 m, the same translation applies to the zero-moment points. Approximating this translation to 0.35 m, the total length of the NSM reinforcement becomes 4.90m + 0.70m = 5.60 m.

To reduce the reinforcement length, the same approach used for beam 2.1 should be followed, utilizing the variation of maximum stress in the reinforcement as a function of bond length, as shown in Figure 14-7.

14.1.4 Tensile Strengthening Design of a Beam-Column Joint Using the FRP-EBR System

Referring to the perimeter frame located between column rows 1 and 3 of the structural system depicted in Figure 14-1, the strengthening design is developed for the corner perimeter joint, which is not entirely confined, at column 3 on level 1.

The joint verification and strengthening design are performed considering the most critical actions that can be transmitted to the joint. These actions are calculated based on the yielding of the longitudinal reinforcement of the weaker element, whether it is beams or columns, that converges at the joint. Specifically, the shear demand in the horizontal direction for external joints can be evaluated using the following equation:

$$V_{\mathrm{j}} = T - V_{\mathrm{c}} = 197.30\,\mathrm{kN} \tag{14.27}$$

where:

- The tensile force in the beam reinforcement is given by:

$$T = \frac{M_{\mathrm{b}}}{0.9 \cdot (h - c)} = \frac{98.1 \cdot 10^{6}}{0.9 \cdot (500 - 30)} = 231.90\,\mathrm{kN} \tag{14.28}$$

- The bending moment acting on the beam can be calculated based on the equilibrium of the joint as:

$$M_{\mathrm{b}} = \left(\left(\frac{M_{\mathrm{Rd,c}}^{\mathrm{sup}}}{\frac{H_{\mathrm{sup}} - h_{\mathrm{b}}}{2}} \right) \cdot \left(\frac{H_{\mathrm{sup}}}{2} \right) + \left(\frac{M_{\mathrm{Rd,c}}^{\mathrm{inf}}}{\frac{H_{\mathrm{inf}} - h_{\mathrm{b}}}{2}} \right) \cdot \left(\frac{H_{\mathrm{sup}}}{2} \right) \right) \cdot \left(\frac{\left(\frac{L_{\mathrm{b}} - h_{\mathrm{c}}}{3} \right)}{\frac{L_{\mathrm{b}}}{3}} \right) = 98.10\,\mathrm{kN} \tag{14.29}$$

- Moment resistance of the upper column (Level 2): $M_{\mathrm{Rd,c}}^{\mathrm{sup}}$ = 39.80 kNm (calculated for an axial load of 63.90 kN);
- Moment resistance of the lower column (Level 1): $M_{\mathrm{Rd,c}}^{\mathrm{sup}}$ = 48.90 kNm (calculated for an axial load of 131.00 kN);
- H_{sup} = 300 cm;
- H_{inf} = 400 cm;
- L_{b} = 550 cm;
- h_{b} = 50 cm;
- h_{c} = 30 cm;
- The shear force in the column above the joint is given by:

$$V_{\mathrm{c}} = \frac{M_{\mathrm{b}} / 2}{\left(\frac{L_{\mathrm{b}} - h_{\mathrm{c}}}{3} \right) \frac{H_{\mathrm{sup}}}{2}} \cdot \frac{L_{\mathrm{b}}}{3} = 34.60\,\mathrm{kN} \tag{14.30}$$

The bending moment acting on the beam (M_b = 98.10 kNm) at the yielding of the two-column moments is lower than the largest moment resistance of the beam (MRD = 107.70 kNm). Thus, the subassembly exhibits a weak-column mechanism, allowing the use of M_b or the strengthening design. Otherwise, the tensile force in the beam reinforcement T would have to be calculated using the largest moment resistance of the beam.

It is important to note that if the strengthening intervention were designed based on global seismic analyses, the forces in the elements converging at the joint would be those derived from seismic analysis.

The diagonal tensile stress within the joint can be calculated as:

$$\sigma_{\mathrm{nt,Sd}} = -\frac{N}{2A_{\mathrm{j}}} + \sqrt{\left(\frac{N}{2A_{\mathrm{j}}}\right)^2 + \left(\frac{V_{\mathrm{j}}}{A_{\mathrm{j}}}\right)^2} = 2.33\mathrm{MPa} \tag{14.31}$$

where:

- Shear force at the joint: V_j = 197.60 kN;
- Axial load in the upper column: N = 63.90 kN;
- Joint area: $A_j = b_j \cdot h_{jc}$ = 72000 mm^2;
  - Effective joint width (b_j = 300 mm) is taken as the minimum of:
    a) The greater of the column section width (30.0 cm) and the beam section width (30.0 cm);
    b) The smaller of the column and beam section widths, both increased by half of the column section height (45.0 cm);
- Height of the joint core: h_{jc} = 240 mm (distance between the outermost layers of column reinforcement).

The diagonal tensile stress, $\sigma_{nt,Sd}$, within the joint is found to be greater than the diagonal tensile strength of the concrete, which can be calculated as:

$$\sigma_{\mathrm{nt,Rd,c}} = 0.30 \cdot \sqrt{f_{\mathrm{cd}}} = 1.16\mathrm{MPa} \tag{14.32}$$

where:

$$f_{\mathrm{cd}} = \frac{f_{\mathrm{cm}}}{FC \cdot \gamma_c} = \frac{22.5}{1.00 \cdot 1.5} = 15.00\mathrm{MPa} \tag{14.33}$$

with assumed values:

- Concrete compressive strength: f_{cm} =22.5 MPa,
- Confidence factor: FC = 1.00 (based on in-situ investigations of the elements under intervention)
- Partial safety factor for brittle mechanisms: γ_c =1.5

The diagonal compressive stress in the joint can be evaluated as:

$$\sigma_{\mathrm{nt,Sd}} = \frac{N}{2A_{\mathrm{j}}} + \sqrt{\left(\frac{N}{2A_{\mathrm{j}}}\right)^2 + \left(\frac{V_{\mathrm{j}}}{A_{\mathrm{j}}}\right)^2} = 3.22\mathrm{MPa} \tag{14.34}$$

which is found to be less than the compressive strength, calculated as:

$$\sigma_{\mathrm{nc,Rd,c}} = 0.50 \cdot f_{\mathrm{cd}} = 7.50\mathrm{MPa} \tag{14.35}$$

FRP Strengthening Strategy

Since the joint shear demand exceeds the joint shear capacity, FRP strengthening is proposed to enhance the overall shear strength of the joint.

A quadri-axial CFRP fabric system is selected for the strengthening, applied with fiber orientations at 0°, 90°, and ±45° relative to the beam axis. The equivalent reinforcement area of the FRP, A_{f}, is calculated using Equation (4.107):

$$A_{\mathrm{f}} = n_{\mathrm{s}} t_{\mathrm{f}} h_{\mathrm{c}} \cos\theta \cdot \left(1 + \tan\theta + 2\tan^2\theta\right) = 134.50\mathrm{mm}^2 \tag{14.36}$$

where:

- n_{s} =1 (number of reinforced joint faces) (Figure 4-27),
- $\theta = \arctan\left(h_{\mathrm{b}} / h_{\mathrm{c}}\right) = 59°$
- t_{f} = 2·0.053 mm = 0.106 mm (total FRP thickness)

The design strain of the FRP composite, $\varepsilon_{\mathrm{fd}}$, can be calculated using the Equation (4.117):

$$\varepsilon_{\mathrm{fd}} = \min\left\{\eta_{\mathrm{a}} \frac{\varepsilon_{\mathrm{fk}}}{\gamma_{\mathrm{f}}}; 34\left(\frac{f_{\mathrm{cm}}^{2/3}}{A_{\mathrm{f}} E_{\mathrm{f}}}\right)^{0.6}\right\} = 3.44‰ \tag{14.37}$$

with:
Concrete compressive strength: f_{cm} = 25 MPa
FRP elastic modulus: E_{f} = 270000 MPa
Characteristic strain: $\varepsilon_{\mathrm{fk}}$ = 0.01
Partial safety factor for FRP: γ_{f} = 1.3
Environmental conversion factor: η_{a} = 0.80 (External Exposure, Carbon/Epoxy System)

The diagonal tensile strength contribution from the FRP reinforcement is evaluated as (4.110):

$$\sigma_{\mathrm{nt,Rd,f}} = \frac{A_{\mathrm{f}} E_{\mathrm{f}} \varepsilon_{\mathrm{fd}}}{b_{\mathrm{c}} \left(h_{\mathrm{c}} / \sin\theta \right)} = 1.19\mathrm{MPa} \tag{14.38}$$

The design diagonal tensile strength of the strengthened joint is obtained through Equation (4.109):

$$\sigma_{\mathrm{nt,Rd}} = \sigma_{\mathrm{nt,Rd,c}} + \sigma_{\mathrm{nt,Rd,f}} = 2.35\mathrm{MPa} \tag{14.39}$$

Anchorage Considerations for FRP Strengthening

To ensure adequate mechanical anchorage, specific construction details must be adopted, such as U-wrappings with unidirectional fabric at the beam ends (Figure 14-8).

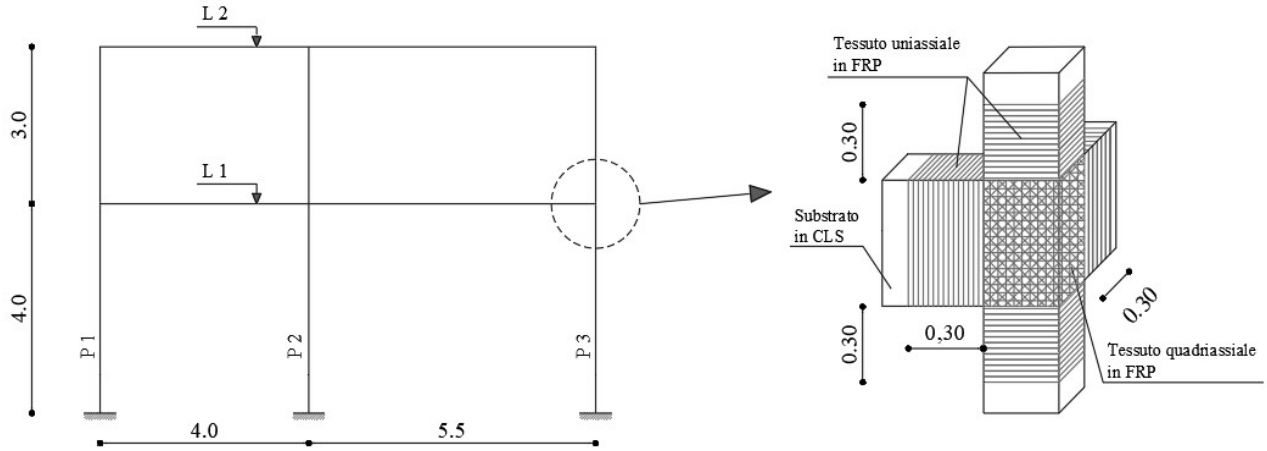

Figure 14-8 – FRP Strengthening Configuration for the Joint (Dimensions in m).

The wrapping of the beam ends with U-jackets may require removing small portions of infill walls, if present.

Alternatively, using mechanical anchors, such as splayed fiber connectors, can significantly reduce disruption to building occupants, allowing for the external application of strengthening to perimeter joints. The design of such anchors follows the guidelines in §4.1.5.

For shear-tension strengthening of beam-column joints, the number of required anchors is determined by verifying:

$$F_{\mathrm{anc,d}}(z) \geq A_{\mathrm{f}} E_{\mathrm{f}} \varepsilon_{\mathrm{fd}} \geq 109.80\mathrm{kN} \tag{14.40}$$

where:

- Effective FRP area A_{f} = 118.2 mm^2 (obtained from (14.36) excluding fibers aligned with the column axis).

In Equation (14.58), the anchored FRP fabric strength, $F_{\mathrm{anc,d}}(z)$, is the strength of the FRP strip obtained from Equation (4.15):

$$F_{\text{anc,d}}(z) = \min\left(k_{\text{k}} \frac{f_{\text{fdm}} b_{\text{f}} t_{\text{f}} + \left[n_{\text{z}}(z) \min\left\{ N_{\text{PO,m}}, N_{\text{DB,k}}, N_{\text{FR,k}} \right\} \right]}{\gamma_{\text{f2}}}; \frac{\eta_{\text{a}} f_{\text{fk}}}{\gamma_{\text{f1}}} b_{\text{f}} t_{\text{f}} \right) = 123.80\text{kN} \quad (14.41)$$

where:

- Reduction factor for anchorage applications: $k_{\text{k}} = 0.7$
- FRP design stress for beam/column nodes: $f_{\text{fdm}} = \varepsilon_{\text{fd}} E_{\text{f}} = 0.00344 \cdot 270000 = 929$ Mpa, with $b_{\text{f}} \cdot t_{\text{f}} = A_{\text{f}} = 118.2$ mm^2
- Number of connectors applied per FRP strip: $n_{\text{z}}(z) = 4$,
- Partial safety factor for FRP at ULS for anchorage: $\gamma_{\text{f2}} = 1.30$ per section § 3.4.1.
- Characteristic tensile strength of FRP: $f_{\text{fk}} = 2700$ MPa
- Environmental conversion factor: $\eta_{\text{a}} = 0.85$
- Partial safety factor for the Ultimate Limit State (ULS) for tensile failure of the reinforcement (Ref. § 3.4.1): $\gamma_{\text{f1}} = 1.30$.

Since the splayed fiber connectors are assumed to be inclined at $\psi = 90^{\text{o}}$, the pull-out (PO) and slip (S) failure modes do not need to be evaluated. Instead, the calculation focuses on the other failure mechanisms, particularly the tensile rupture strength of the splayed fiber, $N_{\text{FR,k}}$:

$$N_{\text{FR,k}} = k_{\text{fan}} \frac{\psi}{\pi} A_{\text{fc}} \eta_{\text{a}} f_{\text{fak}} = 30.00\text{kN} \quad (14.42)$$

where:

- $\eta_{\text{a}} = 0.85$ (environmental factor)
- $f_{\text{fak}} = 1800$ Mpa (characteristic tensile strength of the fiber anchor);
- $k_{\text{FAN}} = 0.5$ (anchorage factor)
- $\psi = 90°$ (converted to radians: π)
- $A_{\text{fc}} = 78.5$ mm^2 (cross-sectional area of the anchor, corresponding to a 10 mm diameter)

Debonding Resistance of the Fiber Anchor from the FRP Reinforcement
The debonding resistance, $N_{\text{DB,k}}$, of the splayed fiber anchor from the FRP reinforcement is:

$$N_{\text{DB,k}} = F_{\text{DB,k}} \frac{\sin\lambda}{\lambda} = 53.00\text{kN} \quad (14.43)$$

where:

- $F_{\text{DB,k}} = \lambda L_{\text{s}}^2 \tau_{\text{Rb,k}} = 55.60\text{kN}$;
- $\tau_{\text{Rb,k}} = \frac{1}{2}\sqrt{f_{\text{Rc,k}} f_{\text{Rt,k}}} = 10.60\text{MPa}$;
- $f_{\text{Rc,k}} = 30$ MPa;
- $f_{\text{Rt,k}} = 15$ MPa;

- $\lambda = 30°$ (0.524 rad);
- $L_s = 100$ mm.

Other Characteristics of the Splayed Fiber Anchors are:

- Embedment depth of the anchor shank: $h_e = 100$ mm;
- Drilled hole depth for the anchor:= 120 mm;
- Anchor hole diameter: $d_h = 14$ mm;
- Semi-opening angle of the fiber spread: $\lambda = 30°$;
- Curvature radius of the fiber bend: $R_b = 10$ mm.

The FRP strengthening layout with splayed fiber anchors is illustrated in Figure 14-9.

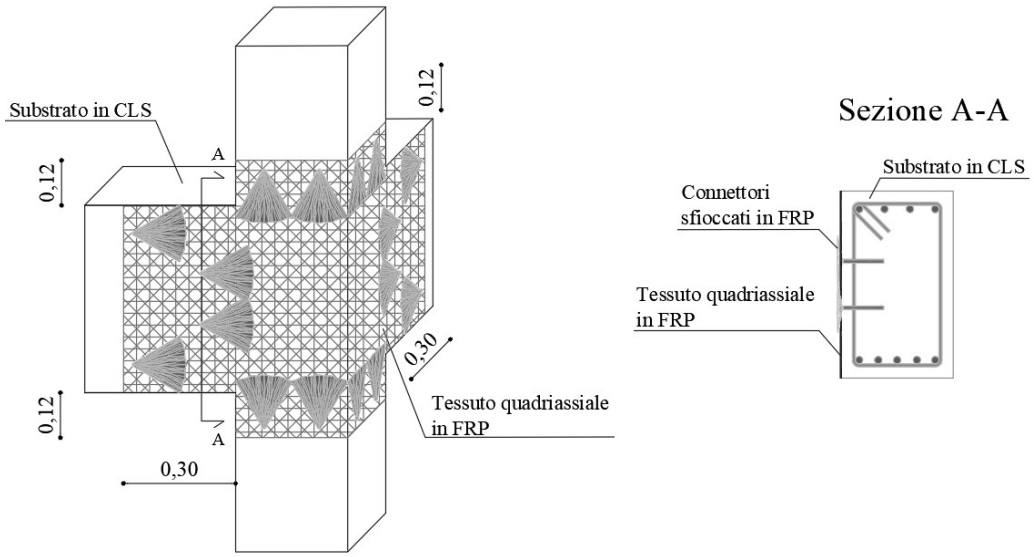

Figure 14-9 – FRP Strengthening Configuration with Splayed Fiber Anchors (Dimensions in m).

The required number of anchors per beam is determined from the calculations (4 anchors per beam in this case).

Each column face receives half the number of beam anchors (2 anchors per column face).

Alternative Anchor Configuration and Design Optimization

If a fixed number of anchors is chosen, the strength of the reinforced joint can be recalculated by equating capacity and demand in Eq.(14.40) and solving for the design strain.
For example, if only 2 anchors per beam are used, the anchored FRP fabric strength, $F_{anc,d}(z)$, from (14.41) is $F_{anc,d}(z) = 91.40$ kN, leading to:

$$\varepsilon_{fdd,anc} = \frac{F_{anc,d}(z)}{A_f E_f} = 2.86‰ \tag{14.44}$$

Diagonal Tensile Strength Contribution from the FRP Reinforcement

The contribution of the FRP system to the diagonal tensile strength is evaluated using Equation (4.110):

$$\sigma_{\mathrm{nt,Rd,f}} = \frac{A_{\mathrm{f}} E_{\mathrm{f}} \cdot \varepsilon_{\mathrm{fdd,anc}}}{b_{\mathrm{c}} \left(h_{\mathrm{c}} / \sin\theta \right)} = 0.99\mathrm{MPa} \tag{14.45}$$

The design diagonal tensile strength of the strengthened joint is calculated using Equation (4.109):

$$\sigma_{\mathrm{nt,Rd}} = \sigma_{\mathrm{nt,Rd,c}} + \sigma_{\mathrm{nt,Rd,f}} = 2.15\mathrm{MPa} \tag{14.46}$$

Final Strength Evaluation of the Strengthened Joint

The strengthened joint's diagonal tensile strength is lower than the maximum shear demand ($\sigma_{\mathrm{nt,Sd}}$ = 2.34 MPa), However, it is 85% higher than the capacity of the unstrengthened joint.

At this strength level, the shear force within the joint, V_{j}, and the bending moment on the beam, M_{b}, corresponding to 90% of the maximum demand calculated using Eq.(14.27).

14.1.5 Strengthening Design for Columns Using FRP-EBR System

The axial-flexural verification of the columns in the examined structure is performed according to current regulations.

Table 14-5 - Design Axial Load and Bending Moment in the Columns

Level	Column	Section	N_{Sd} [kN]	M_{Sd} [kN m]	Eccentricity [cm]	Radius of Gyration [cm]
1	Left lateral	Base	-270.50	7.10	-2.62	5.88
	Left lateral	Top	-279.50	-15.17	5.43	5.88
	Central	Base	-836.70	13.97	-1.67	5.88
	Central	Top	-845.70	-23.33	2.76	5.88
	Right lateral	Base	-383.60	-13.25	3.45	5.88
	Right lateral	Top	-392.60	31.01	-7.90	5.88
2	Left lateral	Base	-129.50	26.27	-20.29	5.88
	Left lateral	Top	-136.30	-15.43	11.32	5.88
	Central	Base	-409.20	45.67	-11.16	5.88
	Central	Top	-416.00	-47.10	11.32	5.88
	Right lateral	Base	-184.30	-58.02	31.48	5.88
	Right lateral	Top	-191.10	64.12	-33.55	5.88

Based on the design axial force and bending moment, a distinction is made between:

- Axial-flexural loading with small eccentricity (when the pressure center is smaller or equal to the radius of gyration).
- Axial-flexural loading with large eccentricity (when the eccentricity is larger than the radius of gyration).

For columns subjected to axial-flexural loading with small eccentricity, the following inequality must be verified:

$$N_{Sd} \leq N_{Rd} \tag{14.47}$$

For columns subjected to axial-flexural loading with large eccentricity, the N-M failure domain of the section is constructed using the mechanical properties of the materials, verifying that the design axial force, N_{Sd}, and bending moment, M_{Sd}, correspond to a point within this domain (Table 14-5).

Table 14-6 - Verification of Axial Strength for Columns

Level	Column	Section	N_{Sd} [kN]	N_{Rd} [kN]	$N_{Rd} > N_{Sd}$
1	Left lateral	Base	-270.50	-1822.47	YES
	Left lateral	Top	-279.50	-1822.47	YES
	Central	Base	-836.70	-1822.47	YES
	Central	Top	-845.70	-1822.47	YES
	Right lateral	Base	-383.60	-1822.47	YES

Table 14-7 - Verification of Bending Strength for Columns

Level	Column	Section	N_{Sd} [kN]	M_{Sd} [kN m]	Verification Satisfied?
1	Right lateral	Top	-392.60	31.01	YES
2	Left lateral	Base	-129.50	26.27	YES

Left lateral	Top	-136.30	-15.43	YES
Central	Base	-409.20	45.67	YES
Central	Top	-416.00	-47.10	YES
Right lateral	Base	-184.30	-58.02	YES
Right lateral	Top	-191.10	64.12	NO

Column Strengthening Strategy
The verification fails for the right lateral column at level 2 (Table 14-7), indicating that strengthening is required for this column using the FRP-EBR system to enhance its axial and flexural capacity.

14.1.5.1 Strengthening of Axially Loaded Columns with Large Eccentricity

This section presents the flexural-strengthening design for the right lateral column at level 2**,** which did not pass the axial-flexural verification under the new loading conditions (Table 14-7).

A flexural-strengthening solution is proposed using one or more layers of unidirectional CFRP fabric with the following geometric and mechanical properties:

1. Equivalent thickness per layer: $t_{f,1}$= 0.167 mm;
2. Layer width: $b_{f,1}$= 250 mm;
3. Elastic modulus: E_f = 270000 MPa;
4. Characteristic tensile strength: f_{fk} = 2700 MPa.

Additionally, a CFRP confinement system is proposed, consisting of one layer of the same CFRP fabric used for flexural strengthening, to prevent premature debonding from the substrate.

- The partial safety factor for FRP tensile rupture, γ_{f1}, is assumed to be 1.30.
- The environmental reduction factor, η_a, is set to 0.80 (Table 3-3, § 3.5.1).

Evaluation of Compressive Strength for Confined Concrete
Due to confinement, the design compressive strength of confined concrete, f_{ccd}, is calculated using Equation (4.93):

$$\frac{f_{ccd}}{f_{cd}} = 1 + \frac{2.6}{\gamma_{Rd}} \cdot \left(\frac{f_{l,eff}}{f_{cd}} \right)^{2/3} \tag{14.48}$$

where:

- f_{cd} = design compressive strength of unconfined concrete, determined according to current regulations.
- $f_{l,eff}$ effective confinement pressure, which depends on the section shape and strengthening method.

The effective confinement pressure is obtained using Equation (4.94):

$$f_{l,eff} = k_{eff} \cdot f_l = k_{eff} \cdot \left(\frac{1}{2} \cdot \rho_f \cdot E_f \cdot \varepsilon_{fd,rid} \right) \tag{14.49}$$

where:

- k_{eff} (≤ 1) is the efficiency coefficient from Equation (4.96)

$$k_{eff} = k_H \cdot k_V \cdot k_\alpha \tag{14.50}$$

- ρ_f is the geometric reinforcement ratio for a rectangular section with continuous wrapping:

$$\rho_f = \frac{2 \cdot t_f \cdot (b + h)}{b \cdot h} \tag{14.51}$$

where

- b and h = the width and depth of the column;
- E_f = FRP elastic modulus;
- $\varepsilon_{fd,rid}$ is the reduced design strain of the FRP, calculated using Equation (4.99):

$$\varepsilon_{fd,rid} = \min\{\eta_a \cdot \varepsilon_{fk} / \gamma_{fl};\ 0.004\} = 0.004 \tag{14.52}$$

Efficiency Coefficients for FRP Confinement

- The vertical efficiency coefficient, k_V, is 1.0 for continuous wrapping along the column's longitudinal axis.
- The orientation efficiency coefficient, k_α, is 1.0, assuming the fibers are perpendicular to the column axis.
- The horizontal efficiency coefficient, k_H, for rectangular sections is calculated using Equation (eq. (4.102)):

$$k_H = 1 - \frac{b'^2 + h'^2}{3 \cdot A_g} \tag{14.53}$$

where:

- b' and h' are the effective section dimensions, following Figure 4-24, § 4.6.2.1.2;
- A_g is the gross cross-sectional area.

Before applying CFRP, it is necessary to round the section corners, ensuring a minimum curvature radius of 20 mm, as specified in §4.6.2.1.2 (2). Thus, it is assumed:

- b' = 260 mm
- h' = 260 mm

Application to the Right Lateral Column at Level 2

Applying the procedure outlined above, the design compressive strength of confined concrete f_{ccd} is calculated using one layer of CFRP fabric (Table 14-8). However, the confinement is not sufficient to significantly increase the compressive strength, in accordance with § 4.6.2 (7).

Table 14-8 - Calculation of Confined Concrete Strength

Section	n_f	k_H	k_{eff}	ρ_f	$f_{l,eff}$ [MPa]	f_{ccd} [MPa]
Top	1	0.50	0.50	0.0022	0.60	21.37*

*: Note: The design compressive strength f_{ccd} is equal to f_{cd} (16.67 Mpa) since $f_{l,eff} / f_{cd}$ is not greater than 0.05.

Iterative Approach for Strengthening Design

Since a single layer of CFRP does not provide effective confinement, an iterative procedure is followed as recommended in Appendix E.

Table 14-9 and Table 14-10) summarize the numerical values obtained during the iterative process. The verification is satisfied by applying two (2) layers of CFRP.

Table 14-9 - Strengthening Design Parameters

Section	n_{Sd}	m_{Sd}	μ_s	u	n_f	μ_f
Top	0.159	0.198	0.134	1	2	0.123

Table 14-10 - Strengthened Section Verification

Section	η_0	η_1	η_2	η_3	η	Failure Mode	$w_{(2)}(\eta)$	m_{Rd} (n_{Sd})	$m_{Rd} > m_{Sd}$
Top	-0.134	0.156	0.279	0.595	0.282	2	0.100	0.296	YES

14.2 EXAMPLE 2 – STRENGTHENING OF A REINFORCED CONCRETE COLUMN USING FRP-EBR IN SEISMIC CONDITIONS

This example considers a reinforced concrete column extracted from a frame structure of an RC building located in a seismic zone. The column has the following geometric dimensions and material properties, derived from original design drawings and in-situ testing:

- Column dimensions**:**
  - Width B = 40 cm, Height H = 40 cm
  - Concrete cover: d_1=d_2=3 cm,
  - Clear height: l = 3.0 m
- Longitudinal reinforcement:
  - Bottom reinforcement*:* A_{s1} = 6.03 cm^2 (3ϕ16),
  - Top reinforcement*:* A_{s2} = 6.03 cm^2 (3 ϕ 16)
- Transverse reinforcement (stirrups):
  - Ties: ϕ 8/30 cm (8 mm diameter stirrups at 30 cm spacing)
- Concrete properties:
  - Compressive strength: f_{cm} =20.00 MPa,
  - Partial safety factor: γ_c=1.5,
  - Confidence factor: FC=1.2;
  - Design strength: f_{cd} = 11.1 MPa;
- Steel properties:
  - Yield strength: f_{ym} = 380.00 MPa,
  - Partial safety factor: γ_s = 1.15,
  - Confidence factor: FC =1.2,
  - Design strength: f_{yd} = 275.4 MPa.

14.2.1 Shear Strengthening Design

In seismic conditions, the column must be ductile, ensuring that shear failure does not occur before the formation of plastic hinges. The design shear force corresponding to the plasticization of the end sections is calculated as:

$$V_{\mathrm{Sd}} = \frac{M_{\mathrm{Rd}}}{L_{\mathrm{V}}} = \frac{147.0kNm}{1.5m} = 98.0kN$$

where:

- L_V = $l/2$ = 1.5 m (shear span).

The shear resistance for existing structures is calculated according to seismic design regulations, using the following formulation:

$$V_{\mathrm{Rd}} = \frac{1}{\gamma_{\mathrm{el}}}\left[V_{\mathrm{N}} + \left(1 - 0.05\min\left(5;\mu_{\Delta\mathrm{pl}}\right)\right)\left(V_{\mathrm{C}} + V_{\mathrm{W}}\right)\right] \tag{14.54}$$

where:

- γ_{el} = 1.15 (elastic behavior factor)
- d = 370 mm (effective depth of tension reinforcement)
- A_c = b d = 148000 mm^2 (column effective cross-sectional area)

- $\rho_{tot} = 0.01$(total reinforcement ratio)
- $L_V = 1500$ mm (shear span)
- $N = 320.00$ kN (axial load on the column)
- $x = (0.25 + 0.85\ N/(A_c f_c))h = 134$ mm, (neutral axis depth, simplified per seismic code recommendations)
- $\rho_s = 0.0008$ (transverse reinforcement ratio)
- $z = 0.9d = 333$ mm (lever arm)
- $V_N = \frac{h-x}{2L_V}\min\left(N, 0.55A_c f_c\right) = 28.30\text{kN}$
- $V_C = 0.16\max\left(0.5, 100\rho_{tot}\right)\left(1 - 0.16\min\left(5, \frac{L_V}{h}\right)\right)\sqrt{f_c}\,A_c = 31.70\text{kN}$
- $V_S = \rho_s b z f_y = 30.70\text{kN}$

In the linear elastic zone (assuming $\mu_{\Delta pl} = 0$ in Equation (14.54)), the shear resistance is:

$$V_{Rd} = 79.00 \text{ kN}.$$

Since the shear resistance is lower than the shear demand ($V_{Rd} < V_{Sd}$), a strengthening system must be designed to prevent shear failure before plastic hinge formation.

A CFRP unidirectional fabric (wet lay-up system) is selected for use in a full-wrap configuration along the entire length of the column, with the following geometric and mechanical properties:

- Equivalent layer thickness: 0.167 mm;
- Elastic modulus in fiber direction: $E_f = 270000$ MPa;
- Characteristic tensile strength: $f_{fk} = 2700$ MPa

Strengthening Configuration

The strengthening system is assumed to consist of two layers of CFRP fabric ($n_f = 2$), applied in discontinuous strips with:

- Strip width: $b_f = 100$ mm
- Strip spacing: $p_f = 200$ mm

The next step is to verify whether this configuration satisfies the inequality $V_{Rd} \geq V_{Sd}$ (14.1).

FRP Contribution to Shear Resistance

For a full-wrap configuration on a rectangular section, the shear resistance contribution, $V_{Rd,f}$, from FRP is evaluated using Mörsch's truss analogy, using the following equation (4.77):

$$V_{Rd,f} = \frac{1}{\gamma_{Rd}} f_{fed} A_{fv} \frac{0.9d}{p_f}(\cot\theta + \cot\beta)\sin^2\beta \qquad (14.55)$$

where:

- Total FRP thickness*:* $t_f = 2\ 0.167 = 0.334$ mm

- Effective FRP area: $A_{fv} = 2\ t_f\ b_f = 66.80\ mm^2$
- Model safety factor: $\gamma_{Rd} = 1.20$

Effective Design Tensile Strength of FRP

For full-wrap FRP on a rectangular section, the effective design tensile strength of the strengthening system is calculated as:

$$f_{fed} = f_{fdd} \cdot \left[1 - \frac{1}{6} \cdot \frac{l_e \cdot \sin\beta}{\min\{0.9 \cdot d, h_w\}}\right] + \frac{1}{2}(\phi_R \cdot f_{fd} - f_{fdd}) \cdot \left[1 - \frac{l_e \cdot \sin\beta}{\min\{0.9 \cdot d, h_w\}}\right] = 734.7\text{MPa} \qquad (14.56)$$

where:

- $\frac{r_c}{b} = 0.4$
- $\phi_R = 0.2 + 1.6 \cdot \frac{r_c}{b} = 0.84$

The maximum stress that the composite can sustain without end debonding failure, f_{fdd}, is calculated as:

$$f_{fdd} = \frac{k_b}{\gamma_{f2}} \cdot \sqrt{\frac{2E_f \Gamma_{Fk}}{t_f}} = 491.03\text{MPa} \qquad (14.57)$$

where:

- $\gamma_{f2} = 1.3$ (partial factor for Ultimate Limit State, SLU),
- $k_b = \sqrt{\frac{2 - b_f / b}{1 + b_f / b}} = 1.18$ characteristic fracture energy factor.
- Γ_{FK} is the characteristic fracture energy, determined as:

$$\Gamma_{Fk} = \frac{k_{Gk}}{4} \frac{\sqrt{f_{cm} f_{ctm}}}{FC} \cdot s_u = 0.18\text{N/mm} \qquad (14.58)$$

assuming:

- $k_{Gk} = 0.60$ (for wet lay-up FRP systems),
- $s_u = 0.25$ mm (slip displacement at peak stress),
- $f_{ctm} = 0.3 \cdot (f_{ck})^{2/3} = 0.3 \cdot (f_{cm} - k)^{2/3} = 1.65\text{MPa}$
- k= 7 (based on Guidelines for In-Place Concrete Strength Assessment, assuming 4-6 concrete compression tests were performed).

The design rupture stress of the composite, f_{fd}, used in Equation (14.62) is:

$$f_{fd} = \eta_a \cdot \frac{f_{fk}}{\gamma_{f1}} = 0.95 \cdot \frac{2700}{1.3} = 1973\ \text{MPa}$$

where:

- Partial safety factor: γ_{fl} = 1.30,
- Environmental conversion factor: η_a = 0.95.

Design Anchorage Length

The optimal design anchorage length, ℓ_{ed}, is calculated as:

$$\ell_{ed} = \max\left\{100\,\text{mm};\ \gamma_{Rd}\frac{\pi}{2}\sqrt{\frac{E_f t_f \cdot s_u}{f_{bm}}}\right\} = \max\left\{100\,\text{mm};163.3\,\text{mm}\right\} = 163.30\text{mm} \qquad (14.59)$$

where:

- γ_{Rd} = 1.20 (model factor),
- $f_{bm} = \frac{k_{Gm}}{2}\frac{\sqrt{f_{cm} f_{ctm}}}{FC} = 3.00\text{MPa}$
- k_{Gm} = 1.25 (for wet lay-up FRP systems).

For calculation of f_{ed} the anchorage length is approximated to $\ell_{ed} = 170mm$.

The shear contribution of the composite is equal to:

$$V_{Rd,f} = \frac{1}{1.2}\cdot 734.7 \cdot 66.8 \cdot \frac{0.9\cdot 370}{150}(\cot 45° + \cot 90°)\sin^2 90° = 90.8\text{kN} \qquad (14.60)$$

FRP contribution is added to the total shear capacity. Thus, the shear capacity of the strengthened column, V_{Rd}, is calculated as:

$$V_{Rd} = \frac{1}{\gamma_{el}}\left[V_N + \left(1 - 0.05\min\left(5;\mu_{\Delta pl}\right)\right)\left(V_C + V_S + V_{Rd,f}\right)\right] \qquad (14.61)$$

where:

- V_C=31.70 kN (shear contribution of concrete),
- V_S=30.70 kN (shear contribution of transverse reinforcement),
- V_N=28.30 kN (shear contribution of axial load),
- Elastic limit factor: γ_{el}=1.15.

Verification of Strengthened Column

In the elastic range ($\mu_{\Delta pl}$ = 0) the shear resistance of the strengthened element is:
V_{Rd} = 157.90 kN.
In plastic ductility demand of $\mu_{\Delta pl}$ = 5, the shear resistance of the strengthened element is:
V_{Rd} = 124.60 kN.

Since the shear resistance in both cases is greater than the shear demand (98.00 kN), the verification is satisfied.

14.2.2 Confinement for Ductility of Axially Loaded and Bending Members

The ductile behavior of the element under cyclic loading conditions is crucial. The goal is to increase the ductility while only slightly enhancing the strength of the reinforced concrete (RC) column subjected to axial load and bending (high eccentricity).

The ultimate curvature of a bent-compressed section can be estimated by assuming a classic parabolic-rectangular stress-strain relationship for confined concrete, where the ultimate strain, ε_{ccu}, is amplified as follows:

$$\varepsilon_{ccu} = 0.0035 + 0.015 \cdot \sqrt{\frac{f_{l,eff}}{f_{cd}}} \tag{14.62}$$

where

- f_{cd} = design compressive strength of unconfined concrete,
- $f_{l,eff}$ = effective confinement pressure.

The formulas for calculating the effective confinement pressure, $f_{l,eff}$ are similar to those used in §14.1.5.1, except for the reduced design strain of the fiber-reinforced polymer (FRP) composite, which is estimated as:

$$\varepsilon_{fd,rid} = \min\left(\eta_a \cdot \frac{\varepsilon_{fk}}{\gamma_{fl}}, 0.6 \cdot \varepsilon_{fk}\right) = 0.006 \tag{14.63}$$

Before applying the CFRP confinement system, it is essential to round the column corners to a minimum radius of 20 mm, as required by §4.6.2.1.2(2). Thus, the adjusted section dimensions are b' = 360 mm and h' = 360 mm.

By applying the procedure described in §14.1.5.1 the ultimate strain of the confined concrete, ε_{ccu}, is determined for a single layer of CFRP fabric. Based on this calculation approach, Table 14-11, summarizes the numerical values of the confinement parameters.

Table 14-11 – Confinement Parameters for the Strengthened Column

Section	n_f	k_H	k_{eff}	ρ_f	$f_{l,eff}$ [MPa]	ε_{ccu}
Top	1	0.46	0.46	0.0017	0.62	0.007

This confinement enhances ductility by increasing the ultimate strain of the concrete.

14.3 EXAMPLE 3 – FLEXURAL STRENGTHENING OF A REINFORCED CONCRETE BEAM USING FRP-EBR SYSTEM

14.3.1 Strengthening with FRP-EBR System

A reinforced concrete (RC) beam extracted from a frame structure is analyzed for flexural strengthening using an externally bonded reinforcement (EBR) FRP system. The beam has the following geometric and material properties, obtained from original design drawings and in-situ testing:

- Cross-section dimensions:
  - Width B = 30 cm, Height H = 50 cm, concrete cover d_1=d_2=3 cm,
  - Span length: l = 4.50 m
- Longitudinal reinforcement:
  - Bottom Reinforcement: A_{s1} = 8.04 cm^2 (4ϕ16),
  - Top Reinforcement: A_{s2} = 4.02 cm^2 (2ϕ16)
- Stirrups ϕ8/15 cm
- Concrete compressive strength: f_{cm} = 25.00 MPa
- Steel yield strength: f_{ym} = 440.00 MPa.

Load and Moment Calculation
Due to the low stiffness of the columns supporting the beam, the loading scheme is approximated as a simply supported beam.

The factored load per unit length in the ultimate limit state (ULS) is:

$$q_d = 64.0 \text{ kN/m}$$

The corresponding maximum internal forces are:

- Maximum bending moment in span: $M_{sd} = q_d \cdot \frac{l^2}{8}$ = 162.00 kNm,
- Maximum shear force at supports: $V_{sd} = q_d \cdot \frac{l}{2}$ = 144.0 kN.

Calculation of the Existing Section's Flexural Capacity
For the flexural resistance calculation, the following design material properties are considered:

- Concrete: f_{cm} =25.00 MPa, γ_c = 1, FC=1.20, f_{cd}=20.80 MPa;
- Steel: f_{ym} = 440.00 MPa, γ_s = 1, FC =1.20, f_{yd} = 366.70 MPa.

Using Equations (14.8) and (14.9) the moment resistance of the existing section is obtained:

$$M_{Rd} = 131.40 \text{ kNm}.$$

Since $M_{Rd} < M_{Sd}$, an increase in flexural resistance of 23% is required.

Strengthening Solution Using FRP-EBR
A flexural strengthening intervention is designed using a wet-lay up unidirectional CFRP fabric applied in the tensile zone, with the following geometric and mechanical properties:

- Equivalent thickness per layer: $t_{f,1}$= 0.337 mm;
- Layer width: b_f = 30 cm (equal to the beam width b);
- Elastic modulus in fiber direction: E_f = 252000 MPa;
- Characteristic tensile strength: f_{fk} = 3500 MPa;
- FRP system classification: C210C (According to the "Guidelines for the Identification, Qualification, and Acceptance Control of Fiber-Reinforced Polymer (FRP) Composites for Strengthening Existing Structures").

Since one layer of CFRP fabric is assumed (n_f = 1), it is necessary to verify whether this strengthening configuration satisfies the inequality $M_{Rd} > M_{Sd}$ (14.1).

Design Verification of the Maximum Usable Strain
The maximum design strain that the FRP composite can sustain, ε_{fd}, is evaluated using Equation (4.51):

$$\varepsilon_{fd} = \min\left\{\eta_a \cdot \frac{\varepsilon_{fk}}{\gamma_{f1}}, \varepsilon_{fdd,2}\right\} = \varepsilon_{fdd,2} = 3.61‰ \tag{14.64}$$

where:

$$\eta_a \cdot \frac{\varepsilon_{fk}}{\gamma_{f1}} = \eta_a \cdot \frac{f_{fk}}{\gamma_{f1}} \frac{1}{E_f} = 0.95 \cdot \frac{3500}{1.3} \cdot \frac{1}{252000} = 0.0101 \tag{14.65}$$

where:

- Partial factor for the tensile strength of the fibers at the Ultimate Limit State, γ_{f1} = 1.30 (Table 3-1, §3.4.1)
- Environmental factor, η_a = 0.95 (Table 3-3, §3.5.1).

Regarding the resistance of the composite against Mode 2 debonding failure, $f_{ffd,2}$, the following results were obtained:

$$f_{fdd,2} = \frac{k_q k_b}{\gamma_{f2}} \sqrt{\frac{2E_f \frac{k_{Gk,2}}{4FC}\sqrt{f_{cm} f_{ctm}} \cdot s_u}{t_f}} = 909.40\text{MPa} \tag{14.66}$$

$$\varepsilon_{fdd,2} = \frac{f_{fdd,2}}{E_f} = \frac{909}{252000} = 3.61‰ \tag{14.67}$$

where:

- $k_{Gk,2}$ = 1.60
- k_q = 1.25
- s_u = 0.25 mm
- $k_b = \max\left(1, \sqrt{\frac{2 - b_f / b}{1 + b_f / b}}\right) = \max(1, 0.7) = 1$
- $t_f = t_{f,1}$= 0.337 mm

- $f_{cm} = 25.00\text{MPa}$
- $f_{ctm} = 0.3 \cdot \left(f_{ck}\right)^{2/3} = 0.3 \cdot \left(f_{cm} - k\right)^{2/3} = 2.06\text{MPa}$
- k =7 (based on the Guidelines for the Evaluation of In-Situ Concrete Properties, under the assumption that between 4 and 6 tests were conducted for the characterization of the concrete's compressive strength).
- γ_{f2} = 1.30 (Table 3-1, §3.4.1)
- FC = 1.20

Flexural Failure Mechanism
The flexural failure mechanism can be classified into two types (refer to Figure 14-3), depending on whether:

- The maximum tensile strain in the FRP reinforcement is reached (Zone 1) or
- The maximum compressive strain in the concrete, ε_{cu}, is reached (Zone 2).

For this case, failure is assumed to occur on the FRP reinforcement side.
Thus, the strain in the FRP reinforcement is set to its design value:

$$\varepsilon_{fd} = \varepsilon_{fdd} = 3.61\ ‰$$

Using Equations (14.6), (14.7), and (14.8), the strains in the other materials are calculated.

To ensure safety, the initial strain ε_0, present at the time of reinforcement application, is neglected. It is assumed that:

- The tensile steel reinforcement undergoes yielding, meaning:

$$\sigma_{s1} = f_{yd} = 366.67\ \text{MPa}$$

- The compressed steel remains in the elastic phase**,** so:

$$\sigma_{s2} = E_s \varepsilon_{s2} \text{ with } E_s = 200000\ \text{MPa}$$

Under these assumptions, the equilibrium equation for translational forces in the section is written, as previously done in Equation (14.9):

$$\psi \cdot b \cdot x \cdot f_{cd} + A_{s2} \cdot \sigma_{s2} - A_{s1} \cdot f_{yd} - A_f \cdot f_{fdd,2} = 0 \qquad (14.68)$$

where the dimensionless coefficient ψ represents the intensity of the resultant compressive stresses relative to $b \cdot x \cdot f_{cd}$.

Iterative Calculation for the Neutral Axis Position
The equation was solved iteratively, assuming trial values for the position of the neutral axis (x), which allowed for the calculation of the corresponding ψ coefficient.
The equation converged when the assumed x value matched the computed x value. Final values obtained are:

- ψ = 0.404
- x = 120 mm

The following material strains confirmed the initial hypotheses:

- Concrete strain: $\varepsilon_c = 1.14$ ‰ < 3.50 ‰,
- Tensile steel strain: $\varepsilon_{s1} = 3.32$ ‰ > $\varepsilon_{yd} = f_{yd} / E_s = 266.7 / 200000 = 1.83$ ‰
- Compressed steel strain: $\varepsilon_{s2} = 0.85$ ‰ < $\varepsilon_{yd} = 1.83$ ‰.

Moment Capacity Verification
Next, the equilibrium equation for rotational forces about the tensile reinforcement was written, as previously done in Equation (14.11):

$$M_{\mathrm{Rd}} = \left[\psi \cdot b \cdot x \cdot f_{cd} \cdot (d - \lambda \cdot x) + A_{s2} \cdot E_s \cdot \varepsilon_{s2} \cdot (d - d_2) + A_f \cdot f_{fdd,2} \cdot d_1)\right] = 169.10\mathrm{kNm} \quad (14.69)$$

where the dimensionless coefficient λ represents the distance of the neutral axis from the extreme compressed fiber, normalized by x. The final result obtained was $\lambda = 0.349$.

Thus, the flexural resistance of the strengthened section is:

$$M_{\mathrm{Rd}} > M_{\mathrm{Sd}} = 162.0 \text{ kNm}$$

This confirms that the FRP reinforcement successfully increases the flexural resistance to meet the required demand.

Anchorage Verification of the FRP Reinforcement
The anchorage verification must be conducted by referencing the maximum tensile stress in the FRP reinforcement at the anchorage section:

$$f_{\mathrm{fdd}} = \frac{k_{\mathrm{b}}}{\gamma_{\mathrm{f2}}} \cdot \sqrt{\frac{2 E_{\mathrm{f}} \Gamma_{\mathrm{Fk}}}{t_{\mathrm{f}}}} = 445.50\mathrm{MPa} \quad (14.70)$$

$$\Gamma_{\mathrm{Fk}} = \frac{k_{\mathrm{Gk}}}{4} \frac{\sqrt{f_{\mathrm{cm}} f_{\mathrm{ctm}}}}{FC} \cdot s_{\mathrm{u}} = 0.224\mathrm{N/mm} \quad (14.71)$$

where, in addition to previously defined symbols:

- $k_{\mathrm{Gk}} = 0.60$ for wet-lay-up systems.

The optimal anchorage length, ℓ_{ed}, is computed using Equation (4.1), assuming $\Gamma_{\mathrm{Fm}} = \frac{1}{2} f_{\mathrm{bm}} s_{\mathrm{u}}$, as:

$$\ell_{\mathrm{ed}} = \max\left\{100\,\mathrm{mm};\ \gamma_{\mathrm{Rd}} \frac{\pi}{2} \sqrt{\frac{E_{\mathrm{f}} t_{\mathrm{f}} \cdot s_{\mathrm{u}}}{f_{\mathrm{bm}}}}\right\} = \max\left\{100\,\mathrm{mm}; 142\,\mathrm{mm}\right\} = 142\,\mathrm{mm} \quad (14.72)$$

with:

- $\gamma_{\mathrm{Rd}} = 1.20$ (model coefficient)

- $f_{bm} = \frac{k_{Gm}}{2}\frac{\sqrt{f_{cm} f_{ctm}}}{FC} = 3.74\text{MPa}$
- $k_{Gm} = 1.25$ for wet-lay-up FRP systems.

For safety purposes, the anchorage length is rounded to $\ell_{ed} = 150$ mm.

Final Reinforcement Length Determination
To ensure that the anchorage is effective, the tensile stress in the reinforcement at the anchorage section must not exceed:

$$f_{fdd} = 445.51 \text{ MPa}.$$

By using this value in Equations (14.9) and (14.11), the moment corresponding to this stress level is:

$$M_{Rd} = 130.20\ kNm$$

This moment is reached at a distance of approximately 1.20 m from the support and is slightly lower than the moment capacity of the unstrengthened section (131.40 kNm).

Thus, for the FRP reinforcement to be effective starting from sections located 1.20 m away from the supports, an anchorage length of at least $\ell_{ed} = 0.15\ m$ beyond these sections is required. The total reinforcement length is therefore 2.4 m (2.10 m + 2 · 0.15 m, Figure 14-10).

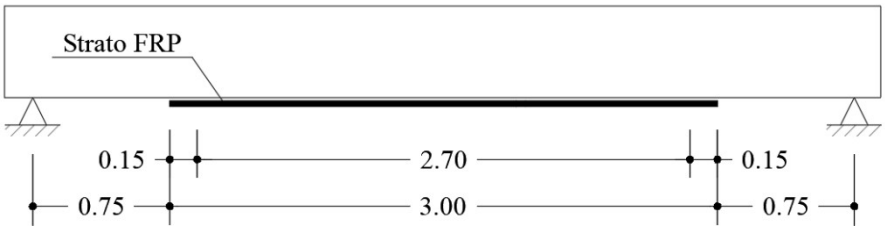

Figure 14-10 –FRP Strengthening layout.

Consideration of Moment Diagram Shift
Since the moment diagram shifts by $0.9d$ = 300mm, the reinforcement ends are extended by 0.30 m towards the beam supports. This results in a total reinforcement length increase of 0.6 m, leading to a final reinforcement length of 3.00 m.

14.3.2 Strengthening with FRP-EBR System and Spike Anchors

To reduce the amount of reinforcement and use a strip width of b_f =16.0 cm instead of 30.0 cm, it is assumed that fan-shaped anchors will be used. These will increase the working strain of the reinforcement by mitigating debonding failure in Mode 2, according to the following expressions:

$$\varepsilon_{fdd,anc} = \frac{F_{anc,d}}{E_f \cdot b_f \cdot t_f} \tag{14.73}$$

$$F_{anc,d} = k_k \cdot \frac{f_{fdm} \cdot b_f \cdot t_f + \left[n_{A,eff} \cdot \min\{N_{PO,m}, N_{S,m}, N_{FD,k}, N_{FR,k}\} \right]}{\gamma_{f2}} \le \frac{\eta_a \cdot f_{fk}}{\gamma_{f1}} b_f \cdot t_f \tag{14.74}$$

$$n_{\mathrm{A,eff}} = \frac{1}{2}\left[n_A + \frac{A_{\mathrm{f}} \cdot \left(f_{\mathrm{fdm,2}} - f_{\mathrm{fdm}} \right)}{F_{\mathrm{A,l}}} \right] \tag{14.75}$$

$$F_{\mathrm{A,l}} = \min\{N_{\mathrm{PO,m}}, N_{\mathrm{S,m}}, N_{\mathrm{FD,k}}, N_{\mathrm{FR,k}}\} \tag{14.76}$$

For b_{f} =160 mm, the flexural capacity of the strengthened section, calculated using Equations (14.67) and (14.68) following the same procedure and assuming $\varepsilon_{\mathrm{fd}}$ = 3.61 ‰, is:

$$M_{\mathrm{Rd}} = 151.30\ kNm > M_{\mathrm{Sd}} = 162.00\ kNm$$

This confirms that, without spike anchors (referred to as “anchors”), the reduced-width FRP strip does not provide sufficient strengthening, thus requiring the use of anchorage techniques.

It is assumed that 2 n_{A} = 6 fan-shaped connectors of the ‘bent anchor’ type will be used, positioned along the entire FRP strip, which is assumed to have a length of:

$$l = 2.10 \text{ m}$$

excluding the anchorage lengths:

$$2\ell_{\mathrm{ed}} = 2 \cdot 0.15m = 0.3m$$

with a constant spacing of:

$$\Delta z = \frac{l}{2n_A - 1} = 0.42\ m$$

and symmetrically distributed with respect to the midspan section (Figure 14-11). The connectors have the following characteristics:

- Opening angle of the fan-shaped fibers: ψ_{a} = 90°, λ = 30°, L_{s} = 130 mm
- Anchor diameter: d_{a} = 10 mm, Connector area: A_{fc} = 78.50 mm^2
- Hole diameter: d_{h} = 15 mm, Effective embedment depth: h_{e} = 100 mm > max (80 mm, 8 d_{a}) = 80 mm
- FRP anchorage tensile strength: f_{fak} = 2000 MPa
- Concrete fracture parameters: f_{Rck} = 80.00 MPa, f_{Rtk} = 30.00 MPa.

Considering the fiber fan opening angle of 30° and L_{s} = 130 mm, the fan-shaped part of the connector covers 130 mm out of the 160 mm corresponding to the reinforcement strip width, thereby complying with the requirement that at least 80% coverage is ensured.

Since the anchors have ψ_{a} = 90°, in Equations (14.26) and (14.65) it is only necessary to calculate the resistances related to the following failure mechanisms:

- Debonding failure of the fan-shaped connector from the FRP reinforcement ($N_{FD,k}$)
- Shear-tension failure of the connector fibers ($N_{FR,k}$)

These values will be computed as follows:

$$N_{\mathrm{FR,k}} = k_{\mathrm{FAN}} \cdot \frac{\psi_{\mathrm{a}}}{\pi} A_{\mathrm{fc}} \cdot \eta_{\mathrm{a}} \cdot f_{\mathrm{fak}} = 37.28\mathrm{kN} \tag{14.77}$$

$$N_{\mathrm{DB,k}} = F_{\mathrm{DB,k}} \cdot \left(\frac{\sin\lambda}{\lambda}\right) = \lambda L_{\mathrm{s}}^2 \cdot \tau_{\mathrm{Rb,k}} \cdot \left(\frac{\sin\lambda}{\lambda}\right) = L_{\mathrm{s}}^2 \cdot \frac{1}{2}\sqrt{f_{\mathrm{Rck}} f_{\mathrm{Rtk}}} \cdot \sin\lambda = 206.89\mathrm{kN} \tag{14.78}$$

$$F_{\mathrm{A,l}} = \min\{N_{\mathrm{FD,k}}, N_{\mathrm{FR,k}}\} = 37.28\mathrm{kN} \tag{14.79}$$

where:

- $F_{\mathrm{DB,k}} = \lambda L_{\mathrm{s}}^2 \cdot \tau_{\mathrm{Rb,k}}$ with $\tau_{\mathrm{Rb}k} = \frac{1}{2}\sqrt{f_{\mathrm{Rck}} f_{\mathrm{Rtk}}}$
- $\eta_{\mathrm{a}} = 0.95$ is the environmental factor defined in §3.4.1
- $k_{\mathrm{FAN}} = 0.50$.

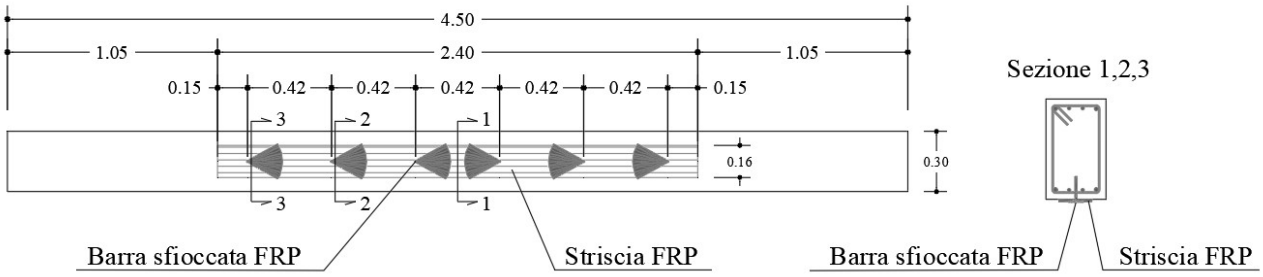

Figure 14-11 – Arrangement of connectors along the reinforcement.

Next, the number of 'effective' connectors, $n_{\mathrm{A,eff}}$, is calculated. This allows identifying the section at a distance:

$$z_{\mathrm{crit}} = (n_{\mathrm{A,eff}} - 1) \cdot \Delta z$$

from the reinforcement anchorage section (in this case, the section at 0.15 m from the end of the reinforcement and 1.20 m from the support) where the end debonding force, $F_{\mathrm{anc,d}}$, (given by Equation (14.65) and calculated considering the mean stress value for end debonding f_{fdm} and the additional contribution of $n_{\mathrm{A,eff}}$ connectors), is equal to the intermediate debonding force calculated at midspan, considering the contribution of the remaining n_{A} - $n_{\mathrm{A,eff}}$ connectors using Equation (14.65) but replacing f_{fdm} with $f_{\mathrm{fdm,2}}$, which refers to intermediate debonding.

$$n_{\mathrm{A,eff}} = \frac{1}{2}\left[n_A + \frac{A_{\mathrm{f}} \cdot \left(f_{\mathrm{fdm,2}} - f_{\mathrm{fdm}}\right)}{F_{\mathrm{A,l}}} \right] = 2.4 \tag{14.80}$$

where, in addition to previously introduced symbols and values:

- $n_{\mathrm{A}} = 3$ (3 connectors from the reinforcement end to the beam midspan)

- $f_{\mathrm{fdm},2} = k_{\mathrm{q}} \sqrt{\dfrac{2E_{\mathrm{f}} \dfrac{k_{\mathrm{Gm},2}}{4FC} \sqrt{f_{\mathrm{cm}} f_{\mathrm{ctm}}} \cdot s_{\mathrm{u}}}{t_{\mathrm{f}}}} = 2111\mathrm{MPa}$, with $k_{\mathrm{Gm},2} = 5.10$
- $f_{\mathrm{fdm}} = \sqrt{\dfrac{E_{\mathrm{f}} \dfrac{k_{\mathrm{Gm}}}{2FC} \sqrt{f_{\mathrm{cm}} f_{\mathrm{ctm}}} \cdot s_{\mathrm{u}}}{t_{\mathrm{f}}}} = 836\mathrm{MPa}$, with $k_{\mathrm{Gm}} = 1.25$.

For safety, it is assumed that $n_{\mathrm{A,eff}} = 2$, meaning that:

- End debonding resistance, f_{fdm}, can be increased by the contribution of $n_{\mathrm{A,eff}} = 2$ connectors using Equation (14.65).
- Intermediate debonding resistance, $f_{\mathrm{fdm},2}$, can be increased by the contribution of (n_{A} - $n_{\mathrm{A,eff}}$) = 1 connector, also using Equation (14.65), assuming $\gamma_{\mathrm{f2}} = 1.3$.

Verification at Midspan (Section 1 in Figure 14-11):

$$F_{anc,\mathrm{d}} = k_{\mathrm{k}} \cdot \frac{f_{\mathrm{fd\,m},2} \cdot b_{\mathrm{f}} \cdot t_{\mathrm{f}} + \left[(n_A - n_{\mathrm{A,eff}}) \cdot \min\{N_{\mathrm{FD,k}}, N_{\mathrm{FR,k}}\} \right]}{\gamma_{\mathrm{f2}}} = 81.40\mathrm{kN} \tag{14.81}$$

Resulting in the following values of stress and strain in the reinforcement:

$$f_{\mathrm{fdd,anc}} = \frac{F_{\mathrm{anc,d}}}{b_{\mathrm{f}} \cdot t_{\mathrm{f}}} = 1509\mathrm{MPa} \ , \qquad \varepsilon_{\mathrm{fdd,anc}} = \frac{f_{\mathrm{fdd,anc}}}{E_{\mathrm{f}}} = 5.99\ ‰ \tag{14.82}$$

For the verification at the section benefiting from 2 anchor connectors (0.42 m from the reinforcement anchorage section and 1.62 m from the support, Section 2 in Figure 14-11):

$$F_{\mathrm{anc,d}} = k_{\mathrm{k}} \cdot \frac{f_{\mathrm{fd\,m}} \cdot b_{\mathrm{f}} \cdot t_{\mathrm{f}} + \left[n_{\mathrm{A,eff}} \cdot \min\{N_{\mathrm{FD,k}}, N_{\mathrm{FR,k}}\} \right]}{\gamma_{\mathrm{f2}}} = 64.40\mathrm{kN} \quad \text{with } \mathrm{n_{A,eff}} = 2 \tag{14.83}$$

Resulting in the following values of stress and strain in the reinforcement:

$$f_{\mathrm{fdd,anc}} = \frac{F_{\mathrm{anc,d}}}{b_{\mathrm{f}} \cdot t_{\mathrm{f}}} = 1195\mathrm{MPa} \, , \qquad \varepsilon_{\mathrm{fdd,anc}} = \frac{f_{\mathrm{fdd,anc}}}{E_{\mathrm{f}}} = 4.74‰ \tag{14.84}$$

For the verification at the reinforcement anchorage section (0.15 m from the reinforcement end and 1.20 m from the support, Section 3 in Figure 14-11), benefiting from 1 anchor connector:

$$F_{\mathrm{anc,d}} = k_{\mathrm{k}} \cdot \frac{f_{\mathrm{fd\,m}} \cdot b_{\mathrm{f}} \cdot t_{\mathrm{f}} + \left[n_{\mathrm{z}} \cdot \min\{N_{\mathrm{FD,k}}, N_{\mathrm{FR,k}}\} \right]}{\gamma_{\mathrm{f2}}} = 44.35\mathrm{kN} \quad \text{con } \mathrm{n_z} = 1 \tag{14.85}$$

Resulting in the following values of stress and strain in the reinforcement:

$$f_{\mathrm{fdd,anc}} = \frac{F_{\mathrm{anc,d}}}{b_{\mathrm{f}} \cdot t_{\mathrm{f}}} = 822.50\mathrm{MPa}\,, \qquad \varepsilon_{\mathrm{fdd,anc}} = \frac{f_{\mathrm{fdd,anc}}}{E_{\mathrm{f}}} = 3.26‰ \tag{14.86}$$

where $k_{\mathrm{k}} = 0.70$, and $\gamma_{\mathrm{f2}} = 1.30$.

At midspan, using Equations (14.9) and (14.11) with $\varepsilon_{\mathrm{fd}} = 5.99$ ‰ instead of 3.61 ‰, the reinforced section's resistant moment is:

$$M_{\mathrm{Rd}} = 165.60 \text{ kNm} > M_{\mathrm{Sd}} = 162.00 \text{ kNm}$$

At reinforcement anchorage sections (0.15 m from the reinforcement end and 1.20 m from the supports), using $\varepsilon_{\mathrm{fd}} = 3.26$ ‰ in Equations (14.9) and (14.11), the resistant moment of the reinforced section is:

$$M_{\mathrm{Rd}} = 148.50 \text{ kNm} > M_{\mathrm{Sd}} = 126.72 \text{ kNm}$$

Finally, considering the shift of the bending moment diagram by an amount equal to $0.9d = 300$ mm, the reinforcement ends are moved an additional 0.30 m toward the beam extremities, resulting in a total increase of 0.6 m in the reinforcement length.

By keeping the spacing between the three anchorage connectors (0.42 m) unchanged on each half of the beam, the moment diagram shift of 0.3 m on each side leads to an increase of 0.6 m in the distance between the two central anchorage connectors.

14.3.3 Shear Strengthening Design of a Beam Using the FRP-EBR System

The analysis considers beam 1.1 of the previously examined frame, for which the applied shear force T_{Sd} at the left support is 144.10 kN.

For the evaluation of the beam's shear resistance, the following mechanical properties of the materials are considered:

- Concrete: f_{cm} =25.00 MPa, γ_c =1.5 (brittle mechanism), FC=1.2; therefore f_{cd} = 13.89 MPa;
- Steel: f_{ym} = 440.00 MPa, γ_s = 1.15 (brittle mechanism), FC =1.2; therefore f_{yd} = 318.84 MPa.

The shear resistance is calculated according to the applicable regulations for existing buildings subject to gravity loads as follows:

$$V_{Rd} = \min\left(V_{Rd,s}, V_{Rd,c}\right) = \min\left(90.4, 439.9\right) = 90.4\text{kN} \tag{14.87}$$

where:

- The shear resistance provided by the transverse reinforcement is computed as:

$$V_{Rd,s} = 0.9d\,\frac{A_s}{s}\,f_{yd}\left(\cot\beta + \cot\theta\right)\sin\beta = 0.9\cdot 470\cdot\frac{100.5}{150}318.84\left(\cot 90° + \cot 45°\right)\sin 90° = 90.40\text{kN} \tag{14.88}$$

- The shear resistance provided by the concrete is evaluated as:

$$\begin{aligned} V_{Rd,c} &= 0.9db\alpha_c \nu f_{cd}\left(\cot\beta + \cot\theta\right)/\left(1+\cot^2\theta\right) = \\ &= 0.9\cdot 470\cdot 300\cdot 1\cdot 0.5\cdot 13.9\left(\cot 90° + \cot 45°\right)/\left(1+\cot^2 45°\right) = 439.90\text{kN} \end{aligned} \tag{14.89}$$

with the following parameter values:

- d = 470 mm
- A_s = 100.5 mm^2
- θ = 45°
- β = 90°
- α_c = 1 (for non-compressed members)
- ν = 0.5

Considering the applied shear force V_{sd}= 144.00 kN shear strengthening intervention is necessary, as the required increase in shear capacity is 59%.

Selection of Strengthening System

It is decided to use the same unidirectional CFRP fabric as in the flexural strengthening design (§14.1.3.1), but in a U-shaped configuration near the supports, where the applied shear force exceeds the beam's shear resistance.

A single layer of CFRP fabric is considered, thus $n_f = 1$, arranged in discontinuous strips of 100 mm width $b_f = 100$ mm at a spacing of $p_f = 150$ mm. A verification is performed to check whether this configuration meets the design inequality $V_{Rd} \geq V_{Sd}$ (14.1).

For a U-shaped FRP layout on a rectangular section, the shear contribution of the FRP system, $V_{Rd,f}$, can be estimated using the Mörsch truss analogy (4.77):

$$V_{Rd,f} = \frac{1}{\gamma_{Rd}} f_{fed} A_{fv} \frac{0.9d}{p_f} (\cot\theta + \cot\beta) \sin^2\beta \tag{14.90}$$

where, in addition to the symbols previously defined, it is assumed:

- $A_{fv} = 2\, t_f\, b_f = 67.4$ mm^2
- $\gamma_{Rd} = 1.20$

The effective design strength of the FRP system, f_{fed}, for a U-shaped configuration is calculated as (4.79):

$$f_{fed} = f_{fdd} \cdot \left[1 - \frac{1}{3} \cdot \frac{l_{ed} \cdot \sin\beta}{\min\{0.9 \cdot d, h_w\}} \right] = 499.00 \cdot \left[1 - \frac{1}{3} \cdot \frac{142 \cdot \sin 90°}{\min\{0.9 \cdot 470, 500\}} \right] = 442.10\text{MPa} \tag{14.91}$$

where:

- $h_w = 500$ mm (assuming the absence of a slab)
- $\ell_{ed} = 142$ mm, (calculated for the previous flexural strengthening in §14.1.3.1)
- The design stress, f_{fdd}, for end-debonding is:

$$f_{fdd} = \frac{k_b}{\gamma_{f2}} \cdot \sqrt{\frac{2 E_f \Gamma_{Fk}}{t_f}} = \frac{1.12}{1.3} \cdot \sqrt{\frac{2 \cdot 252000 \cdot 0.224}{0.337}} = 499.00\text{MPa} \tag{14.92}$$

where:

- $k_b = \sqrt{\frac{2 - b_f / b}{1 + b_f / b}} = \sqrt{\frac{2 - 100/300}{1 + 100/300}} = 1.12$
- $\gamma_{f2} = 1.3$
- $\Gamma_{Fk} = 0.224\text{N/mm}$, was computed for the flexural reinforcement in §14.1.3.1

Verification of Strengthening Effectiveness

The shear contribution of the FRP system is then calculated as:

$$V_{\mathrm{Rd,f}} = \frac{1}{1.2} \cdot 442.10 \cdot 67.4 \cdot \frac{0.9 \cdot 470}{150} (\cot 45° + \cot 90°) \sin^2 90° = 70.00\mathrm{kN} \quad (14.93)$$

The shear resistance of the strengthened beam at the supports is then given by:

$$V_{\mathrm{Rd}} = \min\left(V_{\mathrm{Rd,s}} + V_{\mathrm{Rd,f}}, V_{\mathrm{Rd,c}} \right) = \min\left(90.40 + 70.00, 439.90\right) = 160.40\mathrm{kN} > 144.10\mathrm{kN} = V_{\mathrm{Sd}} \quad (14.94)$$

where:

- $V_{\mathrm{Rd,s}}$ is the shear contribution of the transverse steel reinforcement and
- $V_{\mathrm{Rd,c}}$ is the shear contribution of the concrete, which was computed earlier.

Application of the Shear Strengthening

Since the applied shear force exceeds the shear resistance of the beam only near the supports, the FRP strengthening should be applied only in those regions.

The CFRP U-wraps will extend for 0.90 m from the support, starting at the edge of the column.

15 APPENDIX I (DESIGN EXAMPLES OF FRP REINFORCEMENT FOR MASONRY STRUCTURES)

This appendix presents calculations related to verifying and sizing the FRP reinforcement system for the masonry piers of a perimeter wall in a three-story masonry building.

The example is structured into the following sections:

- Geometry, material properties, and loads;
- Compression-bending verification of existing masonry piers;
- Sizing of the FRP reinforcement system for compression-bending;
- Shear verification of existing masonry piers;
- Sizing of the FRP reinforcement system for shear.

15.1 GEOMETRY, MATERIAL PROPERTIES AND LOADS

The wall consists of two edge piers, each 2.0 m long, and two internal piers, each 3.0 m long. The thickness of the piers varies in height: 500 mm on the first floor, 375 mm on the second floor, and 250 mm on the top floor. The height of the piers, measured at the centerline of the floor bands, is constant along the building and equal to 3.0 m (Figure 15-1).

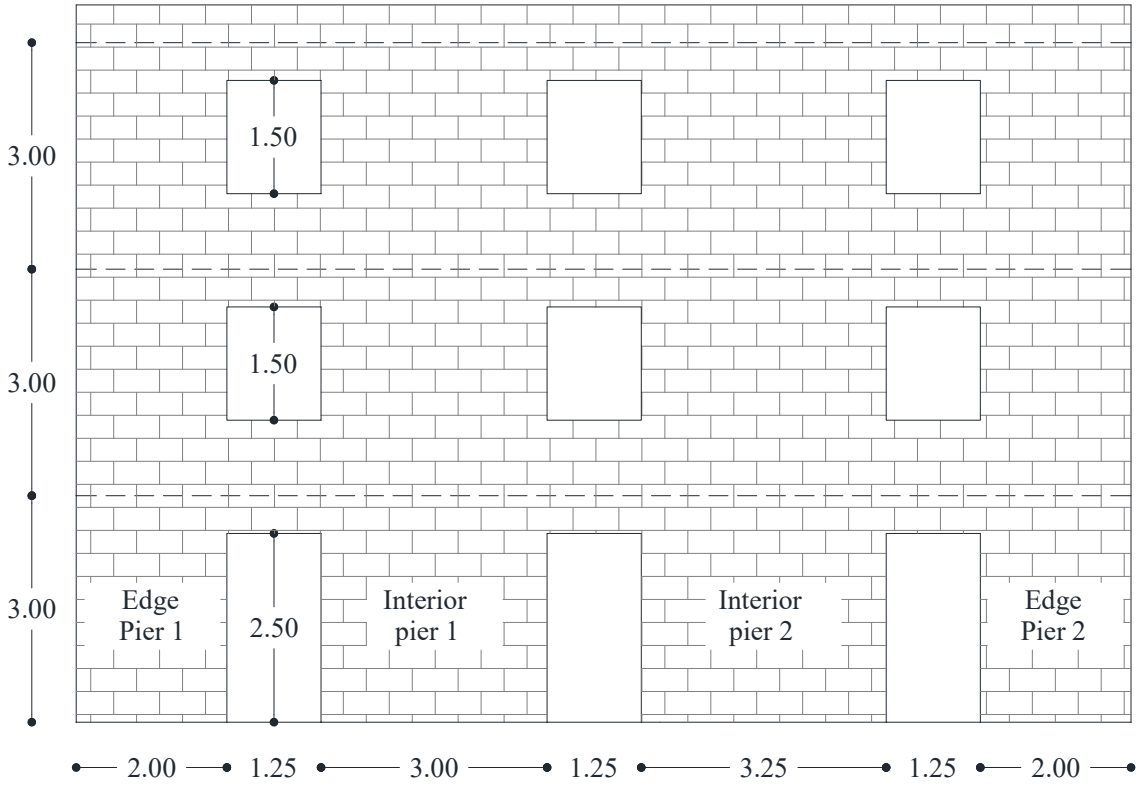

Figure 15-1 – Geometry of the studied wall (dimensions in meters).

Table 15-1 presents the mechanical properties of the masonry and the partial factors used. The assumed constitutive model for masonry follows § 5.2.3(8), with $\bar{\varepsilon}_m$= 2.00 ‰ and ε_{mu}= 3.50 ‰.

Table 15-1 - Masonry Parameters.

Elastic modulus (normal)	E [MPa]	4000
Elastic modulus (shear)	G [MPa]	1000
Unit weight	γ [kN/m^3]	18.0
Confidence factor	FC	1.00
Partial safety factor	γ_M	2.00
Compressive strength (normal to mortar joints)		
Characteristic value	f_{mk} [MPa]	8.00
Design value	f_{md} [MPa]	4.00
Shear strength (without normal stress)		
Characteristic value	f_{vk0} [MPa]	0.80
Block strength		
Average compression strength	f_{bcm} [MPa]	38.00
Average tensile strength	f_{btm} [MPa]	3.80

The reinforcement system used in this example is an in-situ impregnated CFRP unidirectional fabric, except for the intervention against out-of-plane overturning (§ 15.6). The relevant geometric and mechanical parameters are listed in Table 15-2. Table 15-3 presents the partial factors and design values used for verification.

Table 15-2– Geometric and Mechanical Properties of FRP Reinforcement.

Layer thickness	t_f [mm]	0.165
Layer width	b_f [mm]	140
Elastic modulus (fiber direction)	E_f [GPa]	230
Characteristic tensile strain at failure	ε_{fk} [‰]	20.7
Shear reinforcement spacing	p_f [mm]	500

Table 15-3– Partial Factors and Design Values for FRP Reinforcement.

Partial factor for debonding failure	γ_{f2} (§ 3.4.1)	1.30
Partial factor for ULS failure	γ_{f1} (§ 3.4.1)	1.30
Environmental reduction factor	η_a (§ 3.5.1)	0.95
Tensile failure strain	$\eta_a \cdot \varepsilon_{fk}/\gamma_f$ [‰] (§ 5.2.3)	15.10
Load diffusion width	b_d [mm] (§ 5.3.2)	250
Geometric correction factor	k_b (§ 5.3.2)	1.25
Ultimate slip	s_u [mm] (§ 5.3.2)	0.4
Correction factor	k_G [mm] (§ 5.3.2)	0.031
Specific fracture energy	Γ_{Fd} [N/mm] (§ 5.3.2)	0.51
Optimal anchorage length	l_{ed} [mm] (§ 5.3.2)	150
End debonding stress	f_{fdd} [MPa] (§ 5.3.2)	681.97
Intermediate debonding stress	$f_{fdd,2}=2.0 \cdot f_{fdd}$[MPa] (§ 5.3.3)	1363.93
Shear bond stress	f_{bd} [MPa] (§ 5.3.2)	2.50
Intermediate debonding strain	$\varepsilon_{fdd,2}$ [‰] (§ 5.3.3)	5.93
Design strain for FRP reinforcement	ε_{fd} [‰] (§ 5.2.3)	5.93
Partial factor for compression-bending	γ_{Rd} (§ 3.4.2)	1.00
Partial factor for shear	γ_{Rd} (§ 3.4.2)	1.20

The wall is modeled as a frame structure (Figure 15-2), subjected to both vertical loads and concentrated lateral forces applied at the nodes. The structural response was calculated assuming linear elastic behavior of the structural elements. The results of the analysis are presented as diagrams in Figure 15-3; while the corresponding numerical values are summarized in Table 15-4 to Table 15-7 for different piers. Elevation measurements are taken from the fixed base.

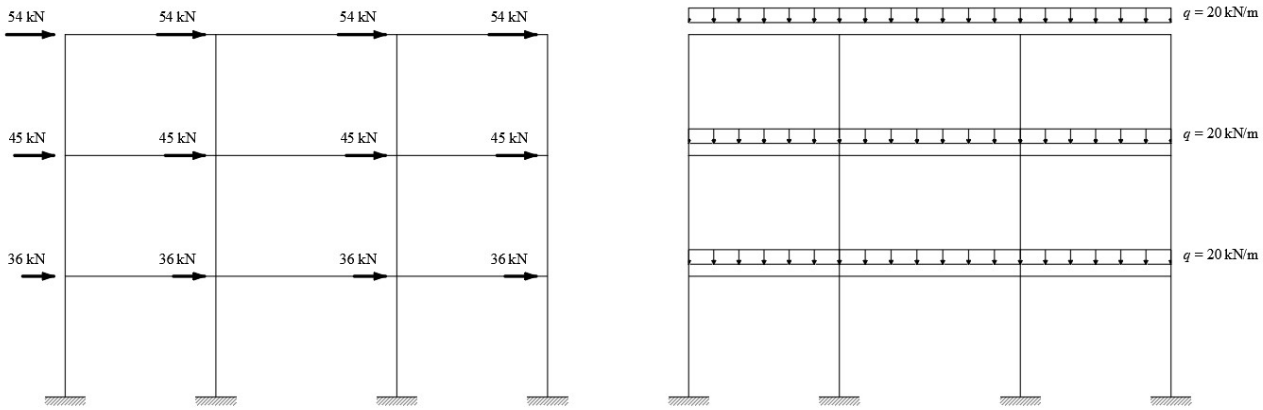

Figure 15-2 – Frame Model and Design Actions.

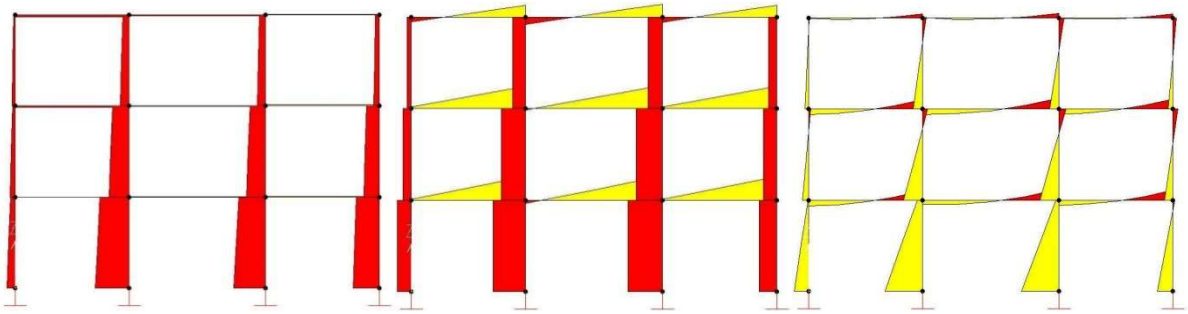

Figure 15-3 – Design Load Diagrams: Axial Load, Shear, and Bending Moment.

Table 15-4 - Design Forces for Edge Pier 1.

Elevation [m]	Panel Length L [cm]	Thickness t [cm]	Axial Load N_{Sd} [kN]	Bending Moment M_{Sd} [kNm]	Shear V_{Sd} [kN]
0	200	50.0	133.38	240.98	76.58
1	200	50.0	115.73	164.40	76.58
2	200	50.0	98.07	87.82	76.58
3	200	50.0	80.41	11.23	76.58
3	200	37.5	84.04	103.39	46.48
4	200	37.5	70.80	56.92	46.48
5	200	37.5	57.56	10.44	46.48
6	200	37.5	44.31	36.04	46.48
6	200	25.0	52.72	55.50	21.85
7	200	25.0	43.89	33.65	21.85
8	200	25.0	35.06	11.81	21.85
9	200	25.0	26.23	10.04	21.85

Table 15-5 – Design Forces for Edge Pier 2.

Elevation [m]	Panel Length L [cm]	Thickness t [cm]	Axial Load N_{Sd} [kN]	Bending Moment M_{Sd} [kNm]	Shear V_{Sd} [kN]
0	200	50.0	434.71	250.51	95.43
1	200	50.0	417.05	155.08	95.43
2	200	50.0	399.39	59.65	95.43
3	200	50.0	381.74	35.78	95.43
3	200	37.5	252.33	131.73	72.51
4	200	37.5	239.09	59.21	72.51
5	200	37.5	225.84	13.30	72.51
6	200	37.5	212.60	85.81	72.51
6	200	25.0	90.50	72.98	45.10
7	200	25.0	81.67	27.89	45.10
8	200	25.0	72.84	17.21	45.10
9	200	25.0	64.01	62.30	45.10

Table 15-6 – Design Forces for Internal Pier 1.

Elevation [m]	Panel Length L [cm]	Thickness t [cm]	Axial Load N_{Sd} [kN]	Bending Moment M_{Sd} [kNm]	Shear V_{Sd} [kN]
0	300	50.0	557.52	619.07	178.52
1	300	50.0	531.03	440.55	178.52
2	300	50.0	504.55	262.04	178.52
3	300	50.0	478.06	83.52	178.52
3	300	37.5	331.42	311.06	131.92
4	300	37.5	311.55	179.14	131.92
5	300	37.5	291.69	47.22	131.92
6	300	37.5	271.82	84.70	131.92
6	300	25.0	143.71	152.28	70.56
7	300	25.0	130.47	81.72	70.56
8	300	25.0	117.22	11.16	70.56
9	300	25.0	103.98	59.40	70.56

Table 15-7 – Design Forces for Internal Pier 2.

Elevation [m]	Panel Length L [cm]	Thickness t [cm]	Axial Load N_{Sd} [kN]	Bending Moment M_{Sd} [kNm]	Shear V_{Sd} [kN]
0	325	50.0	521.43	618.68	189.47
1	325	50.0	494.94	429.21	189.47
2	325	50.0	468.46	239.74	189.47
3	325	50.0	441.97	50.27	189.47
3	325	37.5	315.46	316.02	145.09
4	325	37.5	295.59	170.93	145.09
5	325	37.5	275.73	25.83	145.09
6	325	37.5	255.86	119.26	145.09
6	325	25.0	138.48	152.36	78.50
7	325	25.0	125.24	73.86	78.50
8	325	25.0	111.99	4.64	78.50
9	325	25.0	98.75	83.13	78.50

15.2 VERIFICATION OF PRE-EXISTING MASONRY PIERS UNDER COMBINED AXIAL LOAD AND BENDING (PRESSOFLEXION)

The verification of the pre-existing masonry piers under combined axial load and bending was carried out using the constitutive model assumed in § 15.1. In analogy with the procedure outlined in § 4.3.2.4 for reinforced concrete structures, the ultimate bending moment capacity, M_{Rd} (N_{Sd}), corresponding to the design axial force, N_{Sd}, was evaluated.
For this purpose, two equilibrium equations were used:

1. Equilibrium of translational forces along the element's axis.
2. Equilibrium of rotational forces about the geometric centroid of the section.

Additionally, the linear strain distribution across the section was taken into account.

The verification results are summarized in:

- Table 15-8 for Edge Pier 1
- Table 15-9 for Edge Pier 2
- Table 15-10 for Internal Pier 1
- Table 15-11 for Internal Pier 2

Furthermore, Figure 15-4 compares the design bending moment diagram with the resisting moment capacity. The results indicate that the pressoflexion verification is not satisfied in certain sections of the edge piers.

Proposed Strengthening Solution

To address this issue, FRP reinforcement will be applied continuously along the full height of the edge piers. The FRP strips will be placed at the ends of the piers, maintaining a centerline distance of 10 cm from the edge.

Table 15-8– Verification of Edge Pier 1 Under Combined Axial Load and Bending.

Elevation [m]	Bending Moment Capacity $M_{Rd}(N_{Sd})$ [kNm]	Verification Result $M_{Rd}(N_{Sd}) \geq M_{Sd}$
0	128.93	**Not satisfied**
1	112.38	**Not satisfied**
2	95.67	Satisfied
3	78.79	Satisfied
3	81.69	**Not satisfied**
4	69.13	Satisfied
5	56.46	Satisfied
6	43.66	Satisfied
6	51.33	**Not satisfied**
7	42.93	Satisfied
8	34.45	Satisfied
9	25.89	Satisfied

Table 15-9 –Verification of Edge Pier 2 Under Combined Axial Load and Bending.

Elevation [m]	Bending Moment Capacity $M_{Rd}(N_{Sd})$ [kNm]	Verification Result $M_{Rd}(N_{Sd}) \geq M_{Sd}$
0	387.47	Satisfied
1	373.57	Satisfied
2	359.51	Satisfied
3	345.31	Satisfied
3	231.11	Satisfied
4	220.04	Satisfied
5	208.84	Satisfied
6	197.53	Satisfied
6	86.40	Satisfied
7	78.34	Satisfied
8	70.19	Satisfied
9	61.96	**Not satisfied**

Table 15-10 – Verification of Internal Pier 1 Under Combined Axial Load and Bending.

Elevation [m]	Bending Moment Capacity $M_{Rd}(N_{Sd})$ [kNm]	Verification Result $M_{Rd}(N_{Sd}) \geq M_{Sd}$
0	758.57	Satisfied
1	726.05	Satisfied
2	693.18	Satisfied
3	659.95	Satisfied
3	460.52	Satisfied
4	434.97	Satisfied
5	409.17	Satisfied
6	383.10	Satisfied
6	205.24	Satisfied
7	187.19	Satisfied
8	168.96	Satisfied
9	150.56	Satisfied

Table 15-11 –Verification of Internal Pier 2 Under Combined Axial Load and Bending.

Elevation [m]	Bending Moment Capacity $M_{Rd}(N_{Sd})$ [kNm]	Verification Result $M_{Rd}(N_{Sd}) \geq M_{Sd}$
0	779.35	Satisfied
1	743.04	Satisfied
2	706.38	Satisfied
3	669.37	Satisfied
3	479.45	Satisfied
4	451.21	Satisfied
5	422.72	Satisfied
6	393.95	Satisfied
6	215.44	Satisfied
7	195.67	Satisfied
8	175.71	Satisfied
9	155.59	Satisfied

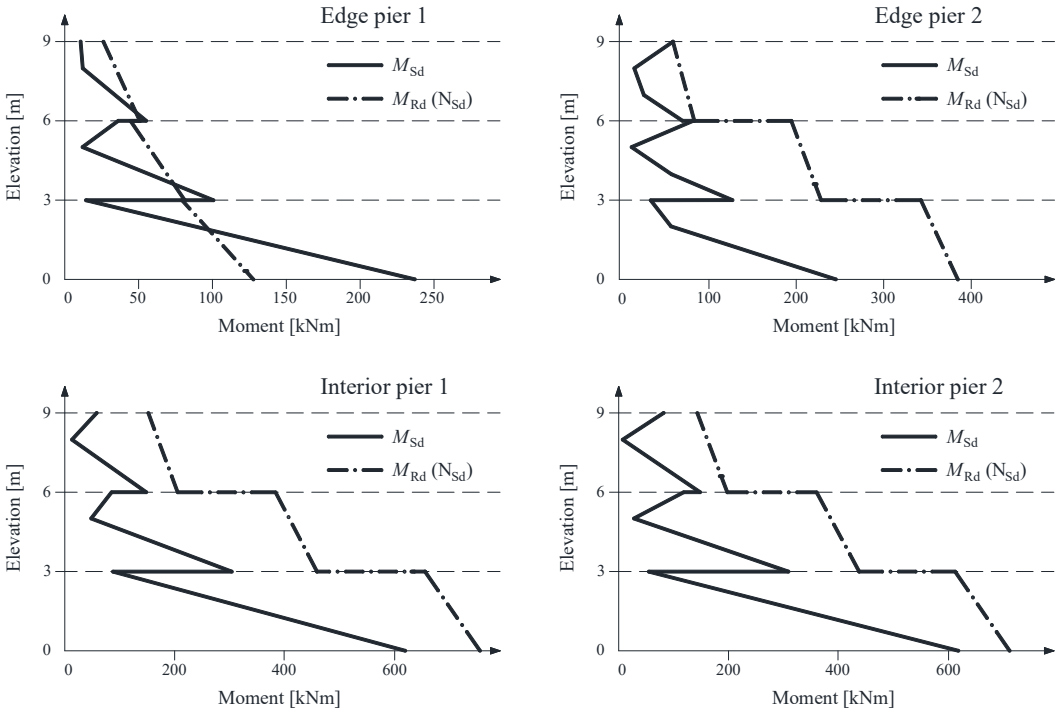

Figure 15-4– Comparison of Design and Resisting Bending Moment Diagrams for Piers.

15.3 SIZING OF THE REINFORCEMENT SYSTEM AND VERIFICATION OF REINFORCED ELEMENTS UNDER COMPRESSION-BENDING

The reinforcement system described in § 15.1, is adopted, and for simplicity, it is assumed to be applied continuously from the lower end of the masonry walls (at elevation 0.0 m) to the upper end (at elevation +9.0 m), both on the external and internal walls.

In particular, it is assumed that the reinforcement anchorage at the base is achieved using a mechanical system.

Moreover, for the stress distribution diagram under Ultimate Limit State (ULS) conditions, a simplified stress-block assumption is adopted, extending over a section portion of depth $\psi \cdot x$, where the formulas for the ψ coefficient can be found in equation (14.10).

The results of the compression-bending verification of the masonry piers reinforced with FRP are reported in Table 15-12 for Edge Pier 1 and in Table 15-13 for Edge Pier 2.

At elevation 0, the presence of a mechanical anchorage for the FRP reinforcement is considered, ensuring sufficient dimensions to allow the fibers to reach their tensile failure.

Table 15-12 – Compression-Bending Verification of Reinforced Masonry Piers: Edge Pier 1.

Section Elevation [m]	Composite Failure Mode	ε_{fd} [‰]	$M_{Rd}(N_{Sd})$ [kNm]	Verification Outcome
0	Tensile failure	15.10	279.56	Satisfied
1	Intermediate debonding	5.93	167.33	Satisfied
2	Intermediate debonding	5.93	151.70	Satisfied
3	Intermediate debonding	5.93	135.91	Satisfied
3	Intermediate debonding	5.93	137.88	Satisfied
4	Intermediate debonding	5.93	126.20	Satisfied
5	Intermediate debonding	5.93	114.41	Satisfied
6	Intermediate debonding	5.93	102.50	Satisfied
6	Intermediate debonding	5.93	108.72	Satisfied
7	Intermediate debonding	5.93	100.99	Satisfied
8	Intermediate debonding	5.93	93.18	Satisfied
9	End debonding	2.97	54.43	Satisfied

Table 15-13 – Compression-Bending Verification of Reinforced Masonry Piers: Edge Pier 2.

Section Elevation [m]	Composite Failure Mode	ε_{fd} [‰]	$M_{Rd}(N_{Sd})$ [kNm]	Verification Outcome
0	Tensile failure	15.10	526.06	Satisfied
1	Intermediate debonding	5.93	415.10	Satisfied
2	Intermediate debonding	5.93	401.53	Satisfied
3	Intermediate debonding	5.93	387.84	Satisfied
3	Intermediate debonding	5.93	278.26	Satisfied
4	Intermediate debonding	5.93	267.73	Satisfied
5	Intermediate debonding	5.93	257.11	Satisfied
6	Intermediate debonding	5.93	246.41	Satisfied
6	Intermediate debonding	5.93	141.10	Satisfied
7	Intermediate debonding	5.93	133.64	Satisfied
8	Intermediate debonding	5.93	126.11	Satisfied
9	End debonding	2.97	86.89	Satisfied

15.4 SHEAR VERIFICATION FOR PIERS

Table 15-14 and Table 15-15 present the shear strength verification results for internal piers 1 and 2, which are not subjected to flexural strengthening. Additionally, Figure 15-5 compares the design shear force with the shear strength for these masonry piers.

The results confirm that the shear verification is satisfied for all sections of these structural elements. Consequently, no shear strengthening is required for these piers.

Shear Verification for Edge Piers Strengthened in Flexure

A similar shear verification was performed for edge piers 1 and 2, which were strengthened in flexure.

The verification results are summarized in:

- Table 15-16 for Edge Pier 1
- Table 15-17 for Edge Pier 2

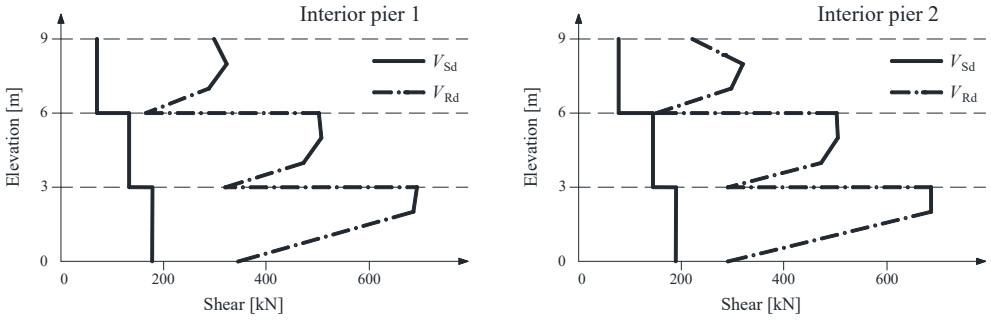

Figure 15-5 – Shear Verification Diagrams for Piers Not Strengthened in Flexure.

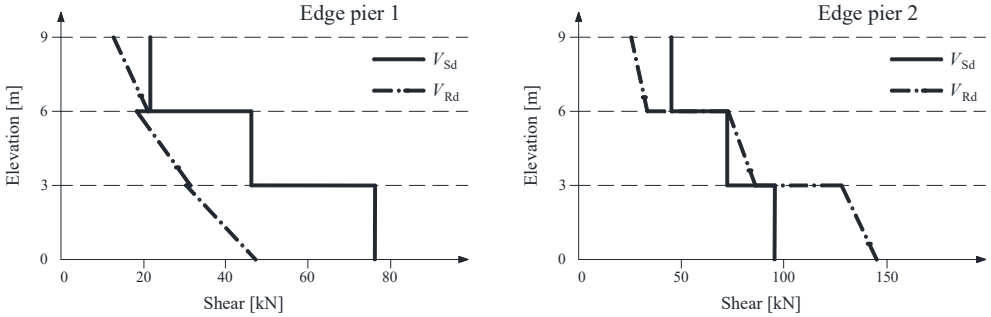

Figure 15-6 – Shear Verification Diagrams for Piers Strengthened in Flexure.

Table 15-14 –Shear Verification for Masonry Piers Not Strengthened in Flexure: Internal Pier 1

Elevation [m]	Design Shear Force V_{Sd} [kN]	Eccentricity e [m]	Effective Length l_c [m]	Characteristic Shear Strength f_{vk} [kN/m^2]	Shear Strength V_{Rd} [kN]	Verification Result $V_{Rd} \geq V_{Sd}$
0	178.52	1.11	1.17	1181.60	345.26	Satisfied
1	178.52	0.83	2.01	1011.20	508.40	Satisfied
2	178.52	0.52	2.94	937.20	689.30	Satisfied
3	178.52	0.17	3.00	927.50	695.60	Satisfied
3	131.92	0.94	1.68	1009.90	318.90	Satisfied
4	131.92	0.57	2.78	919.80	478.60	Satisfied
5	131.92	0.16	3.00	903.70	508.30	Satisfied
6	131.92	0.31	3.00	896.60	504.40	Satisfied
6	70.56	1.06	1.32	974.00	160.90	Satisfied
7	70.56	0.63	2.62	879.60	288.20	Satisfied
8	70.56	0.10	3.00	862.50	323.40	Satisfied
9	70.56	0.57	2.79	859.70	299.40	Satisfied

Table 15-15 –Shear Verification for Masonry Piers Not Strengthened in Flexure: Internal Pier 2

Elevation [m]	Design Shear Force V_{Sd} [kN]	Eccentricity e [m]	Effective Length l_c [m]	Characteristic Shear Strength f_{vk} [kN/m^2]	Shear Strength V_{Rd} [kN]	Verification Result $V_{Rd} \geq V_{Sd}$
0	189.47	1.19	0.94	1243.54	292.38	Satisfied
1	189.47	0.87	1.90	1008.60	478.70	Satisfied
2	189.47	0.51	2.96	926.40	686.60	Satisfied
3	189.47	0.11	3.00	917.90	688.40	Satisfied
3	145.09	1.00	1.49	1025.10	287.30	Satisfied
4	145.09	0.58	2.77	914.00	473.90	Satisfied
5	145.09	0.09	3.00	898.00	505.10	Satisfied
6	145.09	0.47	3.00	891.00	501.20	Satisfied
6	78.50	1.10	1.20	984.70	147.60	Satisfied
7	78.50	0.59	2.73	873.40	298.10	Satisfied
8	78.50	0.04	3.00	859.70	322.40	Satisfied
9	78.50	0.84	1.97	880.00	217.20	Satisfied

Table 15-16 –Shear Verification for Masonry Piers Strengthened in Flexure: Edge Pier 1

Elevation [m]	Design Shear Force V_{Sd} [kN]	Neutral Axis x [m]	Characteris-tic Shear Strength f_{vk} [kN/m^2]	Shear Strength V_{Rd} [kN]	Verification Result $V_{Rd} \geq V_{Sd}$
0	76.58	0.15	1488.40	57.70	**Not satisfied**
1	76.58	0.11	1618.40	45.80	**Not satisfied**
2	76.58	0.10	1568.50	40.00	**Not satisfied**
3	76.58	0.09	1506.50	34.30	**Not satisfied**
3	46.48	0.12	1520.40	35.50	**Not satisfied**
4	46.48	0.11	1466.00	31.20	**Not satisfied**
5	46.48	0.10	1399.80	26.90	**Not satisfied**
6	46.48	0.09	1317.60	22.60	**Not satisfied**
6	21.85	0.15	1371.90	25.30	Satisfied
7	21.85	0.14	1314.60	22.40	Satisfied
8	21.85	0.13	1247.30	19.60	**Not satisfied**
9	21.85	0.07	1370.30	12.60	**Not satisfied**

Table 15-17 –Shear Verification for Masonry Piers Strengthened in Flexure: Edge Pier 2

Eleva-tion [m]	Design Shear Force V_{Sd} [kN]	Neutral Axis x [m]	Characteris-tic Shear Strength f_{vk} [kN/m^2]	Shear Strength V_{Rd} [kN]	Verification Result $V_{Rd} \geq V_{Sd}$
0	95.43	0.34	1812.90	155.60	Satisfied
1	95.43	0.30	1906.80	143.70	Satisfied
2	95.43	0.29	1900.20	138.00	Satisfied
3	95.43	0.28	1893.10	132.20	Satisfied
3	72.51	0.26	1816.90	90.20	Satisfied
4	72.51	0.25	1805.50	85.90	Satisfied
5	72.51	0.24	1793.00	81.60	Satisfied
6	72.51	0.23	1779.30	77.30	Satisfied
6	45.10	0.19	1543.60	37.60	**Not satisfied**
7	45.10	0.18	1511.40	34.70	**Not satisfied**
8	45.10	0.17	1475.10	31.80	**Not satisfied**
9	45.10	0.12	1647.80	24.90	**Not satisfied**

15.5 SHEAR STRENGTHENING DESIGN

A shear reinforcement system consisting of horizontal strips with the same geometric and mechanical properties as those used for flexural strengthening is proposed along the height of the edge piers.

In particular, spacing (p_f) of strips is 50 cm. The results of the verification, conducted in accordance with the application rules of 5.5.1.2.2, are presented in Table 15-18 for Edge Pier 1 and Table 15-19 for Edge Pier 2.

The results confirm that the assumed strip spacing is sufficient to ensure compliance with Ultimate Limit State (ULS) shear verification for the edge piers.

Table 15-18 – Shear Verification with Shear Strengthening: Edge Pier 1

Elevation [m]	Design Shear Force V_{Sd} [kN]	Masonry Contribution $V_{Rd,m}$ [kN]	FRP Contribution $V_{Rd,f}$ [kN]	Strut Resistance $V_{Rd,max}$ [kN]	Shear Strength V_{Rd} [kN]	Verification Result $V_{Rd} \geq V_{Sd}$	Failure Mode
0	76.58	57.70	126.03	1140.00	183.73	Satisfied	FRP failure
1	76.58	45.80	126.03	1140.00	171.83	Satisfied	FRP failure
2	76.58	40.00	126.03	1140.00	166.03	Satisfied	FRP failure
3	76.58	34.30	126.03	1140.00	160.33	Satisfied	FRP failure
3	46.48	35.50	126.03	855.00	161.53	Satisfied	FRP failure
4	46.48	31.20	126.03	855.00	157.23	Satisfied	FRP failure
5	46.48	26.90	126.03	855.00	152.93	Satisfied	FRP failure
6	46.48	22.60	126.03	855.00	148.63	Satisfied	FRP failure
6	21.85	25.30	126.03	570.00	151.33	Satisfied	FRP failure
7	21.85	22.40	126.03	570.00	148.43	Satisfied	FRP failure
8	21.85	19.60	126.03	570.00	145.63	Satisfied	FRP failure
9	21.85	12.60	126.03	570.00	138.63	Satisfied	FRP failure

Table 15-19 – Shear Verification with Shear Strengthening: Edge Pier 2

Elevation [m]	Design Shear Force V_{Sd} [kN]	Masonry Contribution $V_{Rd,m}$ [kN]	FRP Contribution $V_{Rd,f}$ [kN]	Strut Resistance $V_{Rd,max}$ [kN]	Shear Strength V_{Rd} [kN]	Verification Result $V_{Rd} \geq V_{Sd}$	Failure Mode
0	95.43	155.61	126.03	1140.00	281.64	Satisfied	FRP failure
1	95.43	143.70	126.03	1140.00	269.73	Satisfied	FRP failure
2	95.43	137.96	126.03	1140.00	263.99	Satisfied	FRP failure
3	95.43	132.22	126.03	1140.00	258.25	Satisfied	FRP failure
3	72.51	90.17	126.03	855.00	216.20	Satisfied	FRP failure
4	72.51	85.86	126.03	855.00	211.89	Satisfied	FRP failure
5	72.51	81.56	126.03	855.00	207.59	Satisfied	FRP failure
6	72.51	77.25	126.03	855.00	203.28	Satisfied	FRP failure
6	45.10	37.57	126.03	570.00	163.60	Satisfied	FRP failure
7	45.10	34.70	126.03	570.00	160.73	Satisfied	FRP failure
8	45.10	31.83	126.03	570.00	157.86	Satisfied	FRP failure
9	45.10	24.88	126.03	570.00	150.91	Satisfied	FRP failure

Finally, Figure 15-7 provides a schematic representation of the FRP strengthening system layout applied to the shear and flexural strengthening of the studied wall.

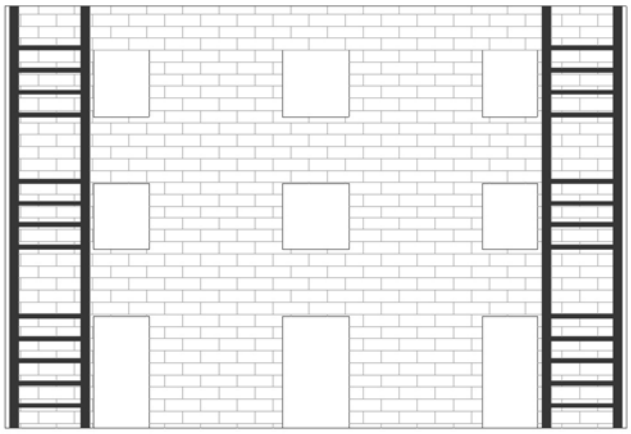

Figure 15-7 – Schematic Layout of the FRP Strengthening System for the Studied Wall.

15.6 CHECK FOR OUT-OF-PLANE WALL OVERTURNING

Following the guidelines outlined in §5.5.1.1.1, this section presents the verification of the strengthening system to be applied to the studied wall against simple overturning (Figure 15-8).

For this purpose, a continuous confinement system is assumed at each of the three-floor levels, consisting of horizontal FRP strips with the same thickness and mechanical properties as those used for flexural strengthening (Figure 15-9).

At the third level, the strengthening system is applied using two overlapping FRP layers, resulting in a total thickness of 0.33 mm. The width of the horizontal strips is as follows:

- 350 mm at the second and third levels,
- 200 mm at the first level.

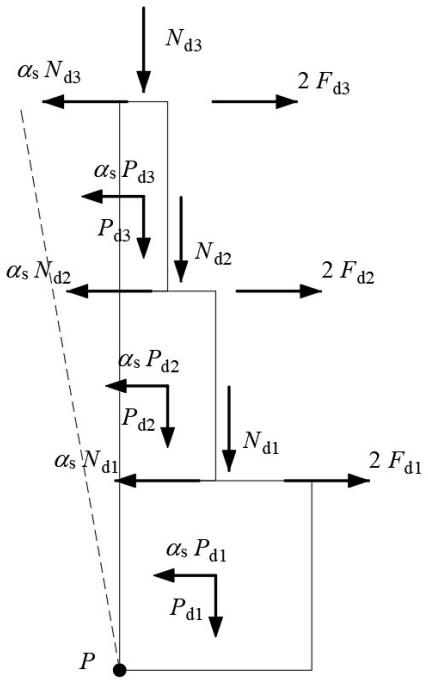

Figure 15-8 – Schematic for Simple Overturning Verification.

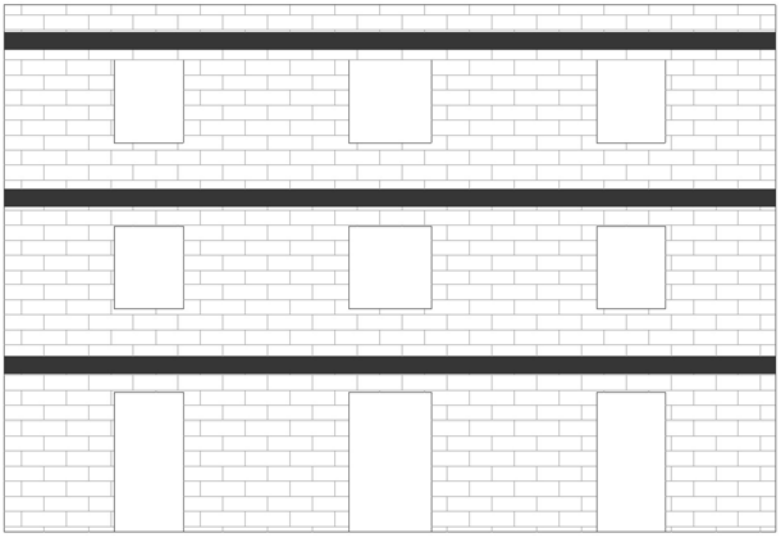

Figure 15-9 – Strengthening Layout for Simple Overturning Verification.

Verification of Restraining Actions
The actions considered for the verification against simple overturning are:

- P_{d1}=288 kN, P_{d2}=243 kN, P_{d3}=162 kN;
- N_{d1}=155 kN, N_{d2}=155 kN, N_{d3}=155 kN;
- Safety coefficient: α_s= 1.5.

The restraining force provided by the FRP confinement system at each floor level are obtained by equilibrium, and they are equal to:

- $2 \cdot F_{d,1}$=188 kN,
- $2 \cdot F_{d,2}$=377 kN,
- $2 \cdot F_{d,3}$=566 kN,

where $F_{d,k}$ represents the tensile force sustained by the FRP strengthening system at the k-th floor level (k = 1, 2, 3).

In this case, assuming that the continuous confinement system is ensured by an adequately extended overlap of the FRP strips or by mechanical anchoring devices, the restraining action provided by the FRP strengthening system is deemed sufficient if its ultimate tensile strength verification is satisfied. The verification condition is:

$F_{d,1} \leq (230000 \cdot 200 \cdot 0.165 \cdot 10^{-3} \cdot 0.0151)$ kN = 115 kN;

$F_{d,2} \leq (230000 \cdot 350 \cdot 0.165 \cdot 10^{-3} \cdot 0.0151)$ kN = 201 kN;

$F_{d,3} \leq (230000 \cdot 350 \cdot 0.330 \cdot 10^{-3} \cdot 0.0151)$ kN =401 kN.

These inequalities confirm that the chosen FRP confinement system is adequate for resisting overturning.